

Durham E-Theses

Exploring Flow Chemistry for the Synthesis and Scale-up of Small Organic Molecules

RUGGERI, MICHELE

How to cite:

RUGGERI, MICHELE (2020) *Exploring Flow Chemistry for the Synthesis and Scale-up of Small Organic Molecules*, Durham theses, Durham University. Available at Durham E-Theses Online: <http://etheses.dur.ac.uk/13768/>

Use policy

The full-text may be used and/or reproduced, and given to third parties in any format or medium, without prior permission or charge, for personal research or study, educational, or not-for-profit purposes provided that:

- a full bibliographic reference is made to the original source
- a [link](#) is made to the metadata record in Durham E-Theses
- the full-text is not changed in any way

The full-text must not be sold in any format or medium without the formal permission of the copyright holders.

Please consult the [full Durham E-Theses policy](#) for further details.



Durham
University

Exploring Flow Chemistry for the Synthesis and Scale-up of Small Organic Molecules

A thesis submitted for the partial fulfilment of the requirement for the

Degree of

Doctor of Philosophy

In the faculty of Science of Durham University

By

Michele Ruggeri

Durham University

Department of Chemistry

University Science Laboratories

South Road

Durham

2020

Statement of Copyright

The copyright of this thesis rests with the author. No quotation from it should be published without prior written consent and information derived from it should be acknowledged.

Declaration

The work described in this thesis was carried out in the Department of chemistry at Durham University between October 2016 and March 2020, under the supervision of Prof. Ian R. Baxendale. All the work is my own work, unless otherwise stated, and has not been submitted previously for a degree at this or any other university.

Michele Ruggeri

ACKNOWLEDGMENTS

First, I would like to thank my supervisor, Professor Ian Baxendale for this opportunity, for making these years an incredible adventure, for all the teachings, support and inspiration he always gave me throughout all the PhD making the lab a place of creativity and fun. Thank you for enduring the Mayhem I brought in your fume hoods.

Many thanks to all the Baxendale's group past and present members for sharing this journey.

Thanks to Dr Amanda Dombrowski and Dr Stephan Djuric from AbbVie for this collaboration, for the continuous support they gave us and for the freedom we had in all the projects.

Thanks to Marcus for all his teachings.

Thanks to don Zauker.

Grazie a Scaligero e Steiner.

Alla mia famiglia, non avrei fatto nulla senza di voi.

Publications

1) Photochemical Flow Synthesis of 3-Hydroxyazetidines

Ruggeri, M.; Dombrowski, A. W.; Djuric, S. W.; Baxendale, I. R.; Photochemical Flow Synthesis of 3-Hydroxyazetidines. *ChemPhotoChem*, **2019**, 3(12), 1212-1218.

Highlighted as an important paper in OPRD in 2019

Org. Process Res. Dev., **2019**, 23, 1773–1783

2) Rearrangement of 3-Hydroxyazetidines into 2-Oxazolines

Ruggeri, M.; Dombrowski, A. W.; Djuric, S. W.; Baxendale, I. R. *J. Org. Chem.* **2020**, 85, 7276-7286.

3) Griffiths, M. O.; Ruggeri, M.; Baxendale, I. R. Photochemical Oximation of Alkanes, *Synlett*, 2020, Accepted.

Abstract

By the late '90s flow chemistry had established itself as a powerful tool for organic synthesis in academia and had started to progressively attract the interest of the industry due to the advantages that it could potentially offer compared to batch processing; among these it is worth mentioning its intrinsic ability to reduce the solvent usage and to dramatically cut the reaction time alongside providing higher purity and selectivity due to the more regulated processing conditions. In addition, it provides a safer way to handle dangerous and hazardous reagents/intermediates and simplifying the scaling up of the process.

This thesis presents a series of molecular preparations involving flow chemistry to expedite the transformation to generate molecules of interest to the pharmaceutical industry.

All the work disclosed has been carried out in the Baxendale's research group at the University of Durham, under the supervision of Professor Ian R. Baxendale. The research has been partially funded and conducted in collaboration with AbbVie under the supervision of Dr Amanda W. Dombrowski and Prof. Stevan W. Djuric.

Chapter 1 describes the first use of flow chemistry for performing Norrish-Yang reactions. The transformation has been exploited to synthesize a range of 3-hydroxyazetidines. The high reproducibility and short residence times of the continuous process enables easy scaling of the transformation allowing easy access to these valuable chemical entities at synthetically useful multi-gram scales. Moreover, a systematic exploration of the constituent structural components was undertaken allowing an understanding of the reactivity and functional group tolerance of the transformation.

Chapter 2 details the chemistry of a novel rearrangement of the previously obtained 3-hydroxyazetidines (Chapter 1) via a Ritter initiated cascade to provide highly substituted 2-oxazolines in high yields. The reaction conditions and substrate scope of the transformation have been studied demonstrating the generality of the process. The derived products can also be functionalized in order to undergo further intramolecular cyclization leading to a new class of macrocycle. The final cyclization step was shown to be a transformation amenable to continuous flow processing allowing for a dramatic reduction in the reaction time and a simple direct scale-up.

Chapter 3 deals with the nitrosation of several alkanes with *tert*-butyl nitrite under flow processing conditions. The continuous approach enabled a marked reduction in the reaction time compared to the analogous batch process. In addition, in order to address the necessity for large excesses of the alkane starting material a continuous recycling process was developed thus allowing the preparation of larger quantities of material in a more atom economic and cost-effective process.

Contents

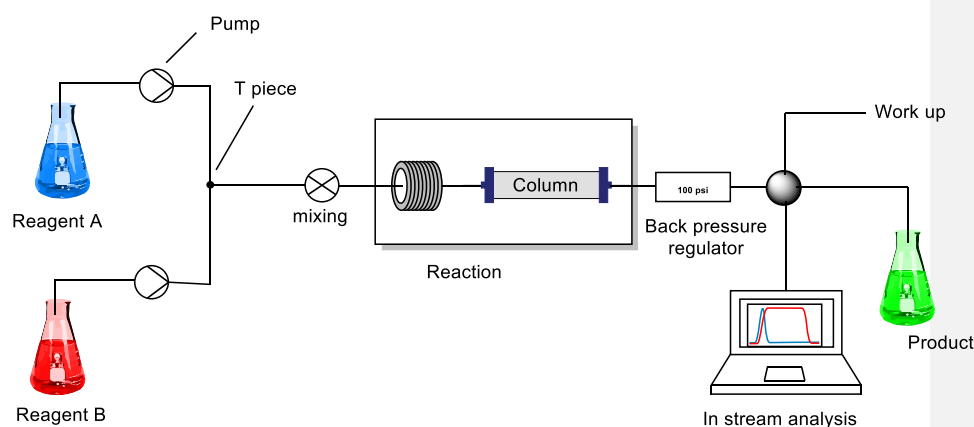
1. Chapter 1:.....	9
1.1 Introduction: flow chemistry	9
1.2 Instrumentation	13
• 1.2.1 Pumps	13
• 1.2.2 Mixing	14
• 1.2.3 Reactor	16
1.3 Photochemistry and Flow	23
1.4 References	33
2. Chapter 2: Photochemical Flow Synthesis of 3-Hydroxyazetidines.....	37
2.1 Azetidines.....	37
• 2.1.1 Literature survey of the synthesis of azetidine rings.....	3940
2.2 The Norrish reaction	4243
2.3 The Yang reaction	4445
2.4 Result and discussion.....	4748
• 2.4.1 Retrosynthesis.....	4748
• 2.4.2 Description of the flow set-up	4950
• 2.4.3 Solvent system	5152
• 2.4.4 Lamps.....	5253
• 2.4.5 Light sources screening.....	5354
• 2.4.6 First approach	5455
• 2.4.7 Substrate screening	5758
2.5 CONCLUSIONS.....	7475
2.6 References	7576
2.7 Experimental.....	8081
• 2.7.1 Materials and Methods.....	8081
• 2.7.2 Synthesis	8182
3. Chapter 3: The rearrangement of 3-hydroxyazetidines to 2-oxazolines.....	113114
3.1 INTRODUCTION: General Oxazoline Synthesis and Applications	113114
• 3.1.1 Synthesis of 2-oxazoline.....	113114
• 3.1.2 Synthesis of 3-oxazolines	121122
• 3.1.3 Use of 2-oxazoline in the pharmaceuticals:.....	122123
• 3.1.4 Industrial application	123124
3.1.5 Asymmetric catalyst.....	124125
3.2 Results and discussions.....	146147

• 3.2.1 Optimization: Acid Screening.....	<u>147148</u>
• 3.2.2 Optimization: Solvent choice	<u>149150</u>
• 3.2.3 Substrate scope.....	<u>150151</u>
• 3.2.4 Investigating Alternative Nucleophiles	<u>157158</u>
• 3.2.5 Further Intramolecular Reactions.....	<u>159160</u>
• 3.2.6 Development of a Flow Process.....	<u>161162</u>
3.3 CONCLUSION.....	<u>162163</u>
3.4 Future work.....	<u>163164</u>
3.5 Experimental Section	<u>163164</u>
3.6 References	<u>183184</u>
4. Chapter 4: Exploring Photoflow Promoted Oximation of Alkanes	<u>189190</u>
4.1 Introduction: Oximes	<u>189190</u>
• 4.1.2 Synthesis of oximes.....	<u>195196</u>
• 4.1.3 Photo oximation of cyclohexane	<u>208209</u>
4.2 Results and discussion	<u>218219</u>
4.3 Conclusion.....	<u>229230</u>
4.4 References	<u>230231</u>
4.5 Experimental	<u>235236</u>
• 4.5.1 Materials and Methods.....	<u>235236</u>
• 4.5.2 Compounds characterization.....	<u>236237</u>

1. Chapter 1:

1.1 Introduction: flow chemistry

Over the last 20 years synthetic chemistry has seen considerable change brought about by the increasing adoption of so called *enabling technologies*^[1]. Among these, flow chemistry can reasonably be considered one of the most influential technologies^[1,2]. Broadly speaking flow chemistry can be defined as the performing of a chemical transformation by pumping the requisite reagents to meet together and be transported along a pipeline (or equivalent processing reactor) whilst reacting to yield the product which exits the reaction chamber at the terminus end of the tube/chip/channel. A general flow process can be depicted as follows (Scheme 1):



Scheme 1: General flow set up.

In this system reagents are pumped by a delivery unit (typically a pump of either HPLC, syringe or peristaltic design), in the case of multiple reacting component they can be mixed together by a specific in-line mixing element before reaching the main residence time reactor. The mixing site can involve active or passive mixing (discussed later). The reactor system can be upgraded with multiple tools for analysis and direct purification. All these elements can be assembled in different configurations to obtain unique and customised set ups to perform different reaction sequences.^[1-5] Despite having multiple components the core of the flow system is the reactor, a device where the entering reagents undergo reaction within a controlled and highly regulated environment. A wide range of activation conditions can be applied to the reactor, including thermal heating, photochemistry^[6,7], microwave

irradiation^[8,9], electrochemistry^[10,11], ultrasound^[12,13] and oscillation^[14,15]. Running a reaction in flow presents several additional advantages over classical batch chemistry. These include better mixing which is easily achieved in a flow system. The Reynold Number (N_{re}) is used to define the flow type and can be generally classified into one of three regimes: laminar, transitional or turbulent based on the degree of mixing (Eq. 1).

$$N_{Re} = D V \rho \mu \quad (\text{Eq. 1})$$

where D is the pipe diameter, V is the velocity, ρ is the density, μ is fluid viscosity.

Generally a laminar flow corresponds to a $N_{Re} = 2,100$ whilst a turbulent flow has a $N_{Re} > 4000$ (Figure 1).

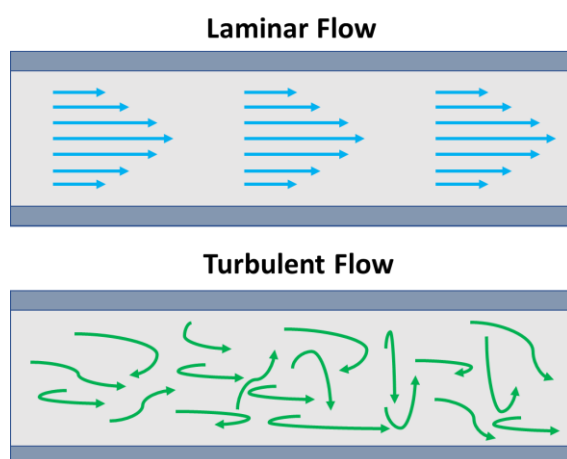


Figure 1: Laminar and turbulent flow regimes.

Normally, in a standard stirred batch experiment the mixing can be in a laminar or in a transitional regime. In this second case what is observed is a turbulent regime near the stirrer bar (overhead propeller stirrer) and a laminar one in the more distant regions of the reactor with the molecules moving from these regions by diffusion (Figure 2).^[16] Inside a pipe reactor the diffusion time between the inner and the outlying region is considerably reduced therefore resulting in a faster mixing. Nonetheless, the mixing efficiency is not determined solely by diffusion, it can be further rationalised using the Damköhler Number (Da ; Eq. 2) a dimensionless unit which can be briefly defined as a ratio between the reaction rate and the mass transfer by diffusion.

$$Da = \frac{\text{reaction rate}}{\text{diffusion rate}} \quad (\text{Eq. 2})$$

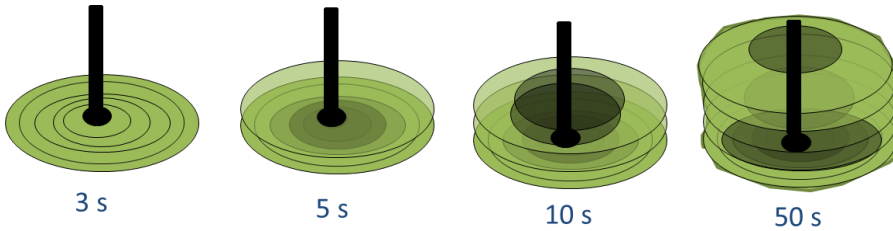


Figure 2: Schematic representation of mixing in a reactor. Fluorescent dye in glycerine (20 L reactor, impeller mixing).

For $Da < 1$ mixing is almost completely achieved before the reaction occurs whereas for $Da > 1$ the mass transfer by diffusion is not as fast as the reaction. In this latter scenario the fast reaction occurs before the mixture has become fully homogeneous. In such situations a higher local concentration of one of the reagents can react further with the product leading to the formation of side product or giving incomplete reaction. The higher achievable mixing in flow diminishes this issue (Figure 3).^[17]

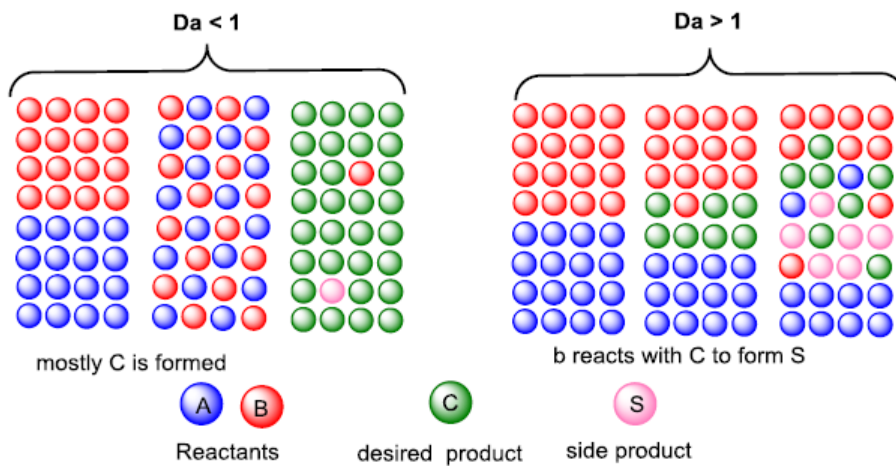


Figure 3: Different scenarios based on Da . (Left): Da number < 1 the solution reaches the homogeneity resulting in high selectivity for the reaction $A+B \rightarrow C$. (Right): The homogeneity

is not reached leading to local concentration gradients of A and B which can react with the product C leading to side product (S).

One of the most attractive aspects of flow chemistry is its ability to enable easy scaling up of the reaction. Normally, in batch, increasing the dimension of the reaction vessel generates problems such as less homogeneous mixing, the production of temperature gradients as heat exchange becomes less efficient or the increasing of the reaction time as prolonged heating periods are needed for the larger volume. These factors can lead to less efficient reaction and the generation of more side products. In flow mode the scaling up of the reaction can be achieved in several ways. The simplest is to increase the apparatus size; using a larger reactor allows the chemist to directly increase the throughput in what is called sizing up in analogy to what is normally performed in traditional batch systems. On the other hand, a flow system can facilitate higher throughput by “equalling up” which increases the number of identical micro-structures in the reactor or by “numbering up” which is the parallel arrangement of identical equipment. This second scaling up strategy can be performed “internally” or “externally”: external numbering up entails the replication of the entire system several times until it produces the desired quantity of product per unit time. This is achieved by employing several reactors with their own pumping system and process control. This method is particularly reliable as a potential failure of one of the replicated reactor components does not affect the others although it does significantly raise the cost due to the number of additional individual components required. Conversely, in the internal numbering up approach only the reactor unit is replicated and the pumping system is shared thus considerably reducing the cost of the set up although a failure under this scenario would affect all the apparatus.

Directly linked with scaling up is the issue of safety. Increasing the quantity of reagents and solvents processed or using greater quantities of toxic or hazardous chemicals is considerably easier and safer in flow because of the low active quantity of material involved in the reactor at any given time. The risk related to potentially harmful intermediates is therefore reduced compared to the batch process where all the chemicals are in the same place at the same time.

1.2 Instrumentation

A basic flow system can be divided in three main blocks: one part dedicated to the delivery of the reagents, one to the mixing and one to the reaction. Although significant emphasis is often placed on the important attributes of the reactor design the delivery pumps are often the most critical components of the system.

1.2.1 Pumps

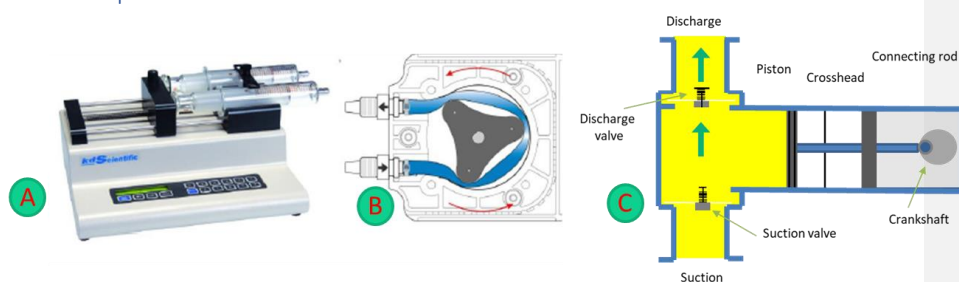


Figure 4: Type of pumping devices: Syringe pumps A (kdsScientific®), peristaltic pump B (PumpsandSystem®), piston pump C.

The selection of a pumping device depends on several factors such as the required flow rate, the reactor pressure drop and the nature of the reagents to be delivered. There are three main types of pump: syringe pumps (Figure 4, A) which allow a very accurate level of control and enable very low flow rates. However, the main drawbacks are that high pressures are not easily available and that the limited volume of the syringe barrel does not easily allow a continuous and uninterrupted delivery. New systems can use two syringes so that as one is used to pump the fluid into the reactor, the second can be refilled enabling a pseudo-continuous process. Alternatively, HPLC pumps (Figure 4, C) allow for a very accurate flow control at higher flow rates and tolerate high fluidic pressure. The main problem with this type of pump is in regard to the use of volatile solvents or very viscous materials which can cause cavitation (in this case the issue can sometimes be by-passed by the use of an additional pressurising the system) and the presence of particles which are not tolerated by piston pumps. An alternative pump design is the peristaltic pump (Figure 4, B) through which it is possible to handle the pumping of modest precipitates and more viscous materials. The main drawback in this case is that they are less accurate and in the main do not tolerate high delivery pressures.

1.2.2 Mixing

As indicated previously mixing is a crucial attribute of any reaction, for this reason several devices have been developed in order to achieve an optimal homogenization of the reaction mixture. Mixing elements can be further divided in two main categories: active and passive components. In active devices the source of energy conducting the mixing comes from outside the system (an example is the use of ultrasound) in the latter, passive form, the mixing depends on the geometric proprieties of the system design itself.

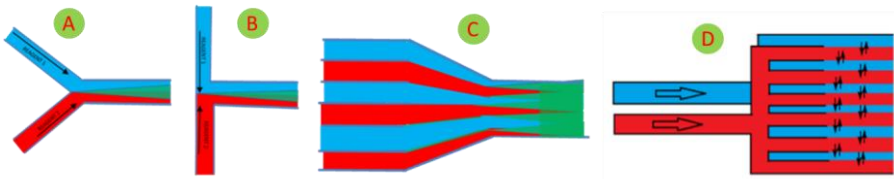


Figure 5: different shaped passive mixing elements; A = Y MIXER, B= T mixer, C, D = multichannel mixers.

For a single-phase reaction, if the transformation does not require fast mixing (e.g. $Da < 1$), a simple T- or Y-connection can be utilised to combine two or more reagent streams (Figure 5 A and B). When improved mixing is required these standard connections might not be enough and for this reason several advanced mixing tools have been developed. In the simplest case the inner diameter of the T-mixer can be reduced and this coupled with a high flow rate can result in what is called engulfment flow where the fluid from one side reaches beyond the centre-line of the T-mixer engulfing the fluid coming from the other side. The engulfment flow has been proven to enhance the mixing^[18-21] although it requires high N_{Re} (around 200).^[22] More sophisticated micromixers are also available, one example is the creation of micro-structured components where the transit of the flow is continuously redirected in order to obtain a form of chaotic mixing (Figure 6).

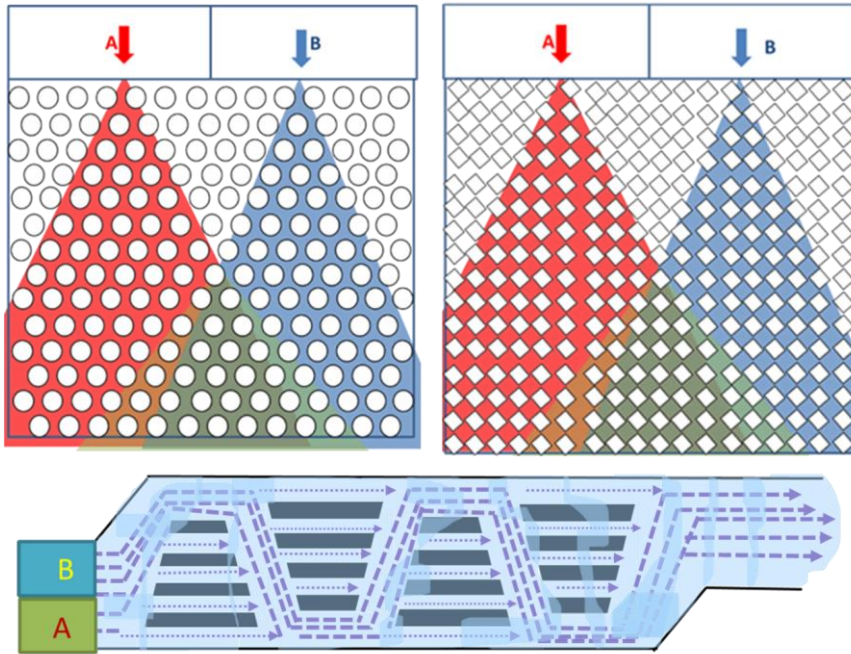


Figure 6: Micromixers with different internal microstructures for promoting chaotic mixing.

Another efficient way to induce mixing is the splitting of the flow into multiple thin streams with the result that the time required for the streams to mix by diffusion upon recombination is considerably reduced.^[18-24] This form of mixing falls into what is called passive mixing, which implies the achievement of reagent mixing occurs via diffusion within the reaction medium within channels or through the use of obstructing objects within the pipe. This second case scenario is called static mixing and the flow rate is responsible for the efficiency of the mixing. When the system is dealing with biphasic or multiphasic mixture or in a case where there is the development of a precipitate (or in case the use of larger channel is required); the use of active mixing can be particularly beneficial^[17]. It entails the mechanical mixing of the mixture and contrary to what occurs in the passive mixing where the mixing efficiency is strictly coupled with the residence time in the active mixing these two factors are decoupled. The mixing can also be achieved by magnetic stirring or by agitation of dedicated reaction vessels, moreover the mixing unit can be submerged in an ultrasonic bath allowing the prevention of aggregates leading to the clogging of the system^[17].

1.2.3 Reactor

Among all the components of a flow apparatus the reactor is the place where the chemical transformation mainly takes place (reaction starts at the site of mixing and hence the mixing element can also be part of or principally the reactor). A great number of reactor devices have been developed ^[17]. Reactors can be placed into one of three general categories: chip-based reactors (including falling film systems), coil reactors and packed bed reactors (Figure 7).

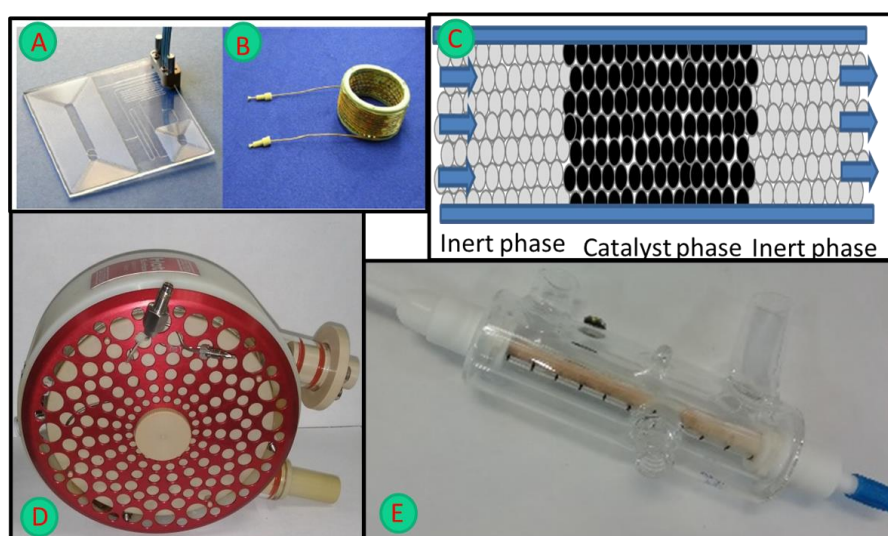


Figure 7: Different reactors: chip based (A), coil (B), packed bed (C), High temperature tube reactor (D), column reactor filled with K_2CO_3 (E).

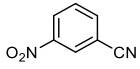
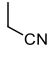
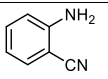
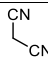
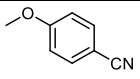
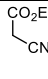
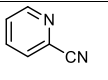
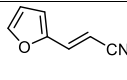
A chip-based reactor (Figure 6 A, average internal channel dimensions between 0.01 and 0.5 mm) comprises a series of channels often etched into a flat surface and enclosed with a bonding layer to prevent channel crossover. The extremely high surface-to-volume ratio makes this type of reactor the best choice when high heat transfer is required.^[25,26] The material of construction is very important and is chosen depending on the use of the reactor; for example, photoreaction requires the use of light transparent material, good heat transfer could use silicon carbide, optics might allow glass to be utilised. Despite these great advantages this kind of reactor remains quite expensive to construct and issues associated with obstruction makes them less useful for the scale up of a reaction.

Coil reactors (Figure 6B and 6D) are generally made out of fluorinated polymers (i.e. PFA, FEP, PTFE), metal/fused silica or additional polymers such as PEEK. When the reaction requires high temperatures and pressures stainless steel or chemically resistant Hastelloy (silicon carbide) reactors are used. Normally temperature regulation is obtained by placing the coil in a special chamber to enhance thermal transfer. If the material of the reactor is chosen correctly then the reactor itself can be used as catalyst for performing transformation like coupling reactions or azides synthesis, i.e. using a copper tube coiled reactor.^[24]

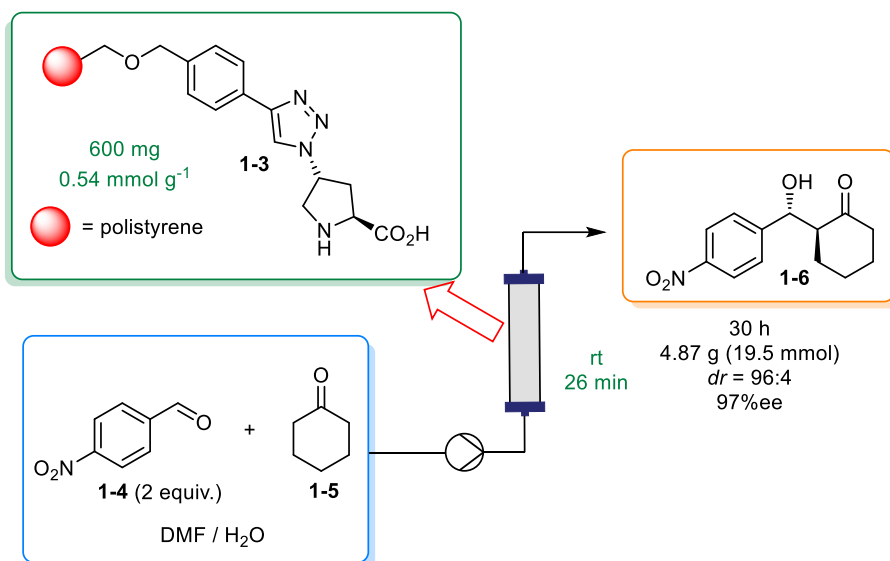
In addition packed bed reactors can be assembled using a heterogeneous component (a reagent or a catalyst) loaded into the tube, channel or cartridge of the reactor.^[25,26] In most cases these reactors are made from in-line columns or cartridges which can be easily filled and emptied and are constructed from a wide range of materials e.g. glass, metal, and polymer. The key aspect of this type of reactor is the very high ratio of catalyst-to-reagent that can be produced in flow compared to a classical stirred batch reactor; the result is often a significant decrease of the reaction time. Moreover, having the reagent/catalyst confined in the cartridge there is a less requirement for purifying the reaction mixture thus reducing the number of required steps. Among the many applications catalytic hydrogenation has been extensively performed by using reactor packed bed units.^[17,27,28] Battilocchio *et al.* performed nitrile hydration in flow using MnO₂ solid supported (Table 1) obtaining the desired product in high yield (94-100%).^[28] Compared to the analogous batch reaction the flow approach allows a reduction in the reaction temperature (T > 140 °C in batch, T 30 < T < 110 °C in flow) and to avoid difficult purification steps and issues linked to the recovery of the catalysts.

Table 1. Solid supported nitrile hydration with MnO₂.

	Substrate	T (°C)	T (min)	Yield (%)		Substrate	T (°C)	T (min)	Yield
1a		100	10	99	1f		100	100	99

1b		100	15	98	1g		70	70	99
1c		110	40	96	1h		100	100	98
1d		110	50	97	1i		30	30	96
1e		100	3	99	1j		80	80	98

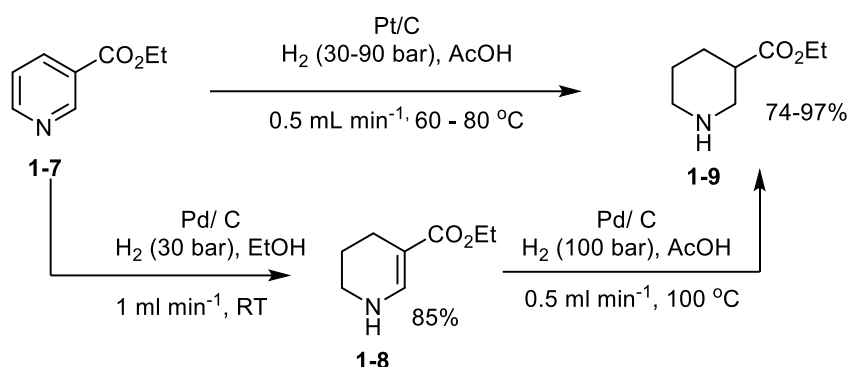
Solid supported catalysts have also been used in flow for performing asymmetric aldol reactions.^[29-35] Pericas *et al.* reported the use of a proline derivatives supported on a Merrifield type resin (Scheme 2). The catalyst was immobilised using a linking Huisgen cycloaddition reaction. The author reported excellent catalyst stability with demonstrated use over 35 hours with no deterioration of the isolated stereoselectivity.



Scheme 2: Asymmetric aldol reaction performed in flow using solid supported proline derivative catalyst.

The Kappe group^[36] reported the heterogeneous hydrogenation of substituted pyridine performed in flow using an H-Cube reactor (Scheme 3). The methodology allows the reaction

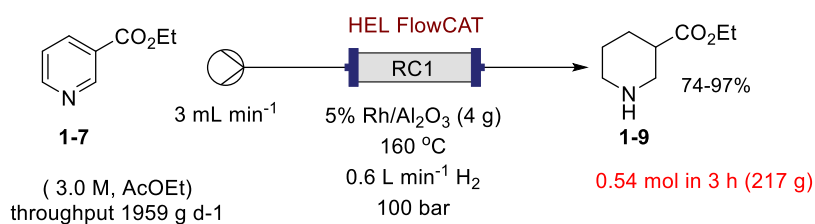
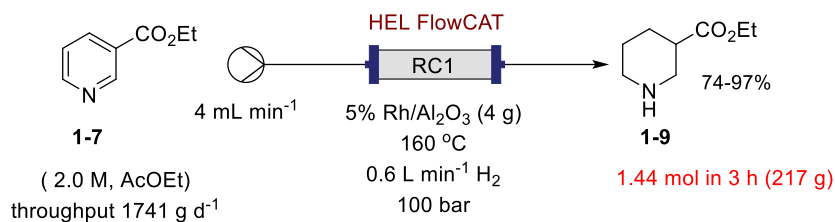
to be achieved in good yields using several different metal catalysts (Pd/C, Pt/C, Rh/C) and in case of ethyl nicotinate (**1-7**; Scheme 3) depending on the combination of H₂ pressure, solvent and catalyst it is possible to discriminate between partial and full hydrogenation (**1-8**, **1-9** Scheme 3).



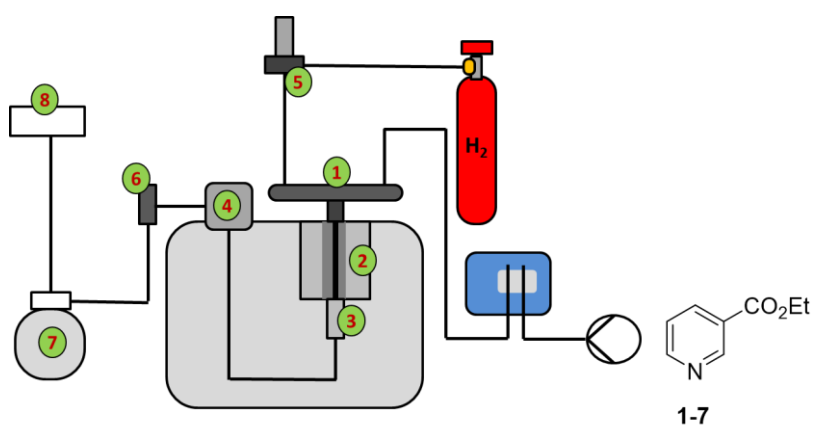
Scheme 3: Kappe's heterogeneous hydrogenation of substituted pyridine in flow using the Thales H-cube reactor.

Hawkins and the Ley group^[37] performed a high intensification of the partial and full hydrogenation of the ethyl nicotinate (Scheme 4). The aim of the group was to develop a process able to deliver a throughput exceeding the kilogram per day. The study was performed using a commercially available HEL FlowCAT reactor^[38]: a benchtop unit which allows to perform the scale up of heterogeneous reactions (Figure 8). One of the features of the Hel flowCAT reactor is that it can operate both under fixed bed and trickle-flow conditions. Fixed bed conditions are characterised by a single-phase flow whilst in the trickle-flow conditions the fluid flows in two distinct phases: liquid and gas

The scale up of the process was performed by using a 3,6 mL RC1 and 12 mL RC2 reactors column loaded with Rh and Al₂O₃T leading to an outstanding throughput of 1959 g d⁻¹.



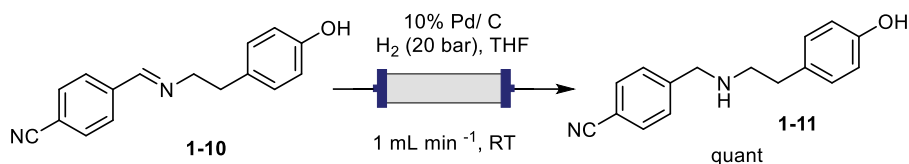
Scheme 4: Continuous Flow Hydrogenation of Ethyl Nicotinate with the HEL FlowCAT reactor.



- | | |
|----------------------------|----------------------------|
| 1 = Liquid/gas mixing zone | 5 = Mass flow controller |
| 2 = Heating jacket | 6 = Pressure release valve |
| 3 = Trickle bed | 7 = Collection vessel |
| 4 = Liquid/gas separator | 8 = H ₂ Venting |

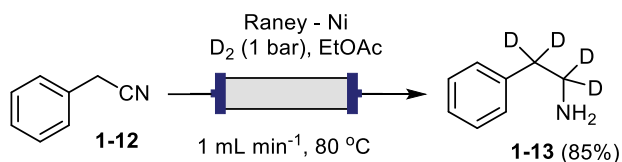
Figure 8: Schematization of the HEL FlowCAT reactor.

Ley's group achieved reduction of various imines in flow using 10% Pd/C (Scheme 5). Interestingly, the author reported that the process can be carried out in the presence of other functional group which would normally be reduced (e.g. pyridines, nitriles).^[39-41]



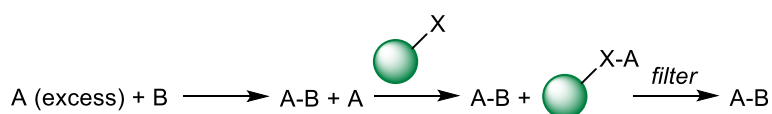
Scheme 5: Reduction of imine in flow using packed bed reactor.

Fulop used the Thales H-cube reactor for the preparation of deuterated compounds by using deuterated water as a D₂ source. This methodology allowed them to reach a deuterium incorporation content of 99% (Scheme 6).^[42]



Scheme 6: Fulop's preparation of deuterated compounds using the Thales H-cube reactor.

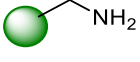
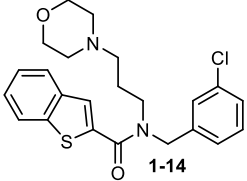
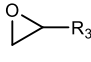
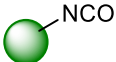
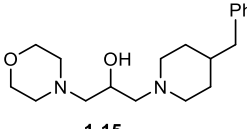
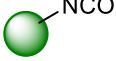
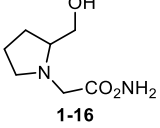
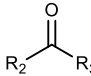
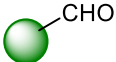
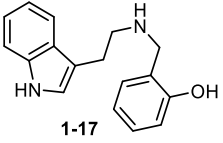
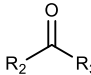
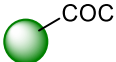
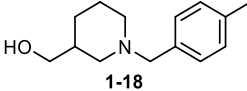
Purification and isolation of the reaction products can also benefit from a flow approach. Of particular value has been the use of solid supported reagents and scavenger resins in order to assist these vital steps. For example, in the case of a reaction performed with an excess of one of the reagents, the purification step can be critical to the point to jeopardise the entire transformation. The use of a scavenger resin, if chosen accordingly, allows selective extraction of the unreacted reagent without need for any further separations or isolations (Scheme 7).^[43-46]



Scheme 7: Schematization of a scavenger process for the removal of excess of one reagent.

Kaldor's group prepared various ureas, thioureas, amides, sulfonamides and carbamates utilising a scavenging agent to remove the excess reagent (Table 2).^[47]

Table 2: Scavengers used by Kaldor's group for the removal of excess starting material.

Limiting reagent	Excess reagent	Scavenger	Solvent / Temp	Representative product	Yield (%)	Purity (%)
R_1R_2NH	R_3NCO R_3COCl R_3SO_2Cl		$CHCl_3$ / RT	 1-14	67	94
	R_1R_2NH		$MeOH$ / RT	 1-15	94	93
$R_3X^{b,e}$	R_1R_2NH		CH_3CN / 30- 60°C	 1-16	96	>95
	R_1NH_2		CH_3Cl / RT	 1-17	73	90
	R_1R_2NH		10% $HOAc$ - $C_2H_4Cl_2$ / RT	 1-18	62	>95
Typically 1.25 - 2 equiv. fold excess; B) piperidinomethyl polystyrene or other supported base is added as an acid scavenger; C) acid chloride or chloroformates; D) reaction was diluted with 2 volumes of CH_2Cl_2 prior to scavenging at room temperature; E) X = halide, sulfonate ester.						

Another crucial step for any chemical process is the ability to analyse the progression of the reaction. For any chemical system, the most basic way to check the status of the reaction is to manually sample the reaction mixture and analyse it off-line. Although this method remains the most used and is sufficient for the requirement of a standard synthetic lab, more detailed reaction monitoring may benefit from alternative methods; this is particularly true in cases of

kinetics studies, extensive optimization and when toxic/ hazardous compounds or intermediates are involved. In such cases the use of on-line and in-line analysis can be additionally useful. An on-line analysis refers to a situation when the reaction mixture is analysed by automatic sampling with no need of any manual transfer, the sample is automatically sent to the analysis device. In case of non-destructive methods IR, UV-vis and NMR the testing can be performed directly in-line by integrating the desired analytical device directly into the flow system thus offering the chance for what is called “real time analysis”^[20] (Figure 9).

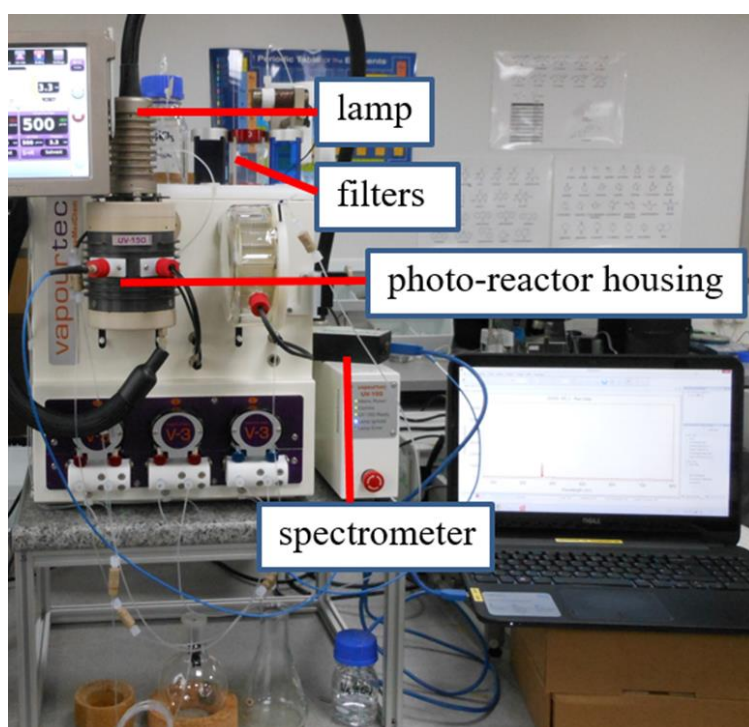


Figure 9: In-line analysis through portable ExemplarLS spectrometer coupled with a Vapourtec UV-150 photoreactor providing information through continuous recording of emission/transmission spectra.

1.3 Photochemistry and Flow

Even as early as the 19th century there was considerable interest in the possibility of using sun light to promote organic chemical reactions. One of the first examples to be studied was the reduction of quinone to hydroquinone by Cannizzaro and Ciamcian.^[48-50] The general interest in this field continued to increase in the following century after the discovery of

several new reactions such as the [2+2] cycloaddition,^[51-53] the photochemistry of ketones^[54-55] and the understanding of new concepts such as the 'excited state'^[56], and the possibility of π^* transition.^[57] At the same time improving chemical knowledge allowed the development of further synthetic applications involving photochemistry, leading to the synthesis of new molecules such as caryophyllene (**1-19**)^[58] and cedrene (**1-20**) (Figure 10).

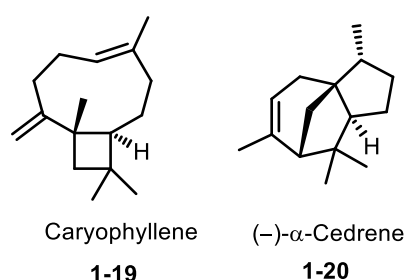


Figure 10: Caryophyllene and α -Cedrene structures.

The reasons why photochemistry has received such intense attention are manifold: one of them was the possibility to form new bonds which were hard or impossible to obtain in other ways and to simplify or reduce the number of steps in the given synthesis of a target structure. Moreover, from a modern environmental stance photochemistry is a very attractive field of study. Indeed, the simplification of a synthesis and the behaviour of the photon as a traceless reagent enhance the environmental characteristics of photochemistry.^[59,60]

Although there have been several examples of industrial synthesis involving photochemistry; for example Vitamin A and D3 by Base and Hoffman-La Roche,^[61] the photochlorination of toluene,^[62] the synthesis of rose oxide^[63] and more recently the preparation of Artemisinin by Sanofi^[64,65] photochemistry still struggles to find a wider prominence in most industry settings. This is partially due to the initial cost of the required instrumentation, as the lamps and filters are often expensive as are the auxiliary cooling system required to counterbalance the high temperature generated by the industrial lamps. Other important considerations also result when switching from a laboratory-based set-up to an industrial scale unit. Amongst these can be dramatic change in reactivity, selectivity and kinetics brought about due to changes in the dimension of the reactor in order to accommodate the large volumes often required.^[66] This problem regarding scaling up a photochemical process is particularly related to a batch approach where the reactor basically constitutes a sealed

light source which is immersed in the reacting solution. From the well-known Lambert-Beer equation it is possible to show that light radiation is not uniform in the reactor because of the absorption of photons and that light intensity decreases with distance travelled from the lamp (Figure 11).

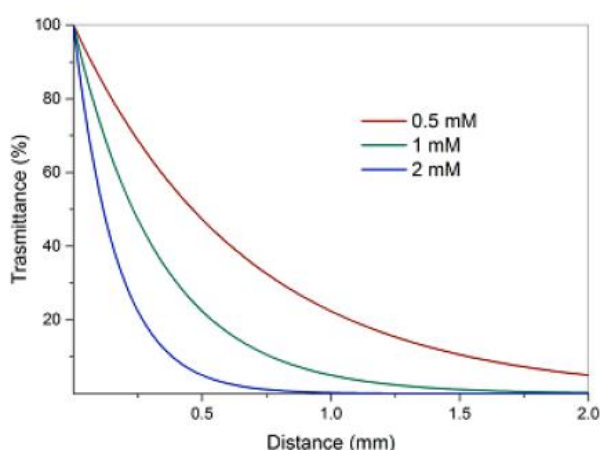


Figure 8: Transmittance vs Distance: The fraction of light available for the photoreaction drops down increasing the distance from the lamp and the concentration of the solution.

$$A = \epsilon c l \quad \text{Eq. 3}$$

The *absorption* (**A**) is proportional to the *extinction coefficient* (ϵ), the concentration **c** and the path length (**l**) but can also be expressed as a negative logarithm of the ratio between transmitted light (**I_o**) and *incident light* (**I**) (Eq. 3 and 4).

$$A = -\log_{10} \frac{I}{I_0} \quad \text{Eq. 4}$$

Using equation 4 we can see that when **A** = 1 corresponds to a situation where **I/I_o** = 0.1 and **I_o** = 10**I** so that 90% of the radiation is absorbed.

To illustrate with an example the photo excitation of valerophenone,^[67] which exhibits a $\pi \rightarrow \pi^*$ transition of $700 \text{ M}^{-1} \text{ cm}^{-1}$ at 280 nm, at a concentration 0.05 M. In order to obtain an absorption of 90% of the incident light, the path length required is only 0.028 cm. If we consider that a $\pi \rightarrow \pi^*$ transition can exhibit an ϵ close to $20000 \text{ M}^{-1} \text{ cm}^{-1}$ this would lead to an absorption of the 90% of light after 0.01 mm. By considering this example it is easy to

understand the main problem for scaling up of a photochemical reaction when using a batch reactor. The solution closest to the lamp effectively screens the bulk solution from the light with any increase of the concentration resulting in an augmentation of this blocking effect.

A solution to this can be to adopt a flow approach.^[68-72] The main difference in a flow-photochemical approach is that at any instant only a small volume of solution, is passing through the reactor and hence is being irradiated whereas the intensity of the incident light has not changed. Therefore, due to the small diameter of the reactor volume compared to its overall surface area, the theoretical light path length has been effectively reduced. This therefore generates a uniform distribution of the radiation through the entire sample. At the same time the continuous progression of the solution in flow allows scale up of the reaction by processing more material through the reactor over time.

An important parameter which can be useful in understanding the efficiency of a reaction is the quantum yield which can be defined as:

$$\Phi = \frac{\text{number of molecules of product}}{\text{number of photons reaching the reactant}} \quad \text{Eq. 5}$$

In general, Φ assumes a value between 0 and 1^[73] where $\Phi = 1$ indicates a chain mechanism.^[74-77] The result Φ is related to the *photon flux* Φ_p : *the number of photons observed per unit of time*. Comparing the Φ_p of a batch reaction to a flow process can aid understanding of the benefits to a photochemical approach by working in flow. Luobiere *et al.*^[78] have calculated that the photon flux achieved for a batch and a flow reactor are similar at 4.1×10^{-6} v's 7.4×10^{-6} Einstein/s. However, dividing these numbers for the associated reactor's volume to obtain the *photon flux density*, the situation is very different, with 0.033 for the batch reactor versus 5.02 Einstein for the flow. These results corroborate additional observations reported by Cambie and Bottecchia^[79] who found a Φ_p 100 times higher for their flow reactor. This difference explains why a photoreaction is generally accelerated under flow conditions and particularly when using a flow micro-reactor.

A third important parameter used to define a photochemical reaction is the photonic efficiency ξ :

$$\xi = \frac{\text{reaction rate}}{\text{photon flux}} \quad \text{Eq.6}$$

Again, here flow reactors show higher values, whilst the batch ξ remain in the range between 0.001-0.0001 a micro reactor can show an increase of 200 times.^[79]

In general, there are two possible approaches which can be adopted when scaling up a photo-flow process. The most straightforward is to increase the flow rate or concentration of the solution thus resulting in a higher throughput. In the first case, it is necessary to maintain the residence time by using a larger reactor volume (extending the reactor length). In the second scenario of increased concentration this should be balanced by an increase in the photon flux to compensate for the increased number of absorbing molecules. The second scaling way is to use more than one reactor run in parallel; called *numbering-up* (see previous introduction section). Depending on the connection between the reactors it is possible to subdivide the numbering up strategy into two distinct categories:^[79] if each reactor is connected with its own pumping system the set-up is called *external numbering-up*. Despite its efficiency it remains the most expensive as often the pump unit is the highest cost part. The alternative set-up is the *internal numbering-up* (Figure 12) in which case the pumps and control system are shared. Internal numbering-up is definitely cheaper but in contrast with the external set-up where a failure on one reactor does not affect the others, in this case any problems in one reactor can jeopardize the entire process.



Figure 9: An example of numbering up for reaction scale up.

Overall photoreactors fall in two categories based upon their internal dimensions, namely, macroflow (also known as mesoflow) and microflow reactors. Microflow reactors are defined as having internal channel dimensions between 0.01 and 0.5 mm (inner diameter), they can thus generally be used with a flow rate from few microliters to low mL flows. Normally these systems are constructed with a series of microchannels etched into a flat surface of glass or metal.^[68, 80] They are characterised by a low material input which together with their high heat and mass transfer properties make the microreactor an excellent choice for working at a lab scale, especially for the optimization of a process using minimal reagents and for kinetics studies. On the other hand, the main disadvantages are a low throughput, a high pressure drop and a tendency to experience obstructions of the channels, i.e. easy reactor blocking.

The characteristic design of a microflow reactor, which generally entails a flat surface, affects their ability to capture incident light both because of the radial character of most of the light sources but also in the case of a planar light (LED) source as its focus is normally wider than the channel dimensions. The main result is that microflow reactors are normally inefficient at exploiting the full capacity of the light source. On the other hand, they allow an extremely precise control of the reaction condition (temp, residence time) making them a powerful tool for reaction screening and for performing transformation on a lab scale.^[68]

A macroflow reactor has a tubing system with an inner diameter higher than 0.5 mm, the comprising coil is normally wrapped around a lamp and the device allows the use of flow rate $> 1 \text{ mL min}^{-1}$ therefore achieving higher throughput and scalability of the process. A great benefit of macroflow reactors is the ability to handle solids which is otherwise not possible using microreactors due to blockages. The main disadvantage is a reduced heat and mass transfer properties. The polymer FEP is widely used due to its excellent transmission properties.^[81,82]

The light source used is generally chosen depending on the absorption range of the reactive species involved in the transformation (Table 3) although other factors like costs, geometry of the system and life time of the light sources play an important role in its choice as well.

Table 3. UV absorption range of some functional groups of organic compounds.

Simple alkene	190-200 nm
Acylic diene	220-250 nm
Cyclic diene	250-270 nm
Styrene	270-300 nm
Saturated ketones	270-280 nm
α,β -Unsaturated ketones	310 – 330 nm
Aromatic ketones/aldehydes	280 – 300 nm
Aromatic compounds	250 – 280 nm

Mercury light sources and CFL (compact fluorescent light) lamps are used respectively for UV and visible light dependent transformations. Their efficiency in terms of lumen per wats (lm/W), long life span and their broad range of emission make them a popular choice for performing a wide range of photoreactions. Medium and low pressure mercury lamps are generally used for performing transformation requiring radiation in the range of 350 - 250 nm whilst high pressure lamps allows emissions to reach 600 nm. Fluorescent black lights offer an emission between 300 - 450 nm. Generally, CFL lamps are easy to use and have thus gained a wide popularity although due to their physical dimension (including hosing) they are not easy to apply in respect to microflow applications i.e. being hard to fit with the microchannels size. LEDs have become very popular because their reduced physical dimensions allow them to be combined with many flow reactors and because their intrinsically reduced emission band permits more selective irradiation to be achieved. Moreover, LEDs generally required much cheaper cooling systems compared to mercury lamps (often simple CPU fans can be used). The use of light filters also permits further tailoring and narrowing of the emission spectra of all light sources thereby targeting only selecting areas of interests.

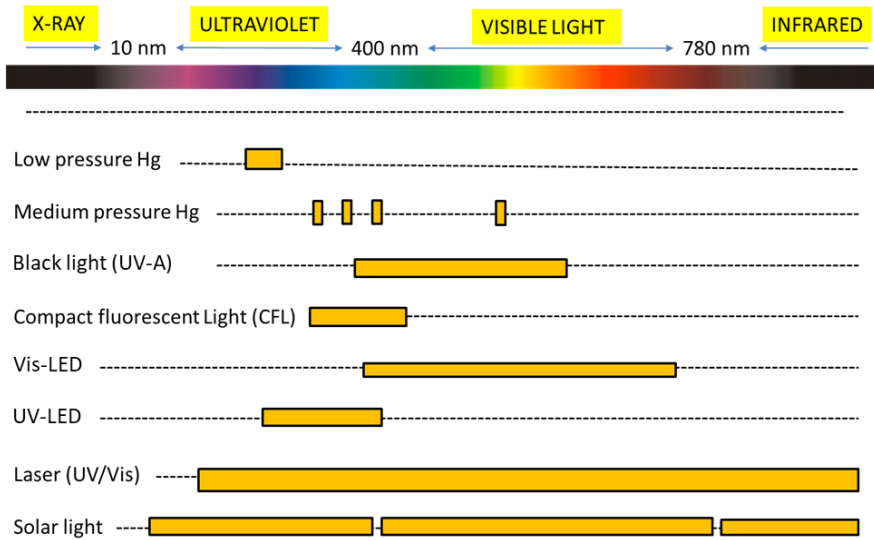


Figure 10: Emission range of some common light sources.

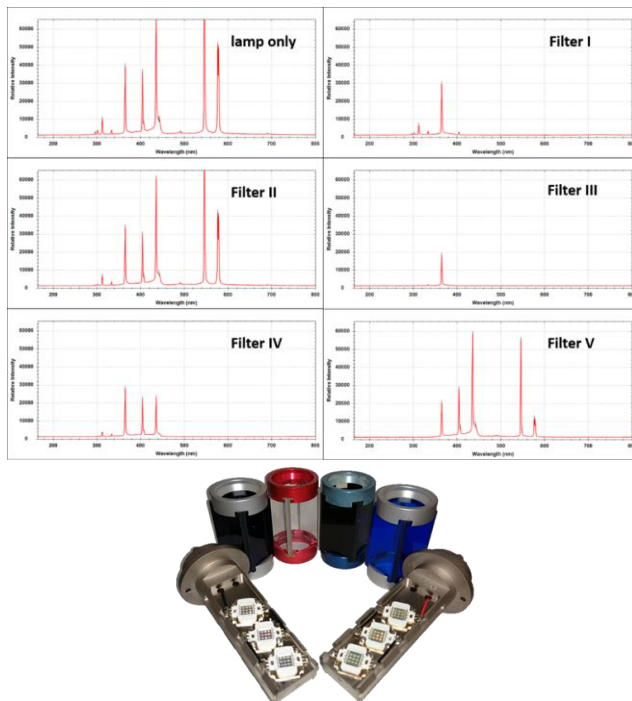


Figure 11: Emission spectra of a Vapourtec medium pressure mercury lamp with different filters (left); UV filters and LED lamps (right).

Although there are countless different possibilities for assembling a photoflow reactor, generally, these can be defined as one of two main approaches: either the light source can be embedded within the reactor (Figure 15A) or conversely the reactor can be placed adjacent to the radiation source (Figure 15B). In the former approach a fine polymer tube is coiled around the reactor housing (Figure 15A, section 5) and the lamp is generally surrounded by a filter (Figure 15A, section 3) for shielding of the undesired radiation. Between the filter and the reactor coil is generally placed a cooling chamber (Figure 15A, section 1) which enables control over the temperature of the reaction. The cooling can be performed by fluxing a cold liquid or a gas through the chamber. The second setup (adjacent alignment of the light and reactor) is often used with chip and microplate reactors where the flat surface of the reactor is easier to couple with an external light source. Nonetheless, this set-up has also been used with mesoreactors and implemented for industrial processes: one example is the PROPHIS plant^[83] (Figure 16) used by the German aerospace centre in Cologne which comprises of four parabolic troughs for collecting the solar light and obtaining the effect of 20 suns on the absorber tube and has a volume of 120 L.

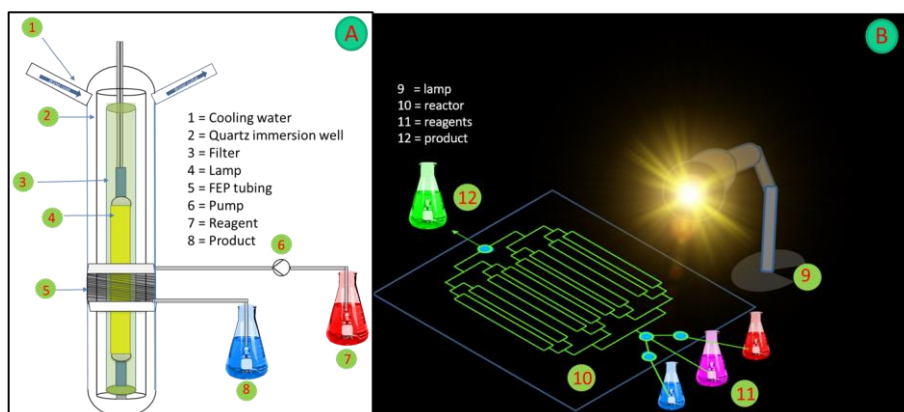


Figure 12: Two possible photoflow setups: the light source is embedded in the reactor (A), the reactor is placed adjacent to the lamp (B).

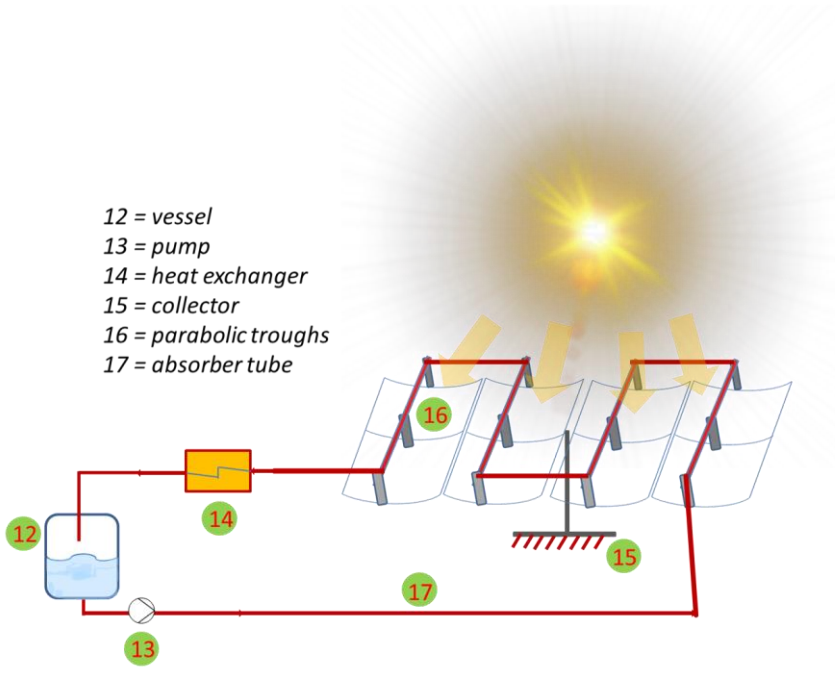


Figure 13: The Prophis plant allowing the use of solar light collectors.

1.4 References

- 1) Reizman, B. J.; Jensen, K. F. *Acc. Chem. Res.* **2016**, *49*, 1786–1796.
- 2) Chanda, A.; Daly, A. M.; Foley, D. A.; LaPack, M. A.; Mukherjee, S.; Orr, J. D.; Reid, G. L.; Thompson, D. R.; Ward, H. W. *Org. Process Res. Dev.* **2015**, *19*, 63–83.
- 3) Yue, J.; Schouten, J. C.; Nijhuis, T. A. *Ind. Eng. Chem. Res.* **2012**, *51*, 14583–14609
- 4) Fabry, D. C.; Sugiono, E.; Rueping, M. *React. Chem. Eng.* **2016**, *1*, 129–133.
- 5) Sans, V.; Cronin, L. *Chem. Soc. Rev.* **2016**, *45*, 2032–2043.
- 6) Manabe, Y.; Kitawaki, Y.; Nagasaki, M.; Fukase, K.; Matsubara, H.; Hino, Y.; Fukuyama, T.; Ryu, I. *Chem. Eur. J.* **2014**, *20*(40), 12750–12753.
- 7) Belluau, V.; Noeureuil, P.; Ratzke, E.; Skvortsov, A.; Gallagher, S.; Motti, C. A.; Oelgemöller, M. *Tetrahedron Lett.*, **2010**, *51*(36), 4738–4741.
- 8) Comer, E.; Organ, M. G. *A J. Am. Chem. Soc.*, **2005**, *127*, 8160–8167.
- 9) Joshua, P. B.; Emiko, K.; Yasuo, N.; Noriyuki, O.; Takeo, Y., *Chem.*, **2019**, *19*(1), 188–203.
- 10) Ian, R. B.; Michael, R. P. *Chim. Oggi – Chem. Today*, **2006**, *24*(3), 41–45.
- 11) Ana, A. F. A.; Thomas, W. J. *Flow Chem.*, **2017**, *7*(3), 94–95.
- 12) Andrijana, M.; Anita, Š.; Tomislav, G.; Bruno, Z.; Silvana, R. M. *RSC Adv.*, **2017**, *7*, 791–800.
- 13) Zhengya, D.; Claire, D.; Keiran, M. C.; Aniket, P. U.; Simon, K. *Materials*, **2020**, *13*, 344–369.
- 14) Milad, A.; Nicholas, C. B.; Klavs, F. J. *Chem. Commun.*, **2015**, *51*, 8916–8919.
- 15) Thomas, M.; Naomi, E. B. B.; Catriona, A. C.; Cameron, J. B.; Jan, S.; Alastair, J. F. *Org. Process Res. Dev.*, **2015**, *19*, 9, 1186–1202.
- 16) Ryan, L. H.; Jonathan, P. M.; Klavs, F. *Angew. Chem. Int. Ed.*, **2011**, *50*, 7502–7519.
- 17) Matthew, B. P.; Bartholomäus, P.; Kerry, G.; Peter, H. S. *Chem. Rev.*, **2017**, *117*, 18, 11796–11893.
- 18) Soleymani, A.; Yousefi, H.; Turunen, I. *Chem. Eng. Sci.*, **2008**, *63*, 5291–5297.
- 19) Ghanem, A.; Lemenand, T.; Della Valle, D.; Peerhossaini, H. *Chem. Eng. Res. Des.* **2014**, *92*, 205–228.
- 20) Nagaki, A.; Togai, M.; Suga, S.; Aoki, N.; Mae, K.; Yoshida, J. *J. Am. Chem. Soc.* **2005**, *127*, 11666–11675.
- 21) Soleymani, A.; Kolehmainen, E.; Turunen, I. *Chem. Eng.*, **2008**, *63*, 21,

5291–5297.

- 22) Mahmut, B. O.; Mustafa, M. A.; Kim, K. Y. *Micromachines*, **2018**, *9*, 5, 210–210.
- 23) Jensen, K. F.; Reizman, B. J.; Newman, S. G. *Lab Chip* **2014**, *14*, 3206–3212.
- 24) Bao, J.; Tranmer, G. K. *Chem. Commun.* **2015**, *51*, 3037–3044.
- 25) Munirathinam, R.; Huskens, J.; Verboom, W. *Adv. Synth. Catal.* **2015**, *357*, 1093–1123.
- 26) Frost, C. G.; Mutton, L. *Green Chem.* **2010**, *12*, 1687–1703.
- 27) Irfan, M.; Glasnov, T. N.; Kappe, C. O. *ChemSusChem* **2011**, *4*, 300–316.
- 28) Battilocchio, C.; Hawkins, J. M.; Ley, S. V. *Org. Lett.*, **2014**, *16*, 1060–1063.
- 29) Ötvös, S. B.; Mándity, I. M.; Fülöp, F. *J. Catal.*, **2012**, *295*, 179–185.
- 30) Ötvös, S. B.; Mándity, I. M.; Fülöp, F. *ChemSusChem*, **2012**, *5*, 266–269.
- 31) Massi, A.; Cavazzini, A.; Zoppo, L. D.; Pandoli, O.; Costa, V.; Pasti, L.; Giovannini, P. P. *Tetrahedron Lett.*, **2011**, *52*, 619–622.
- 32) Bortolini, O.; Caciolli, L.; Cavazzini, A.; Costa, V.; Greco, R.; Massi, A.; Pasti, L. *Green Chem.*, **2012**, *14*, 992–1000.
- 33) Bortolini, O.; Cavazzini, A.; Giovannini, P. P.; Greco, R.; Marchetti, N.; Massi, A.; Pasti, L. *Chem. Eur. J.* **2013**, *19*, 7802–7808.
- 34) Greco, R.; Caciolli, L.; Zaghi, A.; Pandoli, O.; Bortolini, O.; Cavazzini, A.; De Risi, C.; Massi, A. *React. Chem. Eng.*, **2016**, *1*, 183–193.
- 35) Ayats, C.; Henseler, A. H.; Pericàs, M. A. *ChemSusChem* **2012**, *5*, 320–325.
- 36) Irfan, M.; Petricci, E.; Glasnov, T. N.; Taddei, M.; Kappe, C. O. *Eur. J. Org. Chem.*, **2009**, 1327–1334.
- 37) Ouchi, T.; Battilocchio, C.; Hawkins, J. M.; Ley, S. V. *Org. Process Res. Dev.* **2014**, *18*, 11, 1560–1566.
- 38) HEL Group. FlowCAT overview. <http://www.helgroup.com/reactor-systems/hydrogenation-catalysis/flowcat/> (accessed 8-08-2020).
- 39) Saaby, S.; K. R. Knudsen, M. Ladlow, S. V. Ley, *Chem. Commun.* **2005**, 2909–2911.
- 40) Baxendale, I. R.; Deeley, J.; Jones, G. C. M.; Ley, S. V.; Saaby, S.; Tranmer, G. K. *Chem. Commun.* **2006**, 2566–2568.
- 41) Carter, C. F.; Lange, H.; Ley, S. V.; Baxendale, I. R.; Wittkamp, B.; Goode, J. G.; Gaunt, N. L. *Org. Process Res. Dev.*, **2010**, *14*, 393–404.
- 42) Mandity, I. M.; Martinek, T. A.; Darvas, F.; Fulop, F. *Tetrahedron Lett.* **2009**, *50*, 4372–4374.
- 43) Baxendale, I. R.; Ley, S.V. *Nature Rev. Drug Discovery*, **2002**, *1*, 573–586.

- 44) Booth, R.J.; Hodges, J.C. *J. Am. Chem. Soc.*, **1997**, *119*, 4882–4886.
- 45) Monenschein, H.; Wittenberg, R.; Kirschning, A. *Angew. Chem. Int. Ed.*, **2001**, *40*, 650–679.
- 46) Ley, S. V.; Baxendale, I. R.; Bream, R. N.; Jackson, P. S.; Leach, A. G.; Longbottom, D. A.; Nesi, M.; Scott, J. S.; Storer, I.; Taylor, S. J. *J. Chem. Soc., Perkin Trans. 1*, **2000**, 3815–4195.
- 47) Kaldor, S. W.; Siegel, M. G.; Fritz, J. E.; Dressman, B. A.; Hahn, P. J. *Tetrahedron Lett.* **1996**, *37*, 7193–7196.
- 48) Cannizzaro, S.; Fabris, G.; Ber, D. *Chem. Ges.*, **1886**, *19*, 2260–2265.
- 49) Ciamician, G.; Rendiconti, R. *Accad. Naz. Lincei*, **1886**, *25*, 22–23.
- 50) Ciamician, G. *Gazz. Chim. Ital.*, **1886**, *16*, 111–112.
- 51) Ciamician, G.; Silber, P. *Ber.* **1908**, *41*, 1928–1929.
- 52) Buchi, G. M.; Goldman, I. M. *J. Am. Chem. Soc.*, **1957**, *79*, 4741–4748.
- 53) Cookson, R. C.; Crundwell, E.; Hudac, J. *Chem. Ind.*, **1958**, 1003–1005.
- 54) R. G. Norrish and M. E. S. Appleyard, *J. Chem. Soc.*, **1934**, 874–880.
- 55) Ciamician and P. Silber. *Ber. dtsh chem. Ges.*, **1908**, *41*, 1071, 1928–1929.
- 56) Zimmerman, H. E.; Schuster, D. I. *J. Am. Chem. Soc.*, **1961**, *83*, 4486–4487
- 57) Introduction to Organic Photochemistry Von J. D. Coyle; Chichester, New York, Brisbane, Toronto, Singapur, John Wiley & Sons, **1986**.
- 58) Corey, E. J.; Nozoe, S. *J. Am. Chem. Soc.*, **1965**, *87*(24), 5733–5735.
- 59) Anastas, P. T.; Kirchhoff, M. M. *Acc. Chem. Res.*, **2002**, *35*(9), 686–694.
- 60) Anastas, P. T.; Eghbali, N. *Chem. Soc. Rev.*, **2010**, *39*, 301–312.
- 61) O. Isler and R. Rugg, Patent US2798095A, **1957**.
- 62) Bella, E. P. Patent US817991A **1959**.
- 63) Monnerie, N.; Ortner, J. *J. Sol. Energy Eng.*, **2001**, *123*, *2*, 171–174.
- 64) DeRosa, M. C.; Crutchley, R. J. *Coord. Chem. Rev.*, **2002**, *233–234*, 351–371.
- 65) Turconi, T. J.; Griolet, F.; Guevel, R.; Oddon, G.; Villa, R.; Geatti, A.; Hvala, M.; Rossen, K.; Göller, R.; Burgard, A. *Org. Process Res. Dev.* **2014**, *18*, 417–422.
- 66) Karine, L.; Michael, O.; Tristan, A.; Odile, D.C.; Laurent, E. P. *Chem. Eng. Process.*, **2016**, *104*, 120–132.
- 67) Zepp, R. G.; Gumz, M.; Miller, W. L.; Gao, H. *J. Phys. Chem. A.*, **1998**, *102*, 5716–5723.
- 68) Knowles, J. P.; Elliott, L. D.; Booker-Milburn, K. I. *Beilstein J. Org. Chem.*, **2012**, *8*, 2025–2052.

- 69) Garlets, Z. J.; Nguyen, J. D.; Stephenson, C. R. *J. Isr. Chem.*, **2014**, *54*(4), 351–360.
- 70) Schuster, E. M.; Wipf, P. *Isr. J. Chem.*, **2014**, *54*(4), 361–370.
- 71) Plutschack, M. B.; Correia, C. A.; Seeberger, P. H.; Gilmore, K. *Organic Photoredox Chemistry in Flow*; Springer Verlag GmbH: Heidelberg, Germany, **2015**.
- 72) Su, Y.; Straathof, N. J. W.; Hessel, V.; Noël, T. *Chem. Eur. J.*, **2014**, *20*, 10562–10589.
- 73) Studer, A.; Curran, D. P. *Angew. Chem., Int. Ed.*, **2016**, *55*, 58–102.
- 74) Cismesia, M. A.; Yoon, T. P. *Chem. Sci.*, **2015**, *6*, 10, 5426–5434.
- 75) Majek, M.; Filace, F.; Wangelin, A. J. *Beilstein J. Org. Chem.*, **2014**, *10*, 981–989.
- 76) Karkas, M. D.; Matsuura, B. S.; Stephenson, C. R. *J. Science*, **2015**, *349*, 6254, 1285–1286.
- 77) Armido S.; Dennis, P. C. *Angew. Chem., Int. Ed.*, **2016**, *55*, 58–102.
- 78) Aillet, T.; Loubiere, K.; Dechy-Cabaret, O.; Prat, L. *J. Chem. React. Eng.*, **2014**, *12*, 257–269.
- 79) Dario, C.; Cecilia, B.; Natan, J. W. S.; Volker, H.; Timothy, N. *Chem. Rev.*, **2016**, *116*, 17, 10276–10341.
- 80) Maurya, R. A.; Park, C. P.; Kim, D. P. *Beilstein J. Org. Chem.* **2011**, *7*, 1158–1163.
- 81) Cambie, D.; Bottecchia, C.; Straathof, N. J. W.; Hessel, V.; Noel, T. *Chem. Rev.* **2016**, *116*, 10276–10341.
- 82) Hook, B. D. A.; Dohle, W.; Hirst, P. R.; Pickworth, M.; Berry, M. B.; Booker-Milburn, K. I. *J. Org. Chem.* **2005**, *70*, 7558–7564.
- 83) Christian, J.; Karl, H. F.; Jürgen, O. *Photochem. Photobiol. Sci.*, **2005**, *4*, 409–411.

2. Chapter 2: Photochemical Flow Synthesis of 3-Hydroxyazetidines

2.1 Azetidines

Azetidines represent an interesting class of heterocycle possessing valuable chemical and biological features. First reported in 1888,^[1] the related azetidin-2-ones **2-1** have received particular attention due to their structural relationship to β -lactams, the core of several important antibiotic compounds, e.g., penicillin, cephalosporin and monobactam (Figure 1, compounds **2-4/2-7**).^[2-17] Azetidinones (Figure 1, **2-2**) are less prevalent in nature but they have received a growing interest, as chemical precursor of other natural compounds such as ethylideneazetidin-2-carboxylic acid (Figure 1, **2-2b**) which is related to the tripeptide antibiotic polyoxine (Figure 1, **122c**). The hydrate form of the azetidin-2-one **2-3**, namely 3,3-dihydroxyazetidine (Figure 1, **2-3**) has also received particular interest due to its behaviour as a promoter of growing factors and as it has been linked to the growth of *bifidusbacterium*.^[18]

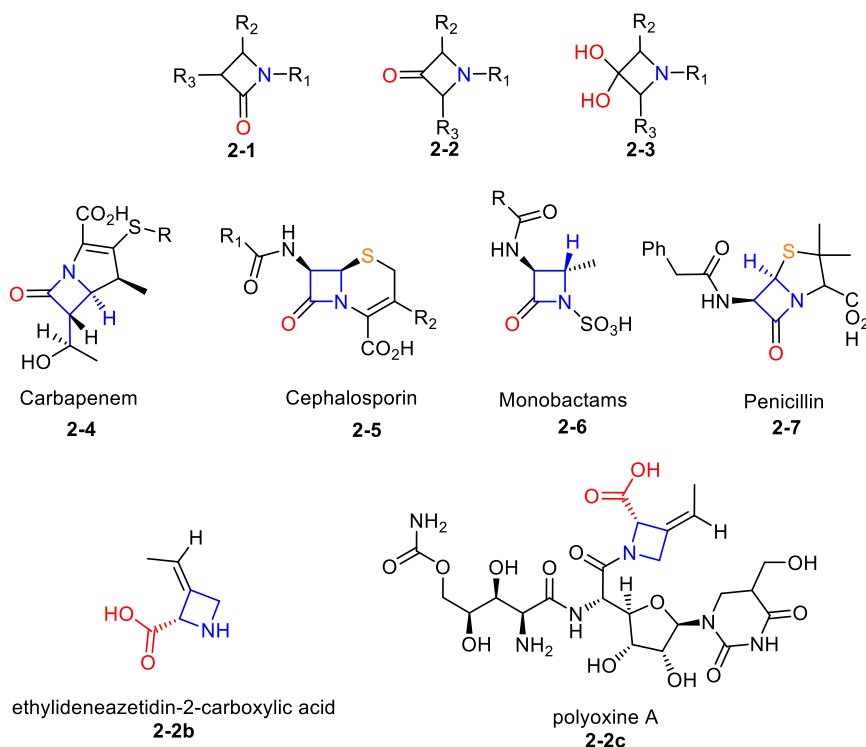


Figure1: Examples of azetidine and azetidinone structures.

The biological activity of the azetidine ring derivatives was established in 1956 through studies on the azetidine-3-carboxylic (Figure 2, 2-8) acid which turned out to be a powerful gametocide, leading to an increase in the general interest of this structure.^[19-21] Subsequently the valuable characteristics of this structure have been found in several other 3-substituted azetidines showing a broad range of biological activity (Figure 2). Interestingly, 3-substituted azetidines have also found value in the area of material chemistry as demonstrated by TNAZ (1,3,3-(trinitroazetidine, Figure 2, 2-16) which has been used as propellant and explosive.^[28-32]

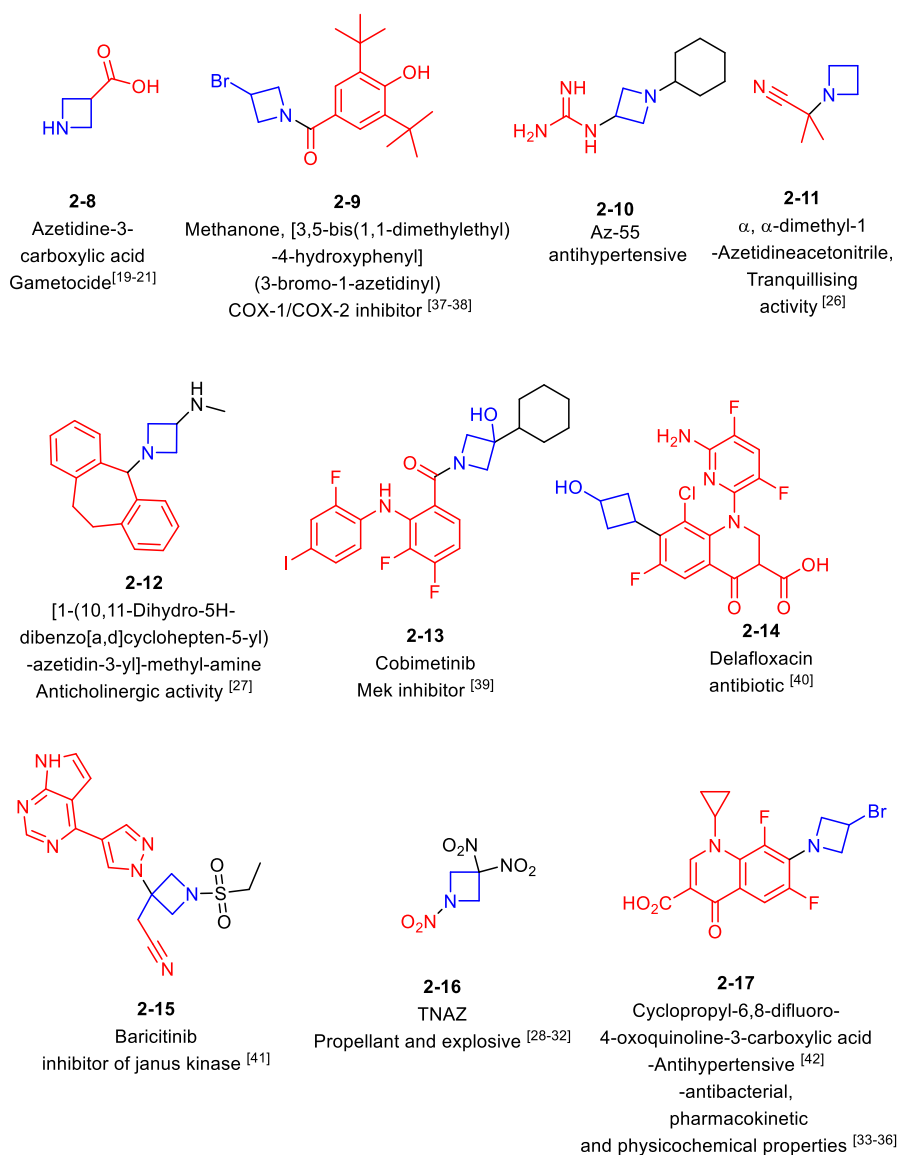


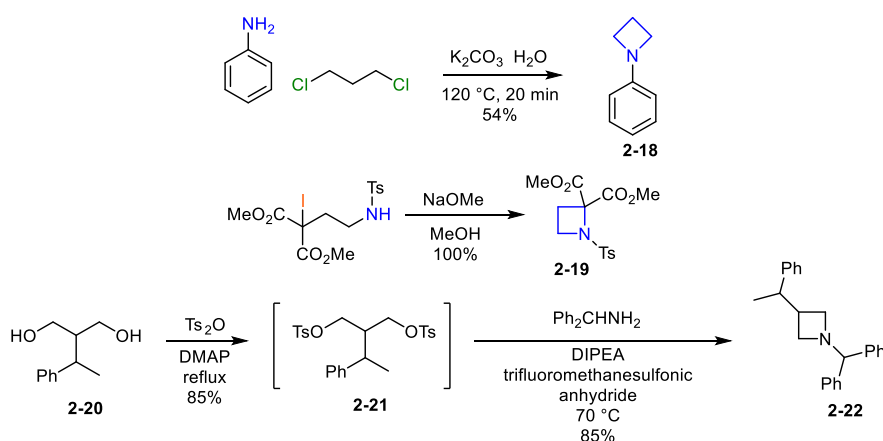
Figure 2: Some application of the azetidinic moiety.

2.1.1 Literature survey of the synthesis of azetidine rings

2.1.1.1 Nucleophilic substitution strategy

The most common synthetic approach to the azetidine ring is via nucleophilic attack by the nitrogen creating the ring (Scheme 1, 2-18).^[43] Normally, a leaving group such as a bromine

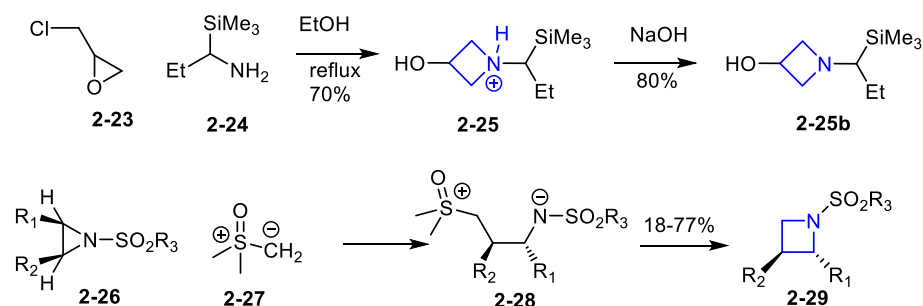
or chlorine is used although iodine often gives better results being a better leaving group (Scheme 1, 2-19).^[44] Additionally the leaving group can be made *in situ* often from an alcohol by conversion to the corresponding tosylate (i.e. 2-21) or mesylate (Scheme 1, 2-22).^[45]



Scheme 1: Synthesis of azetidine ring through nucleophilic substitution.

2.1.1.2 Ring expansion strategy

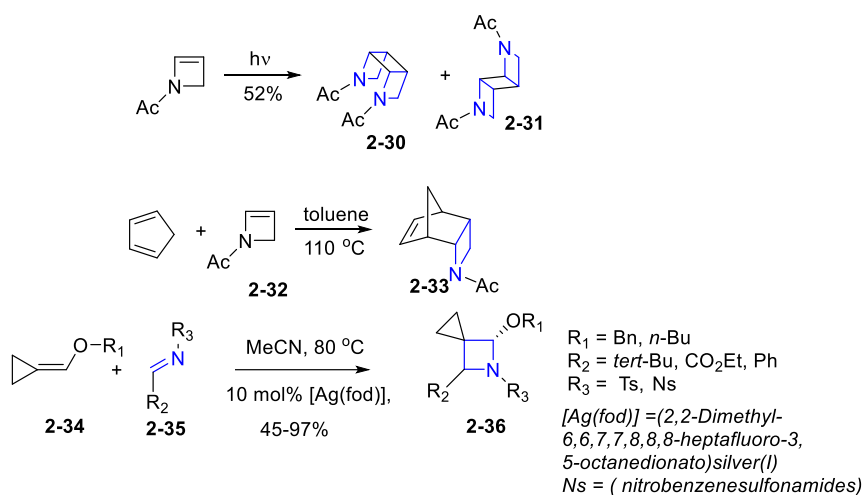
Opening of epoxides is a valuable synthetic method on route to 3-azetidinols and its important derivatives the 3-azetidinone through subsequent oxidation. The protocol as developed by Gartner^[46] uses primary amines in combination with epichlorohydrin (Scheme 2, 2-23), to form *N*-substituted 3-azetidinols, whereas bulky amines react less readily it was observed that the use of silyl functionalised amines (i.e. 2-24) increases the reactivity (2-25b). Aziridine ring opening has also been used, for example by Nadir^[47-52] who reported the use of dimethyloxosulfonium methyide (2-27) to achieve a stereospecific reaction where the *cis* or *trans* aziridine (2-26) leads to the oppositely configured *anti* or *syn* azetidine (2-29).



Scheme 2: azetidine ring formation through ring expansion.

2.1.1.3 Cycloaddition reaction strategy

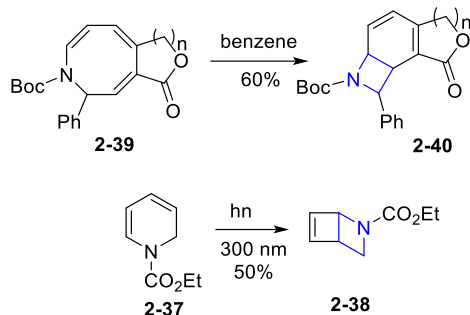
Although cycloaddition reactions are widespread as routes for the synthesis of β -lactams (which can be used as precursor for azetidines), only a few examples involving the direct synthesis of the azetidine ring by cycloaddition have been developed.^[53-56] The 1,2-dihydroazetidine system has been used in a Diels Alder reaction with substituted cyclopentadienes yielding azetidine products in good yields and in photodimerization reactions leading to an interesting mixture of diazotricyclooctane (**Scheme 3**; **2-31**, **2-32**).^[57] Cycloaddition between an imine derivative **2-35** and alkoxyethylene cyclopropane **2-34** turned out to be a very valuable method of preparing spiro-cyclopropane azetidine derivatives **2-36** in excellent yield (**Scheme 3**).



Scheme 3: Azetidine formation through cycloaddition reactions.

2.1.1.4 Ring contraction strategy

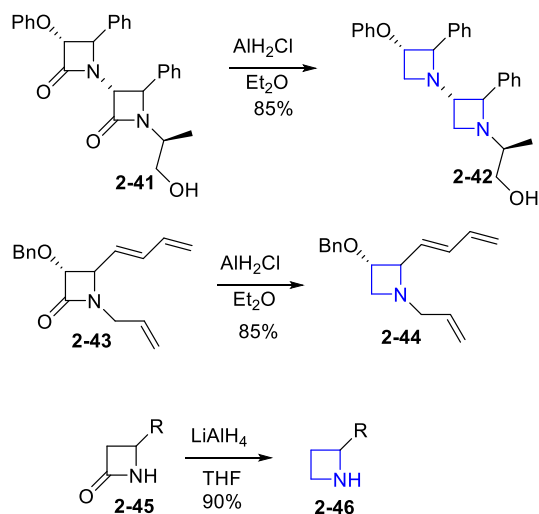
Ring contraction has allowed particular azetidines to be made, for example, ring fused structures have been prepared using electrocyclic 6- π rearrangement of cyclooctatrene systems (**Scheme 4**, **2-39**).^[58] Similarly photo-electrocyclic reaction of dihydropyridine rings affords an azobicyclo ring in good yield (**Scheme 4**, **2-38**).^[59-61]



Scheme 4: Azetidine formation through ring contraction processes.

2.1.1.5 Reduction of azetidinone strategy

2-Azetidinones are largely used in the synthesis of azetidines due to their readiness to undergo reduction. Diborane,^[62] LiAlH_4 ^[62] and Raney nickel^[53] have all been widely used as reducing agents providing the desired products in high yields. Further examples of DIBAL-H and chloroaluminium hydrides (AlH_2Cl or AlHCl_2) have also been reported by Ojima and Alcoide^[63-65] (Scheme 5, **2-42**, **2-44**, **2-46**).

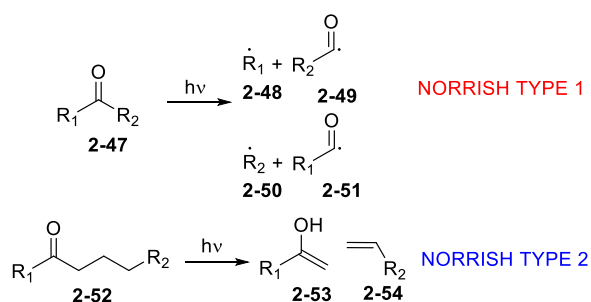


Scheme 5: Azetidine formations via reduction of azetidinones.

2.2 The Norrish reaction

Between 1936 and 1938 Ronald George Norrish published a series of seminal works^[66-69] in which 2 very important photochemical reactions of aldehydes and ketones were presented.

In the first of these reactions a carbonyl compound after a photo excitement was fragmented to an acyl and alkyl radical pair; this reaction is normally observed in the gas phase and is called a Norrish type 1 reaction (Scheme 6). Although it has been intensively studied, so far it has not found major synthetic application. In the second reported transformation a carbonyl compound was fragmented under photochemical activation generating an enol and an olefin. This second process became famous gaining the name a Norrish type 2 reaction (Scheme 6).



Scheme 6: Examples of Norrish type transformations.

These Norrish processes each involve the photon excitation of an electron of the carbonyl functionality with promotion of an electron from a ground state to an excited one. Two distinct transitions are possible a $\pi \rightarrow \pi^*(S_g \rightarrow S_2)$ and $n \rightarrow \pi^*(S_g \rightarrow S_1)$ (Figure 3).

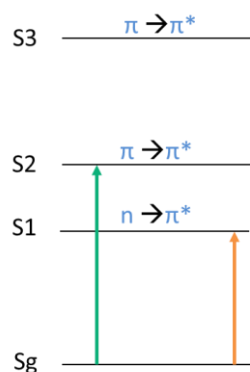
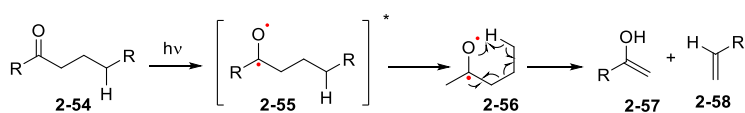


Figure 3: S_1 and S_2 excited states. (S_g = ground state, S_n = excited states)

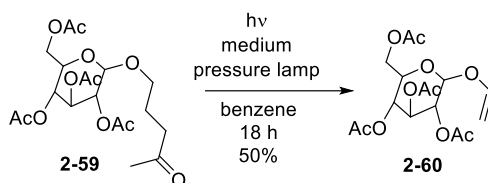
The carbonyl group has two electrons in its π bonding orbital and two pairs of electrons in non-bonding orbitals on the oxygen. Under photo-excitation an electron can be promoted to

the empty π^* -orbital leading to an excited state. Depending on which orbital the electron is excited from we can distinguish two potential transitions. If the promoted electron comes from a non-bonding orbital the transition and resulting excited state have the notation $n-\pi^*$ whereas if it involves an electron from the π bonding orbital its definition is a $\pi-\pi^*$ transition.^[70] These two excited states give rise to different chemical behaviour; in the $n-\pi^*$ the electron which remain in the π orbital provides the oxygen with free radical character, this is not true for the $\pi-\pi^*$ excited state. The free radical character of the oxygen in the $n-\pi^*$ state is strictly related with the Norrish type 2 transformation which is characterized by an intramolecular hydrogen abstraction (Scheme 7). If a γ -hydrogen is available a subsequent 1,5-hydrogen transfer (by oxygen abstraction) can occur generating a bi-radical intermediate which can subsequently fragment leading to an enol and an olefin.



Scheme 7: Norrish type 2 reaction.

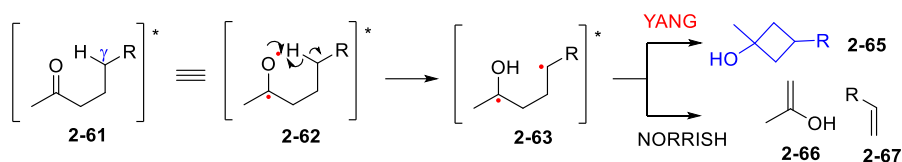
The discovery of this transformation has turned out to have several synthetic applications such as the elimination of protecting groups from carbohydrate systems, synthesis of steroid derivatives and the preparation of isomerically pure alkanes (Scheme 8).^[71-74]



Scheme 8: Elimination of protecting group from a carbohydrate system.

2.3 The Yang reaction

Once the carbonyl oxygen has abstracted a hydrogen, instead of undergoing a fragmentation of the diradical intermediate into an enol and an olefin, it is possible to have a recombination of the radicals resulting in the formation of a new cyclic structure (Scheme 9; 2-65).



Scheme 9: The Yang Reaction.

This transformation, first reported by Yang in 1958,^[75] adopted the name of its discoverer to become the Norrish-Yang reaction, although it is often shorted to simple the Yang reaction. A key feature of the Yang reaction (and in general of all Norrish type 2 transformations) is that they involve a six membered transition state implying a strong preference for the γ -hydrogen activation;^[76] this has been confirmed by Ihmels and Schaffer studying the geometric parameters of the hydrogen abstraction.^[77] According to their investigation, in order to obtain an optimal abstraction the following assembly must be met (Figure 4).

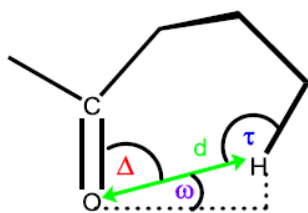
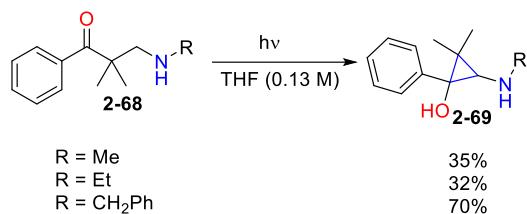


Figure 4: Geometrical parameters involved in the H-abstraction.

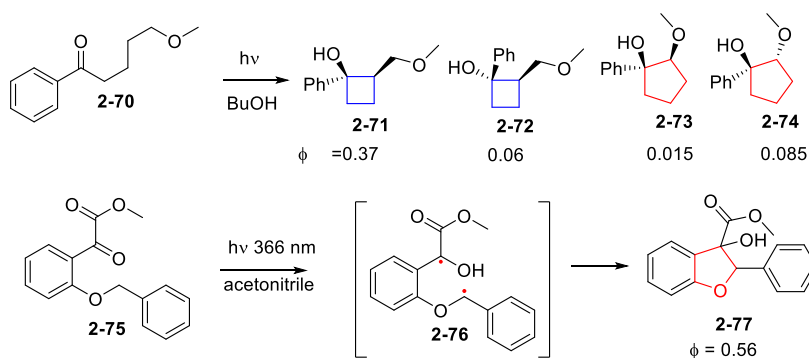
Parameters: d , the distance between the carbonyl oxygen and the hydrogen which should be close to the sum of the van der Waals radii of oxygen and hydrogen (2.72 Å). Δ , the angle between CO and the H should be between 90° and 120° . τ , the angle between the CH and O should have an optimal value of 180° . ω , the angle by which the hydrogen lies outside the plane of the carbonyl group which has an ideal value of 0° .

Despite the inherent preference for γ -hydrogen abstraction, if a hydrogen atom is not available a larger or smaller sized transition state can be adopted leading to different cyclic products. An example of β -abstraction leading to interesting cyclopropane derivatives has previously been reported (Scheme 10).^[78]



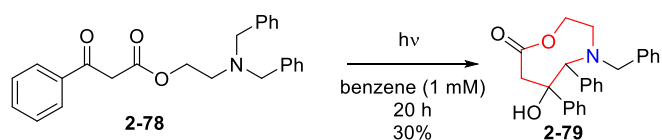
Scheme 10: Example of β -abstraction to form cyclopropanes.

Wagner showed how in the case of δ -alcoxy ketone **2-70** the δ - and γ -abstraction compete leading to the formation of a mixture of cyclic products **2-71** to **2-74** (Scheme 11).^[79] In addition, several cases have been reported in which the γ -hydrogen is not available and thus a δ -H is abstracted leading to the cyclopentanol **2-77** (Scheme 11).



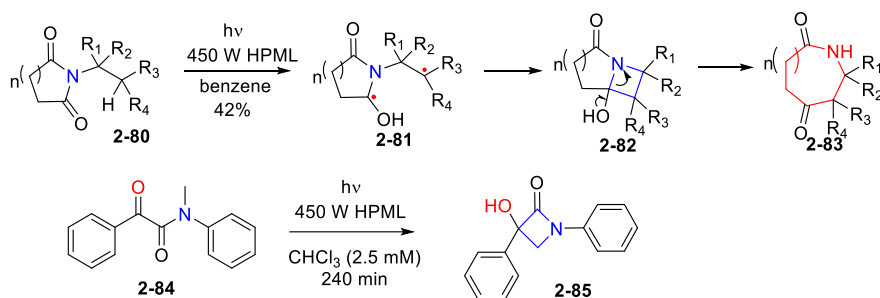
Scheme 11: δ -hydrogen abstraction leading to cyclic.

Further, long distance abstractions are possible. Hasegawa *et al.* has reported the formation of an eight membered lactone ring from 2-(dibenzylamino)ethyl-3-oxo-3-phenylpropanoate (**2-78**, Scheme 12).^[80]



Scheme 12: Cyclization through long distance abstraction.

To increase the synthetic potential of this transformation, a heteroatom can be inserted between the carbonyl and the abstraction site; this can lead to the formation of interesting heterocyclic rings. Succinamide derivatives, for example, form lactam structures with ring enlargement occurring through opening of the azetidine ring initially formed by the Yang reaction^[81] or gaining access to 3,2-hydroxyazetidinone (**2-85**) by positioning a second adjacent carbonyl group, substrate **2-84**^[82] (Scheme 13).



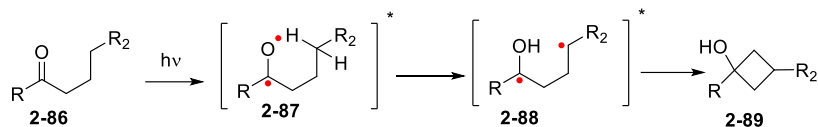
HPML = High-Pressure Mercury Lamp

Scheme 13: Enriched heterocyclic rings via the Yang reaction.

2.4 Result and discussion

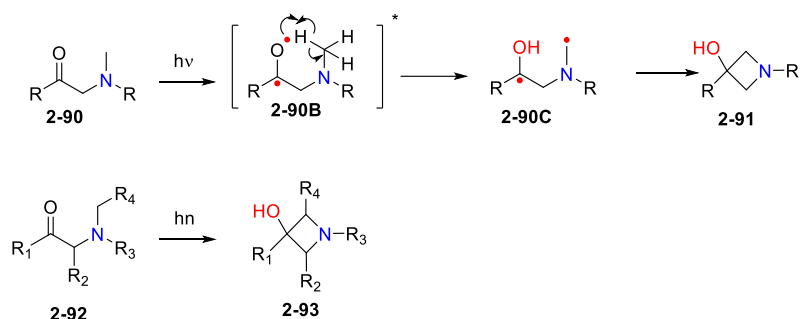
2.4.1 Retrosynthesis

In the Norrish-Yang reaction a carbonyl derivative, under photo-irradiation, is subjected to a promotion from the ground state S_0 to an excited state (normally S_1) by an $n \rightarrow \pi^*$ transition, in which a $2p_y$ non-bonding electron on the oxygen is promoted to the antibonding π^* -orbital. The excited singlet state can then transition to the triplet state through ISC (intersystem crossing). The photoexcitation leads to a di-radical compound (Scheme 13) where the oxygen achieves free radical character. If a suitably positioned hydrogen atom is available the oxygen can abstract it forming a second di-radical structure which can further react intramolecularly forming a cyclohydroxyl derivate (**2-89**, Scheme 14). Normally the abstraction and the cyclization proceed through an open chair transitional state (Figure 4) thus the abstraction involves the γ -proton (favoured by steric factors) leading to a hydroxyl cyclopropane; however if no γ -hydrogen is available the abstraction and succeeding cyclization may give a 3, 5 or even larger cyclic derivative. It is easy to see how the presence of an atom different from the C between the carbonyl and the site of abstraction would lead to a four-member heterocycle.



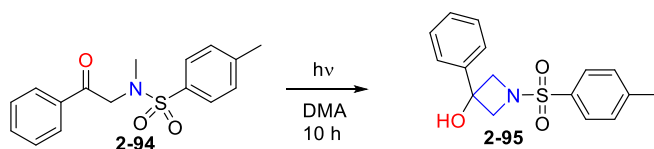
Scheme 14: General cyclization sequence affording cyclobutanols.

The 3-hydroxy azetidine ring **2-91** can be derived from the same reaction using as the starting material a *N*-methyl- β -aminoketone **2-90** in one pot sequence. Indeed, more substituted azetidines can also be obtained by appropriate decoration of the starting ketone (*Scheme 15*).



Scheme 15: Yang reaction affording the 3-hydroxyazetidine moiety.

Among the examples reported in the literature is work presented by Ishida and co-workers^[83] who use a photochemical method to build up an azetidinic intermediate which acts as a CO₂ capture system. In their work the Japanese group reported the conversion of a series of α -amino aryl ketones to their corresponding azetidine ring structures (*Scheme 16*). The reactions were performed using solar light in a Pyrex flask using DMA (*N,N*-dimethylacetamide) as the solvent. Very high conversion (>90%) was claimed by the author but on a very small scale (30 mg), we decided to adopt the same substrate to investigate a photoflow approach.



Scheme 16: Specific substrate used by Ishida.

Although the Yang reaction has been extensively studied over the years the true synthetic value of the transformation has not been fully exploited due to the photochemical processing conditions required (long reaction times, very dilute reaction conditions being required in batch). We embarked on a study of the Yang reaction under flow condition in order to evaluate the impact of a flow set up on this transformation. Indeed, flow chemistry due to its intrinsic characteristics (see introduction) allows an enhancement of many photochemical processes. In this project we aimed to leverage the synthetic potential of the Yang reaction addressing some of the common disadvantages of batch photochemistry (longer reaction time, lower selectivity and critical scalability).

The sulfonamide **2-94** was used as representative substrate as it had previously been shown to be a viable starting material albeit on a very small scale (30 mg). Our aim was to build a collection of derivatives thus studying the effect of structural changes on the reactivity of the general formula of **2-94**.

2.4.2 Description of the flow set-up

A Vapourtec E series system with a UV-150 photochemical reactor equipped with a medium pressure mercury lamp (maximum of emission at 365 nm) and 3 low pressure mercury lamps (peak emissions at 254, 310 and 370 nm) was used. The power of the lamp can be controlled from 75-150 W for the medium pressure lamp while the 3 low pressure lamps have an input power of 9 W and are between 30-40% efficient providing a fixed power output of 3 W.

The flow reactor consists of a 10 mL FEP (fluorinated ethylene propylene) coiled tube housed in the reactor body which allows the connection with the rest of the E-system and the lamp. Moreover, a probe in the reactor body permits the monitoring of temperature and a connection with an external cooling system gas (cylinder with dry ice coolant) is established as well. The temperature tolerated by the reactor is between -5 and 80 °C.

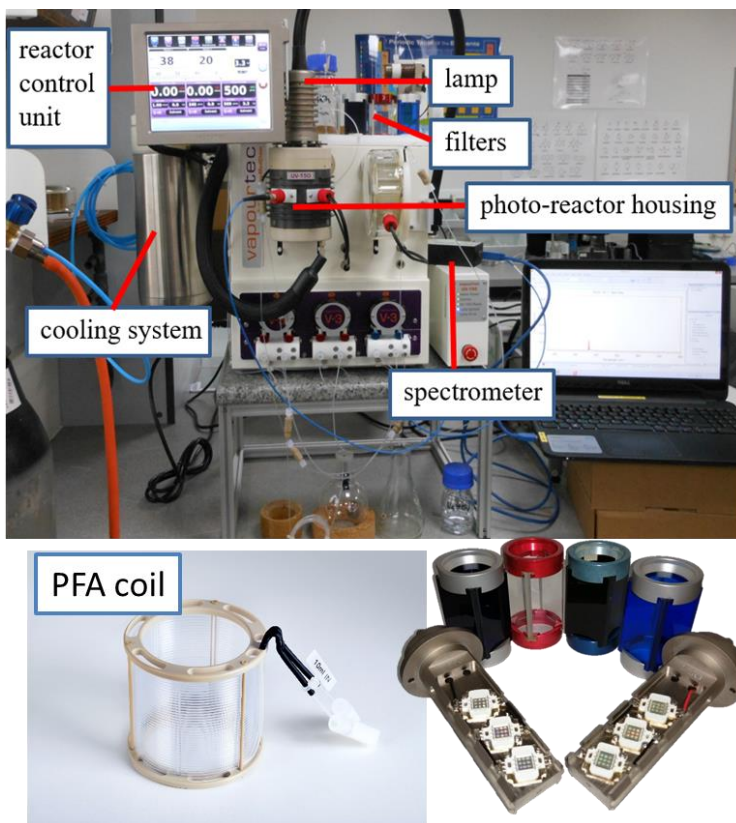
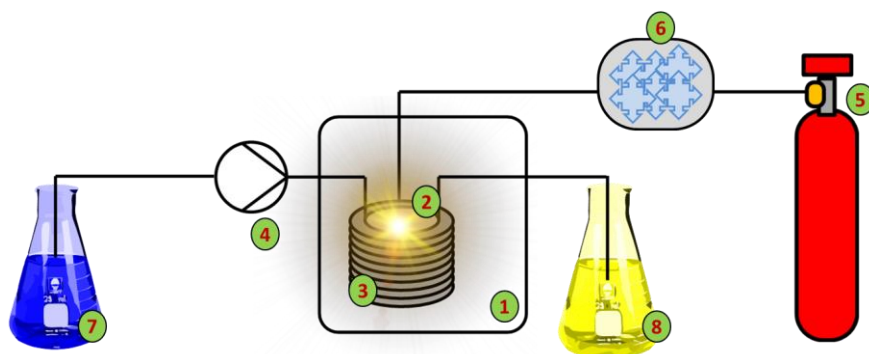


Figure 5: Equipment set-up used in the study.



- | | |
|--------------|-----------------------|
| 1 = Reactor | 5 = Cooling system |
| 2 = Lamp | 6 = Dry ice |
| 3 = Fep coil | 7 = Starting material |
| 4 = Pump | 8 = Reaction product |

Figure 6: Schematic of the flow reactor set-up.

2.4.3 Solvent system

The choice of the solvent is a critical aspect of any photochemical reaction as it can strongly influence the experiment. There are several requirements that a solvent has to meet in order to be used: 1) it must not react with the reagent; 2) it has to dissolve the starting material; 3) it has to be transparent toward the wavelength needed by the compound (the solvent has to absorb in a different range to the compound). The solvent can act as a sensitizer absorbing the radiation and then releasing it to the substrate promoting the desired transition. Additionally, whereas in batch the precipitation of the product is normally welcome, in a flow system it is undesirable as it can obstruct the tube or deposit on the surface of the reactor which might lead to its breakage (blockage) or to a local overheating resulting in melting of the tubing/chip.

Another important factor to bear in mind when choosing the solvent is the effect that it can have on the excited state, particular the polarity of the solvent which can affect the relative energies of the $n \rightarrow \pi^*$ and $\pi \rightarrow \pi^*$ states of ketone leading to a mixing of the $n \rightarrow \pi^*$ triplets and $\pi \rightarrow \pi^*$ triplets. In general, the unreactive $\pi \rightarrow \pi^*$ triplet states are more stabilised by high dielectric and hydrogen bonding solvents. Zepp and co-workers^[84] studied the effect of the solvent on aromatic ketones finding a substantial increase in the lifetime of

the triplet state when changing the solvent from a hydrocarbon to water. This was found to be directly related to the efficiency of the hydrogen abstraction by the oxygen.

Among the various solvents available, the solubility of the reagents narrows the number of possibilities. Water and common alcohols such as methanol, ethanol or *i*PrOH, are normally used in photochemistry due to their low absorption cut-off. Another important factor which has to be considered in the selection of a solvent is the scaling up of the reaction: whereas at lab scale the kind of solvent normally does not represent a concern this is not true when it comes to increasing the quantities of reagent, especially in industrial settings. Hydrocarbon solvents (i.e. pentane, hexane and toluene), or chlorinated (i.e. chloroform, DCM, 1,2-dichlorobenzene and CCl₄) are normally avoided both for environmental and safety reasons.

A good compromise between solubility, absorption cut-off, simplicity of work-up and considerations of safety for scale up of these transformations can be realised using solvents such as acetone, acetonitrile and THF. These solvents exhibit reasonable cut-off (330, 190 and 245 nm respectively) and are compatible with the wavelengths normally involved in carbonyl photo-transformations.

2.4.4 Lamps

Many light sources have been used to perform Yang reactions, from standard mercury lamps^[85] to the use of laser^[86] or excimer lamps^[87]. In our case the available lamps were a medium pressure mercury lamp and 3 low pressure mercury lamps. The medium pressure lamp has an emission spectra (Figure 7) which exhibits a broad range of wavelengths, from 220-600 nm, while for the others the peaks are more localized (Figure 7, B). In addition, by using filters it is possible to partially select the radiation emitted by the medium pressure lamp.

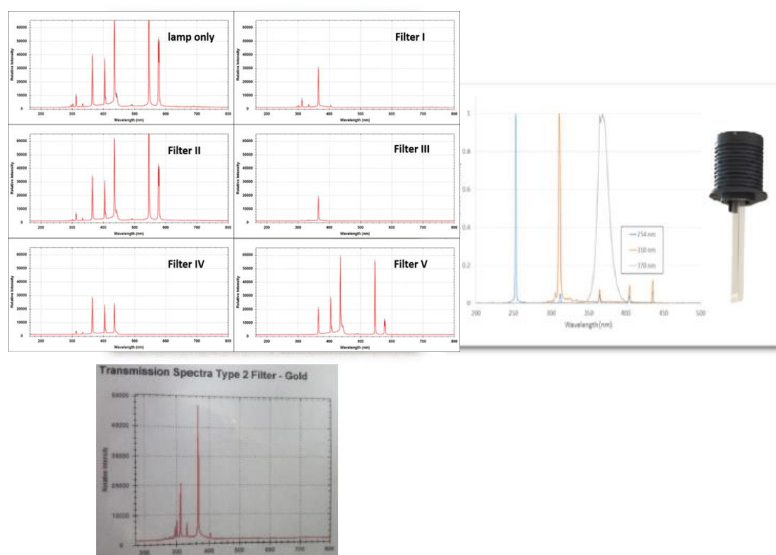


Figure 7: Medium pressure lamp emission spectra with different filters (A), emission spectra of a low-pressure lamp (B), emission with filter used (C).

2.4.5 Light sources screening

As an indication for the subsequent screening of the light sources, the absorption spectra for the starting material **2-94** was recorded and showed two different absorption bands;^[88-91] a strong band around 250 nm pertaining to the $\pi \rightarrow \pi^*$ transition and a weaker absorbance in the range of 280-320 nm relating to the synthetically desirable $n \rightarrow \pi^*$ propagation, which would result in the eventual cyclisation reaction (Figure 8).

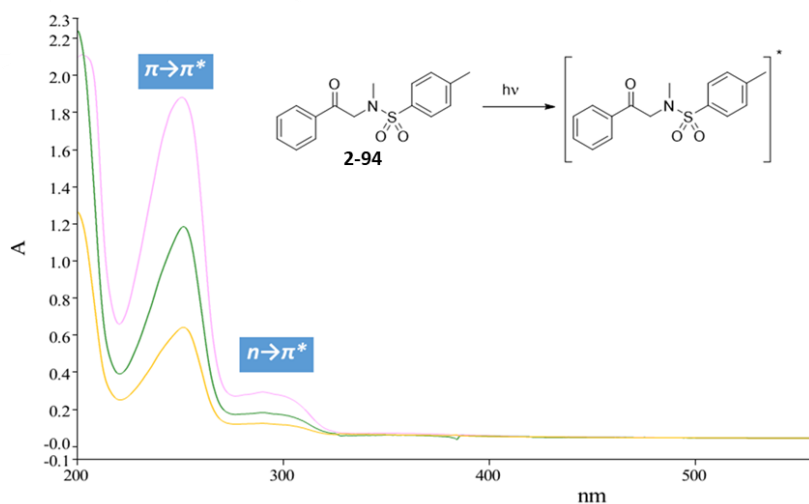


Figure 8: UV spectra of substrate **1-115**. Recorded in MeCN. Yellow (0.05 mM), green (0.1 mM) and pink (0.2 mM).

To perform the flow reaction screening, we utilised a commercially available Vapourtec UV-150 system based upon the E-series peristaltic delivery unit.^[92] A 0.15 M acetonitrile (solvent wavelength cut-off of 190 nm) stock solution of substrate **2-94** was passed at a specified flow rate into a 10 mL photoflow coil reactor and irradiated using a low pressure mercury lamp (150 W; 100% of the lamp power) fitted with a filter ('Gold' filter with transmission 415-250 nm).

2.4.6 First approach

Our first task was to reproduce the original batch process in flow using a long exposure. Substrate **2-94** was tested using different flow rates thus subjecting the material to different exposure times. After an exposure of 7 h the substrate showed high levels of decomposition leading to less than 20% conversion to the desired product. Lower exposure times (achieved using higher flow rates) results in a progressive reduction of the decomposition. Encouragingly, at a flow rate of 1 mL/min (10 min residence time), 90% conversion and a 75% isolated yield following chromatographic purification was achieved. It should be noted that this specific flow rate represented an optimal productivity balancing the consumption of starting material and conversion against the occurrence of several by-products generated

during extended irradiation (decomposition). In addition, it was found to be easier to purify samples comprising mainly residual starting material from incomplete conversion rather than driving the reaction to completion but subsequently having to separate the product from a complex mixture of multiple minor by-products. Indeed, at larger scales purification could be readily achieved by simple crystallisation of the incomplete reactions. Once the flow rate was optimised a range of solvents was then assessed evaluating them for solubility, absorption cut-off, impact on conversion and isolated yield. The solvents DMF, MeCN, THF and MeOH were all comparable, providing essentially equivalent results (~75% isolated yield). Acetone, although effective, gave a lower conversion (60%), which may be indicative of its absorption cut off of 330 nm and hence, competitive absorption. The chlorinated solvents CHCl_3 and DCM indicated some potential solubility issues and were therefore directly discounted. Ultimately, acetonitrile was selected as the primary solvent for convenience of evaporation (discounting DMF) and avoidance of potential radical side reactions, such as proton abstraction (THF and MeOH).

Next, to evaluate the impact of the transmission window the reactor filter was changed to one with a narrower band ('Blue' filter transmission 310-400 nm) which removes most of the irradiation overlapping with the indicated $n \rightarrow \pi^*$ transition. As anticipated, the detected conversion (1 mL/min; 10 min residence time) dropped dramatically to only 10%, thereby confirming our premise and confirming the preferential filter selection ('Gold' transmission 415-250 nm, filter 1 [Figure 9](#)). It should also be noted that using a simple quartz window ('Silver' filter, transmission 280-600 nm, filter 2 [Figure 9](#)) that essentially removes only the long wave IR bands led to substantial substrate decomposition even over very short residence times. Finally, the four lamps were screened in order to compare their effect ([Table 1](#)).

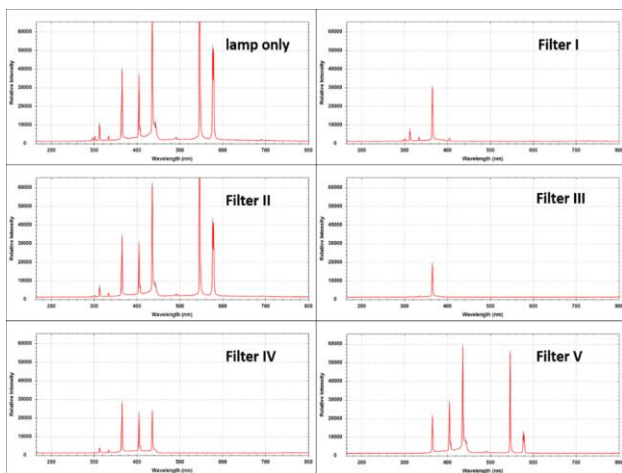
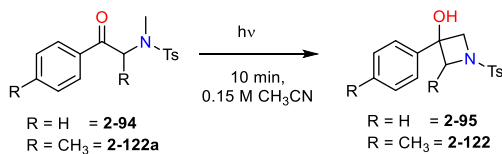


Figure 9: Medium pressure mercury lamp emission spectra with different filters.

Table 1: Lamp screening.



	Lamp 1 (300 / 365 nm)	Lamp 2 (370 nm)	Lamp 3 (310 nm)	Lamp 4 (254 nm)
2-94	90% conv. 70 W 55 °C	7% conv. 7.5 W 25 °C	23% conv. 7.8 W 24 °C	17% conv. 6.8 W 25 °C
2-122A	90% conv. 70 W 55 °C	10% conv. 7.5 W 24 °C	18% conv. 7.6 W 24 °C	10% conv. 7.2 W 25 °C

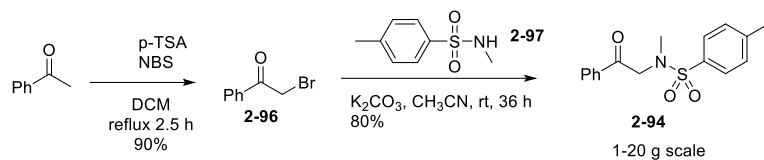
Despite the apparent large gap between the conversions obtained by lamp 1 and the others, the use of the low-pressure lamps is still interesting if parameters such as power and temperature are considered. Indeed, the conversion obtained with lamp 3 (the most efficient of the low-pressure lamps) is less than a quarter that of lamp 1, however, the power used is

ten times lower and the heat produced is also less than half. This data would be of particular interest if designing an industrial scale reactor specifically for scaling this reaction with a view to environmental and economy.

In addition the results obtained with a selective low-pressure mercury lamp (7.8 W) which exhibits a peak emission at 310 nm seemed interesting (Table 1). At the previous standardized flow rate of 1 mL/min the reaction proceeded but with a much-reduced conversion of 23% in accordance with the lower rated lamp power specification. Slowing the flow rate to 0.75, 0.5 or 0.25 mL/min enabled higher conversions of 34, 49 and 59% (for compounds **2-95** and **2-122**) respectively to be achieved, indicating an essentially linear correlation with extended irradiation time. Of particular note was that these reactions were very clean showing only starting materials **2-94** and **2-122a** and products **2-95** and **2-122**. Unfortunately, we deemed the overall throughput would ultimately be too low with such a system as our challenge was to devise a system which could be used to perform larger preparative scale Norrish-Yang reactions. Consequently, although showing high selectivity the low power system was deemed inadequate for our needs and we elected to revert to the original medium pressure lamp (150 W) for all further reactions. In the hope of improving the transformation, we also evaluated the addition of a range of potential photocatalysts (e.g. diphenyl ketone, 2-methylthioxanthone and methylene blue at 10 and 40 mol%); however, none of the catalysts tested showed any advantageous activity across a range of wavelengths for this particular transformation.

2.4.7 Substrate screening

The lack of any existing literature substrate studies and inconsistencies in the reaction conditions previously reported made it hard to generalize the synthetic scope or anticipate new reactivity based upon varying structural functionality. Therefore, we built a collection of functionalised starting materials for a systematic investigation (Scheme 17). The general synthetic route entails a two-step process involving the bromination of the related acetophenone using NBS and *p*-TSA followed by substitution of the halogen with the sulfonamide unit **2-97** by simple nucleophilic substitution carried out in acetonitrile at room temperature.



Scheme 17: Synthesis of starting material 2-94.

Therefore, by starting from the appropriately substituted ketones, a series of additional starting materials were prepared and their resultant solutions pumped through the photoreactor, allowing evaluation of their conversion into the related azetidins (figure 10 and 11).

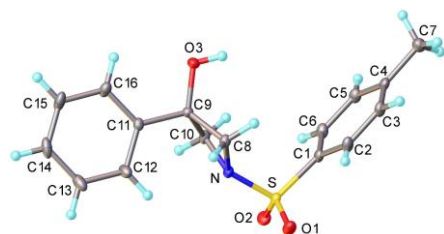


Figure 10: X-ray structure of compound 2-95.

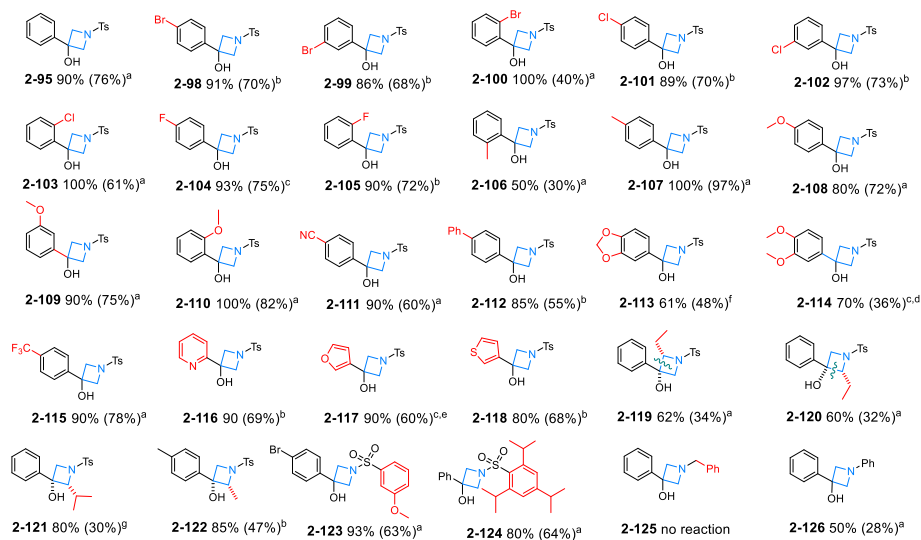


Figure 11: The expanded range of products prepared from the photo-flow Yang reaction.

All reactions were performed at 1 and 5 mmol exploratory scales, results presented are the mean of at least 3 repeat runs at the 5 mmol scale. The % consumption of starting material and % isolated yields (in parentheses) are shown. NMR yields were determined for the crude products using an internal standard of 4-dimethylaminobenzonitrile. All isolated yields were in the range of -1→3% lower than the theoretical yield determined by NMR. ^aGeneral flow conditions; 0.15 M solution of the starting material 1-110 in acetonitrile, flow rate 1 mL/min (10 min residence time), reactor temperature 18-25 °C. ^b Concentration used was 0.075 M. ^cSolvent used was acetone. ^dConcentration used was 0.035 M. ^eConcentration used was 0.02 M. ^fA flow rate of 0.7 mL/min was used and a reactor temperature was 70 °C. ^gA flow rate of 0.5 mL/min was used.

Initially, the aromatic ring was enriched by the addition of bromine and chlorine substitution (Figure 11; 2-98 to 2-103) as versatile handles for subsequent medicinal chemistry derivatisation. The 3- and 4-substituted compounds gave high conversions and were isolated in similarly high yield by column chromatography, indicating that their reactivity was not affected by a halogen substituent at either the *meta* or *para* positions. This was in contrast to the corresponding *ortho* substituted aromatics which although showing high starting material consumption gave significantly more decomposition and thus much lower isolated recoveries (Figure 11; 2-100 & 2-103). We speculated this may be due to the *ortho* substituent imposing a steric impingement on the transition state thereby preventing planarity of the aromatic carbonyl and thus affecting the electronics and desired absorption of the substrate (Figure 12, 13 and 14: conformational modelling). To experimentally test this, we prepared and ran the corresponding 2-substituted methyl and fluoro materials (Figure 11; 2-104 - 2-107). Again,

the difference in reactivity between the 2- and 4-methyl substituents was dramatic. Whereas, the 2- and 4-fluoro substituted reactants showed comparable reactivity as would be expected for the small orbital contracted fluoro group. These additional results indicated the observed effect was as hypothesised mainly steric in nature and not a direct electronic aspect of the potentially inductive halogens. This was further confirmed by assessing the methoxy series (Figure 11; 2-108 – 2-110). The reactivity of which was essentially equivalent for each member, including the 2-methoxy substrate (Figure 11; 2-110), which can preferentially orientate the methyl substituent to minimise steric interactions in the transition state and so easily achieve planarity. A further evidence in this direction was given by some conformational modelling on the starting materials (2-95, 2-100, 2-103, 2-105, 2-106 and 2-110) showing that the co-planarity between the carbonyl group and the aromatic ring was progressively hampered increasing the dimension of the substituent in the *ortho*-position (Figure 12, 13, 14).

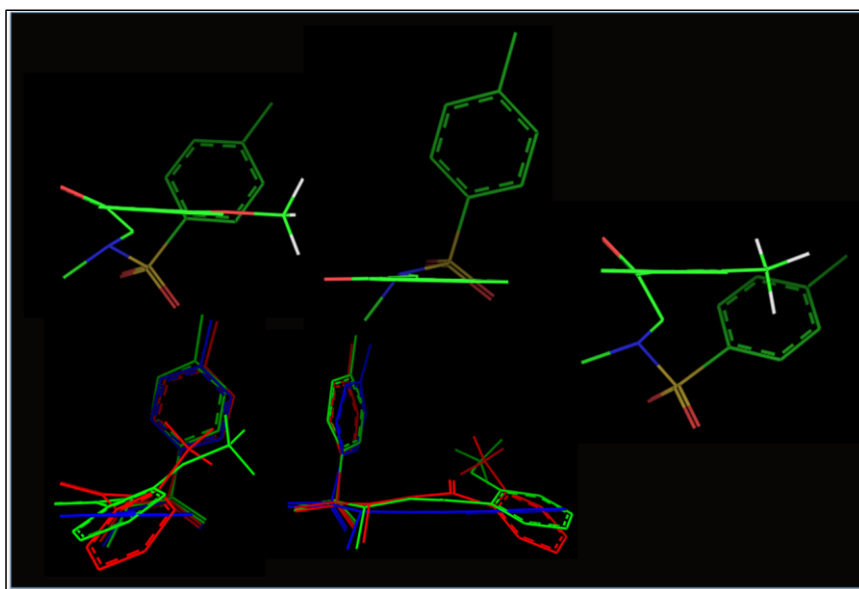


Figure 12: Modelling of compounds 2-95, 2-106, 2-110.

Conformational modelling simulation for compounds 2-95 (Blue), 2-96 (red) and 2-110 (green). The aromatic ring of the ketone moiety twists further out of plane with increasing size of *ortho* group. Compounds energies are reported: *ortho*-H. (Energy = 30.46 kcal mol⁻¹). *Ortho*-Me (Energy = 37.40 kcal mol⁻¹). *Ortho*-OMe (Energy = 37.38 kcal mol⁻¹)

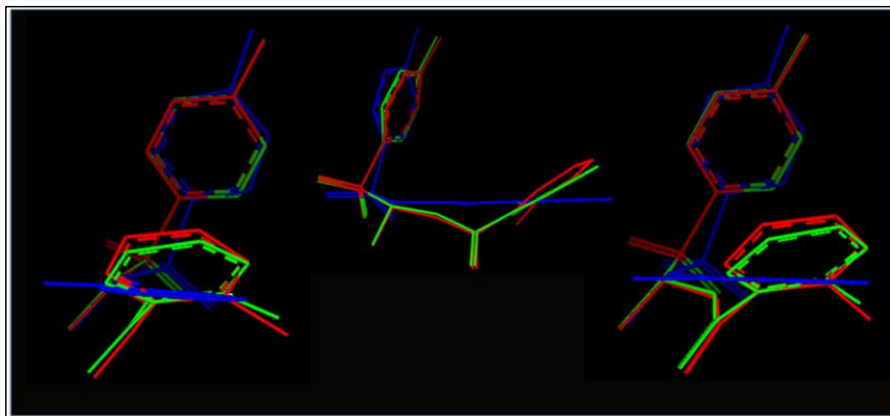


Figure 13: Modelling of compounds **2-95**, **2-100**, **2-103**.

Conformational modelling simulation for compounds **2-95** (Blue), **2-100** (red) and **2-103** (green). The aromatic ring of the ketone moiety twists further out of plane with increasing size of ortho group.

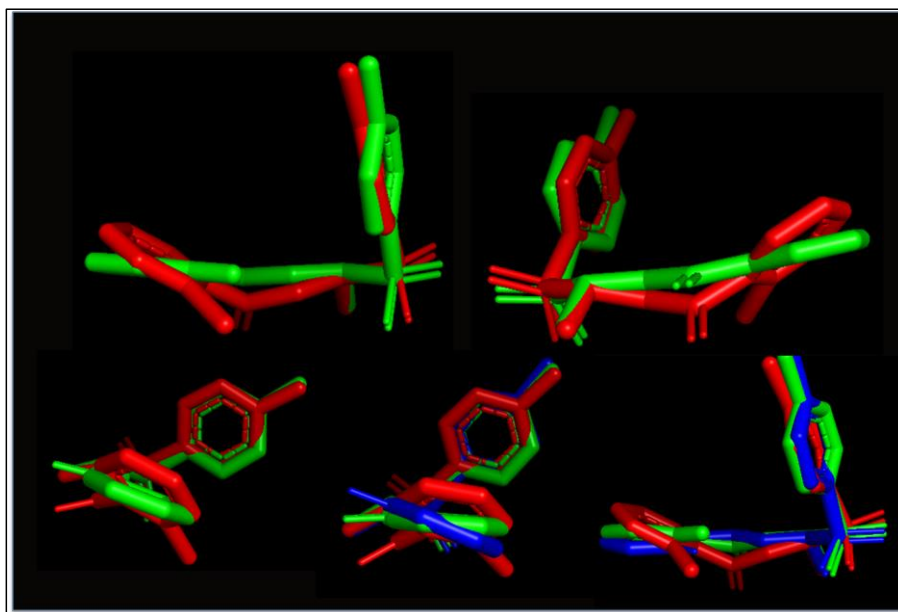
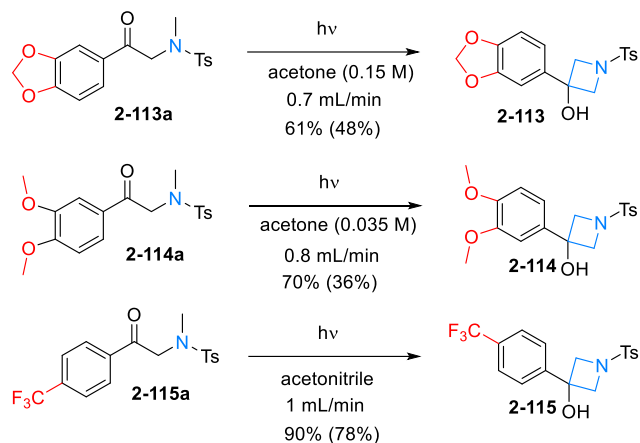


Figure 14: Modelling of compounds **2-95**, **2-100**, **2-103**, **2-105**.

Conformational modelling simulation for compounds **2-95** (Blue), **2-103** (red) and **2-105** (green). The aromatic ring of the ketone moiety twists further out of plane with increasing size of ortho group.

We next probed the installation of various π -donor and acceptor substituents as well as a trifluoromethyl functional group on the phenyl ring (Scheme 18; compounds **2-113** to **2-115**).



Scheme 18: Synthesis of compounds 2-113, 2-114, 2-115.

The % consumption of starting material and % isolated yields (in parentheses) are shown. Medium pressure mercury lamp with “gold filter” (365 nm max) was used.

It appears that strongly electron donating units diminish the reactivity as indicated by the dioxolane **2-113a** and dimethoxy derivative **2-114a**. Under the standard conditions (1 mL/min - 10 min residence time) only 22% conversion, equating to a 10% isolated yield of the corresponding azetidinium **2-113** was obtained. However, wishing to demonstrate that the general conditions could be rapidly re-optimized (Table 2) in flow for poorly reacting substrates we were able to improve the conversion (61%) and enable an isolated yield of 48%.

Table 2: Rapid reoptimization screen for product 2-113.

Entry	Flow rate (mL/min)	Lamp power (%)	Temperature (°C)	Yield (%)
1	1	90	18-25	10
2	0.7	90	18-25	20
3	0.5	90	18-25	15
4	0.7	90	49-52	22
5	0.7	90	70	48
6	0.7	90	80	39

[a]Reactions were performed at 0.15 M concentration in MeCN using a medium pressure mercury lamp equipped with a “Gold Filter” (365 nm max) At the higher temperatures indicated the photoreactor is more stable and easier to control the temperature at a specific set point.

Of particular interest was an observed dependence on temperature in this reaction. Allowing the photoreactor temperature to rise to 70 °C was accompanied by a steady but limited improvement in the yield. Although temperature has been shown to have a positive influence on other photochemical transformations, we, as well as others, are not able to fully account for this effect at this stage.^[93] Indeed, this was in our case a seemingly localised effect as across the range of other substrates evaluated, the best yields were obtained at or below a temperature of 25 °C. The same impact of strongly donating substituents on the phenyl ring was also clearly seen with the equivalent 3,4-dimethoxy substrate **2-114** which initially proved completely inert to the photo induced reaction under the standard condition and showed little benefit when tested with the newly derived conditions established for **2-113** (see above). Interestingly, by changing the solvent, in this particular case to acetone, and using a lower flow rate (0.8 mL/min) we were able to achieve a modest 36% isolated yield of the cyclic product **2-114**. Of note, the addition of 30 mol% diphenyl ketone or acetone to the original acetonitrile solution had no impact on the transformation discounting a photo-catalysed process. Overall, the reactions to form products **2-113** and **2-114** highlight that the aryl electronic contributions do play an important role in the transformation. The implication is that high yields of the desired azetidinol can be attained when there is a good match between the light source and absorbance relating to the $n \rightarrow \pi^*$ propagation. Unfortunately, significant electronic perturbation from strongly electron donating or assumedly withdrawing groups would be expected to shift the absorbance band and alter the transition to the reactive diradical **2-90b** (Scheme 15). Unfortunately, analysis of the UV spectra was not very revealing and did not allow any meaningful conclusions to be drawn. However, by comparing the ¹³C chemical shift of the carbonyl signals for the electron rich aromatic starting materials **2-113a** (191.8 ppm) and **2-114a** (192.0 ppm) against the parent H substituted standard **2-95a** (193.8 ppm) it is clear some donation occurs which is associated with a diminished reactivity (**2-113** and **2-114**). Interestingly, during a wider analysis (Figure 15) we noted a general correlation that substrates with a carbonyl ¹³C signal in the range of 196-193 ppm generally showed good reactivity resulting in high isolated yields under the standard conditions (0.15 M in MeCN, 1 mL/min). In comparison compounds outside this range were typically much lower yielding but could often be improved by changing the processing conditions (i.e. flow rate, solvent or concentration). Although more data is required to confirm this observation, it may with the sophisticated predictive NMR packages currently available enable *in silico* design of idealised substrates for subsequent reaction.

entry	yield	ppm ¹³ C
95	76	193.8 ¹³ C
98	70	193
99	68	192.6
100	40	197.88
101	71	192.91
102	73	192.79
104	75	192.46
105	73	192.15
106	30	197.24
107	85	193.35
108	72	192.26
109	75	193.7
110	82	195.08
111	60	190.2
112	55	193.44
113	48	191.8
114	36	192
115	78	193.3
116	69	194.7
117	60	187
119	34	194.2
120	32	197.66
121	30	193.21
122	47	197.1
123	63	193
124	64	193.32
126	28	196.5
130	40	208.9
131	0	209.06
132	0	202.99
137	74	193.44
133	71	196.24
134	81	194.26
136	76	194.08

- meta and para substituted (compounds 2-119 – 2-122)
- ortho substituted (compounds 2-133 – 2-137)
- N substituted (2-100, 2-105, 2-106, 2-110)

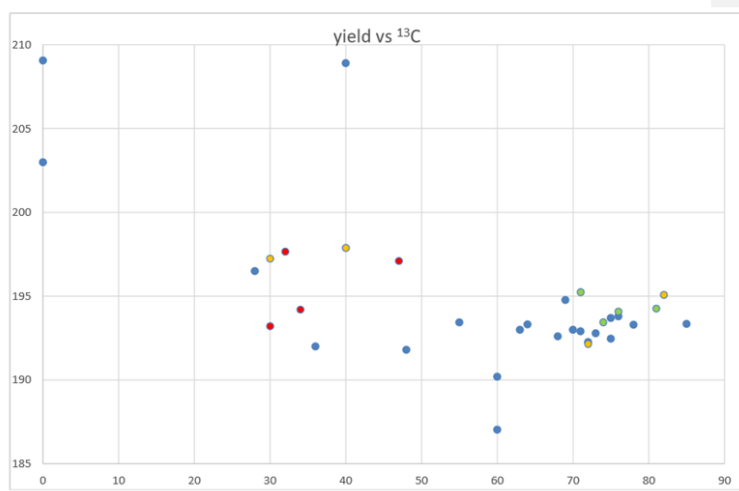
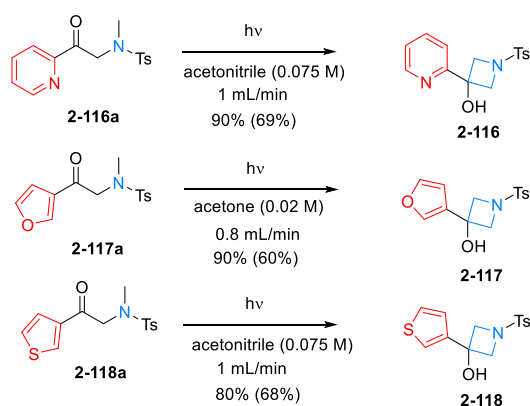


Figure 15: Correlation of ¹³C shift and yield.

Pleasingly, when expanding the substrate range, the direct replacement of the phenyl ring for other simple heteroaromatics (Scheme 19; 1-136 – 1-138, Figure 16) was readily tolerated opening up the feasibility for exploring much greater structural diversity.



Scheme 19: Substrates 2-116 to 2-118.

The % consumption of starting material and % isolated yields (in parentheses) are shown. Medium pressure mercury lamp with "gold filter" (365 nm max) was used.

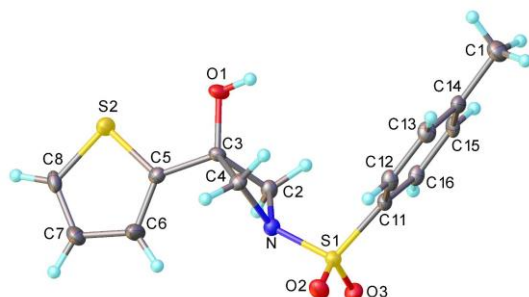
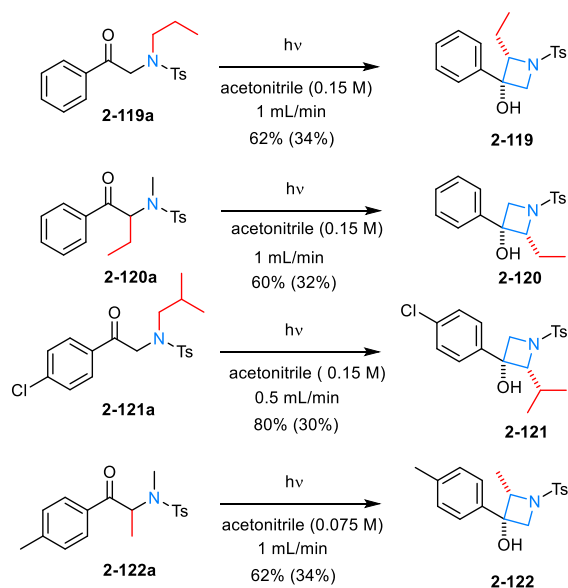


Figure 16: X-Ray structure of compound **2-118**.

Next, we elected to explore the effect of further substitution on the carbon scaffold of the azetidine ring, consequently the additional substrates leading to compounds **2-119** to **2-122** were assembled and tested (Scheme 20, Figure 17).



Scheme 20: Synthesis of compounds **2-119** to **2-122**.

The % consumption of starting material and % isolated yields (in parentheses) are shown. Medium pressure mercury lamp with "gold filter" (365 nm max) was used.

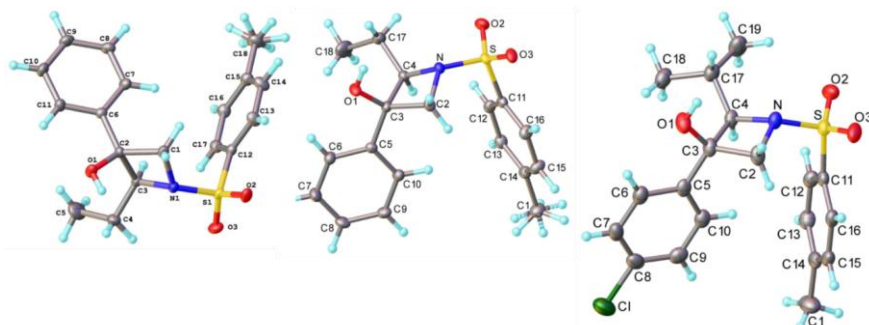


Figure 17: X-Ray structures of compounds **2-119**, **2-120** and **2-121**.

Analysis of the crude products revealed that in each case the material produced was a single diastereoisomer with *syn* disposition of the corresponding hydroxyl and the alkyl groups as confirmed by COSY, NOESY correlation experiments and by single crystal X-ray analysis (Figure 18).

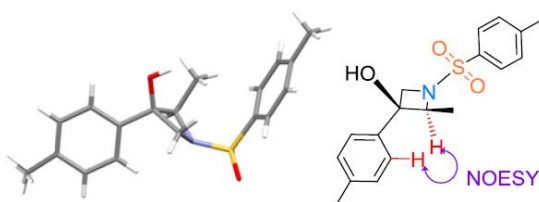
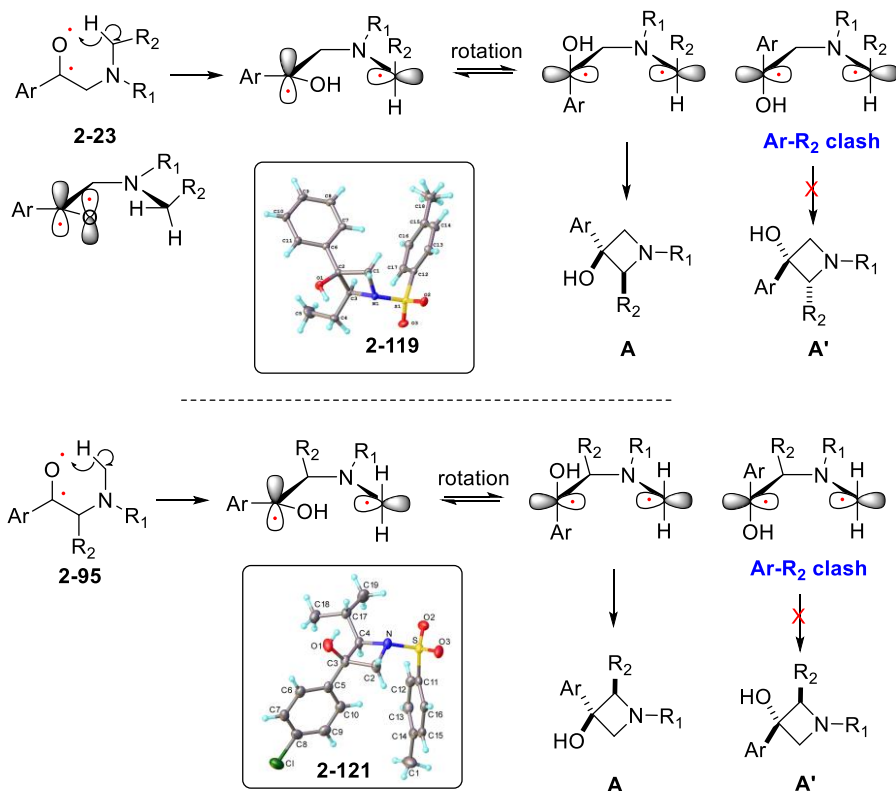


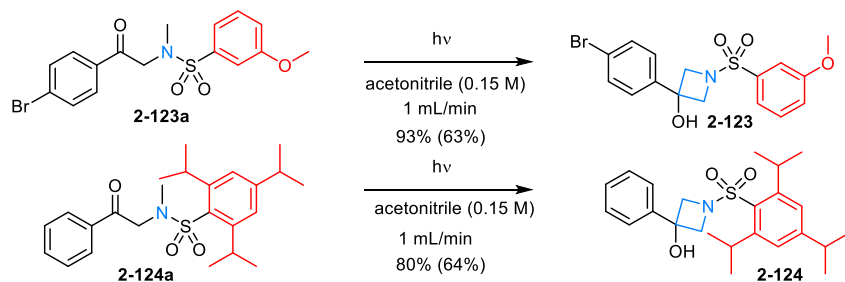
Figure 18: X-ray of substrate **2-122** (left) and protons involved in the NOESY interaction (right).

This observed selectivity is consistent with a predictive model based upon minimization of steric interactions in the ring forming transition state (Scheme 21). It is apparent that by adding additional steric demands to the reaction in the form of these side chains the reaction becomes more challenging as expressed by the lower isolated yields (*cf.* compound **2-95** with **2-119** to **2-122**). Of particular interest was that steric factors were balanced as the regioisomeric starting materials leading to the equivalent products **2-119** and **2-120** were obtained in essentially identical conversion and isolated yield.



Scheme 21: Minimization of steric interactions in the ring forming transition state.

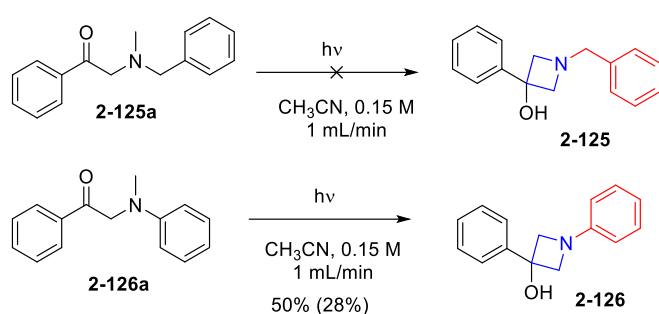
Having identified certain steric constraints which impact the reaction, we wished to explore the modification of the sulfonamide component of the system by adding an electron rich 3-methoxyphenyl and a bulky *tris*-2,4,6-isopropylphenyl ring (Scheme 22; 2-123 & 2-124).



Scheme 22: Substitution on the sulfonamide moiety.

The % consumption of starting material and % isolated yields (in parentheses) are shown. Medium pressure mercury lamp with "gold filter" (365 nm max) was used.

Both substrates (**2-123** & **2-124**) were converted into the corresponding azetidinoles under the standard condition without any appreciable difference in reactivity (Scheme 22). This was in stark contrast with the simple benzyl substituted substrate **2-125a** which failed to yield any of the desired product **2-125** (Scheme 23). Interestingly, removing the methylene group restored some of the reactivity allowing 28% of the corresponding product **2-126** to be isolated.

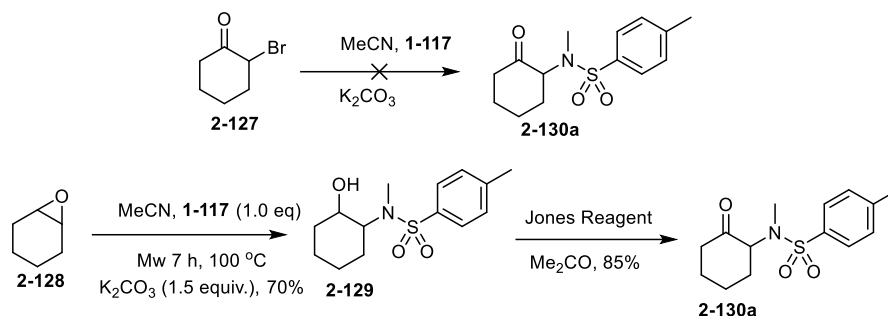


Scheme 23: Change of the spacer between N and the Ar group.

The % consumption of starting material and % isolated yields (in parentheses) are shown. Medium pressure mercury lamp with "gold filter" (365 nm max) was used.

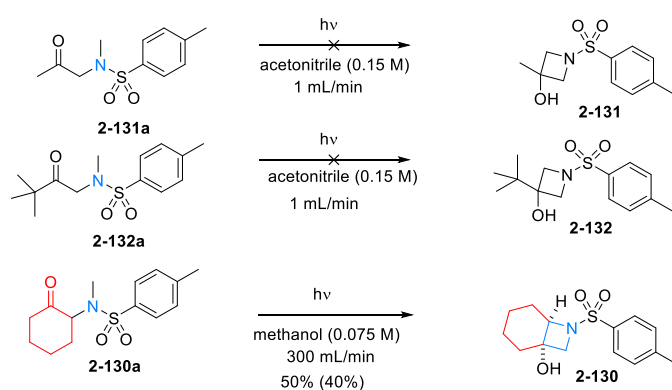
Evidently an electron withdrawing group on the nitrogen helps increase the attached *N*-methyl C-H acidity enabling easier hydride abstraction via the proposed intermediate **2-90b** (Scheme 21), as well as stabilising the resultant radical formed (Scheme 15). This ultimately inspired us to consider other functional groups on the nitrogen which we will discuss below.

Our study has demonstrated that the photochemical process works generally for many aromatic ketones. In order to gauge how a non-aromatic structure responds to the flow processing three aliphatic derivatives were prepared (Scheme 25). The methyl and *tert*-butyl derivatives were prepared by the standard sequence of bromination and substitution with sulfonamide **2-97** (Scheme 25), whereas the cyclohexanone construct, namely, bromocyclohexanone **2-127** proved completely unreactive toward substitution by sulfonamide **2-97**. Compound **2-130a** was therefore prepared starting from the corresponding epoxide **2-128**, which was ring opened and the intermediate alcohol **2-129** subsequently oxidized (Scheme 24).



Scheme 24: The preparation of substrate 2-130a.

The aliphatic sulfonamides (Scheme 25) were each subjected to the optimised flow conditions used previously (0.15 M, 1 mL/min 100% lamp power), compounds **2-131a** and **2-132a** showed no conversion (even increasing the reaction time) whereas compound **2-130a** was converted into the related azetidine **2-130** (Figure 19) but only in modest conversion and isolated yield and required longer reaction time (lower flow rate). As the UV spectra for these compounds all possess a characteristic absorption in the correct region, we expected these compounds would successfully react. Unfortunately, the lack of an aromatic ring seems to significantly affect the reactivity, possibly due to the diminished stability of the reactive intermediate **2-90b** (Scheme 15).^[94] Indeed, even screening a wider range of conditions and solvents no sign of reactivity was ever seen. The fact that the substrate **2-130a** reacts at all is probably due to the more favourable locked geometric configuration which assists its cyclisation.



Scheme 25: Aliphatic sulfonamides.

The % consumption of starting material and % isolated yields (in parentheses) are shown. Medium pressure mercury lamp with "gold filter" (365 nm max) was used.

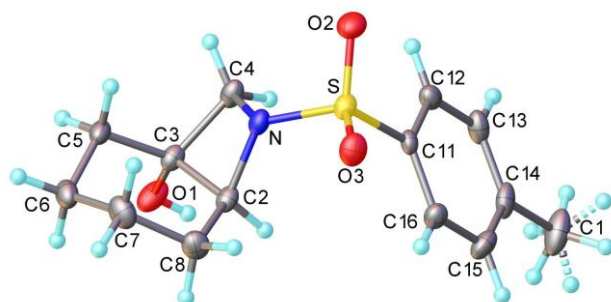
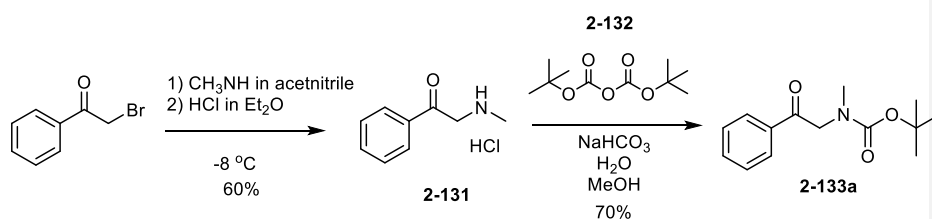


Figure 19: X-Ray structure of compound **2-130**.

Having previously established that although an electron withdrawing substituent on the sulfonamide nitrogen atom was required for successful reaction (*cf* compounds **2-125** and **2-126**) there seemed to be some scope for variation in the functionality (*cf* compounds **2-95**, **2-98**, **2-123**, **2-124**). We therefore decided to explore some simplified amide groups and the synthetically more versatile Boc protection. The Boc group is considerably easier to remove compared with the analogous sulfonamide thus allowing access to the hydroxyzazetidine with a free nitrogen available for further reactions. In order to introduce the Boc group we decided to start from the chlorine salt of the aminoketone (**Scheme 26**, **2-131**) obtained by direct reaction between the related bromoketone and methylamine. Thus, reaction with Boc anhydride **2-132** gives the desired product **2-133** (**Scheme 26**).

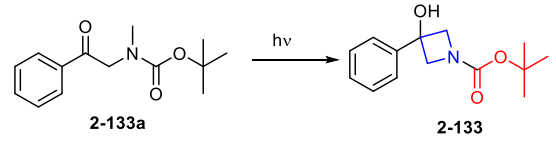


Scheme 26: Generation of Boc derivative **2-133a**.

Attempting the photocatalysed cyclisation using the standard flow condition despite indicating rapid consumption of the starting materials only resulted in low isolated yields of

the corresponding cyclic products (<30%). Thus, we embarked upon a re-optimisation screen which identified the solvent had a pronounced impact on the reaction process for these particular species (Table 3).

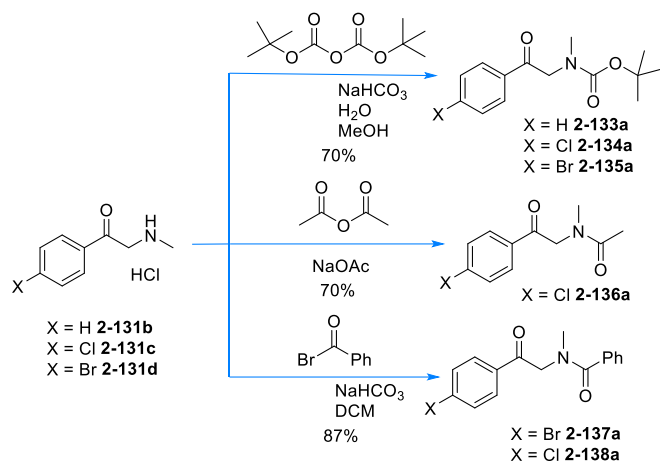
Table 3: Optimization of the reaction of the Boc derivative 2-133a.



Solvent	T(°C)	Flow (mL/min)	Yield (%)
CH ₃ CN (0.15 M)	30	1	25
CH ₃ CN (0.037 M)	30	1	30
MeOH (0.15 M)	30	1	62
MeOH (0.15 M)	30	0.7	62
MeOH (0.15 M)	40	1	63
MeOH (0.075 M)	40	1	69
MeOH (0.037 M)	40	1	71
MeOH (0.037 M)	40	0.8	71
Acetone (0.037 M)	40	1	52

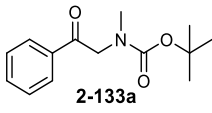
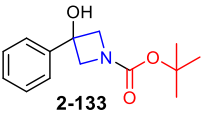
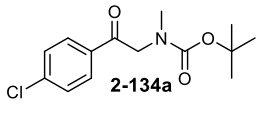
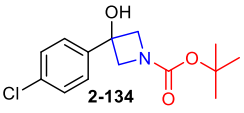
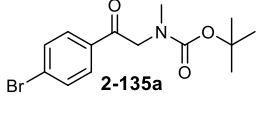
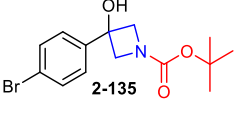
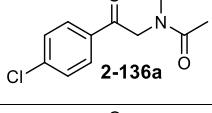
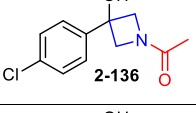
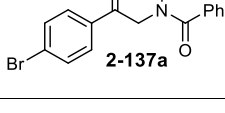
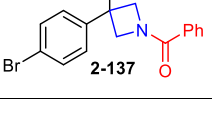
[a] performed with a medium pressure mercury lamp; power = 100%.

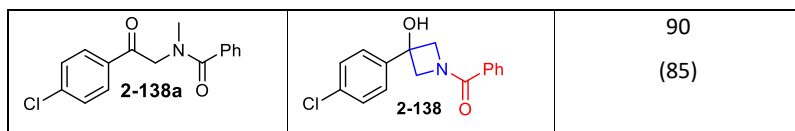
Adopting the newly determined condition the full range of substrates (acetyl, benzoyl and Boc species) were also processed and gave similar improved yields to the corresponding azetidines products (Scheme 27, Table 4, Figure 20).



Scheme 27: Synthesis of starting material for acetyl, benzoyl and Boc derivatives.

Table 4. Cyclization acetyl, benzoyl and Boc derivatives.

Starting material	Product	Conversion% (yield %)
 2-133a	 2-133	100 (71)
 2-134a	 2-134	100 (81)
 2-135a	 2-135	100 (76)
 2-136a	 2-136	100 (74)
 2-137a	 2-137	91 (89)



Performed with a lamp power of 100%, 0.037 M in MeOH at a reactor temperature of 40 °C.

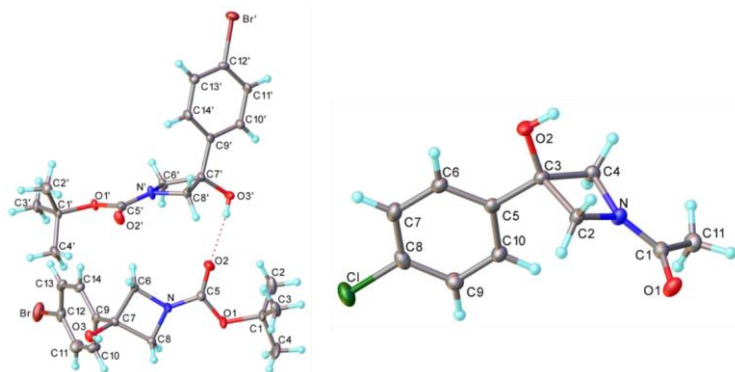
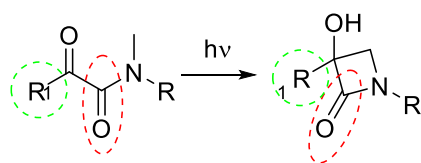


Figure 20: X-Ray structures of **2-135** and **2-136**.

Having determined the general scope and some limitations to the reaction, we wished to demonstrate the robustness and scalability of the processing capabilities of working in flow through the scale up of the transformation. As such five compounds were selected for assess at larger scale production, namely products **2-95**, **2-100**, **2-108** and **2-122**. As an illustration compound **2-101** was directly scaled to 100 mmol (0.15 M concentration in MeCN equating to a required processing volume of 667 mL at 1 mL/min flow rate). In a single continuous run, this material required 11.5 h of processing, including reactor washing. After solvent evaporation, the product could be more expediently isolated by trituration with cold CHCl_3 and following drying *in vacuo* furnished 20.3 g (60%). For larger processing volumes (i.e. **2-108** (64%) and **2-122** (40%), 250 mmol), the mixture was conveniently processed intermittently during a standard working day (8 h), with the reactor flushed with MeCN each night and simply restarted in continuation the following day. In this way, it was trivial to prepare stock solutions of materials and thus generate multi-gram quantities of the products.

2.5 CONCLUSIONS

In conclusion, the Yang reaction has been studied in flow for the first time; starting from a sulfonamide derivative whereby the reactivity in batch was known. The reaction was optimized in a flow reactor showing a remarkable reduction in the reaction time from several hours (batch) to minutes. The initial substrate was progressively extrapolated in order to evaluate the effect of different substituents on the reactivity: initially both the aromatic ring and the sulfonamide fragments were functionalized, then the role of the substituent on the nitrogen was more closely assessed. Several *N*-carbonyl derivatives were subsequently assembled showing a good reactivity toward the cyclization, moreover the Boc protected azetidine particularly represents a valuable substrate giving the chance for deprotection and the use of the free nitrogen for further reactions. The reaction was also scaled up allowing the production of >20 g of product in under 12 h demonstrating the efficiency of the Yang reaction in flow as a valuable synthetic tool. The total NMR conversion calculated using 4-(dimethylamino)benzotrile as an internal standard shows that the results are comparable to what has been previously reported in literature. Moreover, the flow process allows a drastic reduction in the reaction time (10 min) and easy scale up of the reaction. Overall, our study has shown how a flow approach can enhance the potential of this transformation increasing its synthetic utility. In this perspective the scope of this transformation leading to various 3-hydroxy azetidines can be continued investigating more complex structures and alternative substituents on the nitrogen as outlined in the last part of this study. Particularly, the presence of a second carbonyl group on at the α position would bypass the need for an aromatic ketone, thus offering a way to reduce the overall weight of the product and potentially to reach new and intriguing structures (Scheme 28).



Scheme 28: Further scope expansion of the transformation.

2.6 References

- 1) Gabriel, S.; Weiner, J. *Eur. JIC*, **1888**, *21*, 2, 2669–2679.
- 2) Koppel, G. A. In *Small Ring Heterocycles*, Hassner, A., Ed.; Wiley: New York, **1983**; part 2, Vol. 2, p 223.
- 3) Hegedus, L. *Pure Appl. Chem.*, **1983**, *55*, 1743–1745.
- 4) Durckheimer, W.; Blumbach, J.; Lattrell, R.; Scheunemann, K. H. *Angew. Chem.*, **1985**, *97*, 183–205.
- 5) Miller, M. J. *Acc. Chem. Res.*, **1986**, *19*, 49–56.
- 6) Nagahara, T.; Kametani, T. *Heterocycles*, **1987**, *26*, 729–731.
- 7) Cooper, R. D. G.; Daugherty, B. W.; Boyd, D. B. *Pure Appl. Chem.*, **1987**, *59*, 485–492.
- 8) Siriwardane, U.; Chu, S. C. C.; Buynak, J. D.; *Acta Crystallogr., Sect. C, Cryst. Struct. Commun.*, **1988**, *C44*, 391–393.
- 9) Barrett, A.; Sturgess, M. A. *Tetrahedron*, **1988**, *44*, 5615–5652.
- 10) Hart, D. H.; Ha, D. C. *Chem. Rev.* **1989**, *89*, 1447–1465.
- 11) Brown, M. J. *Heterocycles* **1989**, *29*, 2225–2244.
- 12) Backes, J. in *Houden Weyl's Methoden der Organischen Chemie*, Vol XVI/B; Georg Thieme Verlag: Stuttgart, **1991**; p 31.
- 13) Van der Steen, F. H.; Van Koten, G. *Tetrahedron*, **1991**, *47*, 7503–7524.
- 14) Page, M. I.; Ed.; *The Chemistry of β -Lactams*; Chapman and Hall: New York, **1992**.
- 15) George, G. I., Ed.; *The Organic Chemistry of β -Lactams*; VCH Publishers: New York, **1993**.
- 16) De Kimpe, N.; *Azetidines, Azetines and Azetesin Comprehensive Heterocyclic Chemistry II, a Review of the Literature of 1982-1995*, Volume 1B; Pergamon: Oxford, **1996**.
- 17) Sandhu, J. S.; Sain, B. *Heterocycles*, **1987**, *26*, 777–818.
- 18) Matthew, B. P.; Bartholomäus, P.; Kerry, G.; Peter, H. S. *Chem. Rev.*, **2017**, *117*, 18, 11796–11893.
- 19) Peterson, P. J.; Fowden, L. *Nature*, **1963**, *200*, 148–151.
- 20) Takeuchi, T.; Prokop, D. J. *Biochem. Biophys. Acta*, **1969**, *175*, 142–155.
- 21) Prokop, D. J. *Biochem. Biophys. Acta*, **1969**, *175*, 156–164.
- 22) Fyfe, M. C. T.; Gattrell, W.; Rasamison, C. M. Patent PCT Int. Appl. 2007, WO2007116230A1; Chem. Abstr. **2007**, *147*, 469218.

- 23) Isabel, E.; Oballa, R.; Powell, D.; Robichaud, J. Patent PCT Int. Appl. 2007, WO2007143823A1; Chem. Abstr. **2007**, *148*, 78872.
- 24) Josyula, V. P. V. N.; Renslo, A. R.; Patent PCT Int. Appl. 2007, WO 2007004049A1 Chem. Abstr. **2007**, *146*, 142631.
- 25) Okutani, T.; Kaneko, T.; Madusa, K. *Chem. Pharm. Bull.*, **1974**, *22*, 1490–1497.
- 26) Frehel, D.; Heymes A.; Maffrand, J. P.; Eloy, F.; Aubert, D.; Rolland, F. *Eur. J. Med. Chem.*, **1977**, *12*, 447.
- 27) Melloni, P.; Della Torre, A.; Meroni, M.; Ambrosini, A.; Rossi, A. C. *J. Med. Chem.*, **1979**, *22*, 183–191.
- 28) Marchand, A. P.; Rajagopal, D.; Bott, S. G. *J. Org. Chem.*, **1994**, *59*, 1608–1612.
- 29) Archibald, T. G.; Gilardi, R.; Baum, K.; Clifford, G. *J. Org. Chem.*, **1990**, *55*, 2920–2924.
- 30) Hayashi, K.; Kumagai, T.; Nagao, Y. *Heterocycles*, **2000**, *53*, 447–452.
- 31) US Army PCT Int. Appl. (1996) WO 9636602 A1 21/11/1996; Chem. Abstr., **1997**, *126*, 74727.
- 32) Dave, P. R. Patent US 5580988 A 03/12/1996; *Chem. Abstr.*, **1996**, *126*, 47087.
- 33) Okada, T.; Ezumi, K.; Yamakawa, M.; Sato, H.; Tsuji, T.; Tsushima, T.; Motokawa, K.; Komatsu, Y. *Chem. Pharm. Bull.*, **1993**, *41*, 126–131.
- 34) Frigola, J.; Vano, D.; Torrens, A.; Gomez-Gomar, A.; Ortega, E.; Garcia-Granda, S. *J. Med. Chem.*, **1995**, *38*, 1203–1215.
- 35) Frigola, J.; Torrens, A.; Castrillo, J. A.; Mas, J.; Vano, D.; Berrocal, J. M.; Calvet, C.; Salgado, L.; Redondo, J. *J. Med. Chem.*, **1994**, *37*, 4195–4210.
- 36) Frigola, J.; Pares, J.; Corbera, J.; Vano, D.; Merce, R.; Torrens, A.; Mas, J.; Valenti, E. *J. Med. Chem.*, **1993**, *36*, 801–810.
- 37) Altisen, R. C.; Constansa, J. F.; Alvarez, M. I. Patent US 2005182041 A1 18/08/2005.
- 38) Hanagan M. A.; Selby, T. P.; Sharpe, P. L.; Sheth, R. B.; Stevenson, T. M. *Chem. Abstr.*, **2005**, *143*, 229708.
- 39) Ryan H. T.; Edna, F. C.; Shuguang, M.; Susan, W.; Jason, H.; Yuzhong, D.; Isabelle, R.; Mary, G.; Cornelis, E. C. A. H.; Cyrus, K.; Mark, J. D.; Luna, M. *Drug Metab. Dispos.*, **2016**, *44*, 28–39.
- 40) Candel, F. J.; Peñuelas, M. *Drug Des. Devel. Ther.*, **2017**, *11*, 881–891.
- 41) Wallace, D. J.; Furie, R. A.; Tanaka, Y.; Kalunian, K. C.; Mosca, M.; Petri, M. A.; Dörner, T.; Cardiel, M. H.; Gomez, E.; Carmack, T.; Delozier, A. M.; Janes, J. M.; Linnik, M. D.; Bono, S.; Silk, M. E.; Hoffman, R. W. *The Lancet*, **2018**, *392*, 222–231.

- 42) Majek, M.; Filace, F.; Wangelin, A. J. *Beilstein J. Org. Chem.*, **2014**, *10*, 981–989.
- 43) Ju, Y.; Varma, R. S. *J. Org. Chem.*, **2006**, *71*, 135–141.
- 44) Shono, T.; Matsumura, Y.; Katoh, S.; Ohshita, J. *Chem. Lett*, **1988**, *17*(6), 1065–1068.
- 45) Hillier, M. C.; Chen, C.-Y. *J. Org. Chem.*, **2006**, *71*, 7885–7887.
- 46) Gaertner, V. R.; *J. Org. Chem.*, **1967**, *32*, 2972–2976.
- 47) Nadir, U. K.; Arora, A. *Indian J. Chem., Sect. B*, **1998**, *37B*, 163–167.
- 48) Nadir, U. K.; Arora, A. *Indian J. Chem., Sect. B*, **1993**, *32B*, 297–298.
- 49) Nadir, U. K.; Sharma, Ms. R. L.; Koul, V. K. *J. Chem. Soc., Perkin Trans.*, **1991**, *1*, 2015–2019.
- 50) Nadir, U. K.; Sharma, R. L.; Koul, V. K. *Tetrahedron*, **1989**, *45*, 1851–1858.
- 51) Nadir, U. K.; Koul, V. K. *Synthesis*, **1983**, 554–554.
- 52) Malik, S.; Nadir, U. K. *Synlett*, **2008**, 108–110.
- 53) Schrader, T.; Steglich, W. *Synthesis* **1990**, 1153–1156.
- 54) Aben, R. W. M.; Smit, R.; Scheeren, J. W. *J. Org. Chem.*, **1987**, *52*, 365–370.
- 55) Fischer, G.; Fritz, H.; Rihs, G.; Hunkler, D.; Exner, K.; Knothe, L.; Prinzbach, H. *Eur. J. Org. Chem.*, **2000**, 743–762.
- 56) Trupp, B.; Fritz, H.; Prinzbach, H.; Irngartinger, H.; Reifenstahl, U. *Chem. Ber.*, **1991**, 1777–1794.
- 57) Dave, P. R.; Duddu, R.; Li, J.; Surapaneni, R.; Gilardi, R. *Tetrahedron Lett.*, **1998**, *39*, 5481–5484.
- 58) Davies, H. M. L.; Matasi, J. J.; Ahmed, G. J. *J. Org. Chem.*, **1996**, *61*, 2305–2313.
- 59) Krow, G. R.; Lin, G.; Yu, F. *J. Org. Chem.*, **2005**, *70*, 590–595.
- 60) Krow, G. R.; Lester, W. S.; Lin, G.; Fang, Y.; Carroll, P. J. *J. Org. Chem.*, **2003**, *68*, 1626–1629.
- 61) Beeken, P.; Bonfiglio, J. N.; Hasan, I.; Piwinski, J. J.; Weinstein, B.; Zollo, K. A.; Fowler, F. *W. J. Am. Chem. Soc.*, **1979**, *101*, 6677–6682.
- 62) Alberto, B.; Stefano, C.; Franca, M. C. *Chem. Rev.* **2008**, *108*, 3988–4035.
- 63) Ojima, I.; Zhao, M.; Yamato, T.; Nakahashi, K.; Yamashita, M.; Abe, R. *J. Org. Chem.*, **1991**, *56*, 5263–5277.
- 64) Alcaide, B.; Almendros, P.; Salgado, N. R. *J. Org. Chem.*, **2000**, *65*, 3310–3321.
- 65) Alcaide, B.; Polanco, C.; Sierra, M. A. *J. Org. Chem.* **1998**, *63*, 6786–6796.
- 66) T. M. Sugden: Photochemistry and Reaction Kinetics. Cambridge University Press, **1967**, ISBN-10: 0521040655.

- 67) Norrish, R. G. W.; Bamford, C. H. *Nature*, **1936**, 140, 195–196.
- 68) Bamford, C. H.; Norrish, R. G. W. *J. Chem. Soc.* **1938**, 1521–1531.
- 69) Bamford, C. H. Norrish, R. G. W. *J. Chem. Soc.* **1938**, 1531–1544.
- 70) Peter, A.; L.; George, F. V. *J. Chem. Educ.*, **1964**, 41, 535–541.
- 71) Neckers, D. C.; Kellogg, R. M.; Prins, W. L.; Schoustra, B. *J. Org. Chem.* **1971**, 36, 1838–1840.
- 72) Cottier, L.; Remy, G.; Descotes, G. *Synthesis* **1979**, 711–712.
- 73) Bemasconi, G.; Cottier, L.; Descotes, G.; Remy, G. *Bull. Soc. Chim. Fr.* **1979**, 322–325.
- 74) Binkley, R. W.; Jarrell, H. F. *J. Carbohydr. Nucleosides, Nucleotides* **1980**, 7, 347–364.
- 75) Yang, N. C.; Yang, D. D. H. *J. Am. Chem. Soc.*, **1958**, 80, 2913–2914.
- 76) Axel, G. G.; Heike, H. *J. Am. Chem. Soc.*, **2002**, 124, 396–403.
- 77) Ihmels, H.; Scheffer, J. R. *Tetrahedron*, **1999**, 55, 885–907
- 78) Abdul-Baki, A.; Rotter, R.; Schrauth, T.; Roth, H. *J. Arch. Pharm.*, **1978**, 311, 341–345.
- 79) Wagner, P. J.; Zepp, R. G. *J. Am. Chem. Soc.* **1971**, 93, 4958–4959.
- 80) Hasegawa, T.; Miyata, K.; Ogawa, T.; Yoshihara, N.; Yoshioka, M. *Chem. Commun.* **1985**, 363–364.
- 81) Hasegawa, T.; Miyata, K.; Ogawa, T.; Yoshihara, N.; Yoshioka, M. *J. Chem. Soc., Perkin Trans.*, **1997**, 2979–2982.
- 82) Anoklase, J. A.; Josepha, L. J.; Nilotpal, B.; Angel, U.; Sivaguru, J. *J. Am. Chem. Soc.*, **2009**, 131, 11314–11315.
- 83) Ishida, N.; Shimamoto, Y.; Murakami, M. *Angew. Chem.*, **2012**, 51, 11750–1175.
- 84) Zepp, R. G.; Gumz, M.; Miller, W. L.; Gao, H. *J. Phys. Chem. A.*, **1998**, 102, 5716–5723.
- 85) Ahmad, A.; Hamamy, E.; John, H.; John, T. *J. Chem. Soc., Perkin Trans.*, **1983**, 1, 573–580.
- 86) Adam, W.; Sven, G.; Wilson, R. M. *Eur JIC.*, **1989**, 122, 561–564.
- 87) Erica, N. D.; Darren, S. L.; Luke, D. E.; Jing, J.; Kevin, I. B. M.; Martyn, P.; Michael, W. G. *Green Chem.*, **2017**, 19, 1431–1438.
- 88) Catalan, J.; Catalan, J. P. *Phys. Chem.*, **2011**, 13, 4072–4082.
- 89) Swenton, J. S. *J. Chem. Educ.*, **1969**, 46, 217–225.
- 90) Porter, G.; Suppan, P. *Pure Appl. Chem.*, **1964**, 9, 499–506.
- 91) Leermakers, P. A.; Vesley, G. F. *J. Chem. Educ.*, **1964**, 41, 535–541.
- 92) <https://www.vapourtec.com/products/flow-reactors/photochemistry-uv-150-photochemical-reactor-features/21/07/2020>

93) P. Melchiorre in *Organic synthesis in the Excited State, enhancing the potential of organocatalysis with light*, presented to the 7th European workshop in drug synthesis, Siena, 22 May 2018.

93) Griesbeck, A.; Mattay, J. *Synthetic Organic Photochemistry*. Boca Raton: CRC Press, **2004**. ISBN 9780824757366.

2.7 Experimental

2.7.1 Materials and Methods

Chemicals: The chemicals used were obtained from the companies Sigma-Aldrich/Fluka, Alfa Aesar, TCI or Fluorochem and were used without further purification.

Chromatography: For the TLC chromatography Merck TLC Aluminium oxide 60 F254 with glass backing were used. Detection was carried out either by UV absorption or by treatment of the plate with an acidic solution of potassium permanganate and drying using a hand held hot-air dryer.

NMR-Spectroscopy: The NMR spectra were recorded on a Bruker Avance-400 and Varian VNMRS-700 spectrometer in the indicated solvent at a temperature of 297 K. Commercially available deuterated chloroform, methanol or DMSO was used as a solvent. The spectra were always set to the reference value of the solvent, for example chloroform (for ^1H -NMR spectra to 7.26 ppm and for ^{13}C -NMR spectra to 77.00 ppm). For the exact analysis and assignment of the signals in more complex compounds, COSY, HSQC and HMBC spectra were additionally added. Chemical shifts were reported in ppm and coupling constants J in hertz (Hz). The following abbreviations were used for the multiplicities of the signals: s (singlet), d (doublet), t (triplet), q (quartet), m (multiplet).

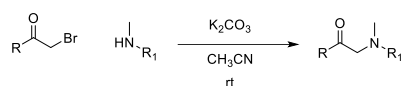
MS-Spectroscopy: GCMS spectra were obtained using an Agilent 6890N gas chromatograph coupled with an Agilent 5973 inert mass selective detector operating in EI mode with a custom-built Anature auto sampler/injector or by Durham University Mass Spectrometry service. Electrospray (ES) mass spectra were obtained using a TQD mass spectrometer (Waters UK, Ltd; all were obtained by Durham University Mass Spectrometry service).

IR-Spectroscopy: The infrared spectra were recorded with a PerkinElmer Spectrum One IR spectrometer. The samples were measured by the ATR method (attenuated total reflection). The evaluation was limited to the bands characteristic of the compound. The position of the absorption bands in the IR spectrum was expressed in wave numbers $\tilde{\nu}$ (cm^{-1}).

Melting point determination: The melting point was determined using an Electrothermal 9100 capillary melting point device. The melting point range was recorded for the determination of melting points for powdered solids.

2.7.2 Synthesis

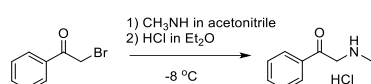
Synthesis of products 2-95 to 1-146a.



The α -bromoacetophenone derivative (10 mmol) was dissolved in acetonitrile (1 M), and K_2CO_3 (1.5 equiv.) and the appropriate sulfonamide (1 equiv.) were added. The mixture was stirred vigorously at room temperature until complete disappearance of the sulfonamide starting material as determined by TLC. The inorganic solids were dissolved by the addition of water (30 mL), and the mixture was extracted with EtOAc (50 mL), washed with brine (30 mL), dried over Na_2SO_4 and the solvent removed by evaporation under reduced pressure. The crude product was purified by column chromatography or by crystallization when possible.

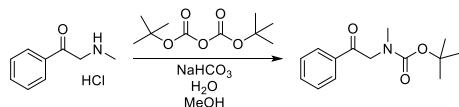
Compounds **2-105**, **2-103** and **2-111** were synthesized using DMF instead of acetonitrile, the reaction was monitored by mass spectra and stirred until disappear of the α -bromoacetophenone starting material. The reaction was worked up by addition of EtOAc (40 mL) and the mixture was extracted with water (50 mL) until removal of DMF (clean water solution), washed with brine (30 mL), and dried over Na_2SO_4 , the solvent was then evaporated and the crude material purified by column chromatography.

Synthesis of the *N*-methyl 2-oxo-2-phenylethanaminium chloride (**2-131b**).

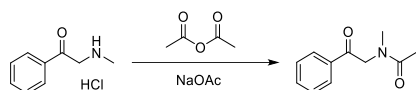


A solution of CH_3NH_2 (2.2 mL; 9 M in MeOH) was added to acetonitrile (6 mL) and the solution was cooled at $-8\text{ }^\circ\text{C}$ with an ice-acetone bath. The α -bromoacetophenone derivative (20 mmol) was dissolved in acetonitrile (20 mL) and added slowly to the cold solution. The mixture was monitored by TLC and stirred until the complete disappearance of the ketone starting material. Et_2O was added and the mixture was filtered removing the ammonium salt. The solution was cooled to $-10\text{ }^\circ\text{C}$ and HCl (2 M solution in Et_2O ; 1 equiv.) was slowly added dropwise. The formed precipitate was filtered and purified by trituration with acetone.

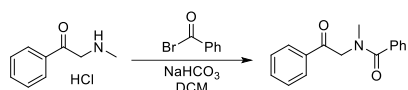
Synthesis of the *N*-methyl *tert*-butyl 1-oxo-1-phenylethan-2-ylcarbamate (2-133a - 2-137ab)



To a solution of *N*-methyl 2-oxo-2-phenylethan-1-aminium chloride in MeOH (1 M) was added NaHCO₃ (4 equiv.) and the solution was cooled to 0 °C. A portion of di-*tert*-butyl dicarbonate (1.5 equiv.) was added and the mixture was stirred at room temperature for 48 h. The solvent was evaporated under reduced pressure, EtOAc (40 mL) was added and the solution was extracted with water (30 mL), washed with brine (20 mL) and crystallised from a mixture of Et₂O / MeOH.



A suspension of 2-oxo-2-phenylethane ammonium chloride (20 mmol) in Ac₂O (15 mL) and NaOAc (3 g) was stirred for 24 h at room temperature. Water (20 mL) was added and the mixture diluted with EtOAc (35 mL), extracted with NaHCO₃ (20 mL), brine (20 mL) and dried over Na₂SO₄. The solvent was evaporated under reduced pressure and the product was crystallised from EtOAc / Hexane.

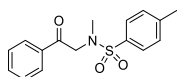


A biphasic mixture of saturated aqueous solution of NaHCO₃ (50 mL) and DCM (40 mL) was cooled in an ice bath. To the mixture was added 2-oxo-2-phenylethane ammonium chloride (21 mmol) and benzoyl bromide (31.5 mmol) and the mixture was stirred for 24 h. To the mixture was added water (20 mL), the organic phase was separated, washed with brine (30 mL), dried over Na₂SO₄ and the solvent evaporated under reduced pressure. The product was purified by crystallisation from Et₂O / MeOH.

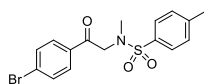
General Procedure for the Photocyclization

The α -aminoketone starting material **1** was dissolved in acetonitrile at the chosen concentration (typically 0.15 M), and the solution was pumped through the photoreactor at

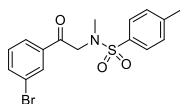
the given flow rate (typically 1 mL/min). The temperature of the reactor was kept between 20–25 °C using N₂ gas cooling. The outflow from the reactor was collected into a flask, and after solvent evaporation, it was purified by normal phase column chromatography (EtOAc/Hexane) or by trituration with cold CHCl₃.



N,4-Dimethyl-N-(2-oxo-2-phenylethyl)benzene sulfonamide (2-95a).^[4] Isolated yield 80%; ¹H NMR (400 MHz, CDCl₃) δ 7.99 – 7.94 (m, 2H), 7.72 (d, *J* = 8.3 Hz, 2H), 7.64 – 7.55 (m, 1H), 7.48 (dd, *J* = 8.3, 7.1 Hz, 2H), 7.33 (d, *J* = 8.4 Hz, 2H), 4.56 (s, 2H), 2.82 (s, 3H), 2.44 (s, 3H); ¹³C NMR (101 MHz, CDCl₃) δ 193.8 (C), 143.7 (C), 134.9 (C), 134.8 (C), 133.9 (CH), 129.8 (CH), 128.9 (CH), 128.3 (CH), 127.6 (CH), 56.1 (CH₂), 35.7 (CH₃), 21.6 (CH₃); IR (neat) ν = 2909.6 (s), 1692.3 (s, CO), 1338.2 (s), 1158.7 (s, SO₂), 1228.7 (s, C-N), 741.2 (s), 666.9 (s), 544.8 (s) cm⁻¹; HR-MS calculated for C₁₆H₁₈NO₃S 304.1007, found 304.1018 (Δ = 3.6 ppm, mDa = 0.1); Melting point: 118-119 °C.

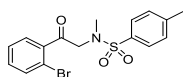


N-(2-(4-Bromophenyl)-2-oxoethyl)-N,4-dimethylbenzene sulfonamide (2-98a).^[4] Isolated yield 63%; ¹H NMR (400 MHz, CDCl₃) δ 7.89 (d, *J* = 8.4 Hz, 2H), 7.73 (d, *J* = 8.3 Hz, 2H), 7.65 (d, *J* = 8.4 Hz, 2H), 7.36 (d, *J* = 8.3 Hz, 2H), 4.50 (s, 2H), 2.81 (s, 3H), 2.47 (s, 3H); ¹³C NMR (101 MHz, CDCl₃) δ 193.0 (C), 143.8 (C), 134.4 (C), 133.4 (C), 132.1 (CH), 129.9 (CH), 129.7 (CH), 129.2 (C), 127.58 (CH), 56.1 (CH₂), 35.6 (CH₃), 21.6 (CH₃); IR (neat) ν = 3064.1 (s), , 1697.6 (s, CO), 1584.6 (s), 1155.5 (s), 1325.7 (SO₂), 1221.9 (s, C-N), 541.7 (s, CBr), 291.8 (s) cm⁻¹; HR-MS calculated for C₁₆H₁₇⁷⁹BrNO₃S 382.0113, found 382.0117 (Δ = 1.0 ppm); Melting point: 87.0-89.5 °C.

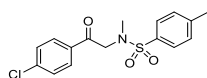


N-(2-(3-Bromophenyl)-2-oxoethyl)-N,4-dimethylbenzene sulfonamide (2-99a). Isolated yield 57%; ¹H NMR (400 MHz, CDCl₃) δ 8.10 (t, *J* = 1.8 Hz, 1H), 7.95 (ddd, *J* = 7.8, 1.8, 1.0 Hz, 1H), 7.77 – 7.73 (m, 3H), 7.43 – 7.34 (m, 3H), 4.54 (s, 2H), 2.84 (s, 3H), 2.47 (s, 3H); ¹³C NMR (101 MHz, CDCl₃) δ 192.6 (C), 143.8 (C), 136.7 (CH), 136.4 (C), 134.6 (C), 131.2 (CH), 130.4

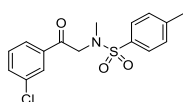
(CH), 129.7 (CH), 127.5 (CH), 126.9 (CH), 123.1 (C), 56.1 (CH₂), 35.6 (CH₃), 21.6 (CH₃); IR (neat) $\nu = 1706.4$ (CO), 1335.8 (s), 1157.6 (s, SO₂), 1217.1 (s, CN), 761.2(s), 546.7 (s, C-Br) cm⁻¹; HR-MS calculated for C₁₆H₁₇⁷⁹BrNO₃S 382.0113, found 382.0123 ($\Delta = 2.6$ ppm); Melting point: 105.1-107.1 °C (crystallised from EtOAc / Hexane).



N-(2-(2-Bromophenyl)-2-oxoethyl)-N,4-dimethylbenzene sulfonamide (2-100a). Isolated yield 55%; ¹H NMR (400 MHz, CDCl₃) δ 7.67 (d, $J = 8.3$ Hz, 2H), 7.59 – 7.55 (m, 1H), 7.45 – 7.41 (m, 1H), 7.36 (td, $J = 7.5, 1.3$ Hz, 1H), 7.33 – 7.27 (m, 3H), 4.45 (s, 2H), 2.85 (s, 3H), 2.39 (s, 3H); ¹³C NMR (101 MHz, CDCl₃) δ 197.88 (C), 143.72 (C), 138.69 (C), 134.83 (C), 133.73 (CH), 132.34 (CH), 129.73 (CH), 128.99 (CH), 127.61 (CH), 127.47 (CH), 118.82 (C), 58.33 (CH₂), 35.74 (CH₃), 21.54 (CH₃); IR (neat) $\nu = 1710.0$ (m, CO), 1336.5 (s), 1215.7 (m), 1158.9 (s, SO₂), 1215.7 (s, C-N), 746.0 (s), 546.9 (s) cm⁻¹; HR-MS: calculated for C₁₆H₁₇⁷⁹BrNO₃S 382.0113, found 382.0108 ($\Delta = -1.3$ ppm, -0.5 mDa).

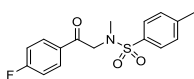


N-(2-(4-Chlorophenyl)-2-oxoethyl)-N,4-dimethylbenzene sulfonamide (2-101a).^[4] Isolated yield 73%; ¹H NMR (400 MHz, CDCl₃) δ 7.94 (d, $J = 8.6$ Hz, 2H), 7.71 (d, $J = 8.3$ Hz, 2H), 7.45 (d, $J = 8.6$ Hz, 2H), 7.34 (d, $J = 8.3$ Hz, 2H), 4.48 (s, 2H), 2.79 (s, 3H), 2.44 (s, 3H); ¹³C NMR (101 MHz, CDCl₃) δ 192.91 (C), 143.94 (C), 140.53 (C), 134.58 (C), 133.14 (C), 129.95 (CH), 129.88 (CH), 129.30 (CH), 127.70 (CH), 56.29 (CH₂), 35.76 (CH₃), 21.70 (CH₃); IR (neat) $\nu = 1691.9$ (s, CO), 1338.7 (s, SO₂), 1158.8 (s, SO₂), 1225.2 (s, NC), 1088.0 (s), 818.9 (s), 756.5 (w), 649.5 (s), 574.8 (s, CCl) cm⁻¹; HR-MS calculated for C₁₆H₁₇³⁵ClNO₃S 338.0618, found 338.0632 ($\Delta = 4.1$ ppm, mDa = 0.14); Melting point: 106-108 °C (crystallised from EtOAc / Hexane).

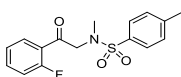


N-(2-(3-Chlorophenyl)-2-oxoethyl)-N,4-dimethylbenzene sulfonamide (2-102a). Isolated yield: 58%; ¹H NMR (400 MHz, CDCl₃) δ 7.92 (t, $J = 1.8$ Hz, 1H), 7.88 (dt, $J = 7.9, 1.8$ Hz, 1H), 7.71 (d, $J = 8.3$ Hz, 2H), 7.57 (ddd, $J = 7.9, 1.8, 1.0$ Hz, 1H), 7.43 (t, $J = 7.9$ Hz, 1H), 7.34 (d, $J =$

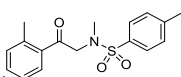
8.3 Hz, 2H), 4.52 (s, 2H), 2.81 (s, 3H), 2.45 (s, 3H); ^{13}C NMR (101 MHz, CDCl_3) δ 192.79 (C), 143.92 (C), 136.33 (C), 135.32 (C), 134.75 (C), 133.92 (CH), 130.32 (CH), 129.88 (CH), 128.41 (CH), 127.69 (CH), 126.59 (CH), 56.26 (CH_2), 35.78 (CH_3), 21.71 (CH_3); IR (neat) ν = 3677.5, 2918.6 (s), 1707.8 (s, CO), 1335.6 (s, SO_2), 1157.1 (s, SO_2) 1219.4 (s, C-N) 771.0 (s), 656.7 (s), 546.7 (s, C-Cl) cm^{-1} ; HR-MS calculated for $\text{C}_{16}\text{H}_{17}\text{NO}_3\text{S}^{35}\text{Cl}$ 338.0618, found 338.0619 (Δ = 2.7 ppm); Melting point: 93-96 °C (crystallised from MeOH / Et_2O).



***N*-(2-(4-Fluorophenyl)-2-oxoethyl)-*N*,4-dimethylbenzene sulfonamide (2-104a).** Isolated yield 65%; ^1H NMR (400 MHz, CDCl_3) δ 8.04 (m, 2H), 7.71 (d, J = 8.2 Hz, 2H), 7.37 – 7.31 (m, 2H), 7.15 (m, 2H), 4.48 (s, 2H), 2.79 (s, 3H), 2.44 (s, 3H); ^{13}C NMR (101 MHz, CDCl_3) δ 192.46 (C), 166.2 (C, d, J = 256.3 Hz), 143.9 (C), 134.5 (C), 131.3 (CH, d, J = 9.5 Hz), 131.2 (C, d, J = 2.9 Hz), 129.8 (CH), 127.7 (CH), 116.1 (CH, d, J = 22.0 Hz), 56.2 (CH_2), 35.7 (CH_3), 21.7 (CH_3); IR (neat) ν = 1690 (s, CO), 1595.2 (s), 1336.6 (s), 1153.1 (s, SO_2), 1228.7 (C-F), 1162.7 (s, CN), 733.3 (s), 546.8 (s) cm^{-1} ; HR-MS calculated for $\text{C}_{16}\text{H}_{17}\text{FNO}_3\text{S}$ 322.0913, found 322.0912 (Δ = 0.3 ppm, -0.1 mDa).

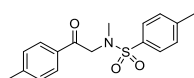


***N*-(2-(4-Fluoro)-2-oxoethyl)-*N*,4-dimethylbenzene sulfonamide (2-105a).** Isolated yield 47%; ^1H NMR (400 MHz, CDCl_3) δ 7.89 (td, J = 7.5, 1.9 Hz, 1H), 7.72 (d, J = 8.3 Hz, 2H), 7.56 (m, 1H), 7.34 – 7.31 (m, 2H), 7.30 – 7.21 (m, 1H), 7.15 (ddd, J = 11.2, 8.3, 1.9 Hz, 1H), 4.58 (d, J = 3.4 Hz, 2H), 2.89 (s, 3H), 2.44 (s, 3H); ^{13}C NMR (101 MHz, CDCl_3) δ 192.15 (C, d, J = 5.6 Hz), 163.44 (C), 160.91 (C), 143.58 (C), 135.62 (CH), 135.53 (CH), 130.94 (CH, d, J = 3.1 Hz), 128.69 (CH, d, J = 212.9 Hz), 124.94 (CH, d, J = 3.2 Hz), 123.36 (C, d, J = 14.7 Hz), 116.76 (CH, d, J = 23.7 Hz), 59.78 (CH_2 , d, J = 11.7 Hz), 36.02 (CH_3), 21.69 (CH_3); IR (neat) ν = 1687.6 (m), 1608.4 (m), 1337.8 (m), 1160.7 (m), 925.4 (s), 844.8 (m), 810.8 (m), 769.1 (s), 737.4 (s), 658.7 (s), 548.2 (s), 527.5 (s) cm^{-1} ; HR-MS calculated for $\text{C}_{16}\text{H}_{27}\text{FNO}_3\text{S}$ 322.0913, found 322.0912 (Δ = -0.3 ppm, -0.1 mDa); Melting point: 103-106.8 °C (crystallised CH_3OH / Et_2O).

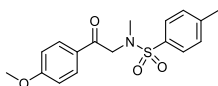


Field Code Changed

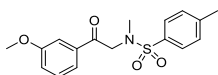
***N*-(2-(2-Methyl)-2-oxoethyl)-*N*,4-dimethylbenzene sulfonamide (2-106a)**. Isolated yield 83%; ¹H NMR (400 MHz, CDCl₃) δ 7.69 (d, *J* = 8.3 Hz, 2H), 7.65 (dd, *J* = 7.5, 1.4 Hz, 1H), 7.37 (td, *J* = 7.5, 1.4 Hz, 1H), 7.31 – 7.20 (m, 4H), 4.43 (s, 2H), 2.82 (s, 3H), 2.43 (s, 3H); ¹³C NMR (101 MHz, CDCl₃) δ 197.24 (C), 143.55 (C), 138.73 (C), 134.94 (C), 134.90 (C), 132.11 (CH), 132.04 (CH), 129.66 (CH), 128.56 (CH), 127.42 (CH), 125.79 (CH), 57.63 (CH₂), 35.71 (CH₃), 21.46 (CH₃), 21.12 (CH₃); IR (neat) ν = 1698.4 (m), 1333.8 (m), 1157.6 (s, SO₂), 662.2 (m), 546.3 (s) cm⁻¹; HR-MS calculated for C₁₇H₂₀NO₃S 318.1164, found 318.1165 (Δ = 0.3 ppm, 0.1 mDa).



***N*-4-Dimethyl-*N*-(1-oxo-1-(*p*-tolyl)propan-2-yl)benzenesulfonamide (2-107a)**. Isolated yield 75%; ¹H NMR (400 MHz, CDCl₃) δ 7.87 (d, *J* = 8.0 Hz, 2H), 7.72 (d, *J* = 8.0 Hz, 2H), 7.33 (d, *J* = 8.0 Hz, 2H), 7.27 (d, *J* = 8.0 Hz, 2H), 4.53 (s, 2H), 2.81 (s, 3H), 2.44 (s, 3H), 2.41 (s, 3H); ¹³C NMR (101 MHz, CDCl₃) δ 193.35 (C), 144.89 (C), 143.68 (C), 134.80 (C), 132.32 (C), 129.75 (CH), 129.54 (CH), 128.42 (CH), 127.61 (CH), 56.02 (CH₂), 35.64 (CH₃), 30.98 (CH₃), 21.60 (CH₃); IR (neat) ν = 1692.9 (m), 1603.0 (m), 1334.6 (s), 1164.8 (s), 969.1 (m), 926.7 (s), 814.9 (s), 737.7 (s), 653.7 (s), 547.0 (s), 459.6 (m) cm⁻¹; HR-MS calculated for C₁₇H₂₀NO₃S 318.1164, found 318.1175 (Δ = 3.5 ppm, 1.1 mDa); Melting Point 115-117 °C (crystallised Hexane / EtOAc).

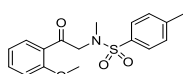


***N*-(2-(4-Methoxyphenyl)-2-oxoethyl)-*N*,4-dimethylbenzene sulfonamide (2-108a)**. Isolated yield 78%; ¹H NMR (400 MHz, CDCl₃) δ 7.96 (d, *J* = 8.9 Hz, 1H), 7.70 (d, *J* = 8.3 Hz, 1H), 7.31 (d, *J* = 8.3 Hz, 1H), 6.93 (d, *J* = 8.9 Hz, 1H), 4.46 (s, 2H), 3.85 (s, 3H), 2.78 (s, 3H), 2.42 (s, 3H); ¹³C NMR (101 MHz, CDCl₃) δ 192.26 (C), 164.12 (C), 143.70 (C), 134.71 (C), 130.78 (CH), 129.76 (CH), 127.85 (C), 127.64 (CH), 114.06 (CH), 55.95 (CH₂), 55.61 (CH₃), 35.65 (CH₃), 21.61 (CH₃); IR (neat) ν = 1684.3 (s), 1584.2 (s), 1342.7 (s), 1260.2 (s), 1153.4 (s, SO₂), 1006.3 (m) cm⁻¹; HR-MS calculated for C₁₇H₂₀NO₄S 334.1113, found 334.1117 (Δ = 4.5 ppm, -0.4 mDa);

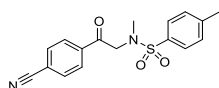
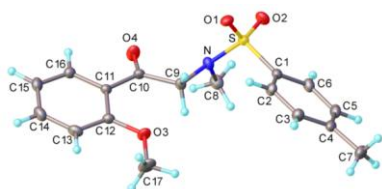


***N*-(2-(3-Methoxyphenyl)-2-oxoethyl)-*N*,4-dimethylbenzene sulfonamide (2-109a)**. Isolated yield 75%; ¹H NMR (400 MHz, CDCl₃) δ 7.72 (d, *J* = 8.2 Hz, 2H), 7.55 (dt, *J* = 8.0, 1.2 Hz, 1H),

7.50 (dd, $J = 2.7, 1.2$ Hz, 1H), 7.38 (t, $J = 8.0$ Hz, 1H), 7.33 (d, $J = 8.2$, Hz, 2H), 7.14 (ddd, $J = 8.0, 2.7, 1.2$ Hz, 1H), 4.54 (s, 1H), 3.85 (s, 2H), 2.82 (s, 1H), 2.44 (s, 1H); ^{13}C NMR (101 MHz, CDCl_3) δ 193.70 (C), 160.00 (C), 143.77 (C), 136.10 (C), 134.87 (C), 129.94 (CH), 129.83 (CH), 127.66 (CH), 120.89 (CH), 120.67 (CH), 112.49 (CH), 56.28 (CH_2), 55.62 (CH_3), 35.70 (CH_3), 21.68 (CH_3); IR (neat) $\nu = 2909.6$ (s), 1693.9 (m) 1593.9 (w), 1597.1 (w), 1486.0 (w), 1426.3 (w), 1332.3 (m), 1262.7 (m), 1194.0 (w), 789.8 (w), 661.9 (m), 544.5 (s) cm^{-1} ; HR-MS calculated for $\text{C}_{17}\text{H}_{20}\text{NO}_4\text{S}$ 334.1113, found 334.1110 ($\Delta = -0.9$ ppm, -0.3 mDa).

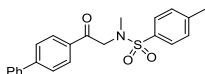


***N*-(2-(2-Methoxyphenyl)-2-oxoethyl)-*N*,4-dimethylbenzene sulfonamide (2-110a).** Isolated yield 58%; ^1H NMR (400 MHz, CDCl_3) δ 7.75 (dd, $J = 7.8, 1.8$ Hz, 1H), 7.71 (d, $J = 8.3$ Hz, 2H), 7.49 (ddd, $J = 8.4, 7.8, 1.8$ Hz, 1H), 7.32 – 7.28 (m, 2H), 7.04 – 6.94 (m, 2H), 4.62 (s, 2H), 3.92 (s, 3H), 2.87 (s, 3H), 2.42 (s, 3H); ^{13}C NMR (101 MHz, CDCl_3) δ 195.08 (C), 159.17 (C), 143.30 (C), 135.83 (C), 134.73 (CH), 130.87 (CH), 129.57 (CH), 127.61 (CH), 125.37 (C), 120.97 (CH), 111.61 (CH), 60.27 (CH_2), 55.66 (CH_3), 35.84 (CH_3), 21.64 (CH_3); IR (neat) $\nu = 3489.2$ (w), 1682.7 (w), 1596.3 (w), 1333.9 (m), 1156.0 (m), 923.6 (w), 550.4 (m), 548.0 (s), 518.1 (m) cm^{-1} ; HR-MS calculated for $\text{C}_{17}\text{H}_{20}\text{NO}_4\text{S}$ 334.1113, found 334.1113 ($\Delta = 4.5$ ppm, 0.0 mDa); Melting point: 151-152.5 $^\circ\text{C}$ (crystallised EtOAc / Hexane). X-Ray data: CCDC 1909069; Formula: $\text{C}_{17}\text{H}_{19}\text{NO}_4\text{S}$, Unit Cell Parameters: a 7.0323(2) b 15.1708(5) c 30.0395(10) Pbca.

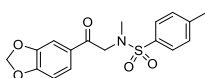


***N*-(2-(4-Cyanophenyl)-2-oxoethyl)-*N*,4-dimethylbenzene sulfonamide (2-111a).** Isolated yield 70%; ^1H NMR (400 MHz, CDCl_3) δ 8.08 (d, $J = 8.7$ Hz, 2H), 7.80 (d, $J = 8.7$ Hz, 2H), 7.74 (d, $J = 8.0$ Hz, 2H), 7.31 (d, $J = 8.0$ Hz, 2H), 4.44 (s, 2H), 2.63 (s, 3H), 2.42 (s, 3H); ^{13}C NMR (101 MHz, CDCl_3) δ 190.2 (C), 143.6 (C), 137.0 (C), 135.9 (C), 132.7 (CH), 129.8 (CH), 129.5 (CH), 127.3 (CH), 117.7 (C), 117.2 (C), 30.2 (CH_2), 29.4 (CH_3), 21.6 (CH_3); IR (neat) $\nu = 3268.5$ (s),

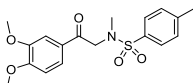
3091.2 (s), 3046.9 (s), 2224.2 (s), 1706.8 (s, CO), 1316.3 (s, SO₂), 1154.7 (s, SO₂), 1089.1 (s), 824.6 (s), 673.3 (s), 541.4 (s) cm⁻¹; HR-MS calculated for C₁₇H₁₇N₂O₃S 329.0960, found 329.0974 (Δ = 4.4 ppm, mDa = 0.14).



N-(2-((1,1'-Biphenyl)-4-yl)-2-oxoethyl)-N,4-dimethylbenzene sulfonamide (2-112a). Isolated yield 68%; ¹H NMR (400 MHz, CDCl₃) δ 8.06 (d, *J* = 8.4 Hz, 1H), 7.75 (d, *J* = 8.3 Hz, 1H), 7.70 (d, *J* = 8.4 Hz, 1H), 7.65 – 7.59 (m, 1H), 7.48 (t, *J* = 7.4 Hz, 1H), 7.44 – 7.38 (m, 1H), 7.34 (d, *J* = 8.3 Hz, 1H), 4.58 (s, 1H), 2.84 (s, 2H), 2.45 (s, 2H); ¹³C NMR (101 MHz, CDCl₃) δ 193.44 (C), 146.58 (C), 143.76 (C), 139.70 (C), 134.82 (C), 133.52 (C), 129.81 (CH), 129.10 (CH), 129.01 (CH), 128.52 (CH), 127.68 (CH), 127.49 (CH), 127.36 (CH), 56.25 (CH₂), 35.74 (CH₃), 21.67 (CH₃); IR (neat) ν = 2921.4 (s), 1699.7 (s, CO), 1601.5 (s), 1340.5 (s), 1324.8 (s), 1228.4 (s), 1150.5 (s), 759.35 (s), 957.9 (s), 542.59 (s) cm⁻¹; HR-MS calculated for C₂₂H₂₂NO₃S 380.1320, found 380.1328 (Δ = 2.1 ppm, 0.8 mDa); Melting Point: 138.7-141 °C (crystallised Hexane / EtOAc).

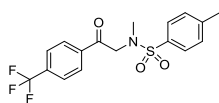


N-(2-(Benzo[d][1,3] dioxol-5-yl)-2-oxoethyl)-N,4-dimethylbenzene sulfonamide (2-113a). Isolated yield 80%; ¹H NMR (400 MHz, CDCl₃) δ 7.70 (d, *J* = 8.3 Hz, 2H), 7.61 (dd, *J* = 8.2, 1.7 Hz, 1H), 7.41 (d, *J* = 1.7 Hz, 1H), 7.32 (d, *J* = 8.3 Hz, 2H), 6.85 (d, *J* = 8.2 Hz, 1H), 6.04 (s, 2H), 4.44 (s, 2H), 2.79 (s, 3H), 2.43 (s, 3H); ¹³C NMR (101 MHz, CDCl₃) δ 191.8 (C), 152.4 (C), 148.4 (C), 143.7 (C), 134.7 (C), 129.7 (CH), 129.5 (C), 127.6 (CH), 124.9 (CH), 108.2 (CH), 108.0 (CH), 102.0 (CH₂), 56.0 (CH₂), 35.6 (CH₃), 21.6 (CH₃); IR (neat) ν = 1686.2 (s, CO), 1602.7 (s), 1487.9 (s), 1446.3 (s), 1301.9 (s), 1251.2 (s), 1156.7 (s), 1035.3 (s), 982.2 (s), 933.3 (s), 881.5 (s), 806.8 (s), 741.4 (s), 645.7 (s), 536.2 (s) cm⁻¹; HR-MS calculated for C₁₇H₁₈NO₅S 348.0906, found 348.0921 (Δ = 4.3 ppm, 1.5 mDa), Melting point: 84-87 °C (crystallised EtOAc / Hexane).

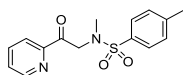


N-(2-(3,4-Dimethoxyphenyl)-2-oxoethyl)-N,4-dimethylbenzene sulfonamide (2-114a). Isolated yield 80%; ¹H NMR (400 MHz, CDCl₃) δ 7.69 (d, *J* = 8.0 Hz, 2H), 7.65 (dd, *J* = 8.4, 2.0 Hz, 1H), 7.53 (d, *J* = 2.0 Hz, 1H), 7.30 (d, *J* = 8.0 Hz, 2H), 6.88 (d, *J* = 8.4 Hz, 1H), 4.44 (s, 2H),

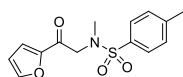
3.92 (s, 3H), 3.90 (s, 3H), 2.76 (s, 3H), 2.40 (s, 3H); ^{13}C NMR (101 MHz, CDCl_3) δ 192.00 (C), 153.90 (C), 149.12 (C), 143.68 (C), 134.58 (C), 129.74 (CH), 127.87 (C), 127.57 (CH), 123.24 (CH), 110.61 (CH), 110.29 (CH), 56.16 (CH_3), 56.09 (CH_3), 55.99 (CH_2), 35.57 (CH_3), 21.58 (CH_3); IR (neat) ν = 1683.7 (s), 1584.7 (s), 1341.6 (s), 1261.4 (s), 1151.7 (s, SO_2), 1008.8 (m) cm^{-1} ; HR-MS calculated for $\text{C}_{18}\text{H}_{22}\text{NO}_5\text{S}$ 364.1219, found 364.1207 (Δ = -3.3 ppm, -1.2 mDa); Melting point: 132.5-133.9 $^\circ\text{C}$.



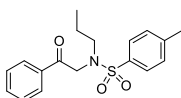
N-(2-(4-Trifluoromethyl)-2-oxoethyl)-N,4-dimethylbenzenesulfonamide (2-115a).^[4] Isolated yield 70%; ^1H NMR (400 MHz, CDCl_3) δ 8.10 (d, J = 8.0 Hz, 2H), 7.72 (m, 4H), 7.34 (d, J = 8.0 Hz, 2H), 4.53 (s, 2H), 2.80 (s, 3H), 2.44 (s, 3H); ^{13}C NMR (101 MHz, CDCl_3) δ 193.30 (C), 144.05 (C), 137.44 (C), 135.11 (q, J = 32.7 Hz, C), 134.43 (C), 129.92 (CH), 128.90 (CH), 127.67 (CH), 125.99 (q, J = 3.8 Hz, CH), 123.55 (q, J = 272.9 Hz, C), 56.53 (CH_2), 35.80 (CH_3), 21.68 (CH_3); IR (neat) ν = 1704.7 (m), 1322.7 (s), 1122.2 (m), 1161.0 (s), 1126.6 (s), 1066.2 (s), 735.9 (m), 550.7 (m) cm^{-1} ; HR-MS calculated for $\text{C}_{17}\text{H}_{17}\text{F}_3\text{NO}_3\text{S}$ 372.0881, found 372.0877 (Δ = -0.4 mDa).



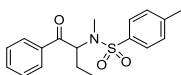
N,4-Dimethyl-N-(2-oxo-2-(pyridin-2-yl)ethyl)benzenesulfonamide (2-116a). Isolated yield 30%; ^1H NMR (400 MHz, CDCl_3) δ 8.65 – 8.57 (m, 1H), 7.97 (d, J = 7.8 Hz, 1H), 7.82 (td, J = 7.8, 1.5 Hz, 1H), 7.73 (d, J = 8.1 Hz, 2H), 7.48 (ddd, J = 7.8, 4.8, 1.5 Hz, 1H), 7.31 (d, J = 8.1 Hz, 2H), 4.91 (s, 2H), 2.89 (s, 3H), 2.41 (s, 3H); ^{13}C NMR (101 MHz, CDCl_3) δ 194.77 (C), 152.03 (C), 149.07 (CH), 143.42 (C), 137.16 (CH), 135.61 (C), 129.71 (CH), 127.92 (CH), 127.50 (CH), 121.97 (CH), 55.88 (CH_2), 35.91 (CH_3), 21.60 (CH_3); IR (neat) ν = 3056.5 (w), 1714.5 (m), 1598.2 (w), 1434.0 (w), 1335.8 (s), 1225.8 (w), 1159.6 (s), 1089.4 (m), 970.3 (m), 925.6 (m), 792.2 (s), 681.15 (m), 646.9 (m), 548.4 (s) cm^{-1} ; HR-MS calculated for $\text{C}_{15}\text{H}_{17}\text{N}_2\text{O}_3\text{S}$ 305.0960, found 305.0950 (Δ = -3.3 ppm, -1.0 mDa).



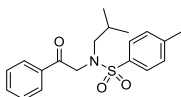
***N*-(2-(furan-2-yl)-2-oxoethyl)-*N*,4-dimethylbenzenesulfonamide (2-117a).** ^1H NMR (400 MHz, CDCl_3) δ 7.94 (d, $J = 4.0$ Hz, 1H), 7.75 – 7.64 (m, 3H), 7.32 (d, $J = 8.0$ Hz, 2H), 7.15 (t, $J = 4.0$ Hz, 1H), 4.41 (s, 2H), 2.82 (s, 3H), 2.43 (s, 3H); ^{13}C NMR (101 MHz, CDCl_3) δ 187.03 (C), 143.90 (C), 141.09 (C), 134.76 (CH), 134.44 (C), 133.48 (CH), 129.84 (CH), 128.58 (CH), 127.64 (CH), 56.52 (CH_2), 35.85 (CH_3), 21.66 (CH_3). IR (neat) $\nu = 1704.3$ (m), 1290.6 (m), 1150.1 (s), 726.5 (s), 547.9 (s) cm^{-1}



4-Methyl-*N*-(2-oxo-2-phenylethyl)-*N*-propylbenzene sulfonamide (2-119a). Isolated yield 32%; ^1H NMR (400 MHz, CDCl_3) δ 7.94 (d, $J = 7.3$ Hz, 2H), 7.74 (d, $J = 8.1$ Hz, 2H), 7.59 (t, $J = 7.3$ Hz, 1H), 7.47 (t, $J = 7.3$ Hz, 2H), 7.29 (d, $J = 8.1$ Hz, 2H), 4.74 (s, 2H), 3.28 – 3.15 (m, 2H), 2.42 (s, 3H), 1.50 (hex, $J = 7.4$ Hz, 2H), 0.81 (t, $J = 7.4$ Hz, 3H); ^{13}C NMR (101 MHz, CDCl_3) δ 194.20 (C), 143.37 (C), 137.00 (C), 135.05 (C), 133.85 (CH), 129.62 (CH), 128.92 (CH), 128.16 (CH), 127.57 (CH), 53.09 (CH_2), 50.20 (CH_2), 21.66 (CH_3), 21.37 (CH_2), 11.21 (CH_3); IR (neat) $\nu = 2981.3$ (s), 1696.4 (s), 1584.9 (s), 1393.8 (s), 1342.9 (s), 1251.5 (s), 1155.8 (s), 801.7 (s) cm^{-1} ; HR-MS calculated for $\text{C}_{18}\text{H}_{22}\text{NO}_3\text{S}$ 332.1320 found, 332.1327 ($\Delta = 2.1$ ppm, 0.7 mDa); Melting point: 59.9-61.7 $^\circ\text{C}$ (crystallised Et_2O / Hexane).

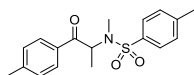


***N*,4-Dimethyl-*N*-(1-oxo-1-phenylbutan-2-yl)benzene sulfonamide (2-120a).** Isolated yield 40%; ^1H NMR (400 MHz, CDCl_3) δ 8.02 (d, $J = 7.4$ Hz, 2H), 7.58 (m, 3H), 7.47 (t, $J = 7.4$ Hz, 2H), 7.18 (d, $J = 7.9$ Hz, 2H), 5.45 (t, $J = 7.4$ Hz, 1H), 2.81 (s, 3H), 2.36 (s, 3H), 1.92 (dt, $J = 13.7, 7.4$ Hz, 1H), 1.45 (dt, $J = 13.7, 7.4$ Hz, 1H), 0.92 (t, $J = 7.4$ Hz, 3H); ^{13}C NMR (101 MHz, CDCl_3) δ 197.66 (C), 143.47 (C), 136.25 (C), 135.86 (C), 133.64 (CH), 129.62 (CH), 128.86 (CH), 128.75 (CH), 127.34 (CH), 60.34 (CH), 29.92 (CH_3), 21.55 (CH_3), 21.26 (CH_2), 11.05 (CH_3); IR (neat) $\nu = 1685.0$ (s), 1330.2 (s), 1149.7 (s), 567.2 (s), 544.6 (s) cm^{-1} ; HR-MS calculated for $\text{C}_{18}\text{H}_{22}\text{NO}_3\text{S}$ 332.1320, found 332.1326 ($\Delta = 1.8$ ppm, 0.6 mDa); Melting point: 79.0-80.2 $^\circ\text{C}$ (crystallised Hexane / EtOAc).



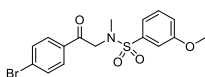
***N*-(2-(4-Chlorophenyl)-2-oxoethyl)-*N*-isobutyl-4-methylbenzene sulfonamide (2-121a).**

Isolated yield 20%; ^1H NMR (400 MHz, CDCl_3) δ 7.88 (d, $J = 8.6$ Hz, 2H), 7.70 (d, $J = 8.1$ Hz, 2H), 7.45 (d, $J = 8.6$ Hz, 2H), 7.29 (d, $J = 8.1$ Hz, 2H), 4.66 (s, 2H), 3.04 (d, $J = 7.5$ Hz, 2H), 2.42 (s, 3H), 1.81 – 1.63 (m, 1H), 0.84 (s, 3H), 0.83 (s, 3H); ^{13}C NMR (101 MHz, CDCl_3) δ 193.21 (C), 143.52 (C), 140.40 (C), 136.63 (C), 133.37 (C), 129.67 (CH), 129.64 (CH), 129.29 (CH), 127.64 (CH), 56.18 (CH₂), 53.86 (CH₂), 27.06 (CH₃), 21.70 (CH₃), 20.12 (CH₃); IR (neat) $\nu = 1703.7$ (m), 1287.9 (m), 1154.9 (s), 1090.0 (s), 726.5 (s), 547.9 (s) cm^{-1} ; HR-MS calculated for $\text{C}_{19}\text{H}_{23}\text{NO}_3\text{S}$ 380.1087, found 380.1088 ($\Delta = 0.3$ ppm, 0.1 mDa).



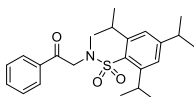
***N*-4-Dimethyl-*N*-(1-oxo-1-(*p*-tolyl)propan-2-yl)benzene sulfonamide (2-122a).**

Isolated yield 65%; ^1H NMR (400 MHz, CDCl_3) δ 8.01 (d, $J = 8.3$ Hz, 2H), 7.67 (d, $J = 8.3$ Hz, 2H), 7.30 – 7.24 (m, 4H), 5.64 (q, $J = 6.9$ Hz, 1H), 2.69 (s, 3H), 2.42 (s, 3H), 2.41 (s, 3H), 1.14 (d, $J = 6.9$ Hz, 3H); ^{13}C NMR (101 MHz, CDCl_3) δ 197.1 (C), 144.6 (C), 143.7 (C), 136.1 (C), 132.5 (C), 129.8 (CH), 129.5 (CH), 129.2 (CH), 127.5 (CH), 55.3 (CH), 29.8 (CH₃), 21.8 (CH₃), 21.6 (CH₃), 12.5 (CH₃); IR (neat) $\nu = 2923.6$ (s), 1685.1 (s, CO), 1603.0 (s), 1446.6 (s), 1250.0 (s), 1156.3 (s), 1087.7 (s), 1035.0 (s), 982.2 (s), 806.4 (s), 536.1 (s) cm^{-1} ; HR-MS calculated for $\text{C}_{18}\text{H}_{22}\text{NO}_3\text{S}$ 332.1320, found 332.1335 ($\Delta = 4.5$ ppm, 1.5 mDa); Melting point: 67-70 °C (EtOAc / Hexane).



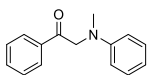
***N*-(2-(4-Bromophenyl)-2-oxoethyl)-3-methoxy-*N*-methylbenzene sulfonamide (2-123a).**

Isolated yield 40%; ^1H NMR (400 MHz, CDCl_3) δ 7.85 (d, $J = 8.6$ Hz, 2H), 7.62 (d, $J = 8.6$ Hz, 2H), 7.48 – 7.37 (m, 2H), 7.33 (dd, $J = 2.6, 1.3$ Hz, 1H), 7.13 (ddd, $J = 8.0, 2.6, 1.3$ Hz, 1H), 4.51 (s, 3H), 3.85 (s, 3H), 2.82 (s, 3H); ^{13}C NMR (101 MHz, CDCl_3) δ 193.00 (C), 160.07 (C), 138.77 (C), 133.50 (C), 132.31 (CH), 130.32 (CH), 129.94 (CH), 129.34 (C), 119.73 (CH), 119.28 (CH), 112.52 (CH), 56.16 (CH₂), 55.80 (CH₃), 35.82 (CH₃). IR (neat) $\nu = 1720.3$ (m), 1280.6 (m), 1160.3 (s), 740.5 (s), 548.2 (s) cm^{-1} .

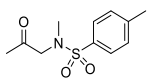
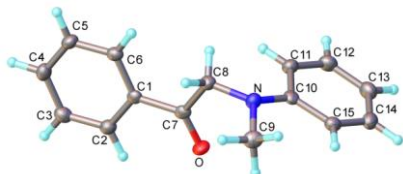


2,4,6-Triisopropyl-*N*-methyl-*N*-(2-oxo-2-phenylethyl)benzene sulfonamide (2-124a).

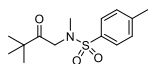
Isolated yield 40%; ^1H NMR (400 MHz, CDCl_3) δ 7.96 (d, $J = 7.4$ Hz, 2H), 7.60 (t, $J = 7.4$ Hz, 1H), 7.48 (t, $J = 7.4$ Hz, 2H), 7.17 (s, 2H), 4.71 (s, 2H), 4.22 – 4.06 (m, 2H), 2.96 – 2.84 (m, 1H), 2.82 (s, 3H), 1.29 – 1.20 (m, 18H); ^{13}C NMR (101 MHz, CDCl_3) δ 193.32 (C), 153.49 (C), 151.98 (C), 150.66 (C), 135.24 (C), 133.86 (CH), 128.95 (CH), 128.16 (CH), 124.15 (CH), 53.28 (CH_2), 34.96 (CH), 34.30 (CH), 29.68 (CH_3), 24.95 (CH_3), 23.68 (CH_3); IR (neat) $\nu = 2958.9$ (m), 1702.3 (m), 1549.3 (m), 1317.2 (m), 1152.1 (s), 883.2 (m), 735.1 (s), 547.1 (m) cm^{-1} ; HR-MS calculated for $\text{C}_{24}\text{H}_{34}\text{NO}_3\text{S}$ 416.2259, found 416.2275 ($\Delta = 3.8$ ppm, 1.6 mDa).



2-(Methyl(phenyl)amino)-1-phenylethan-1-one (2-126a).^[5] Isolated yield 65%. ^1H NMR (400 MHz, CDCl_3) δ 8.00 (d, $J = 7.2$ Hz, 2H), 7.62 (t, $J = 7.6$ Hz, 1H), 7.51 (t, $J = 7.6$ Hz, 2H), 7.32 – 7.14 (m, 2H), 6.74 (t, $J = 7.2$ Hz, 1H), 6.70 (d, $J = 7.6$ Hz, 2H), 4.79 (s, 2H), 3.12 (s, 3H); ^{13}C NMR (101 MHz, CDCl_3) δ 196.5 (C), 149.3 (C), 135.6 (C), 133.6 (CH), 129.3 (CH), 128.9 (CH), 127.9 (CH), 117.1 (CH), 112.3 (CH), 59.0 (CH_2), 39.6 (CH_3); IR (neat) $\nu = 1692.8$ (s, CO), 1595.7 (s), 1506.7 (s), 1215.3 (s, CN), 1256.2 (s, CN), 748.7 (s), 689.17 (s) cm^{-1} ; HR-MS calculated $\text{C}_{15}\text{H}_{16}\text{NO}$ 226.1232, found 226.1240 ($\Delta = 3.5$ ppm); X-Ray data: CCDC 1909071; Formula: $\text{C}_{17}\text{H}_{19}\text{NO}_4\text{S}$, Unit Cell Parameters: a 8.6115(11) b 9.5954(10) c 29.077(4) Pbca.

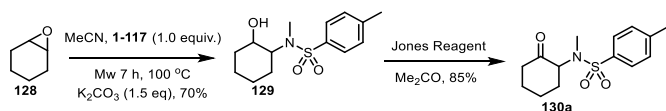


***N*,4-Dimethyl-*N*-(2-oxopropyl)benzene sulfonamide (2-131a).** Isolated yield 50%; ^1H NMR (400 MHz, CDCl_3) δ 7.52 (d, $J = 8.1$ Hz, 2H), 7.19 (d, $J = 8.1$ Hz, 2H), 3.75 (s, 2H), 2.63 (s, 3H), 2.27 (s, 3H), 2.03 (s, 3H); ^{13}C NMR (101 MHz, CDCl_3) δ 202.99 (C), 143.41 (C), 134.15 (C), 129.47 (CH), 127.03 (CH), 58.90 (CH_2), 35.72 (CH_3), 26.65 (CH_3), 21.13 (CH_3); IR (neat) $\nu = 1694.0$ (s), 1603.7 (s), 1321.1 (s), 1229.7 (s), 1153.9 (s), 1091.8 (s), 974.4 (s), 757.8 (s), 421.1 (s) cm^{-1} ; HR-MS: calculated for $\text{C}_{11}\text{H}_{16}\text{NO}_3\text{S}$ 242.0851 found, 242.0854 ($\Delta = 4.7$ ppm, 0.3 mDa).



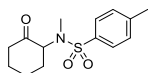
N,4-Dimethyl-N-(2-2,2dimethyl-oxobutyl)benzene sulfonamide (2-132a). Isolated yield 45%; ^1H NMR (400 MHz, CDCl_3) δ 7.64 (d, $J = 8.1$ Hz, 2H), 7.27 (d, $J = 8.1$ Hz, 1H), 4.16 (s, 2H), 2.75 (s, 3H), 2.38 (s, 3H), 1.10 (s, 9H); ^{13}C NMR (101 MHz, CDCl_3) δ 209.06 (C), 143.39 (C), 135.60 (C), 129.58 (CH), 127.38 (CH), 53.76 (CH₂), 43.29 (C), 35.44 (CH₃), 26.69 (CH₃), 26.22 (CH₃). IR (neat) $\nu = 1680.3$ (s), 1623.3 (s), 1311.5 (s), 1166.2 (s), 1100.7 (s), 980.1 (s), 760.2 (s), 424.7 (s) cm^{-1}

Synthesis of compound 2-130a



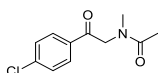
A mixture of cyclohexene oxide (1.96 g, 20 mmol, 1.0 equiv.), *N*-methyl-*p*-tosylamide (1.2 equiv.) and K_2CO_3 (1.5 equiv.) in acetonitrile (20 mL) was loaded into a Biotage 20 mL microwave vial. The solution was stirred and irradiated for 7 h at 90 °C. After cooling water (20 mL) was added and the mixture was extracted with EtOAc (30 mL x 2) washed with brine (25 mL) and dried over Na_2SO_4 . The solvent was removed under reduced pressure to obtain as a colourless oil which was used in the next step without further purification.

The amino alcohol intermediate (2.83 g; 10 mmol) was dissolved in acetone (100 mL) and freshly prepared Jones reagent (Aldrich; Cat No. 758035) was slowly added dropwise until the solution remained red. The solution was stirred for an additional 2 h. Isopropyl alcohol (10 mL) was added, and the mixture stirred for 10 min, the mixture was diluted with Et_2O (200 mL). The solution was washed sequentially with NaHCO_3 (100 mL), saturated NaHCO_3 (50 mL), brine (50 mL) and dried over Na_2SO_4 . The solvent was removed by evaporation to obtain a white solid which was purified by column chromatography (EtOAc / Hexane 6:4).

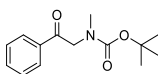


2-(Methyl(phenyl)amino)cyclohexan-1-one (2-130a). Isolated yield 60%; ^1H NMR (400 MHz, CDCl_3) δ 7.20 (d, $J = 7.1$ Hz, 2H), 6.76 – 6.69 (m, 3H), 4.38 – 4.31 (m, 1H), 2.91 (s, 3H), 2.59 – 2.51 (m, 1H), 2.40 (m, 1H), 2.26 – 2.18 (m, 1H), 2.16 – 1.93 (m, 3H), 1.86 – 1.61 (m, 2H); ^{13}C

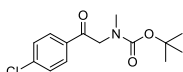
NMR (101 MHz, CDCl₃) δ 208.9 (C), 149.9 (C), 129.2 (CH), 117.4 (CH), 113.4 (CH), 67.3 (CH), 42.1 (CH₂), 34.3 (CH₃), 31.7 (CH₂), 27.1 (CH₂), 25.3 (CH₂); IR (neat) ν = 1594.6 (CO), 1496.5 (s), 1215.2 (s, CN), 748.5 (s), 690.6 (s) cm⁻¹; HR-MS calculated for C₁₃H₁₈NO 204.1388, found 204.1385 (Δ = -1.5 ppm, -0.3 mDa).



N-(2-(4-Chlorophenyl)-2-oxoethyl)-N-methylacetamide (2-137a).^[7] Isolated yield 55%; ¹H NMR (400 MHz, CDCl₃) δ 7.86 (d, *J* = 8.6 Hz, 2H), 7.41 (d, *J* = 8.6 Hz, 2H), 4.76 (s, 2H), 3.07 (s, 3H), 2.16 (s, 3H); ¹³C NMR (101 MHz, CDCl₃) δ 193.44 (C), 171.36 (C), 140.10 (C), 133.51 (C), 129.45 (CH), 129.14 (CH), 53.98 (CH₂), 37.39 (CH₃), 21.42 (CH₃); IR (neat) ν = 2920.0 (W), 1691.7 (s), 1627.8 (s, CO), 1584.8 (m), 1396.2 (s), 1294.4 (m), 1219.2 (s), 1074.5 (s), 1004.5 (m), 965.4 (m), 814.5 (s), 703.7 (s), 562.7 (m), 552.3 (m) cm⁻¹; HR-MS: calculated for C₁₁H₁₃NO₂³⁵Cl 226.0635, found 226.0630 (Δ = -2.2 ppm, -0.5 mDa); Melting point 119.0-120.9 °C (recrystallized from Hexane / EtOAc).

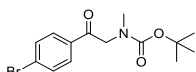


tert-Butyl methyl(2-oxo-2-phenylethyl)carbamate (2-133a).^[6] Isolated yield 50%; NMR data show the presence of rotamers. ¹H NMR (400 MHz, CDCl₃) δ 7.95 – 7.89 (m, 2H), 7.61 – 7.52 (m, 1H), 7.51 – 7.37 (m, 2H), 4.66 (d, 2H), 2.95 (d, 3H), 1.47 (d, 9H); ¹³C NMR (101 MHz, CDCl₃) δ 195.24 (C), 194.90 (C), 156.33 (C), 155.80 (C), 135.39 (C), 135.36 (C), 133.57 (CH), 133.53 (CH), 128.88 (CH), 128.76 (CH), 127.97 (CH), 127.80 (CH), 80.10 (C), 80.06 (C), 55.77 (CH₂), 55.16 (CH₂), 35.79 (CH₃), 35.70 (CH₃), 28.46 (CH₃), 28.31 (CH₃); IR (neat) ν = 2978.1 (s), 2930.3 (s), 1686.12 (s, CO), 1144.9 (s), 881.3 (s), 753.4 (s), 688.8 (s), 632.5 (s) cm⁻¹; HR-MS: calculated for C₁₄H₁₈NO₃ 248.1287, found 248.1274 (Δ = -5.2 ppm, -1.3 mDa).



tert-Butyl (2-(4-chlorophenyl)-2-oxoethyl)(methyl)carbamate (2-134a). Isolated yield 52%; NMR data show the presence of rotamers. ¹H NMR (400 MHz, CDCl₃) δ 7.91 – 7.82 (m, 2H), 7.46 – 7.38 (m, 2H), 4.57 (app. d, 2H), 2.93 (app. d, 3H), 1.41 (app. d, 9H); ¹³C NMR (101 MHz, CDCl₃) δ 194.26 (C), 193.82 (C), 156.27 (C), 155.66 (C), 140.07 (C), 140.00 (C), 133.63 (C),

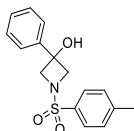
129.44 (CH), 129.24 (CH), 129.12 (CH), 80.28 (C), 80.20 (C), 55.71 (CH₂), 55.12 (CH₂), 35.82 (CH₃), 35.69 (CH₃), 28.45 (CH₃), 28.31 (CH₃); IR (neat) ν = 3060.1 (s), 2951.4 (s), 1689.7 (s), 1627.3 (s, CO), 1584.3 (s), 1396.4 (s), 1218.9 (s), 1069.8 (s), 1004.4 (s), 813.2 (s), 703.33 (s), 551.8 (s) cm⁻¹; HR-MS: calculated for C₁₄H₁₇NO₃³⁵Cl 282.0897, found 282.0883 (Δ = -5 ppm, -1.4 mDa); Melting point: 82-85 °C (crystallised from CHCl₃).



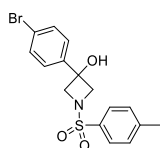
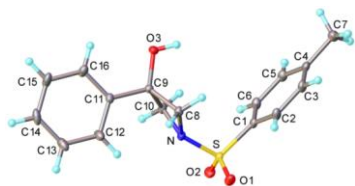
tert-Butyl (2-(4-bromophenyl)-2-oxoethyl)(methyl)carbamate (2-136a). Isolated yield 40%;

¹H NMR (400 MHz, CDCl₃) δ 7.71 – 7.65 (m, 2H), 7.47 (dd, J = 13.5, 8.5 Hz, 2H), 4.48 (d, J = 26.4 Hz, 2H), 2.83 (d, J = 10.2 Hz, 3H), 1.31 (d, J = 48.2 Hz, 9H); ¹³C NMR (101 MHz, CDCl₃) δ 194.08 (C), 193.77 (C), 155.95 (C), 155.39 (C), 133.77 (C), 131.93 (CH), 131.81 (CH), 129.25 (CH), 129.10 (CH), 128.44 (C), 128.39 (C), 79.87 (C), 79.77 (C), 55.43 (CH₂), 54.85 (CH₂), 35.54 (CH₃), 35.45 (CH₃), 28.19 (CH₃), 28.04 (CH₃); IR (neat) ν = 3414.6 (s), 3289.4 (s), 2978.6 (s), 1665.3 (s, CO), 1428.9 (s), 1366.8 (s), 1116.9 (s), 1009.8 (s), 821.2 (s) cm⁻¹; HR-MS: calculated for C₉H₁₁⁷⁹BrNO 228.0024 found, 228.0027 (Δ = 1.3 ppm, 0.3 mDa); Melting point: 90.6-91.9 °C (crystallised from Hexane / EtOAc).

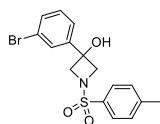
Synthesis of the azetidion-3-ol products (2-95 – 2-139).



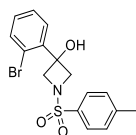
3-Phenyl-1-tosylazetidion-3-ol (2-95).^[1] 0.15 M in CH₃CN, isolated yield 76%; ¹H NMR (400 MHz, DMSO-*d*₆) δ 7.76 (d, J = 8.0 Hz, 2H), 7.53 (d, J = 8.0 Hz, 2H), 7.31 – 7.17 (m, 5H), 6.35 (s, 1H), 3.93 (d, J = 8.5 Hz, 2H), 3.83 (d, J = 8.5 Hz, 2H), 2.47 (s, 3H); ¹³C NMR (101 MHz, DMSO-*d*₆) δ 144.63 (C), 144.13 (C), 130.9 (C), 130.4 (CH), 128.8 (CH), 128.5 (CH), 127.8 (CH), 125.0 (CH), 69.0 (C), 65.7 (CH₂), 21.5 (CH₃); IR (neat) ν = 3478.8 (OH), 3062.7 (s), 2963.6 (CH), 1132.2 (s), 1147.8 (SO), 1184.5 (s), 700.7 (s), 612.9 (s), 670.8 (s), 533.2 (s) cm⁻¹; HR-MS calculated for C₁₆H₁₈NO₃S 304.1007, found 304.1008 (Δ = 0.3 ppm, 0.1 mDa). Melting point: 126.5-128.5 °C (crystallised from EtOAc). X-Ray data: CCDC 1909065; Formula: C₁₆H₁₇NO₃S, Unit Cell Parameters: a 12.8320(9) b 5.7430(4) c 19.8741(14) P21/n.



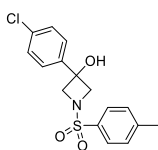
3-(4-Bromophenyl)-1-tosylazetididin-3-ol (2-98). 0.075 M in CH₃CN, isolated yield 70%; ¹H NMR (400 MHz, DMSO-*d*₆) δ 7.74 – 7.69 (m, 2H), 7.47 (ddd, *J* = 9.3, 6.5, 5.3 Hz, 4H), 7.19 – 7.13 (m, 2H), 6.42 (s, 1H), 3.89 (d, *J* = 9.0 Hz, 2H), 3.79 (d, *J* = 9.0 Hz, 2H), 2.44 (s, 3H); ¹³C NMR (101 MHz, DMSO-*d*₆) δ 144.2 (C), 143.1(C), 131.0 (CH), 130.4 (C), 130.0 (CH), 128.36 (CH), 127.0 (CH), 120.5 (C), 68.2 (C), 65.0 (CH₂), 21.0 (CH₃); IR (neat) ν = 3441.2 (m, OH), 2980.6 (w, CH), 1596.8 (w), 1488.7 (m, C=C), 1331.8 (s), 1146.6 (s, SO), 1181.7 (m, C-N), 825.7 (s), 675.6 (s), 617.4 (s), 533.8 (s, C-Br) cm⁻¹; HR-MS calculated for C₁₆H₁₆⁷⁹BrNO₃S 382.0113, found 382.0103 (Δ = -2.6 ppm, -1.0 mDa); Melting point: 160-162 °C (crystallised from EtOAc).



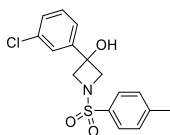
3-(3-Bromophenyl)-1-tosylazetididin-3-ol (2-99). 0.075 M in CH₃CN, isolated yield: 68%; ¹H NMR (400 MHz, CDCl₃) δ 7.76 (d, *J* = 7.8 Hz, 2H), 7.49 – 7.13 (m, 6H), 4.04 (d, *J* = 8.9 Hz, 2H), 3.98 (d, *J* = 8.9 Hz, 2H), 2.48 (s, 3H); ¹³C NMR (101 MHz, CDCl₃) δ 144.7 (C), 144.3 (C), 131.2 (CH), 131.0 (C), 130.2 (CH), 130.0 (CH), 128.4 (CH), 127.8 (CH), 123.2 (CH), 122.8 (C), 69.8 (C), 65.4 (CH₂), 21.7 (CH₃); IR (neat) ν = 3468.2 (w, OH), 1595.0 (w), 1561.0 (w), 1333.0 (m, SO₂), 1183.8 (s, CN), 1148.8 (s, SO₂), 792.0 (s, CBr), 672.9 (s), 611.8 (s), 533.2 (s) cm⁻¹; HR-MS calculated for C₁₆H₁₇NO₃S⁷⁹Br 382.0113, found 382.0107 (Δ = -1.6 ppm, -0.6 mDa).



3-(1-Bromophenyl)-1-tosylazetididin-3-ol (2-100). 0.15 M in CH₃CN, isolated yield: 40%; ¹H NMR (400 MHz, CDCl₃) δ 7.71 (d, *J* = 8.3 Hz, 2H), 7.55 – 7.50 (m, 1H), 7.32 – 7.22 (m, 3H), 7.20 – 7.12 (m, 2H), 4.35 (d, *J* = 9.9 Hz, 2H), 4.08 (d, *J* = 9.9 Hz, 2H), 2.39 (s, 3H); ¹³C NMR (101 MHz, CDCl₃) δ 144.37 (C), 139.37 (C), 134.23 (CH), 131.56 (C), 130.30 (CH), 129.87 (CH), 128.38 (CH), 127.81 (CH), 127.46 (CH), 121.61 (C), 72.60 (C), 62.50 (CH₂), 21.66 (CH₃); IR (neat) ν = 3467.2 (w), 3065.8 (w), 2995.8 (w), 1337.7 (m), 1157.3 (s), 716.7 (m), 675.2 (s), 550.7 (m) cm⁻¹; HR-MS calculated for C₁₆H₁₇NO₃S⁷⁹Br 382.0113, found 382.0130 (Δ = 4.5 ppm, 1.7 mDa).

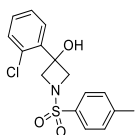


3-(4-Chlorophenyl)-1-tosylazetididin-3-ol (2-101). 0.075 M in CH₃CN, isolated yield: 71%; ¹H NMR (400 MHz, *d*₆-DMSO) δ 7.74 (d, *J* = 8.2 Hz, 2H), 7.51 (d, *J* = 8.2 Hz, 2H), 7.37 – 7.31 (d, *J* = 8.7 Hz, 2H), 7.28 – 7.22 (d, *J* = 8.7 Hz, 2H), 6.44 (s, 1H), 3.92 (d, *J* = 9.0 Hz, 2H), 3.82 (d, *J* = 9.0 Hz, 2H), 2.46 (s, 3H); ¹³C NMR (101 MHz, *d*₆-DMSO) δ 144.2 (C), 142.7 (C), 132.0 (C), 130.4 (C), 129.9 (CH), 128.3 (CH), 128.1 (CH), 126.6 (CH), 68.2 (C), 65.1 (CH₂), 21.0 (CH₃); IR ν = 3640.6 (w, OH), 2975.6 (w), 1490.3 (m, SO₂), 1329.7 (s, SO₂), 1311.6 (s, CN), 1182.7 (m), 1149.9 (s), 1087.2 (s), 1149.9 (s), 1087.2 (s), 812.11 (s), 827.1 (s), 673.6 (s, CCl) cm⁻¹; Melting point: 173-175 °C (crystallised from EtOAc); HR-MS: calculated for C₁₆H₁₇³⁵ClNO₃S 338.0618, found 338.0623 (Δ = 1.5 ppm, -0.5 mDa).

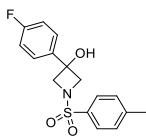


3-(3-Chlorophenyl)-1-tosylazetididin-3-ol (2-102). 0.075 M in CH₃CN, isolated yield: 73 %; ¹H NMR (400 MHz, CDCl₃) δ 7.77 (d, *J* = 8.3 Hz, 2H), 7.41 (d, *J* = 8.3 Hz, 2H), 7.27 – 7.23 (m, 3H), 7.19 (m, 1H), 4.05 (d, *J* = 9.3 Hz, 2H), 3.99 (d, *J* = 9.3 Hz, 2H), 2.48 (s, 3H); ¹³C NMR (101 MHz, CDCl₃) δ 144.8 (C), 144.2 (C), 134.7 (C), 131.1 (C), 130.1 (CH), 130.0 (CH), 128.6 (CH), 128.3 (CH), 125.0 (CH), 122.8 (CH), 70.0 (C), 65.6 (CH₂), 21.8 (CH₃); IR (neat) ν = 3447.1 (m, OH), 3063.1 (w), 2925.2 (w), 1421.5 (m), 1333.0 (s, SO₂), 1301.77 (m), 1185.2 (s, CN), 1147.3 (s, SO₂), 1596.5 (m), 1569.0 (w), 532.9 (s, CCl) cm⁻¹; Melting point: 128-131 °C (crystallised from

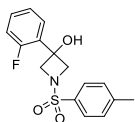
EtOAc); HR-MS calculated for $C_{16}H_{17}^{35}ClNO_3S$ 338.0618, found 338.0619 ($\Delta = 0.3$ ppm, -0.1 mDa).



3-(2-Chlorophenyl)-1-tosylazetididin-3-ol (2-103). 0.15 M in CH_3CN , isolated yield: 61%; 1H NMR (400 MHz, $CDCl_3$) δ 7.73 (d, $J = 8.1$ Hz, 2H), 7.40 – 7.16 (m, 6H), 4.40 – 4.32 (m, 2H), 4.09 – 4.03 (m, 2H), 2.41 (s, 3H); ^{13}C NMR (101 MHz, $CDCl_3$) δ 144.39 (C), 137.89 (C), 132.58 (C), 131.73 (C), 130.90 (CH), 130.22 (CH), 129.89 (CH), 128.44 (CH), 127.33 (CH), 127.18 (CH), 71.60 (C), 62.58 (CH_2), 21.72 (CH_3); IR (neat) $\nu = 3459.2$ (w), 1596.5 (w), 1337.6 (m), 1155.0 (s), 1080.0 (m), 880.8 (m), 777.5 (m), 676.3 (s), 676.3 (s), 547.9 (s), 522.7 (s), 460.3 (m) cm^{-1} ; HR-MS calculated for $C_{16}H_{17}ClNO_3S$ 338.0618, found 338.0618 ($\Delta = 0.0$ ppm, 0.0 mDa).

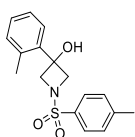


3-(4-Fluorophenyl)-1-tosylazetididin-3-ol (2-104). 0.15 M in acetone, isolated yield 75%; 1H NMR (400 MHz, $CDCl_3$) δ 7.76 (d, $J = 8.3$ Hz, 2H), 7.39 (d, $J = 8.3$ Hz, 2H), 7.35 – 7.27 (m, 2H), 6.99 (t, $J = 8.7$ Hz, 2H), 4.06 (d, $J = 9.0$ Hz, 2H), 3.97 (d, $J = 9.0$ Hz, 2H), 2.47 (s, 3H); ^{13}C NMR (101 MHz, $CDCl_3$) δ 162.5 (C, d, $J = 247$ Hz), 144.6 (C), 138.1 (C, d, $J = 3.3$ Hz), 131.3 (C), 129.8 (CH), 129.5 (CH, d, $J = 144$ Hz), 126.5 (CH, d, $J = 8.2$ Hz), 115.6 (CH, d, $J = 21.5$ Hz), 70.1 (C), 65.5 (CH_2), 21.7 (CH_3); IR (neat) $\nu = 3450.0$ (w, OH), 2985.4 (w), 2865.0 (w), 1608.0 (w), 1597.2 (w), 1513.4 (m), 1333.7 (s), 1228.0 (m, CF), 1148.2 (s, SO_2), 1181.5 (m, CN), 832.8 (s), 674.8 (s), 514.4 (s) cm^{-1} ; HR-MS calculated for $C_{16}H_{17}FNO_3S$ 322.0913, found 322.0912 ($\Delta = -0.3$ ppm, -0.1 mDa); Melting point: 131-133 °C (crystallised from EtOAc).

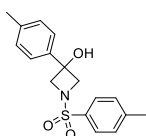


3-(2-Fluorophenyl)-1-tosylazetididin-3-ol (2-105). 0.075 M in CH_3CN , isolated yield 72%; 1H NMR (400 MHz, $CDCl_3$) δ 7.72 (d, $J = 8.3$ Hz, 2H), 7.35 – 7.26 (m, 3H), 7.23 (td, $J = 7.7, 1.4$ Hz,

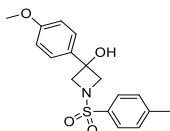
1H), 7.10 (td, $J = 7.7, 1.4$ Hz, 1H), 7.02 (ddd, $J = 11.2, 7.7, 1.4$ Hz, 1H), 4.28 (dd, $J = 9.8, 0.8$ Hz, 2H), 4.01 (dd, $J = 9.8, 0.8$ Hz, 2H) 2.42 (s, 3H); ^{13}C NMR (101 MHz, CDCl_3) δ 160.58 (d, $J = 247.5$ Hz, C), 144.41 (C), 131.57 (C), 130.69 (d, $J = 8.6$ Hz, CH), 129.89 (CH), 128.45 (CH), 128.06 (d, $J = 12.5$ Hz, C), 127.16 (d, $J = 3.7$ Hz, CH), 124.50 (CH), 116.40 (d, $J = 21.5$ Hz, CH), 69.32 (C), 63.24 (CH_2), 21.71 (CH_3); IR (neat) $\nu = 3477.4$ (m, OH), 1491.0 (m), 1452.4 (m), 1334.0 (s), 1300.9 (s), 1147.4 (s), 841.3 (s), 815.9 (s), 765.9 (s), 664.9 (s), 616.11 (s), 545.8 (s) cm^{-1} ; HR-MS calculated for $\text{C}_{16}\text{H}_{17}\text{FNO}_3\text{S}$ 322.0913, found 322.0922 ($\Delta = 2.8$ ppm, 0.9 mDa).



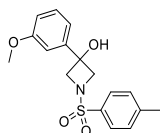
3-(2-Methyl)-1-tosylazetididin-3-ol (2-106). 0.15 M in CH_3CN , isolated yield 30%; ^1H NMR (400 MHz, CDCl_3) δ 7.74 (d, $J = 8.3$ Hz, 2H), 7.36 – 7.25 (m, 3H), 7.14 (dd, $J = 7.6, 1.7$ Hz, 1H), 6.95 – 6.86 (m, 2H), 4.22 (d, $J = 9.6$ Hz, 2H), 3.94 (d, $J = 9.6$ Hz, 2H), 3.82 (s, 3H), 2.42 (s, 3H); ^{13}C NMR (101 MHz, CDCl_3) δ 156.72 (C), 144.15 (C), 131.72 (C), 129.92 (CH), 129.81 (CH), 128.86 (C), 128.47 (CH), 125.86 (CH), 120.97 (CH), 111.10 (CH), 70.25 (C), 62.80 (CH_2), 55.50 (CH_3), 21.69 (CH_3); IR (neat) $\nu = 3466.37$ (w), 1337.1 (m), 1156.0 (s), 1089.8 (m), 760.82 (m), 727.2 (m), 666.5 (s), 549.2 (s), 539.4 (s), 514.6 (m), 457.3 (m) cm^{-1} ; HR-MS calculated for $\text{C}_{17}\text{H}_{20}\text{NO}_3\text{S}$ 338.1164, found 338.1174 ($\Delta = 3.1$ ppm, 1.0 mDa).



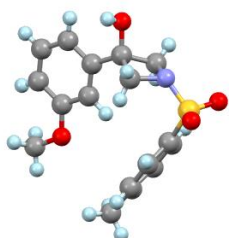
3-(4-Methyl)-1-tosylazetididin-3-ol (2-107). 0.15 M in CH_3CN , isolated yield 85%; ^1H NMR (400 MHz, $\text{DMSO}-d_6$) δ 7.75 (d, $J = 8.0$ Hz, 2H), 7.53 (d, $J = 8.0$ Hz, 2H), 7.10 – 7.03 (m, 4H), 6.29 (s, 1H), 3.89 (d, $J = 8.5$ Hz, 2H), 3.81 (d, $J = 8.5$ Hz, 2H), 2.47 (s, 3H), 2.26 (s, 3H); ^{13}C NMR (101 MHz, $\text{DMSO}-d_6$) δ 181.86 (C), 178.44 (C), 174.18 (C), 168.11 (C), 167.68 (CH), 166.32 (CH), 166.07 (CH), 162.25 (CH), 106.20 (C), 103.04 (CH_2), 58.76 (CH_3), 58.22 (CH_3); IR (neat) $\nu = 3472.4$ (m), 1330.9 (s), 1181.2 (s), 1148.1 (s), 814.4 (s), 710.1 (m), 678.8 (s), 603.9 (s), 547.5 (s), 516.0 (s), 456.6 (m) cm^{-1} ; HR-MS calculated for $\text{C}_{17}\text{H}_{20}\text{NO}_3\text{S}$ 318.1164, found 318.1163 ($\Delta = -0.3$ ppm, -0.1 mDa); Melting point: 141.0-143.5 $^\circ\text{C}$ (crystallised from CH_3CN).

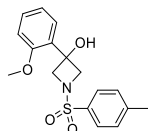


3-(4-Methoxyphenyl)-1-tosylazetididin-3-ol (2-108). 0.15 M in CH₃CN, isolated yield 72%; ¹H NMR (400 MHz, CDCl₃) δ 7.74 (d, *J* = 8.0 Hz, 2H), 7.37 (d, *J* = 8.0 Hz, 2H), 7.22 (d, *J* = 8.8 Hz, 2H), 6.82 (d, *J* = 8.8 Hz, 2H), 4.06 (d, *J* = 9.3 Hz, 2H), 3.93 (d, *J* = 9.3 Hz, 2H), 3.78 (s, 3H), 2.46 (s, 3H); ¹³C NMR (101 MHz, CDCl₃) δ 159.4 (C), 144.5 (C), 134.3 (C), 131.4 (C), 129.9 (CH), 128.5 (CH), 126.0 (CH), 114.0 (CH), 70.3 (C), 65.3 (CH₂), 55.4 (CH₃), 21.7 (CH₃); IR (neat) ν = 3457.9 (OH), 2979.7 (s), 1517.1 (s), 1330.1 (s), 1146.9 (s, SO₂), 1146.9 (s), 829.8 (s), 677.4 (s), 526.9 (s) cm⁻¹; HR-MS calculated for C₁₇H₁₉NO₄S 334.1117, found 334.1113 (Δ = 4.12 ppm, 0.4 mDa); Melting point: 141.7-142.9 °C (crystallised from Hexane / EtOAc).

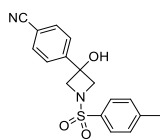
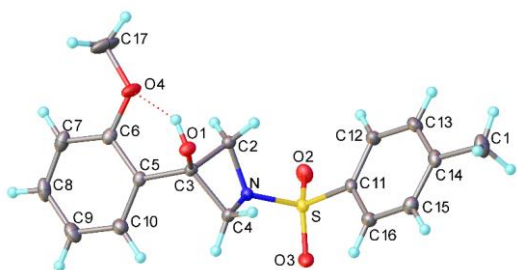


3-(3-Methoxyphenyl)-1-tosylazetididin-3-ol (2-109). 0.15 M in CH₃CN, isolated yield 75%; ¹H NMR (400 MHz, CDCl₃) δ 7.79 (d, *J* = 7.8 Hz, 2H), 7.42 (d, *J* = 7.8 Hz, 2H), 7.34 – 7.21 (m, 1H), 6.96 – 6.79 (m, 3H), 4.12 (d, *J* = 8.2 Hz, 2H), 3.99 (d, *J* = 8.2 Hz, 2H), 3.80 (s, 3H), 2.50 (s, 3H); ¹³C NMR (101 MHz, CDCl₃) δ 159.96 (C), 144.60 (C), 143.70 (C), 131.33 (C), 130.03 (CH), 129.95 (CH), 128.64 (CH), 116.84 (CH), 113.54 (CH), 110.63 (CH), 70.50 (C), 65.39 (CH₂), 55.42 (CH₃), 21.77 (CH₃); IR (neat) ν = 3849.9 (m, OH), 1581.2 (m), 1435.8 (m), 1332.6 (s), 1156.0 (s), 1045.5 (s), 804.1 (s), 782.6 (s), 619.6 (s), 547.2 (s), 520.2 (s) cm⁻¹; HR-MS calculated for C₁₇H₂₀NO₄S 334.1113, found 334.1101 (Δ = -0.12 ppm, -1.2 mDa); X-Ray data: CCDC 1909067; Formula: C₁₇H₁₉NO₄S, Unit Cell Parameters: a 14.0517(6) b 18.3265(8) c 6.2061(3) Pna21.



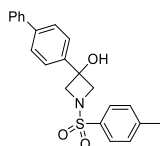


3-(2-Methoxyphenyl)-1-tosylazetididin-3-ol (2-110). 0.15 M in CH₃CN, isolated yield 82%; ¹H NMR (400 MHz, CDCl₃) δ 7.74 (d, *J* = 8.3 Hz, 2H), 7.36 – 7.24 (m, 3H), 7.14 (dd, *J* = 7.6, 1.7 Hz, 1H), 6.96 – 6.85 (m, 2H), 4.22 (d, *J* = 9.6 Hz, 2H), 3.94 (d, *J* = 9.6 Hz, 2H), 3.82 (s, 3H), 2.42 (s, 3H); ¹³C NMR (101 MHz, CDCl₃) δ 156.72 (C), 144.15(C), 131.72 (C), 129.92 (CH), 129.81 (CH), 128.86 (C), 128.47 (CH), 125.86 (CH), 120.97 (CH), 111.10 (CH), 70.25 (C), 62.80 (CH₂), 55.50 (CH₃), 21.69 (CH₃); IR (neat) ν = 3454.6 (w), 1596.3 (w), 1489.7 (w), 1434.6 (w), 1322.9 (m), 1339.4 (s), 1150.9 (s), 1144.5 (s), 1126.8 (s), 1089.3 (s), 991.8 (s), 817.5 (s), 755.6 (s), 688.8 (s), 617.5 (s), 507.6 (s) cm⁻¹; HR-MS calculated for C₁₇H₁₉NO₄S 318.1164, found 318.1174 (Δ = 3.1 ppm, 1.0 mDa); Melting point 136.6-138.0 °C (crystallised EtOAc-Hexane); X-Ray data: CCDC 1909066; Formula: C₁₇H₁₉NO₄S, Unit Cell Parameters: a 8.1107(4) b 15.4959(7) c 25.5787(11) Pbca.

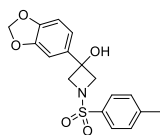


4-(3-Hydroxy-1-tosylazetididin-3-yl)benzonitrile (2-111). 0.15 M in CH₃CN, isolated yield 60%; ¹H NMR (400 MHz, DMSO-*d*₆) δ 7.78 (d, *J* = 8.4 Hz, 2H), 7.74 (d, *J* = 8.1 Hz, 2H), 7.51 (d, *J* = 8.1 Hz, 2H), 7.45 (d, *J* = 8.4 Hz, 2H), 6.61 (s, 1H), 3.95 (d, *J* = 8.8 Hz, 2H), 3.84 (d, *J* = 8.8 Hz, 2H), 2.46 (s, 3H); ¹³C NMR (101 MHz, DMSO-*d*₆) δ 149.09 (C), 144.36 (C), 132.28 (CH), 130.43 (C), 130.07 (CH), 128.40 (CH), 125.77 (CH), 118.68 (C), 110.26 (C), 68.37 (C), 64.99 (CH₂), 21.13

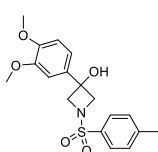
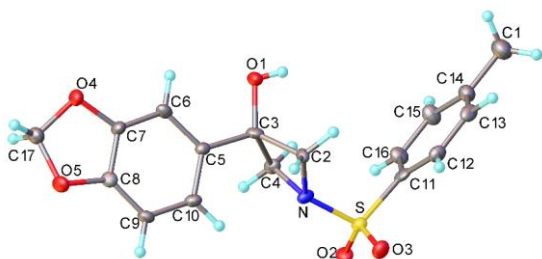
(CH₃); IR (neat) ν = 3420.7 (OH), 2230.8 (s, CN), 1517.1 (s), 1324.3 (s), 1162.3 (s, SO₂), 542.3 (s) cm⁻¹; HR-MS calculated for C₁₇H₁₇N₂O₃S 329.1000, found 329.0966 (Δ = 4.0 ppm, 0.6 mDa).



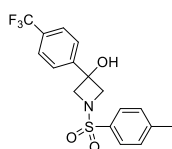
3-((1,1'-Biphenyl)-4-yl)-1-tosylazetididin-3-ol (2-112). 0.075 M in CH₃CN, isolated yield 55%; ¹H NMR (400 MHz, DMSO-*d*₆) δ 7.77 (d, *J* = 7.7 Hz, 2H), 7.67 – 7.50 (m, 6H), 7.46 (t, *J* = 7.7 Hz, 2H), 7.34 (m, 3H), 6.41 (s, 1H), 3.98 (d, *J* = 8.5 Hz, 2H), 3.87 (d, *J* = 8.5 Hz, 2H), 2.45 (s, 3H); ¹³C NMR (101 MHz, DMSO-*d*₆) δ 144.18 (C), 142.85 (C), 139.63 (C), 139.22 (C), 130.57 (C), 130.01 (CH), 128.94 (CH), 128.38 (CH), 127.49 (CH), 126.60 (CH), 126.44 (CH), 125.31 (CH), 68.53 (CH), 65.26 (CH₂), 21.10 (CH₃); IR (neat) ν = 3100.8 (OH), 1323.1 (s), 1150.7 (s), 758.5 (s), 541.99 (s) cm⁻¹; HR-MS calculated for C₂₂H₂₂NO₃S 380.1320, found 380.1325 (Δ = 1.3 ppm, 0.5 mDa); Melting point: 170-172.8 °C (crystallised from CHCl₃).



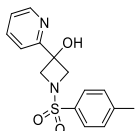
3-(Benzo[d][1,3]dioxol-5-yl)-1-tosylazetididin-3-ol (2-113). 0.15 M in CH₃CN (Flow rate 0.7 mL/min), isolated yield 48%; ¹H NMR (400 MHz, DMSO-*d*₆) δ 7.74 (d, *J* = 7.8 Hz, 2H), 7.51 (d, *J* = 7.8 Hz, 2H), 6.79 (d, *J* = 8.2 Hz, 1H), 6.69 (dd, *J* = 8.2, 1.9 Hz, 1H), 6.55 (s, 1H), 6.30 (s, 1H), 5.98 (s, 2H), 3.88 (d, *J* = 8.6 Hz, 2H), 3.78 (d, *J* = 8.6 Hz, 2H), 2.45 (s, 3H); ¹³C NMR (101 MHz, DMSO-*d*₆) δ 147.23 (C), 146.37 (C), 144.23 (C), 137.66 (C), 130.46 (C), 129.99 (CH), 128.35 (CH), 118.03 (CH), 107.64 (CH), 105.43 (CH), 101.02 (CH₂), 68.69 (C), 65.30 (CH₂), 21.09 (CH₃); IR (neat) ν = 3458.5 (w), 3356.2 (w), 3259.6 (w), 1596.1 (w), 1492.9 (m), 1147.4 (m), 813.5 (s), 671.0 (s), 524.02 (s), 504.03 (s) cm⁻¹; HR-MS calculated for C₁₇H₁₈NO₅S 348.0906, found 348.0925 (Δ = 5.5 ppm, 1.5 mDa); Melting point: 134-137.0 °C (crystallised MeOH-Et₂O); X-Ray data: CCDC 1909064; Formula: C₁₇H₁₇NO₅S, Unit Cell Parameters: a 11.9795(10) b 5.7940(4) c 22.8815(16) P21/n.



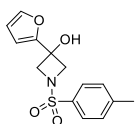
3-(3,4-Dimethoxyphenyl)-1-tosylazetididin-3-ol (2-114) 0.035 in acetone isolated yield 36%; ^1H NMR (400 MHz, CDCl_3) δ 7.75 (d, $J = 7.9$ Hz, 2H), 7.37 (d, $J = 7.9$ Hz, 2H), 6.89 – 6.73 (m, 3H), 4.08 (d, $J = 8.7$ Hz, 2H), 3.94 (d, $J = 8.7$ Hz, 2H), 3.84 (s, 3H), 3.80 (s, 3H), 2.45 (s, 3H); ^{13}C NMR (101 MHz, CDCl_3) δ 149.10 (C), 148.85 (C), 144.49 (C), 134.70 (C), 131.37 (C), 129.95 (CH), 128.58 (CH), 116.99 (CH), 110.96 (CH), 108.07 (CH), 70.38 (C), 65.34 (CH_2), 56.02 (CH_3), 55.97 (CH_3), 21.72 (CH_3); HR-MS calculated for $\text{C}_{18}\text{H}_{22}\text{NO}_5\text{S}$ 364.1219 found 364.1220 ($\Delta = 0.3$ ppm, 0.1 mDa); Melting point: 131-133.0 °C. IR (neat) $\nu = 3101.2$ (OH), 1325.3 (s), 1154.2 (s), 750.0 (s), 540.13 (s) cm^{-1}



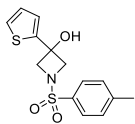
3-(2-Chlorophenyl)-1-tosylazetididin-3-ol (2-115). 0.15 M in CH_3CN , isolated yield 78%; ^1H NMR (400 MHz, CDCl_3) δ 7.78 (d, $J = 8.3$ Hz, 2H), 7.59 (d, $J = 8.3$ Hz, 2H), 7.50 (d, $J = 8.2$ Hz, 2H), 7.41 (d, $J = 8.2$ Hz, 2H), 4.10 (d, $J = 9.5$ Hz, 2H), 4.01 (d, $J = 9.5$ Hz, 2H), 2.49 (s, 3H); ^{13}C NMR (101 MHz, CDCl_3) δ 146.11 (C), 144.89 (C), 131.18 (C), 130.25 (C, q, $J = 36.5$ Hz), 130.13 (CH), 128.58 (CH), 125.67 (CH, q, $J = 3.5$ Hz), 125.11 (CH), 123.9 (C, q, $J = 123.9$ Hz), 69.95 (C), 65.62 (CH_2), 21.77 (CH_3); IR (neat) $\nu = 3462.2$ (w), 1621.30 (w), 1597.8 (w), 1329.2 (s), 1316.8 (s), 1151.6 (s), 1111.0 (s), 1076.5 (s), 1076.5 (s), 1015.6 (m), 840.0 (m), 677.5 (m), 605.8 (m) cm^{-1} ; HR-MS calculated for $\text{C}_{17}\text{H}_{17}\text{NO}_3\text{F}_3\text{S}$ 372.0881, found 372.0880 ($\Delta = -0.3$ ppm, -0.1 mDa).



3-(2-Pyridin)-1-tosylazetididin-3-ol (2-116). 0.075 M in CH₃CN, isolated yield 69%; ¹H NMR (400 MHz, CDCl₃) δ 8.47 (d, *J* = 4.9 Hz, 1H), 7.93 – 7.89 (m, 1H), 7.85 (td, *J* = 7.6, 1.5 Hz, 1H), 7.80 (d, *J* = 8.0 Hz, 2H), 7.43 (d, *J* = 8.0 Hz, 2H), 7.32 (ddd, *J* = 7.6, 4.9, 1.5 Hz, 1H), 4.02 (d, *J* = 8.9 Hz, 2H), 3.95 (d, *J* = 8.9 Hz, 2H), 2.49 (s, 3H); ¹³C NMR (101 MHz, CDCl₃) δ 159.81 (C), 146.82 (CH), 144.64 (C), 138.52 (CH), 130.13 (CH), 128.85 (CH), 123.62 (CH), 119.35 (CH), 114.75 (C), 68.48 (C), 65.72 (CH₂), 21.82 (CH₃); IR (neat) ν = 2948.8 (w), 1595.0 (w), 1343.3 (m), 1161.9 (s), 1091.8 (m), 909.3 (s), 726.5 (s), 670.3 (s), 615.3 (m), 550.7 (s) cm⁻¹; HR-MS calculated for C₁₅H₁₇N₂O₃S 305.0960, found 305.0951 (Δ = -2.9 ppm, -0.9 mDa).

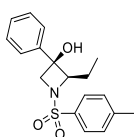
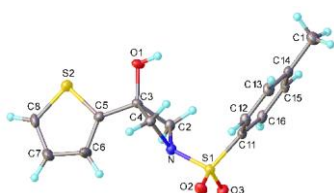


3-(2-Furan)-1-tosylazetididin-3-ol (2-117). 0.02 M in acetone, isolated yield 60%; ¹H NMR (400 MHz, CDCl₃) δ 7.70 (d, *J* = 8.0 Hz, 2H), 7.35 (d, *J* = 8.0 Hz, 1H), 7.23 (dd, *J* = 1.9, 0.9 Hz, 1H), 6.26 (dd, *J* = 3.3, 0.9 Hz, 1H), 6.21 (dd, *J* = 3.3, 0.9 Hz, 1H), 4.08 (d, *J* = 9.4 Hz, 2H), 3.89 (d, *J* = 9.4 Hz, 2H), 2.44 (s, 3H); ¹³C NMR (101 MHz, CDCl₃) δ 153.73 (C), 144.42 (C), 142.67 (CH), 131.16 (C), 129.88 (CH), 128.47 (CH), 110.55 (CH), 106.64 (CH), 66.57 (C), 63.20 (CH₂), 21.67 (CH₃); IR (neat) ν = IR (neat) ν = 3345.4 (m), 3074.5 (w), 2970.1 (w), 2830.3 (w), 1453.8 (m), 1300.7 (m), 1250.3 (m), 1187.3 (m), 1150.7 (s), 1073.8 (s), 1055.4 (s), 1000.6 (m), 830.7 (m), 670.4 (s), 543.5 (s) cm⁻¹; HR-MS calculated for C₁₄H₁₆NO₄S 294.0800, found 294.0811 (Δ = -0.3 ppm, -0.1 mDa).

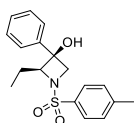
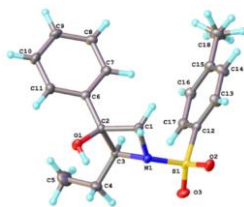


3-(2-Thiophen)-1-tosylazetididin-3-ol (2-118). 0.02 M in acetone (flow = 0.8 mL/ min), isolated yield 68%; ¹H NMR (400 MHz, CDCl₃) δ 7.74 (d, *J* = 8.0 Hz, 2H), 7.38 (d, *J* = 8.0 Hz, 2H), 7.22 (dd, *J* = 5.1, 1.2 Hz, 1H), 6.92 (dd, *J* = 5.1, 1.2 Hz, 1H), 6.83 (dd, *J* = 3.6, 1.2 Hz, 1H), 4.06 (d, *J* = 8.7 Hz, 2H), 4.01 (d, *J* = 8.7 Hz, 2H), 2.46 (s, 3H); ¹³C NMR (101 MHz, CDCl₃) δ 146.70 (C), 144.62

(C), 131.19 (C), 130.03 (CH), 128.61 (CH), 127.30 (CH), 125.66 (CH), 123.87 (CH), 69.07 (C), 65.99 (CH₂), 21.76 (CH₃); IR (neat) ν = 3426.4 (m), 3088.2 (w), 2989.1 (w), 2861.4 (w), 1328.7 (m), 1295.6 (m), 1243.4 (m), 1190.6 (m), 1147.2 (s), 1085.1 (s), 1064.8 (s), 994.2 (m), 913.8 (m), 850.1 (m), 819.9 (m), 783.6 (m), 698.9 (s), 674.7 (s), 616.3 (s), 535.5 (s) cm⁻¹; HR-MS calculated for C₁₄H₁₅NO₃S₂ 310.0572, found 310.0586 (Δ = 4.5 ppm, 1.4 mDa); Melting point: 139-141 °C (crystallised from MeOH / Et₂O); X-Ray data: CCDC 1909072; Formula: C₁₄H₁₅NO₃S₂, Unit Cell Parameters: a 12.1475(6) b 5.7937(3) c 20.2726(9) P21/n.

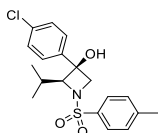
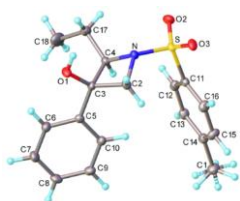


2-Ethyl-3-phenyl-1-tosylazetid-3-ol (2-119). 0.15 M in CH₃CN (0.8 mL/min), isolated yield 34%; ¹H NMR (400 MHz, DMSO-*d*₆) δ 7.76 (d, *J* = 8.1 Hz, 2H), 7.53 (d, *J* = 8.1 Hz, 2H), 7.15 – 7.05 (m, 3H), 6.69 (dd, *J* = 8.0, 1.7 Hz, 1H), 6.31 (s, 1H), 3.82 (d, *J* = 9.5 Hz, 2H), 3.77 (d, *J* = 9.5 Hz, 2H), 3.67 (dd, *J* = 9.5, 4.8 Hz, 1H), 2.48 (s, 3H), 2.03 (m, 1H), 1.71 (ddd, *J* = 10.6, 7.5, 4.8 Hz, 1H), 0.69 (t, *J* = 7.5 Hz, 3H); ¹³C NMR (101 MHz, DMSO-*d*₆) δ 144.23 (C), 144.00 (C), 130.60 (C), 129.98 (CH), 128.40 (CH), 127.91 (CH), 126.94 (CH), 124.49 (CH), 76.19 (CH), 71.10 (C), 63.11 (CH₂), 22.78 (CH₂), 21.04 (CH₃), 9.51 (CH₃); IR (neat) ν = 3437.0 (m, OH), 3054.7 (w), 2965.2 (w), 2877.9 (w) 1329.5 (s), 1149.2 (s), 1084.9 (s), 831.6 (m), 815.5 (m) 756.4 (s), 703.1 (s), 674.2 (s), 613.4 (s) cm⁻¹; HR-MS calculated for C₁₈H₂₂NO₃S 332.1320, found 332.1327 (Δ = 2.1 ppm, 0.7 mDa); Melting point: 149.5-150.8 °C (crystallised from CHCl₃); X-Ray data: CCDC 1909064; Formula: C₁₈H₂₂NO₃S, Unit Cell Parameters: a 9.1996(5) b 9.8006(5) c 10.3959(6) P-1.



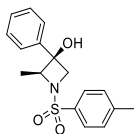
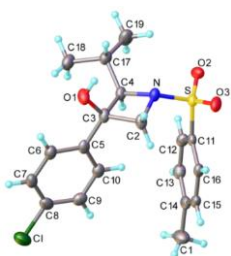
2-Ethyl-3-phenyl-1-tosylazetid-3-ol (2-120). 0.15 M in CH₃CN (0.8 mL/min), isolated yield 32%; ¹H NMR (400 MHz, CDCl₃) δ 7.77 (d, *J* = 8.0 Hz, 2H), 7.39 (d, *J* = 8.0 Hz, 2H), 7.23 – 7.13 (m, 3H), 6.96 – 6.88 (m, 2H), 4.01 – 3.85 (m, 3H), 2.49 (s, 3H), 2.05 (m, 1H), 1.91 (m, 1H), 0.81 (t, *J* = 7.5 Hz, 3H); ¹³C NMR (101 MHz, CDCl₃) δ 144.38 (C), 142.44 (C), 131.86 (C), 129.95 (CH), 128.60 (CH), 128.50 (CH), 127.73 (CH), 124.74 (CH), 76.00 (CH), 73.09 (C), 63.65 (CH₂), 23.28 (CH₂), 21.73 (CH₃), 9.88 (CH₃); IR (neat) ν = 3454.0 (m, OH), 2966.2 (w), 2877.7 (w), 1596.8 (w), 1404.8 (w), 1328.2 (s), 1157.6 (s), 1096.8 (s), 896.5 (w), 846.7 (w), 821.7 (m), 746.6 (s), 706.2 (s), 668.1 (s), 551.6 (s), 534.7 (s) cm⁻¹; HR-MS calculated for C₁₈H₂₂NO₃S 332.1320, found 332.1326 (Δ = 1.8 ppm, 0.6 mDa); Melting point: 156-158 °C (MeOH); X-Ray data: CCDC 1909074; Formula: C₁₈H₂₂NO₃S, Unit Cell Parameters: a 9.2258(11) b 9.8099(14) c 10.3977(13)

P-1.

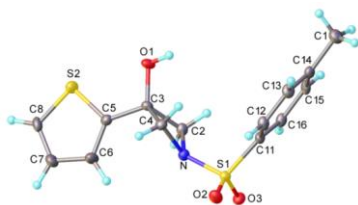


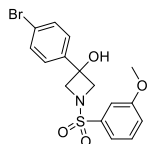
3-(4-Chlorophenyl)-2-isopropyl-1-tosylazetid-3-ol (2-121). 0.15 M in CH₃CN (0.5 mL/min), isolated yield 30%; ¹H NMR (400 MHz, CDCl₃) δ 7.72 (d, *J* = 8.0 Hz, 2H), 7.34 (d, *J* = 8.0 Hz, 2H), 7.14 (d, *J* = 8.6 Hz, 2H), 6.87 (d, *J* = 8.6 Hz, 2H), 4.06 (d, *J* = 10.0 Hz, 1H), 3.91 (dd, *J* = 10.0, 1.1

Hz, 1H), 3.79 (dd, $J = 10, 1.1$ Hz, 1H), 2.48 (s, 3H), 2.29 (m, 1H), 1.13 (d, $J = 6.8$ Hz, 3H), 0.84 (d, $J = 6.8$ Hz, 3H); ^{13}C NMR (101 MHz, CDCl_3) δ 144.49 (C), 141.43 (C), 133.73 (C), 132.49 (C), 129.89 (CH), 128.69 (CH), 128.65 (CH), 126.43 (CH), 80.28 (CH), 72.80 (C), 64.27 (CH_2), 29.38 (CH), 21.75 (CH_3), 19.45 (CH_3), 19.10 (CH_3); IR (neat) $\nu = 3444.2$ (w, OH), 2960.6 (w), 2875.4 (w), 1331.9 (m), 1115.4 (s), 1088.7 (s), 908.1 (m), 814.9 (s), 729.4 (s), 409.4 (s) cm^{-1} ; HR-MS calculated for $\text{C}_{19}\text{H}_{23}\text{NO}_3\text{S}^{35}\text{Cl}$ 380.1087, found 380.1097 ($\Delta = 2.6$ ppm, 1 mDa); Melting point: 194-196 °C (crystallised from MeOH); X-Ray data: CCDC 1909074; Formula: $\text{C}_{19}\text{H}_{22}\text{NO}_3\text{S}$, Unit Cell Parameters a 11.3556(5) b 9.6431(5) c 17.4421(8) P21/n.

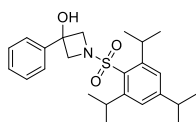


2-Methyl-3-(*p*-tolyl)-1-tosylazetid-3-ol (2-122). 0.075 M in CH_3CN , isolated yield 47%; ^1H NMR (400 MHz, CDCl_3) δ 7.76 (d, $J = 8.2$ Hz, 2H), 7.38 (d, $J = 7.9$ Hz, 2H), 7.01 (d, $J = 7.9$ Hz, 2H), 6.82 (d, $J = 8.2$ Hz, 2H), 4.14 (q, $J = 6.5$ Hz, 1H), 3.95 – 3.85 (m, 2H), 2.48 (s, 3H), 2.28 (s, 3H), 1.41 (d, $J = 6.5$ Hz, 3H); ^{13}C NMR (101 MHz, CDCl_3) δ 144.3 (C), 138.8 (C), 137.8 (C), 131.9 (C), 129.9 (CH), 129.2 (CH), 128.5 (CH), 124.7 (CH), 73.1 (C), 70.5 (CH), 63.0 (CH_2), 21.7 (CH_3), 21.0 (CH_3), 14.4 (CH_3); IR (neat) $\nu = 3457.0$ (br. OH), 2985.4 (s), 28.65.0 (s, SO), 1228.0 (s, CF), 1181.5 (s), 832.8 (s), 674.8 (s), 514.4 (s) cm^{-1} ; HR-MS calculated for $\text{C}_{18}\text{H}_{22}\text{NO}_3\text{S}$ 332.1320, found 332.1326 ($\Delta = 1.8$ ppm); Melting point: 108-110 °C (crystallised from MeOH).

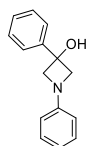




3-(4-Bromophenyl)-1-((3-methoxyphenyl)sulfonyl)azetidin-3-ol (2-123). 0.15 M in CH₃CN, isolated yield 63%; ¹H NMR (400 MHz, CDCl₃) δ 7.48 (t, *J* = 8.0 Hz, 1H), 7.39 (t, *J* = 8.0 Hz, 3H), 7.34 – 7.27 (m, 1H), 7.22 – 7.10 (m, 3H), 4.01 (s, 4H), 3.85 (s, 3H); ¹³C NMR (101 MHz, CDCl₃) δ 160.20 (C), 141.36 (C), 135.33 (C), 131.72 (CH), 130.50 (CH), 126.45 (CH), 122.12 (C), 120.57 (CH), 119.81 (CH), 113.29 (CH), 69.86 (C), 65.58 (CH₂), 55.88 (CH₃); IR (neat) ν = 3429.3 (w, OH), 3069.7 (w), 1594.4 (m), 1479.8 (m), 1241.6 (s), 1148.4 (s), 1037.9 (s), 907.3 (m), 726.1 (s), 697.9 (s), 983.8 (s), 588.5 (s) cm⁻¹; HR-MS: calculated for C₁₇H₁₇NO₄S⁷⁹Br 398.0062, found 398.0068 (Δ = 3.8 ppm, 0.6 mDa).

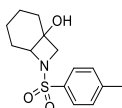


3-Phenyl-1-((2,4,6-triisopropylphenyl)sulfonyl)azetidin-3-ol (2-124). 0.15 M in CH₃CN, isolated yield 64%; ¹H NMR (400 MHz, CDCl₃) δ 7.58 (d, *J* = 7.2 Hz, 2H), 7.37 (t, *J* = 7.2 Hz, 2H), 7.30 (t, *J* = 7.2 Hz, 1H), 7.18 (s, 2H), 4.31 – 4.08 (m, 6H), 2.98 – 2.85 (m, 1H), 1.27 (m, 18H); ¹³C NMR (101 MHz, CDCl₃) δ 153.61 (C), 151.77 (C), 150.67 (C), 142.65 (C), 128.69 (CH), 128.11 (CH), 124.67 (CH), 123.98 (CH), 70.18 (C), 63.92 (CH₂), 34.32 (CH), 29.80 (CH), 25.03 (CH₃), 23.66 (CH₃); IR (neat) ν = 3478.5 (w), 1340.4, 1170.8 (s), 901.7 (m), 666.4 (s), 540.4 (s), 520.3 (m) cm⁻¹; HR-MS calculated for C₂₄H₃₄NO₃S 416.2259, found 416.2263 (Δ = 4.5 ppm, 0.4 mDa).

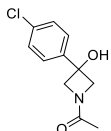
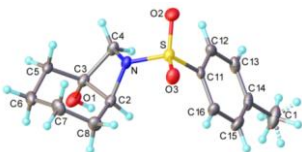


1,3-Diphenylazetidin-3-ol (2-126).^[5] 0.15 M in CH₃CN, isolated yield 28%; ¹H NMR (400 MHz, CDCl₃) δ 7.67 – 7.59 (m, 2H), 7.48 – 7.39 (m, 2H), 7.40 – 7.32 (m, 1H), 7.32 – 7.25 (m, 2H), 6.83 (tt, *J* = 7.6, 1.1 Hz, 1H), 6.58 (dd, *J* = 7.6, 1.1 Hz, 2H), 4.29 (dd, *J* = 7.7, 0.9 Hz, 2H), 4.13 (dd, *J* = 7.7, 0.9 Hz, 2H); ¹³C NMR (101 MHz, CDCl₃) δ 151.35 (C), 143.6 (C), 129.1 (CH), 128.7 (CH), 127.8 (CH), 124.8 (CH), 118.2 (CH), 112.1 (CH), 72.4 (C), 67.2 (CH₂); HR-MS calculated for

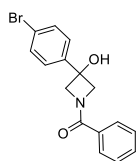
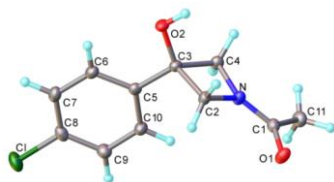
C₁₅H₁₆NO 226.1232, found 226.1245 (Δ = 3.6 ppm, 0.7 mDa); Melting point: 77-80 °C (crystallised from MeOH).



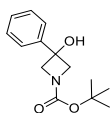
7-Tosyl-7-azabicyclo[4.2.0]octan-1-ol (2-130). 0.075 M in MeOH, isolated yield 40%; ¹H NMR (400 MHz, CDCl₃) δ 7.65 (d, J = 8.1 Hz, 1H), 7.33 (d, J = 8.1 Hz, 1H), 3.53 (m, 1H), 3.47 (dd, J = 6.7, 0.7 Hz, 1H), 3.18 (d, J = 6.7 Hz, 1H), 1.99 – 1.79 (m, 3H), 1.67 – 1.42 (m, 4H), 1.33 – 1.19 (m, 1H); ¹³C NMR (101 MHz, CDCl₃) δ 144.26 (C), 131.10 (C), 129.82 (CH), 128.58 (CH), 70.11 (CH), 67.57 (C), 63.51 (CH₂), 35.41 (CH₂), 24.80 (CH₂), 21.68 (CH₃), 20.05 (CH₂), 19.62 (CH₂); IR (neat) ν = 3481.6 (w, OH), 2937.2 (w), 1598.6 (w), 1304.6 (m), 1333.9 (m), 1156.2 (s), 1091.2 (m), 816.2 (m), 714.6 (m), 662.7 (s), 599.5 (s), 550.4 (m) cm⁻¹; HR-MS calculated for C₁₄H₂₀NO₃S 282.1164, found 282.1174 (Δ = -4.6 ppm, -1.0 mDa); X-Ray data: CCDC 1909071; Formula: C₁₄H₁₉NO₃S, Unit Cell Parameters: a 5.4874(3) b 11.3120(7) c 22.1706(13) P212121.



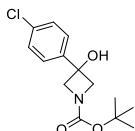
1-(3-(4-Chlorophenyl)-3-hydroxyazetidin-1-yl)ethan-1-one (2-137). 0.075 M in CH₃OH, isolated yield 70%; ¹H NMR (400 MHz, CDCl₃) δ 7.37 (d, J = 8.6 Hz, 2H), 7.28 (d, J = 8.6 Hz, 2H), 4.31 (d, J = 9.1 Hz, 1H), 4.24 (d, J = 9.1 Hz, 1H), 4.14 (s, 2H), 1.82 (s, 3H); ¹³C NMR (101 MHz, CDCl₃) δ 171.38 (C), 142.05 (C), 133.48 (C), 128.60 (CH), 126.17 (CH), 69.77 (C), 66.01 (CH₂), 63.22 (CH₂, rotamer), 19.04 (CH₃); IR (neat) ν = 3186.0 (m), 2979.8 (w), 2937.7 (w), 1607.9 (s, CO), 1484.5 (s), 1422.2 (s), 1244.6 (s), 1008.7 (m), 826.1 (s), 738.5 (s), 535.9 (s), 452.0 (m) cm⁻¹; HR-MS calculated for C₁₁H₁₃NO₂Cl 226.0635, found 226.0638 (Δ = 1.3 ppm, 0.3 mDa); X-Ray data: CCDC 1909066; Formula: C₁₁H₁₂ClNO₂, Unit Cell Parameters: a 10.4122(4) b 10.8600(4) c 10.1440(5) P21/c.



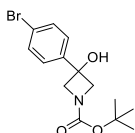
(3-(4-Bromophenyl)-3-hydroxyazetidin-1-yl)(phenyl)methanone (2-138). 0.075 M in CH₃OH, isolated yield 89%; ¹H NMR (599 MHz, DMSO-*d*₆) δ 7.70 (d, *J* = 7.9 Hz, 2H), 7.56 (d, *J* = 7.9 Hz, 2H), 7.53 – 7.49 (m, 3H), 7.46 (t, *J* = 7.5 Hz, 2H), 4.55 (d, *J* = 8.8 Hz, 1H), 4.41 (d, *J* = 8.8 Hz, 1H), 4.27 (app. s, 2H); ¹³C NMR (101 MHz, DMSO-*d*₆) δ 169.47 (C), 143.83 (C), 133.02 (C), 131.14 (CH), 128.49 (CH), 127.87 (CH), 127.19 (CH), 120.46 (CH), 79.26 (C), 70.01 (C), 68.18 (CH₂), 64.09 (CH₂ rotamer); IR (neat) ν = 3294.2 (s), 2980.7 (s), 1685.8 (s), 1602.4 (s, CO), 1447.2 (s), 1245.1 (s), 1156.1 (s), 953.7 (s), 806.2 (s), 645.0 (s), 534.3 (s) cm⁻¹; HR-MS calculated for C₁₆H₁₅NO₂⁷⁹Br 332.0286, found 332.0299 (Δ = 3.9 ppm, 1.3 mDa); Melting point: 88.5-91.0 °C (crystallised from CHCl₃); X-Ray data: CCDC 1909066; Formula: C₁₆H₁₄BrNO₂, Unit Cell Parameters: a 7.1854(6) b 15.5462(11) c 25.176(2) P212121.



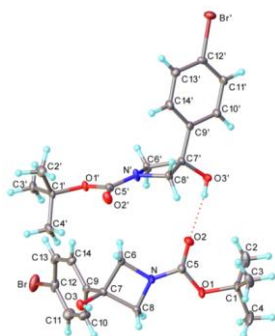
tert-Butyl 3-hydroxy-3-phenylazetidine-1-carboxylate (2-133). 0.075 M in CH₃OH, isolated yield 70%; ¹H NMR (400 MHz, CDCl₃) δ 7.46 (d, *J* = 7.5 Hz, 2H), 7.33 (t, *J* = 7.5 Hz, 2H), 7.28 – 7.22 (m, 1H), 4.16 (q, *J* = 9.1 Hz, 2H), 1.41 (s, 9H); ¹³C NMR (101 MHz, CDCl₃) δ 156.62 (C), 143.68 (C), 128.47 (CH), 127.58 (CH), 124.64 (CH), 80.01 (C), 70.87 (C), 64.45 (CH₂), 28.39 (CH₃); IR (neat) ν = 3385.0 (br., OH), 2975.0 (m), 1675.1 (s, CO), 1393.0 (s), 1366.7 (s), 1154.7 (s), 759.4 (m), 759.4 (m), 730.6 (s), 699.6 (s), 589.5 (w), 549.5 (w), 460.2 (w), 425.9 (w) cm⁻¹; HR-MS calculated for C₉H₁₂NO 150.0919, found 150.0929 (Δ = 6.7 ppm, 1.0 mDa).

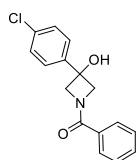


tert-Butyl 3-(4-chlorophenyl)-3-hydroxyazetidine-1-carboxylate (2-134). 0.075 M in CH₃OH, isolated yield 71%; ¹H NMR (400 MHz, DMSO-*d*₆) δ 7.51 (d, *J* = 8.4 Hz, 2H), 7.42 (d, *J* = 8.4 Hz, 2H), 4.13 – 3.87 (m, 4H), 1.40 (s, 9H); ¹³C NMR (101 MHz, DMSO-*d*₆) δ 155.79 (C), 143.71 (C), 131.70 (C), 128.15 (CH), 126.54 (CH), 78.89 (C), 69.25 (C), 64.74 (CH₂), 28.05 (CH₃); IR (neat) ν = 3417.4 (w, OH), 2980.8 (m), 2883.2 (w), 1666.2 (s), 1427.6 (s), 1367.4 (s), 1237.4 (m), 1159.1 (s), 1118.8 (s), 824.1 (m), 765.9 (m), 532.3 (w) cm⁻¹; HR-MS calculated for C₁₀H₉NO₃³⁵Cl (M-trBuO-) 226.0271, found 226.0275 (Δ = 1.8 ppm, 0.4 mDa); Melting point: 138.4-140.8 °C (crystallised from CHCl₃).



tert-Butyl 3-(4-bromophenyl)-3-hydroxyazetidine-1-carboxylate (2-136). 0.075 M in CH₃OH, isolated yield 72%; ¹H NMR (400 MHz, CDCl₃) δ 7.44 (d, *J* = 8.6 Hz, 2H), 7.35 (d, *J* = 8.6 Hz, 2H), 4.14 (d, *J* = 9.3 Hz, 2H), 4.09 (d, *J* = 9.3 Hz, 2H), 1.40 (s, 9H); ¹³C NMR (101 MHz, CDCl₃) δ 156.59 (C), 142.94 (C), 131.53 (CH), 126.51 (CH), 121.52 (C), 80.23 (C), 70.45 (C), 64.47 (CH₂), 28.41 (CH₃); IR (neat) ν = 3414.6 (w, OH), 3289.4 (w), 2978.6 (w), 1665.3 (s, CO), 1428.9 (s), 1366.8 (s), 1234.4 (m, SO₂), 1116.9 (s), 1009.8 (s), 821.2 (s), 529.4 (m) cm⁻¹; HR-MS calculated for C₉H₁₁NO⁷⁹Br (M-trBuO-) 228.0024, found 228.0027 (Δ = 1.3 ppm, 0.3 mDa); Melting point: 158-161 °C (crystallised from CDCl₃); X-Ray data: CCDC 1909076; Formula: C₁₄H₁₈BrNO₃, Unit Cell Parameters: a 10.7025(7) b 11.3028(7) c 12.7165(8) P-1.





(3-(4-Chlorophenyl)-3-hydroxyazetidin-1-yl)phenylmethanone (2-139). ^1H NMR (400 MHz, CDCl_3) δ 7.56 (d, $J = 8.0$ Hz, 2H), 7.41 (m, 5H), 7.31 (d, $J = 8.0$ Hz, 2H), 4.44 (m, 4H); ^{13}C NMR (101 MHz, CDCl_3) δ 170.73 (C), 141.86 (C), 133.75 (C), 132.63 (C), 131.54 (CH), 128.81 (CH), 128.61 (CH), 128.00 (CH), 126.24 (CH), 71.07 (C), 68.85 (CH_2), 64.05 (CH_2); IR (neat) $\nu = 3290.6$ (s), 2977.3 (s), 1690.4 (s), 1609.7 (s, CO), 1460.3 (s), 1245.1 (s), 970.8 (s), 806.2 (s), 670.0 (s), 542.7 (s) cm^{-1} ; HR-MS calculated for $\text{C}_{16}\text{H}_{15}\text{NO}_2\text{Cl}$ 288.0791, found 288.0793 ($\Delta = 0.7$ ppm, 0.2 mDa).

3. Chapter 3: The rearrangement of 3-hydroxyazetidines to 2-oxazolines

3.1 INTRODUCTION: General Oxazoline Synthesis and Applications

Oxazolines are a class of 5 membered ring heterocycles which along with the less oxidised structural analogues oxazolidines and oxazoles share the same 1,3 distributed nitrogen and oxygen ring pattern (Figure 1)

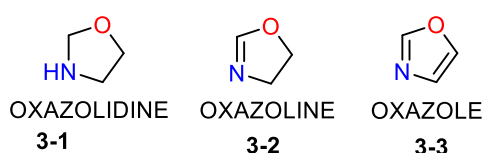


Figure 4: Oxazo class of heterocyclic compounds

Depending on the position of the unsaturation various structures can be generated, namely, 2-oxazoline (**3-2**), 3-oxazoline (**3-2b**), and 4-oxazoline (**3-2c**), numbering from oxygen, through to the nitrogen (Figure 2)

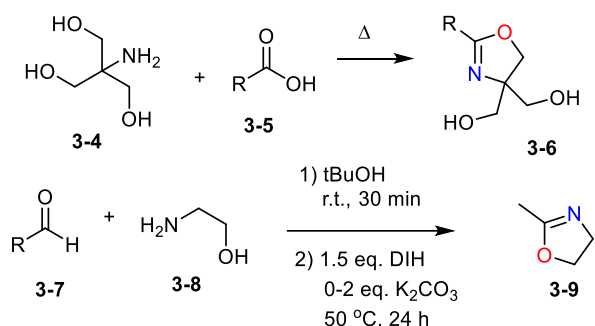


Figure 5: Oxazoline's isomers

2-Oxazolines were first synthesized by Andreasch in 1885^[1] by heating several amidine salts and amino alcohols, amid his study of allyl urea derivatives. Their structures were later assigned by Sigmund Gabriel in 1889^[2].

3.1.1 Synthesis of 2-oxazoline

One of the simplest ways to prepare the oxazoline ring is via the reaction between an amino alcohol and a carboxylic acid (scheme 1), for example, 2-phenyl-4,4-bis(hydroxymethyl)-2-oxazoline (**3-6**) has been synthesized in refluxing benzoic acid for 20 hours using azeotropic distillation with xylene to remove generated H₂O^[3]. The equivalent reaction with an aldehyde gives the corresponding oxazolidine which can be subsequently oxidised giving the desired mono-unsaturated product **3-9**.^[4]

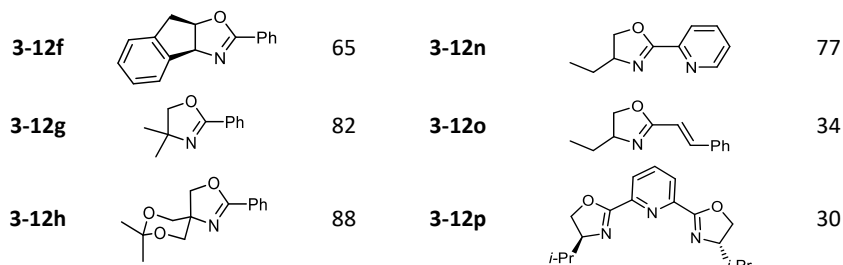


Scheme 4: Synthesis of 2-oxazolines through reaction between carboxylic acids and aldehydes with aminoalcohol.

Schwekendiek and Glorius developed a one-pot synthesis involving the use of *N*-bromosuccinimide (NBS) as an auxiliary oxidising agent. (Table 1) The reaction employs mild condition and allows the synthesis of a variety of substrates, moreover enantiomeric purity is retained during the transformation.^[5]

Table 1: Enantioselective synthesis of 2-oxazolines through secondary oxidation of intermediate oxazolidine with NBS.

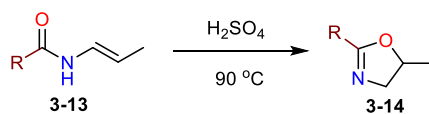
Product	Yield (%)	Product	Yield (%)
3-12a	88	3-12i	42
3-12b	91	3-12j	93
3-12c	70	3-12k	76
3-12d	80	3-12l	83
3-12e	81	3-12m	68



^aGeneral reaction conditions: **3-10** (1 mmol), 2-7 (1 mmol), 4 Å MS (1.5 g), CH₂Cl₂ (6 mL), rt, 14 h; NBS (1 mmol), rt, 0.5 h. NBS (1 mmol), rt, 0.5 h.

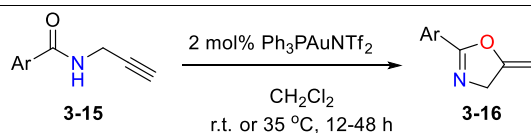
Several examples have also been reported where 2-oxazolines have been prepared starting from amides. Early attempts entailed the use of allyl amides with concentrated H₂SO₄ to induce cyclisation and dehydration^[6,7](Table 2), more recently propargylic amides have been used in combination with gold,^[8] ZnI₂ and FeCl₃^[9] catalysts (Table 3 and 4).

Table 2: Synthesis of 2-oxazolines through cyclization of amides by treatment with H₂SO₄.



Compound No.	R group	Yield (%)
3-14a	2-Methyl	60
3-14b	2-Phenyl	77
3-14c	2- <i>p</i> -Tolyl	50
3-14d	2- <i>p</i> -Fluorophenyl	40
3-14e	2- <i>p</i> -Nitrophenyl	74
3-14f	2- <i>p</i> -Dimethylaminophenyl	52
3-14g	2- <i>p</i> -Anisyl	15

Table 3: Synthesis of 2-oxazolines through cyclization of propargylic amide gold catalysed.



Product	T (°C)	Yield	Product	T (°C)	Yield
---------	--------	-------	---------	--------	-------

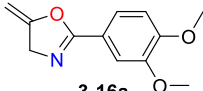
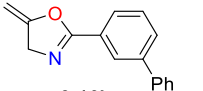

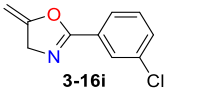
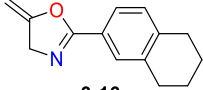
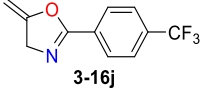
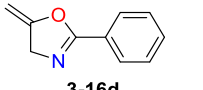
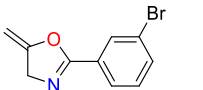
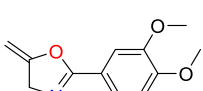
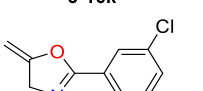
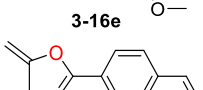
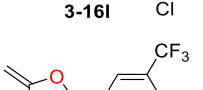
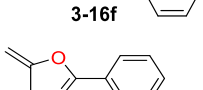
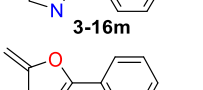
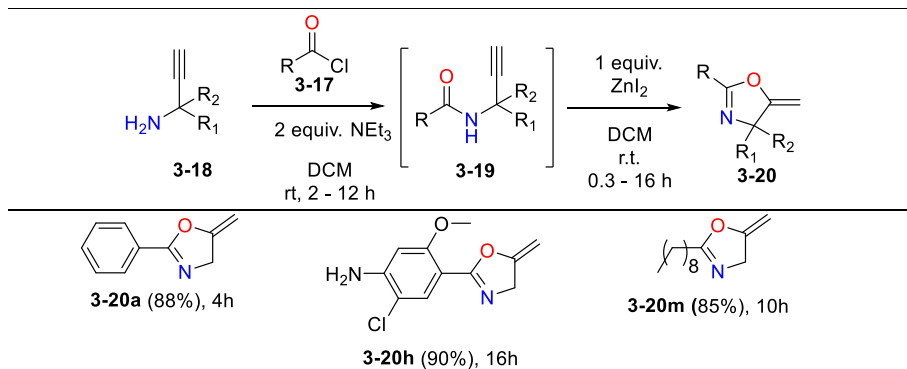
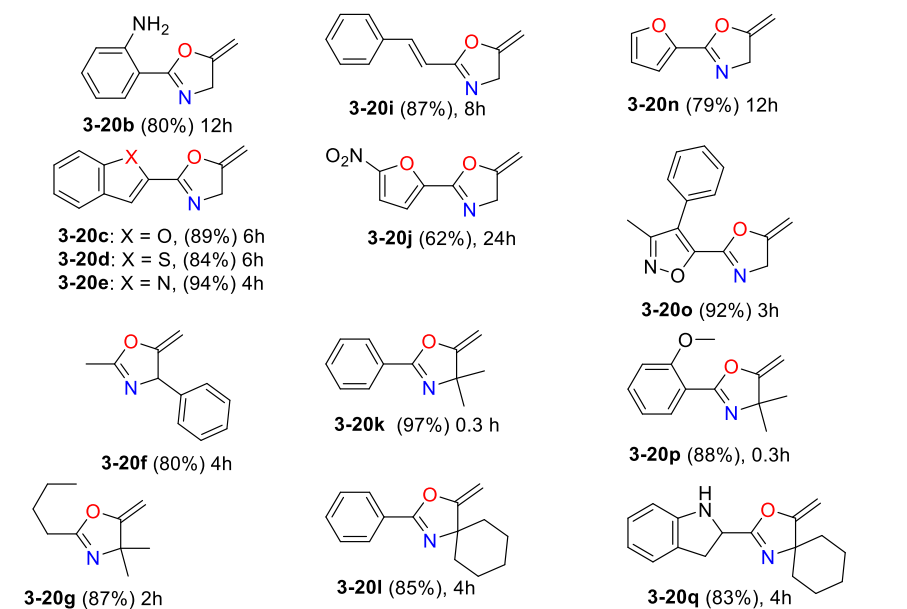
 3-16a	20	83	 3-16h	12	84
 3-16b	6	78	 3-16i	14	80
 3-16c	12	80	 3-16j	12	88
 3-16d	12	91	 3-16k	36	81
 3-16e	48	59	 3-16l	12	91
 3-16f	24	70	 3-16m	12	88
 3-16g	16	80	 3-16n	48	90

Table 4: Synthesis of methylene-3-oxazoline derivatives through ZnI_2 promoted cyclization of propargyl amides





Nitriles react with epoxides when treated with strong acid leading to the cyclic product, this transformation has been used to obtain several 2-oxazolines^[10,11] (Table 5).

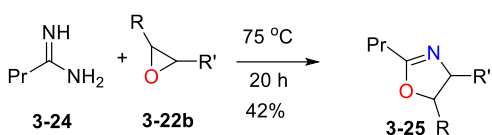
Table 5: 2-oxazolines through reaction between nitriles and epoxides.

R	R ₁	Yield (%)	Ratio 2,4- : 2,5-
CH ₃	H	11	-
C ₆ H ₅	H	20	-
CH ₃	ClCH ₂	37	0 : 100
C ₆ H ₅	ClCH ₂	21	0 : 100
CH ₃	CH ₃	11	48 : 52
C ₆ H ₅	CH ₃	14	59 : 41
CH ₃	C ₆ H ₅	24	97 : 3
C ₆ H ₅	C ₆ H ₅	42	93 : 7

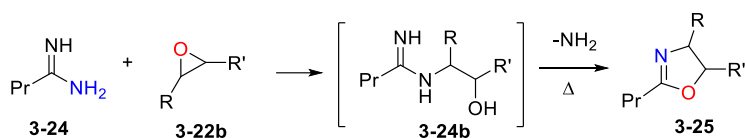
A series of 2-propyl-2-oxazolines have been prepared by Lambert and Kristofferson using the reaction between butyramidine and epoxides^[12] (Table 6). According to the authors the

reaction proceeds from intermediate **3-24b** which cyclises after eliminating ammonia (Scheme 2).

Table 6: 2-oxazolines through reaction between butyramidine and epoxides.



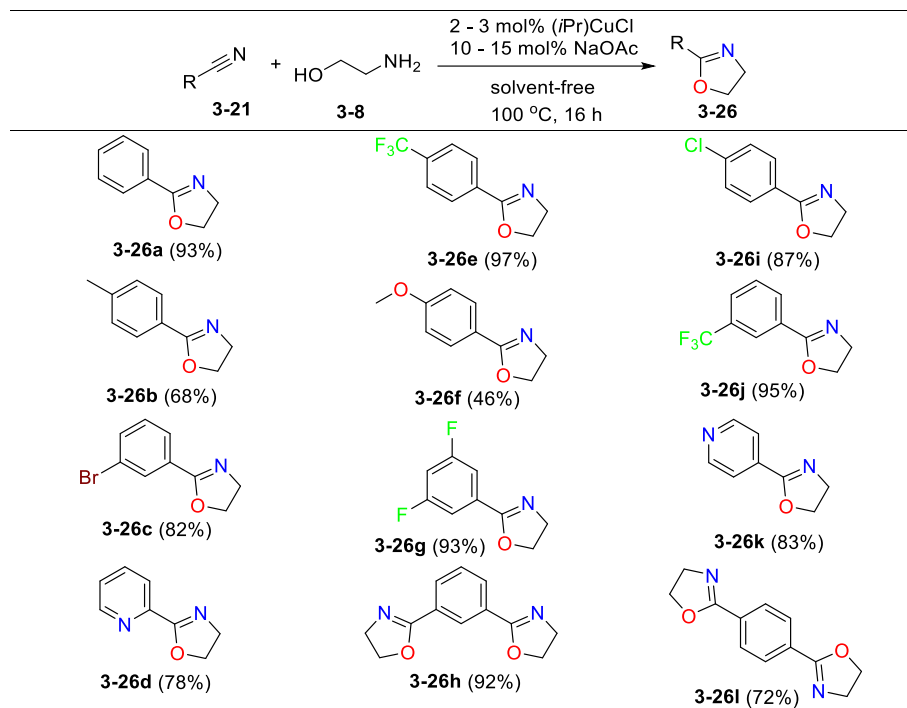
R	R'	Yield (%)
H	H	40
H	CH ₃	80
H	CH ₂ CH ₃	82
CH ₃	CH ₃	42



Scheme 5: Reaction mechanism proposed by Lambert and Kristofferson for the reaction between butyramidine and epoxides.

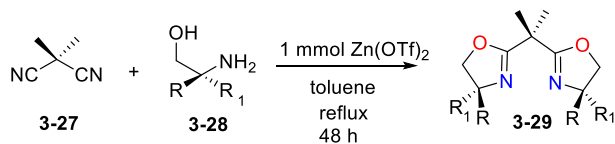
Nitriles have also been used in combination with Cu or Zn catalysts making it possible to directly react them with amino alcohols leading to the 5 membered ring^[13, 14] (Table 7 and 8).

Table 7: Synthesis of 2-oxazolines through reaction between amino alcohols and nitriles Cu catalysed.



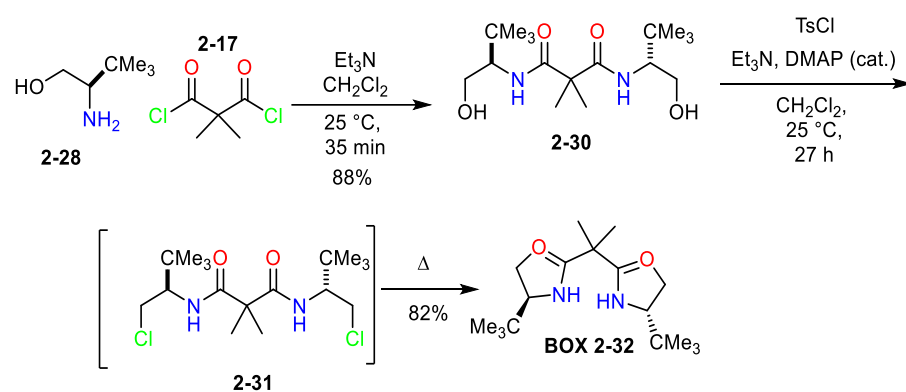
Reaction condition: nitrile (1mmol), alcohol (2mmol), [Cu(Cl)(iPr)] (0.02 mmol), NaOAc (0.1 mmol), 100 °C, solvent free, 16 h.

Table 6: Synthesis of 2-oxazolines through reaction between amino alcohols and nitriles Cu catalysed.



Entry	Groups	Reaction time (h)	Yield
3-29a	R' = H, R = Ph	2	95
3-29b	(R' = H, R = CH ₂ Ph)	2	100
3-29c	(R' = H, R = <i>i</i> Pr)	2	90
3-29d	(R' = H, R = <i>t</i> Bu)	3	90
3-29e	(R' = H, R = Me)	2	75
3-29f	(R' = H, R = Indanyl)	2	100
3-29g	(R' = Me, R = Ph)	3	85

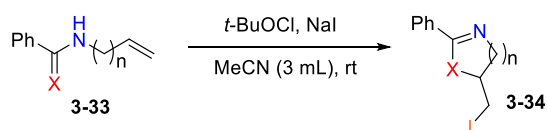
Another straightforward protocol for the assembly of the oxazoline structure starts from an amino alcohol and involves its conversion to the related amide by reaction with an acyl chloride, its subsequent reaction with tosyl chloride then generates the alkyl chloride (alcohol to chloride) which reacts intramolecularly to form the desired product^[15-19] (Scheme 3).



Scheme 6: Evans' route to Box ligands 2-32.

The group of Minataka has performed the cyclization of various alkenyl benzamides using a *tert*-BuOCl/Nal system. The method was shown to be quite general and allowed the synthesis of several different heterocycles. The reaction mechanism involves the formation of a cyclic iodonium ion obtained by reaction with the *t*-BuOCl generate *in situ*^[20] (Table 9)

Table 9: Minataka's synthesis of 2-oxazolines by cyclization of alkenyl benzamides using a *tert*-BuOCl/Nal system

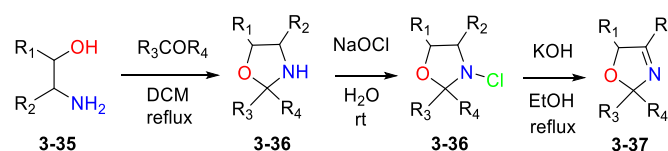


<i>n</i>	X	<i>t</i> -BuOCl (equiv.)	Nal (equiv.)	Time (h)	Yield (%)
1	O	1.1	1.1	5	95
2	O	1.1	1.1	24	82
1	S	1	1	5	77
2	S	1.1	1.1	24	47

3.1.2 Synthesis of 3-oxazolines

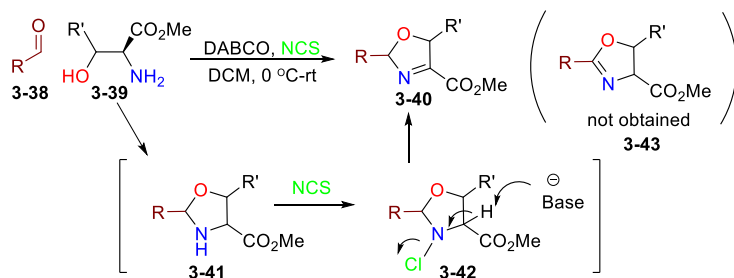
Although the practical utilization of 3-oxazolines has been neglected compared to the most used 2-oxazolines, several syntheses have been developed: Favreau and Fellous assembled the heterocycle starting from the condensation of an amino alcohol and a ketone ^[21] (Table 10).

Table 10: Synthesis of 3-oxazolines by condensation of amino alcohols and ketones.



	R ₁	R ₂	R ₃	R ₄	Yield 2-36	Yield 2-37
a	H	H	Et	Me	80	66
b	H	H	<i>i</i> -Pr	Me	87	65
c	Me	H	Et	Me	85	66
d	Me	H	<i>i</i> -Pr	Me	76	55
e	H	Et	Et	Me	91	83
f	H	Et	<i>i</i> -Pr	Me	83	72

Murai and Fujioka ^[22] showed a one-pot synthesis of 3-oxazoline-4-carboxylates **3-40** starting from aldehydes. The transformation involves the formation of the oxazolidine ring followed by chlorination of the nitrogen and subsequent elimination (Scheme 4 and Table 11).



Scheme 7: Mechanism proposed for the 3-oxazoline-4-carboxylates from aldehydes and amino alcohols.

Table 11: Synthesis of 3-oxazoline-4-carboxylates from aldehydes and amino alcohols.

	RCHO	R'	Yield (%)
3-38a		H	84
3-38b		H	82
3-38c		Me	83
3-38d		Me	84
3-38e		H	82
3-38f		H	90
3-38g		H	89
3-38h		H	87
3-38i		H	96
3-38j		H	91
3-38 k		H	84

The types of application where these molecules have been successfully used are extremely wide ranging due to the multiple properties of this heterocycle. Furthermore, the importance of the molecules is shown by the continued development of new methods.

3.1.3 Use of 2-oxazoline in the pharmaceuticals:

The 2-oxazoline heterocycle motif is found in many drugs with many different therapeutic indications making it a valuable structure in medicinal chemistry. It is a prominent functional units in several biologically active molecules (antimicrobial,^[23,24] anti-inflammatory,^[3] anti-malarial,^[26,27] antibacterial,^[28-30] antitumor,^[31,32] anti-viral,^[33] antipyretic,^[34] antituberculous,^[35] CNS stimulant activity,^[37,38] antioxidant^[39]) and several natural products^[15] (Figure 3) indicating its further biological activity.

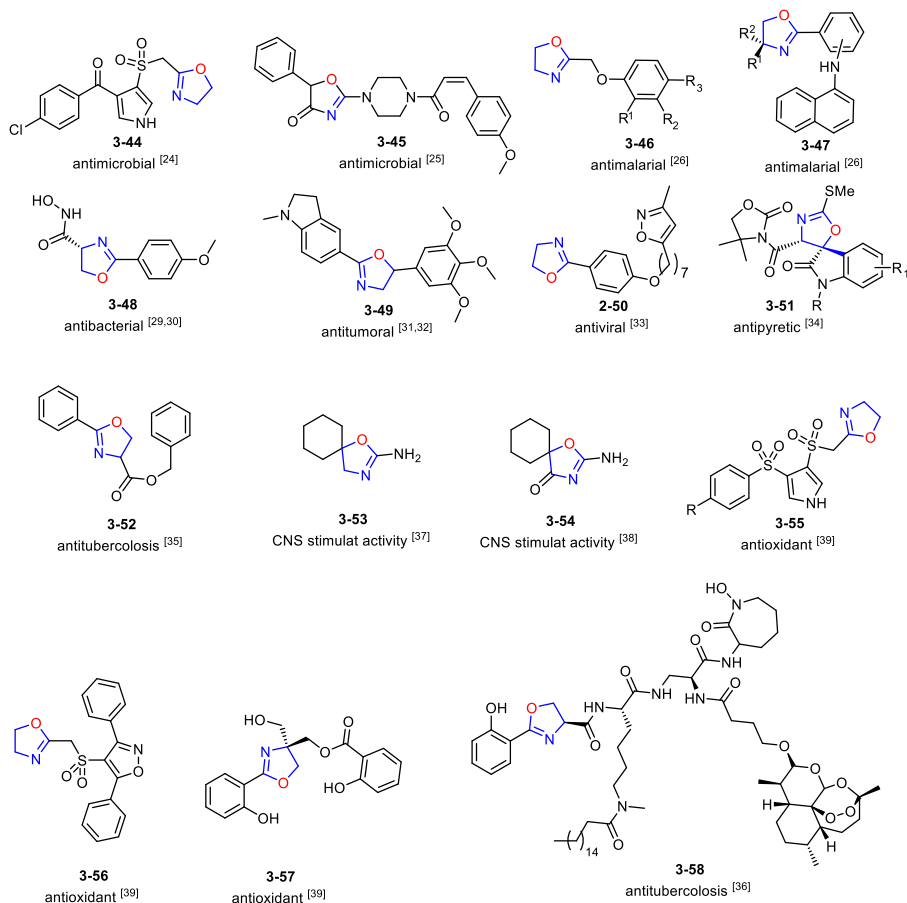


Figure 3: Pharmaceutical relevant molecules containing the 2-oxazoline moiety.

3.1.4 Industrial application

These heterocyclic species have found value in several industrial applications thus increasing their interest to their study (Figure 4).

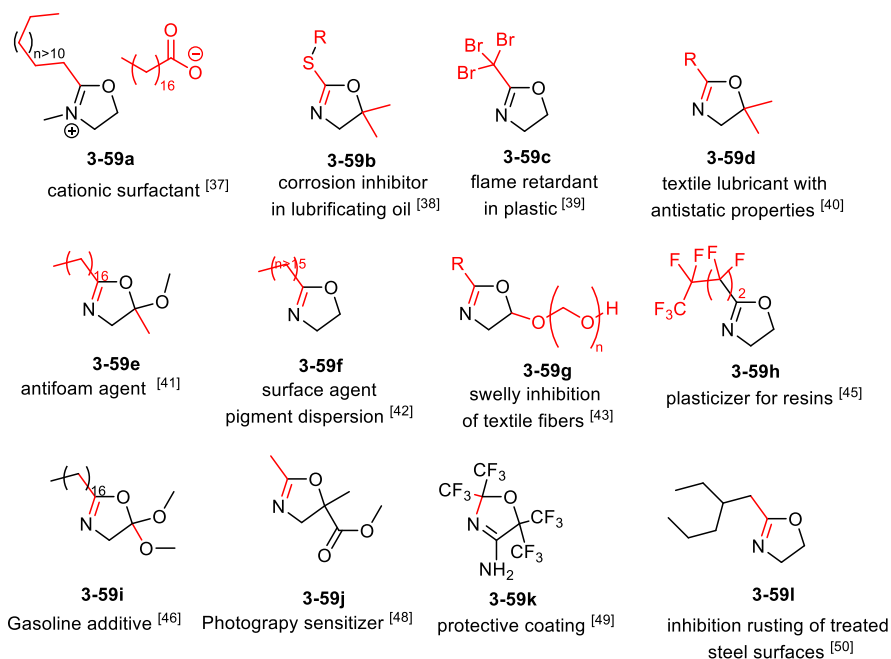


Figure 4: Industrial relevant molecules containing the 2-oxazoline moiety.

3.1.5 Asymmetric catalyst

The most widespread application of 2-oxazolidines is as ligands. Since the first reported example of a ligand containing the oxazoline ring by the Brunner group in 1986 several different ligands have been developed. Most popular examples comprise pyridine *bis*(oxazoline) (Pybox)^[43], *bis*(oxazoline),^[52-57] phosphinooxazolines (PHOX),^[58-60] trisoxazolines (Tox)^[61,62] and several other related systems.^[63-69] (Figure 5).

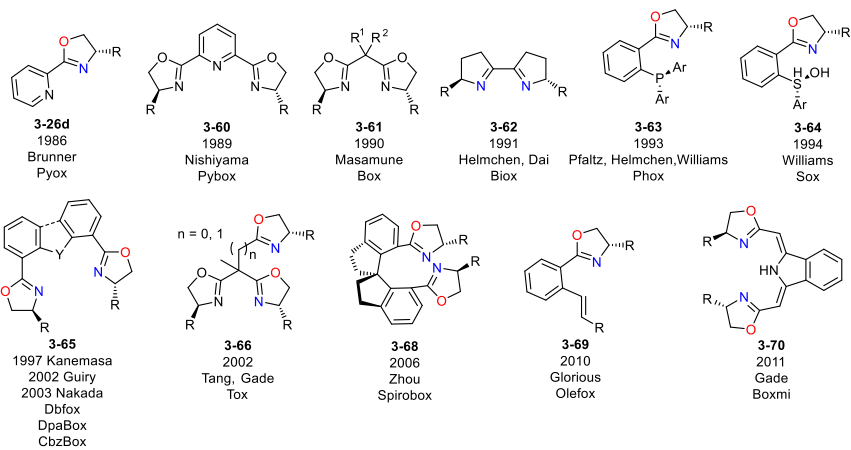


Figure 5: Oxazoline based asymmetric ligands.

Chiral oxazoline-based ligands are among the most popular ligands in asymmetric catalysis. The reasons are essentially two: firstly, they can be easily synthesized by starting from cheap amino alcohols which allow access to a wide range of different derivatives and secondly, they permit to perform efficiently a large variety of crucial enantioselective transformation.^[70]

3.1.5.1 C₂-symmetric Box

Generally, among the Lewis acid catalysis, the catalyst is often a cation associated (by coordination or bound) with an optically active ligand resulting in a chiral complex with at least one Lewis acid vacant site able to induce the coordination and the activation of the reagent. In order to enhance a high enantioselectivity the reagent must possess the right orientation allowing it to favour the attack on a specific face. C₂-symmetric chiral ligands allow to reduce half the variables required for a good face selectivity and C₂-symmetric bis-oxazolines also called BOX's are some of the most popular ligands which fulfil these requisites^[71] (Figure 6 and Table 12).

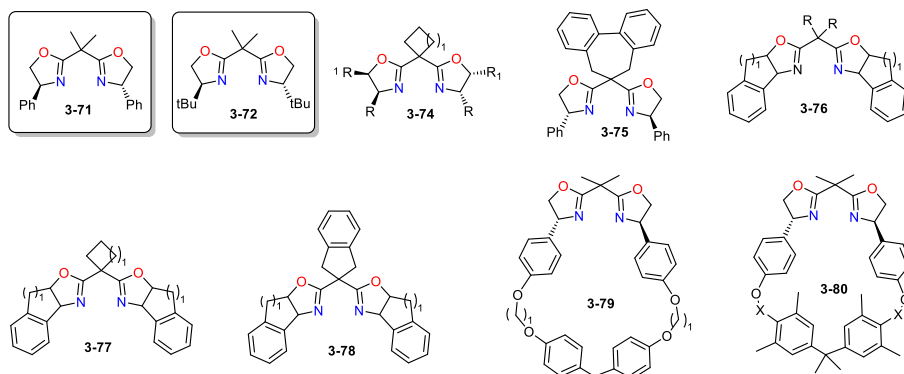


Figure 6: C₂-symmetric BOX catalysts.

BOX	R	BOX	R
3-73	Me	3-73r	CMe ₂ SMe
3-73b	Et	3-73s	CH(Ph)OH
3-73c	<i>i</i> -Pr	3-73t	CH(Ph)OMe
3-73d	CH ₂ Ph	3-73u	CH(Ph)OSiMe ₂ - <i>t</i> Bu
3-73e	CH ₂ CHMe ₂	3-73v	CH(Ph)OCOPh
3-73f	CH ₂ C ₆ H ₁₁	3-73w	2-Me-C ₆ H ₄
3-73g	(1-adamantyl)	3-73x	2-OMe-C ₆ H ₄
3-73h	(1-naphtyl)	3-73y	4-OMe-C ₆ H ₄
3-73i	(2-naphtyl)	3-73z	4-Cl-C ₆ H ₄
3-73j	CH ₂ OH	3-73aa	2OH-5- <i>t</i> Bu-C ₆ H ₃
3-73k	CH ₂ OCOPh	3-73ab	2-OMe-5- <i>t</i> Bu-C ₆ H ₃
3-73l	CH ₂ OTBDPS	3-73ac	2-(OCH ₂ CH ₂ Cl)-5- <i>t</i> Bu-C ₆ H ₃
3-73m	CH(Me)OH	3-73ad	2-OMe-5-Cl-C ₆ H ₃
3-73n	CH(Me)OCOPh	3-73ae	CH ₂ -1-naphtyl
3-73o	CMe ₂ OSiMe ₃	3-73af	CH ₂ -2-naphtyl
3-73p	CH ₂ SMe	3-73ag	CH(Ph)OH
3-73q	CH ₂ CH ₂ SMe	3-73ah	CH(Ph)OMe

Table 7: C₂-symmetric BOX catalysts.

Generally, the BOX ligand with a spacer consisting of one carbon atom use the two nitrogen as a bidentate ligand although there are few exceptions^[71] where complexes formed with the BOX ligand behaves as a monodentate ligand; for example $\{\text{Ag}[(\text{S})\text{-1}]\text{OTf}(\text{0.5H}_2\text{O})\}$ and $\{\text{Ag}[(\text{S})\text{-3d}]\text{OTf}\}$.^[72] Here the Ag ion coordinates two nitrogens belonging to two different BOX ligands leading to a single stranded polymer with a helical coordination, this system possesses a 2-fold symmetry displaying a left handed helicity and a zigzag conformation. In addition the oxazoline (S)-3-72 (Figure 6) with CuOTf·0.5C₆H₆^[73] polymerises forming a single-strained helical with a 3-fold symmetry where the box bridges two bidentate Cu.^[71] (Figure 7)

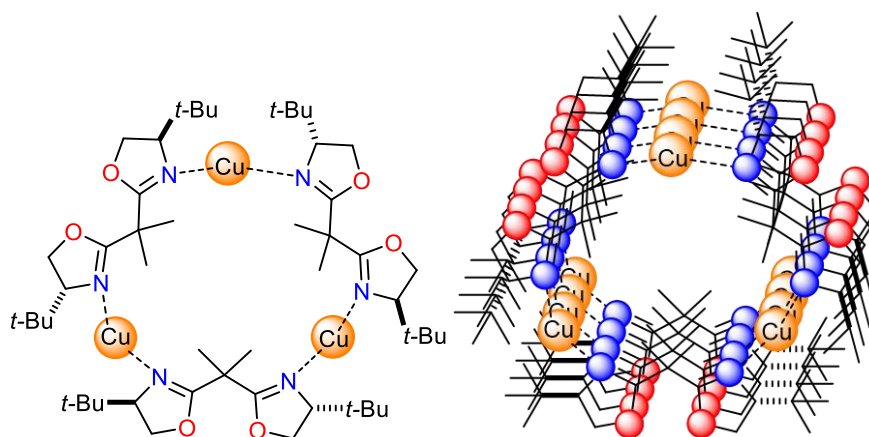


Figure 7: C_2 symmetric Oxazoline complex with Cu, behaving as a monodentate ligand.

In general, a bidentate ligand where the cation is coordinated by two nitrogens from the same BOX allows the formation of a much more rigid species resulting in an enhancement of the discriminating ability between the two diastereofaces of the reagent.^[71] For this reason, Mono-BOX species behaving as a bidentate ligand are some of the most popular complexes in asymmetric catalysis. Copper(II) remains the most used metal with these compounds.^[71] For BOX's **3-71** and **3-72** a distorted square-planar coordination is normally observed leading to a coordination number of 4 although the use of a counter ion like triflate can expand it to five due to the formation of a distorted square pyramid-geometry.^[71] The anion plays an important role in the distortion of the structure compared to the ideal plane of box and cation: $[(S)\text{-1}\cdot\text{CuBr}_2]$ and $[(S)\text{-1}\cdot\text{CuCl}_2]$ show this effect as Cl and Br induce a large distortion with the halogens positioned in quadrant free from substituent ^[74] (Figure 2) whereas the hydrated complex shows more planar features, with the dihedral angles O-Cu-N-C equal to -11.3° and -7.2 and the two molecules of water pointing in the direction of the aromatic substituents (Figure 8) ^[75-77].

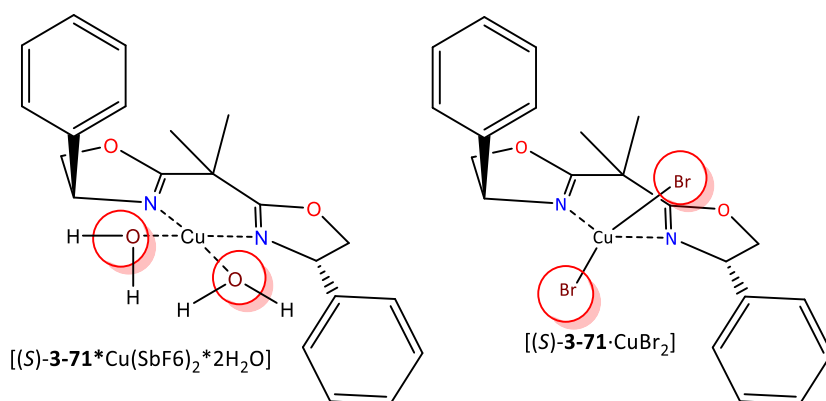


Figure 8: Different geometries of the complex (S)-3-71 with Cu: distorted square-planar coordination in the hydrated form (left) and distortion of the geometry for effect of the ion Br (right).

Complexes of (S)-3-72 with Cu have been extensively studied showing the importance of the counter ion in influencing the coordination number.^[71,75,76] For example, when associated with SbF_6 , (S)-3-72 assumes a distorted planar square structure where two water molecules are included as happen with (S)-3-71 (Figure 9) although in this second case the distortion effect is augmented and the ligands are pushed far from the *tert*-butyl group with a big impact on the dihedral angles O-Cu-N-C which become $+30.2^\circ$ and $+35.9^\circ$ [75-78].

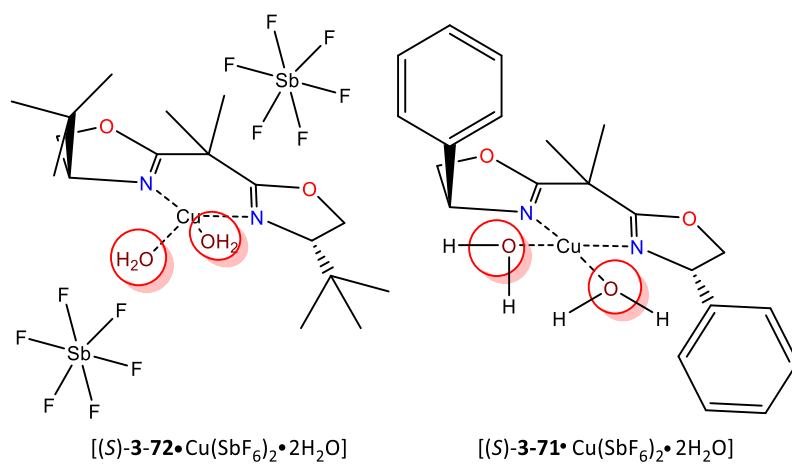
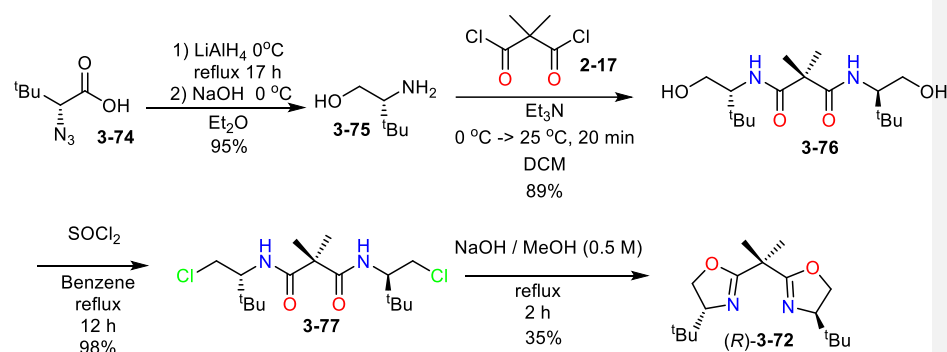
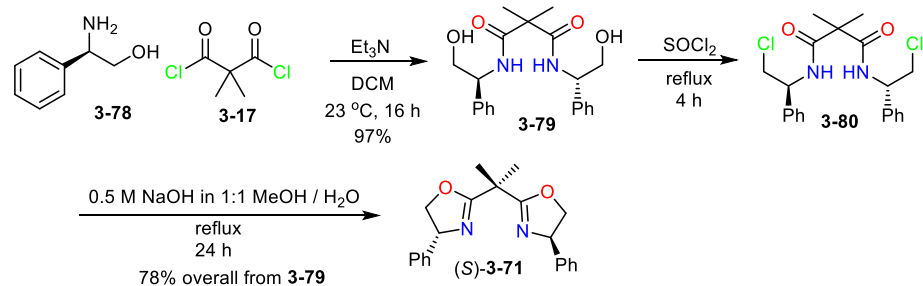


Figure 9: different effects of SbF_6 on the distortion of the geometry in (S)-3-72 (left) compared to (S)-3-71 (right).

Since the end of last century, these ligands have gained a great deal of popularity to the point that some of them have been widely commercialised: for example ligands (*R*)-**3-72**, (*S*)-**3-72** and (*S*)-**3-73** have become some of the most used ligands in scientific literature^[71]. The synthesis of box ligands was first explored in the pioneering work of Corey^[55] and Evans^[54]. The oxazoline's frame is obtained by reaction of a β -amino alcohol and a malonic acid derivative (Schemes 5 and 6).

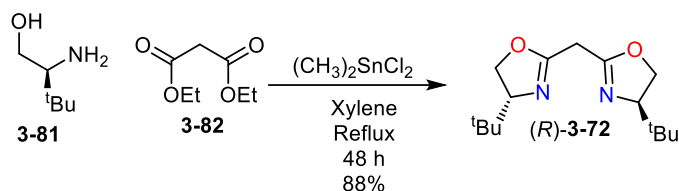


Scheme 8: Corey's synthesis of the Box (*R*)-**3-72**.



Scheme 9: Evans' synthesis of the Box (*S*)-**3-71**.

The cyclization step has been developed using alternative conditions; one example is the Masamune protocol^[79] which uses Me_2SnCl_2 in refluxing xylene (Scheme 7).



Scheme 10: Musamune's cyclization using $(\text{CH}_3)_2\text{SnCl}_2$.

Other reagents used for the cyclization are $\text{CH}_3\text{SO}_3\text{H}$,^[80] Me_2SnCl_2 ,^[52,53] ZnCl_2 ,^[81] DAST (diethylaminosulfur trifluoride),^[82] or $\text{CF}_3\text{SO}_3\text{H}$ and $\text{BF}_3 \cdot \text{Et}_2\text{O}$.^[83]

3.1.5.2 Reactions:

3.1.5.2.1 Cyclopropanation

The BOX ligand (*S*)-**3-72** and CuOTf catalyse the cyclopropanation of alkenes with diazoacetates showing excellent yield, diastereoselectivity and enantioselectivity^[86]. Interestingly, BOX **3-72** with Cu(I) salts gives better results compared to its use with Cu(II) or the alternative BOX ligand **3-71** (Table 13, entry 2, 3)^[84,85]

The selectivity is also dependent on the diazoester, particularly, *trans* selectivity is enhanced by increasing the steric demand (entry 6, Table 13). Trisubstituted alkenes were used in order to gauge the limitations of the BOX ligands for these reactions (entries 12-20, Table 13).^[52,53,86] In the experimentation the ligand (*S*)-**3-72** showed a much higher enantioselectivity compared with (*S*)-**3-71** (entries 13-16, Table 13) although they led to the same absolute configuration.

Table 13: Asymmetric Cyclopropanations of Alkenes with Diazoacetates 3-84 Catalysed by Box Complexes.

	R_1	$\text{R}_{2,3}$	R_4	R	box	MX_n	yield	3-85:23-86	3-85 ee(%)	3-86 ee	ref
1	Ph	H	H	Et	(<i>S</i>)- 3-72	Cu(OTf)_2	77	73:27	99 (1 <i>R</i> ,2 <i>R</i>)	97(1 <i>R</i> ,2 <i>S</i>)	54,73,84,85
2	Ph	H	H	Et	(<i>S</i>)- 3-72	Cu(I)^a	81	71:29	91 (1 <i>R</i> ,2 <i>R</i>)	88(1 <i>R</i> ,2 <i>S</i>)	85
3	Ph	H	H	Et	(<i>R</i>)- 3-71	CuOTf	77	70:30	65 (1 <i>S</i> ,2 <i>S</i>)	54(1 <i>S</i> ,2 <i>R</i>)	84
4	Ph	H	H	<i>t</i> -Bu	(<i>S</i>)- 3-72	CuOTf	75	81:19	96 (1 <i>R</i> ,2 <i>R</i>)	93(1 <i>R</i> ,2 <i>S</i>)	54
5	Ph	H	H	2,6-DMP ^b	(<i>S</i>)- 3-72	CuOTf	68	86:14	97 (1 <i>R</i> ,2 <i>R</i>)	96(1 <i>R</i> ,2 <i>S</i>)	54
6	Ph	H	H	2,6-BHT ^c	(<i>S</i>)- 3-72	CuOTf	85	94:6	99 (1 <i>R</i> ,2 <i>R</i>)		54

7	Ph	H	H	CH(C ₆ H ₁₁) ₂	(S)- 3-72	CuOTf	83	88:12	97 (1 <i>R</i> ,2 <i>R</i>)	87
8	Bn	H	H	2,6-BHT	(S)- 3-72	CuOTf	d	99:1	99 (1 <i>R</i> ,2 <i>R</i>)	54
9	H	Ph	H	Et	(S)- 3-72	CuOTf	d		99 (1 <i>S</i>)	54
10	H	Me	H	Et	(S)- 3-72	CuOTf	d		99 (1 <i>S</i>)	54
11	C=CMe ₂	Me	H	L-methyl	(S)- 3-72	CuOTf	60	84:16	24 (1 <i>R</i> ,2 <i>R</i>)	52, 53
12	CH ₂ OAc	Me	H	Et	(S)- 3-71	Cu(I)	47	49:51	69 (1 <i>R</i> ,2 <i>R</i>)	20
13	CH ₂ OAc	Me	H	Et	(S)- 3-72	CuOTf	50	80:20	95 (1 <i>R</i> ,2 <i>R</i>)	3
14	CH ₂ OSiMe ₃	Me	H	Et	(S)- 3-71	CuOTf	52	64:36	66	47
15	CH ₂ OSiMe ₃	Me	H	Et	(S)- 3-72	CuOTf	33	76:24	87	d
16	CH ₂ OCH ₂ Ph	Me	H	Et	(S)- 3-72	CuOTf	74	88:12	93	d
17	CH ₂ Otrityl	Me	H	Et	(S)- 3-72	CuOTf	46	82:18	87	d
18	CH ₂ OCOPh	Me	H	Et	(S)- 3-72	CuOTf	82	82:18	92	d
19	CH ₂ OCOC ₆ H ₄ OMe	Me	H	Et	(S)- 3-72	CuOTf	61	91:9	92	12
20	Ph	Me	H	Et	(S)- 3-72	CuOTf	62	72:28	89 (1 <i>S</i> ,2 <i>S</i>)	80
21	Ph	H	F	Et	(S)- 3-72	CuOTf	56	81:19	93 (1 <i>S</i> ,2 <i>S</i>)	89
22	Ph	H	F	<i>t</i> -Bu	(S)- 3-72	CuOTf	28	81:19	92 (1 <i>S</i> ,2 <i>S</i>)	>98
23	<i>p</i> -ClPh	H	F	L-methyl	(S)- 3-72	CuOTf	64	82:18	93	91
24	Ph	H	F	Et	(S)- 3-72	CuOTf	62	64:36	65	d
25	C ₆ H ₉	Me	F	Et	(S)- 3-72	CuOTf	28		16	d

^a X = not reported. ^b 2,6-DMP is 2,6 dimethylphenyl. ^c 2,6-BHT is 2,6-di-*tert*-butyl-4-methylphenyl. ^d Not reported.

3.1.5.2.2 Aldol like reactions

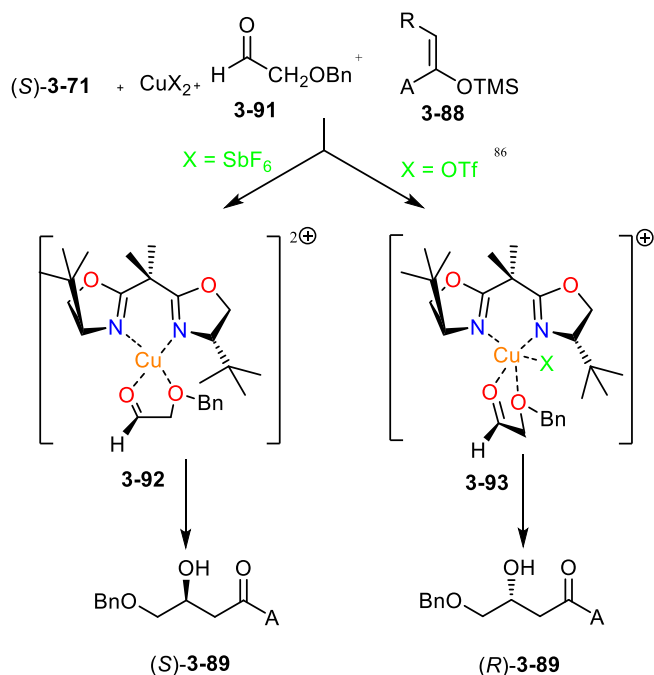
The Mukaiyama reaction was one of the first transformations studied with the BOX ligands which turned out to be able to catalyse the addition of aldehydes or ketones to silylacetals.^[71] The aldehyde or ketones **3-87** must possess a group capable of coordinating to the Lewis acid (Table 14).

Table 14: Catalysed Enantioselective Mukaiyama-Aldol Reactions between Aldehydes **3-87** (R₁=H) and Trimethylsilylketene acetals **3-88**.

Entry	R	A	R ²	BOX	MX _n	Solvent	Anti/syn	87 ee	88 ee	Ref
1	CH ₂ OBn	<i>St</i> -Bu	H	(S)- 3-71	Zn(SbF ₆) ₂	DCM		85 (S)		95
2	CH ₂ OBn	<i>St</i> -Bu	H	(S)- 3-71	Cu(OTf) ₂	DCM		9 (R)		90
3	CH ₂ OBn	<i>St</i> -Bu	H	(S)- 3-72	Cu(OTf) ₂	DCM		91 (R)		71,90,95
4	CH ₂ OBn	<i>St</i> -Bu	H	(S)- 3-72	Zn(SbF ₆) ₂	DCM		64 (S)		90
5	CH ₂ OBn	OEt	H	(S)- 3-72	Cu(OTf) ₂	DCM		50 (R)		90
6	CH ₂ OBn	Me	H	(S)- 3-72	Cu(OTf) ₂	DCM		38 (R)		90
7	CH ₂ OBn	Ph	H	(S)- 3-72	Cu(OTf) ₂	DCM		51 (R)		90
8	CH ₂ OBn	<i>St</i> -Bu	Me	(S)- 3-72	Cu(OTf) ₂	DCM	81:19	84 (R,S)		90
9	CO ₂ Et	SPh	H	(S)- 3-71	Cu(OTf) ₂	DCM		91 (S)		71
10	Ph	Ph	Me	(S)- 3-72	Cu(OTf) ₂	H ₂ O	10:90	a	15	71

The chiral environment generated influences not only the substituent but also cation and anion play a fundamental role (Table 14, entries 1-4). Evans^[90] suggested that changing the

counter ion (Table 14, entry 3 and 4) can induce an inversion of the configuration by causing a change in the coordination number (Scheme 8).



Scheme 11: Inversion of the configuration due to a change in the coordination number.

If the counter ion does not behave as an auxiliary ligand (e.g. SbF_6) the complex assume a square planar conformation and the attack of the nucleophile occurs on the *Si* face leading to the $(S)\text{-}3\text{-}89$ product as major product whereas when the counter ion play a direct role as the ligand (e.g. OTf) the geometry changes toward a pyramidal square structure thus attacking preferably the *Re* face leading to the $(R)\text{-}3\text{-}89$ product (Scheme 8).

3.1.5.2.3 Radical processes

The use of bicyclo-oxazolines as chiral catalysts has found application in several free radical processes. The chiral Lewis acids can control the transfer of an atom or group allowing delivery of the substituent selectively to a particular face (Figure 10). The reaction is normally performed generating the radical from α -halo carbonyl compounds or from conjugate addition to a β -carbon atom.

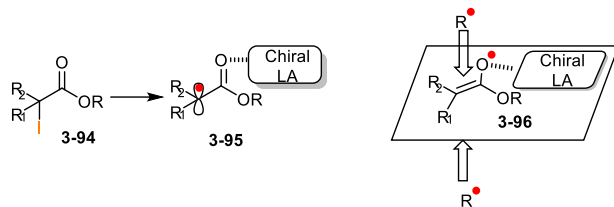


Figure 10: Chiral control over the transfer of an atom or group by Lewis acid.

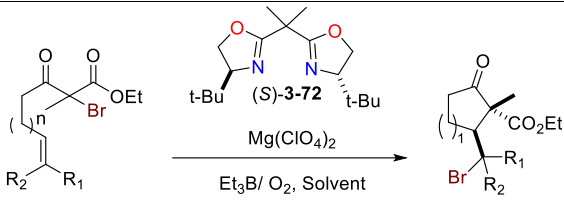
The use of BOX ligated Lewis acids can catalyse the coupling between the radical generated from the halo derivative **3-97** and Et_3B (used as initiator) and allyl silanes or stannanes **3-98** leading to the β -bromo derivative **3-99** which can then eliminate ZBr_2 leading to the corresponding alkene. Changing the ion and counter ion can dramatically affect the outcome of the transformation: the salt $\text{Zn}(\text{OTf})_2$ and MgI_2 give opposite enantiomers (Table 15).^[91]

Table 15. Reaction of 3-(α -bromoacyl)-2-oxazolidinone with allyl silanes and stannanes.

Entry	R	Z	BOX	MX_2	Yield (%)	ee (%) (conf)
1	Et	SnBu_3	(<i>R</i>)- 3-71	$\text{Zn}(\text{OTf})_2$	84	42 (<i>S</i>)
2	Et	$\text{Si}(\text{OEt})_3$	(<i>R</i>)- 3-71	$\text{Zn}(\text{OTf})_2$	65	60 (<i>S</i>)
3	CH_2tBu	SnBu_3	(<i>R</i>)- 3-71	$\text{Zn}(\text{OTf})_2$	63	74 (<i>R</i>)
4	CH_2tBu	SnMe_3	(<i>R</i>)- 3-71	$\text{Zn}(\text{OTf})_2$	88	90 (<i>R</i>)
5	CH_2tBu	SnMe_3	(<i>R</i>)- 3-71	MgI_2	86	68 (<i>S</i>)
6	CH_2tBu	SnMe_3	(<i>S</i>)- 3-72	MgI_2	61	78 (<i>R</i>)

Yang^[92] performed highly enantioselective atom-transfer radical cyclizations by using chiral Lewis acids. The transformation allowed the creation of various chiral centres and also to install a halogen in the product. The chiral ligand (*S*)-**3-72** in combination of $\text{Mg}(\text{ClO}_4)_2$ catalyses the cyclization of unsaturated β -keto esters through atom transfer (Table 16).

Table 16: cyclization of unsaturated β -keto esters through atom transfer.

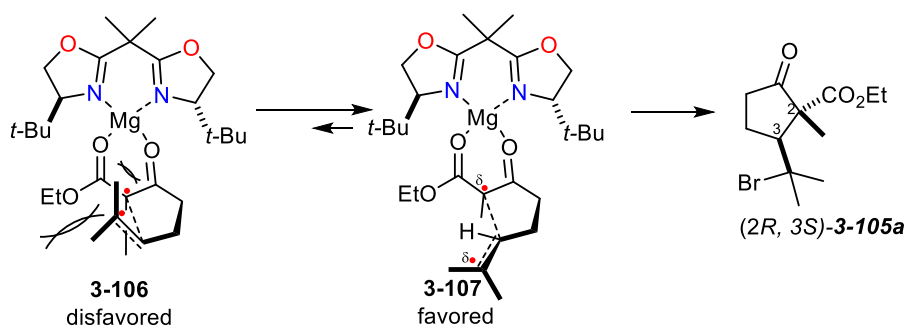


3-101a n = 1, R₁ = R₂ = Me
3-102b n = 2, R₁ = Et, R₂ = H
3-103c n = 2, R₁ = H, R₂ = Et
3-104d n = 2, R₁ = R₂ = Me

Entry	Substrate	Catalyst (equiv.)	Solvent	Time (h)	Yield (%)	ee (%)
1	3-101	1.1	DCM	7.5	68	71
2	3-101	1.1	Toluene	5	67	94
3	3-101	0.5	Toluene	7	65	93
4	3-101	1.1	Toluene	9	53	21
5	3-102	1.0	Toluene	9.5	57(1/1.2) ^c	68/78 ^d
6	3-102	0.3	Toluene	12	58(1/1) ^c	74/87 ^d
7	3-103	0.3	Toluene	9.5	81(1/1.4) ^c	74/95 ^d
8	3-104	1.1	Toluene	7.5	62	93
9	3-104	0.5	Toluene	7.5	53	94

^a MS 4Å (500 mg/mmol substrate); ^b 1.0 equiv. of water was added. ^c ratio of product b: product c; ^d ee's for product b and c

The high selectivity of the process has been rationalised using the transitional state in which Mg is tetrahedral (Scheme 9): here, due to the bulky tert-Bu-groups of the ligand the cyclization on the *Re*-face is favoured over the *Si*-face and the resulting transition state **3-107** experiences lower steric interactions thus resulting in the product **3-105**.^[92, 93]



Scheme 12: Rationalization of the selectivity in 5-exo cyclization.

The same ligand has been used by Yang^[94] with Mg(ClO₄)₂ for performing enantioselective tandem cyclizations: The author reports that the use of DCM gives poor enantiomeric excess which can be increased using molecular sieves although this decreases the yield on the contrary using toluene improves considerably the ee although reducing the yield of the transformation (Table 17).

Table 17: Tandem cyclization by atom-transfer.

entry	substrate	T (°C)	Tolvent	Product	Yield (%)	ee (%)
1	3-108	-78	DCM	3-110	41	13
2 ^a	3-108	-78	DCM	3-110	24	33
3	3-109	-40	Toluene	3-111	23	82
4	3-109	-20	Toluene	3-111	16	84

^a MS 4Å was added

3.1.5.2.4 Diels alder

The Diels-Alder reaction together with the aldol addition represents a benchmark of the efficiency of a chiral catalyst and most of the ligand classes have been assessed with these reactions.^[71] Since Corey in 1991 used (**S**)-**3-71** for catalysing the Diels-Alder reaction between 3-acryloyl-2-oxazolidinone and cyclopentadiene showing an endo selective process (3-113:3-114 =96:4) and 82% ee for (**1R,2R,4R**)-**3-113** [simplified (**R**)-**3-113**]^[55] the interest for this particular transformation grew considerably up to the point that acryloyl and crotonoyl oxazolidinones became a standard for gauging the efficiency of catalysts toward the Diels-Alder reaction.^[71]

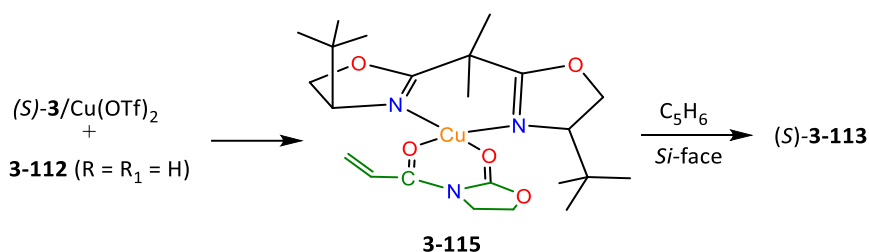
Table 18: Box catalysed enantioselective Diels-Alder between cyclopentadiene and 3-acryloyl-2-oxazolidinones ($R = H$).

$\text{3-112 (R = R}_1 = \text{H)}$
 $(1R,2R,4R)\text{-3-113}$
 3-114

Entry	R ¹	box	MX _n	additives	Solvent	Yield (%)	Endo / Exo	Endo ee (%)	[ref]
1	H,H	(S)-3-71	FeI ₃ /I ₂		DCM	85	96:4	82 (R)	55
2	H,H	(S)-3-71	Cu(OTf) ₂		DCM	92	95:5	30 (S)	95,96
3	H,H	(S)-3-72	Cu(OTf) ₂		DCM	86	98:2	>98 (S)	95,96,97,102
4	H,H	(S)-3-72	Cu(OTf) ₂		THF	>98	97:3	98 (S)	95
5	H,H	(S)-3-72	Cu(OTf) ₂		MeNO ₂	>98	92:8	84 (S)	95
6	H,H	(S)-3-72	Cu(OTf) ₂		MeCN	87	92:8	58 (S)	95
7	H,H	(S)-3-72	Cu(SbF ₆) ₂		DCM	>95	96:4	>98 (S)	95,103
8	H,H	(S)-3-72	Cu(ClO ₄) ₂ ^d		DCM	85	97:3	60 (S)	101
9	H,H	(S)-3-72	Co(OTf) ₂		DCM	85	90:10	50 (S)	95
10	H,H	(S)-3-72	Mn(OTf) ₂		DCM	80	85:15	50 (S)	95
11	H,H	(S)-3-72	Ni(OTf) ₂		DCM	75	90:10	40 (S)	95
12	H,H	(S)-3-72	Zn(OTf) ₂		DCM	85	95:5	38 (S)	95
13	H,H	(S)-3-72	LiOTf		DCM	89	85:15	14 (S)	95
14	H,H	(S)-3-72	Cd(OTf) ₂		DCM	80	90:10	10 (S)	95
15	H,H	(S)-3-72	Sm(OTf) ₃		DCM	78	80:20	Racemate	95
16	H,H	(S)-3-72	Lu(OTf) ₃		DCM	75	75:25	racemate	95
17	(R)-Bn	(S)-3-72	Cu(OTf) ₂		DCM	100	99:1	>98 (S) ^b	95,96
18	(S)-Bn	(S)-3-72	Cu(OTf) ₂		DCM	20	>95:5	36 (S) ^b	95,96
19	H,H	(R)-3-71	Mg(ClO ₄) ₂		DCM	>98	93:7	73 (S)	99,98,100
20	H,H	(R)-3-71	Mg(ClO ₄) ₂	2H ₂ O	DCM	>98	95:5	73 (R)	99,98,100
21	H,H	(R)-3-71	Mg(ClO ₄) ₂	2MeOH	DCM	>98	91:9	42 (R)	98
22	H,H	(R)-3-71	Mg(ClO ₄) ₂	2EtOH	DCM	>98	91:9	16 (R)	98
23	H,H	(R)-3-71	Mg(ClO ₄) ₂	2tBuOH	DCM	>98	92:8	33 (R)	98
24	H,H	(R)-3-71	Mg(ClO ₄) ₂	(CH ₂ OH) ₂	DCM	>98	91:9	58 (R)	98
25	H,H	(R)-3-71	Mg(ClO ₄) ₂	TMU ^c	DCM	>98	96:4	51 (R)	100
26	H,H	(R)-3-71	Mg(ClO ₄) ₂	Py or Et ₃ N	DCM	0	0	0	100
27	H,H	(R)-3-71	Mg(OTf) ₂		DCM	>98	92:8	88 (R)	97,100
28	H,H	(R)-3-71	Mg(OTf) ₂	2H ₂ O	DCM	>98	92:8	86 (R)	100
29	H,H	(R)-3-71	Mg(OTf) ₂	TMU ^c	DCM	>98	93:7	88 (R)	100
30	H,H	(S)-3-71	MgI ₂ /I ₂		DCM	>98	94:6	76 (R)	68
31	H,H	(R)-3-71	Zn(OTf) ₂		DCM	>98	90:10	32 (R)	97
32	H,H	(R)-3-71	Zn(ClO ₄) ₂ ^d		DCM	>98	92:8	20 (R)	85
33	H,H	(R)-3-71	Zn(ClO ₄) ₂	MS ^d	DCM	>98	92:8	73 (S)	85
34	H,H	(R)-3-71	Zn(SbF ₆) ₂		DCM	>90	98:2	92 (R)	68,103
35	H,H	(R)-3-71	Ni(ClO ₄) ₂ ^d		DCM	97	88:12	52 (R)	64
36	H,H	(S)-3-71	Cu(ClO ₄) ₂ ^d		DCM	84	97:3	41 (S)	101

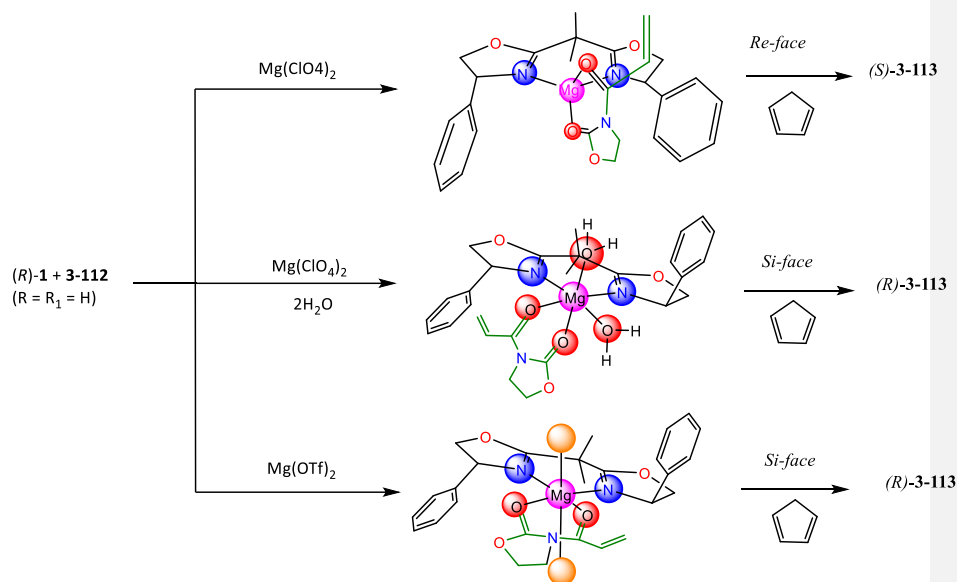
^aHexahydrate sat. ^bMajor endo diastereoisomer. ^cTMU is tetramethylurea. ^dMolecular sieves are 4 Å

Evans showed how the BOX ligand **3-72** and Cu(II)^[95,96,102-105] in combination with both OTf and SbF₆ counter ions (entries 3-8) give the best results. The asymmetric induction [(S)-**3-72** gives (S)-**3-29**] arises from the intermediate **3-115** (Scheme 10) which has a square planar geometry.



Scheme 13. Asymmetric induction arising from the square-planar intermediate 3-115.

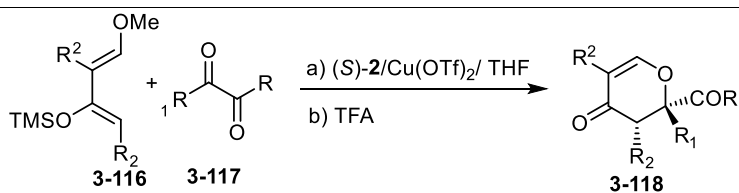
The use of (*R*)-**3-71** as catalyst reveals a unique behaviour: it seems that its enantioselectivity is not just influenced by the counter ion but also by external species which can work as auxiliary ligands: the use of perchlorate gives (*S*)-**3-113** as product (Table 18) but when it is used in combination with 2 equivalent of water or ethylene glycol or tetramethylurea (entries 27-29 Table 18) then the product obtained is the (*R*)-**3-114**. Conversely, when triflate is used as counter ion the product obtained is (*R*)-**3-113** but in this case the addition of water or other additives does not affect the selectivity of the process (Table 18). This interesting effect where the enantioselectivity of the process is inverted by adding an achiral additive has been rationalised^[63] considering that water and tetramethylurea in combination with perchlorate are able to induce an expansion in the coordination number bringing the complex from a tetrahedral geometry (coordination number = 4) to octahedral (coordination number = 6), on the contrary in case triflate is used, two of them coordinate in the axial position, therefore, the coordination number is always 6 and it is not affected by water or tetramethylurea. (Scheme 11) Among the 3 intermediate the tetrahedral geometry allows the cyclopentadiene to attack the *Re* face of the dienophile whereas an octahedral geometry results in the approach of the diene on the *Si* face (Scheme 11).



Scheme 14: Asymmetric induction resulting by expansion of the coordination sphere due to auxiliary ligands.

Hetero Diels-Alder processes have been also extensively studied. Jorghensen^[106] reported the reaction between activated ketones and the Danishefsky's diene catalysed by (*S*)-**3-72**/Cu(OTf)₂/THF (Table 19). The enantiomeric purity of the transformation together with the low loading of the catalyst makes this transformation comparable to a bio-enzymatic reaction.^[106,71]

Table 19: Enantioselective Hetero-Diels Alder reaction between diene **3-116** and diketones **3-117**.

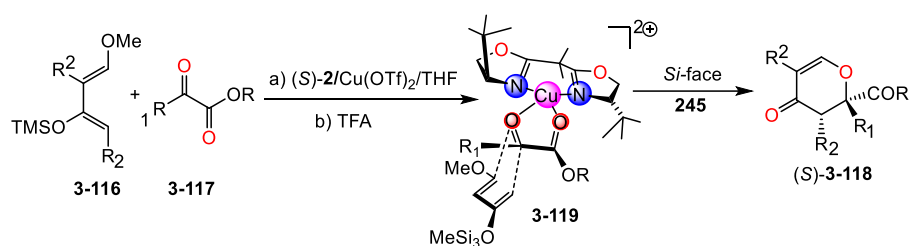


Entry	R	R ₁	R ₂	BOX	MX _n	Yield (%)	ee (%)	[ref]
1 ^o	OEt	Me	H	(<i>R</i>)- 3-71	Cu(SbF ₆) ₂	24	23 (<i>S</i>)	106
2 ^o	OEt	Me	H	(<i>R</i>)- 3-71	Cu(OTf) ₂	85	35 (<i>S</i>)	106
3 ^o	OEt	Me	H	(<i>S</i>)- 3-72	Cu(SbF ₆) ₂	37	89 (<i>S</i>)	106
4 ^o	OEt	Me	H	(<i>S</i>)- 3-72	Cu(OTf) ₂	78	>99 (<i>S</i>)	106
5	OMe	Me	H	(<i>S</i>)- 3-72	Cu(OTf) ₂	96	>99 (<i>S</i>)	109, 106

6	OMe	Et	H	(S)- 3-72	Cu(OTf) ₂	80	94 (S)	106
7	OEt	<i>i</i> -Pr	H	(S)- 3-72	Cu(OTf) ₂	42	37 (S)	106, 107
8	OEt	Ph	H	(S)- 3-72	Cu(OTf) ₂	77	77 (S)	106, 107
9	OEt	Ph	H	(S)- 3-72	Sc(OTf) ₃	26	6	107
10	OEt	Ph	H	(S)- 3-72	Yb(OTf) ₃	70	4	107
11	OEt	Ph	H	(S)- 3-72	In(OTf) ₃	26	9	107
12	Me	Me	H	(S)- 3-72	Cu(OTf) ₂	90	94 (S)	106
13	Et	Me	H	(S)- 3-72	Cu(OTf) ₂	77	98 (S)	106
14	Et	Et	H	(S)- 3-72	Cu(OTf) ₂	84	90 (S)	106
15	Ph	Me	H	(S)- 3-72	Cu(OTf) ₂	95	94 (S)	106
16 ^o	Et	(CH ₂) ₈ Me	H	(S)- 3-72	Cu(OTf) ₂	77	47 (S)	108
17	OMe	Me	Me	(S)- 3-72	Cu(OTf) ₂	75	96 (S)	106
18	OEt	Ph	Me	(S)- 3-72	Cu(OTf) ₂	57	99 (S)	106
19	Me	Me	Me	(S)- 3-72	Cu(OTf) ₂	60	91 (S)	106

^o Reaction run in DCM

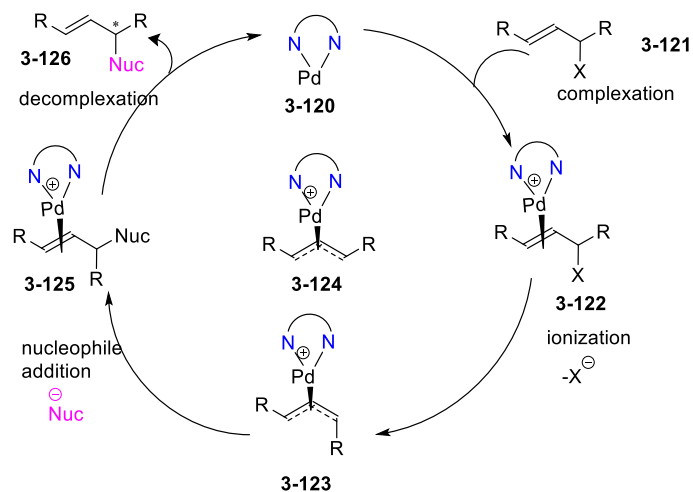
The approach of the diene on the *Re*-face of the square planar complex is hampered by the tert-butyl group therefore leading to the (S)-**3-118** arising from the attack on the *Si* face of the ketone coordinated to the Cu.



Scheme 15: Asymmetric induction of the intermediate 3-119.

3.1.5.2.5 Palladium chemistry

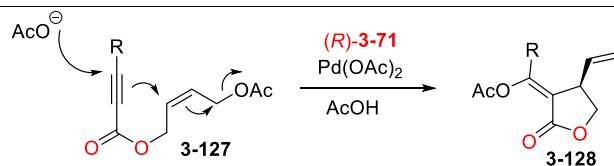
Box catalysts have also been tested on the palladium chemistry. One of the first application was in the field of Pd-catalysed nucleophilic allylic substitution reactions. The mechanism proposed entails the attack on the halo-allyl **3-121** by the BOX-Pd complex leading to a couple of diastereoisomer complexes, thus, reaction with the nucleophile followed by a decomplexation gives the optically active product (Scheme 13).



Scheme 16: Nucleophilic allylic substitution reactions mechanism.

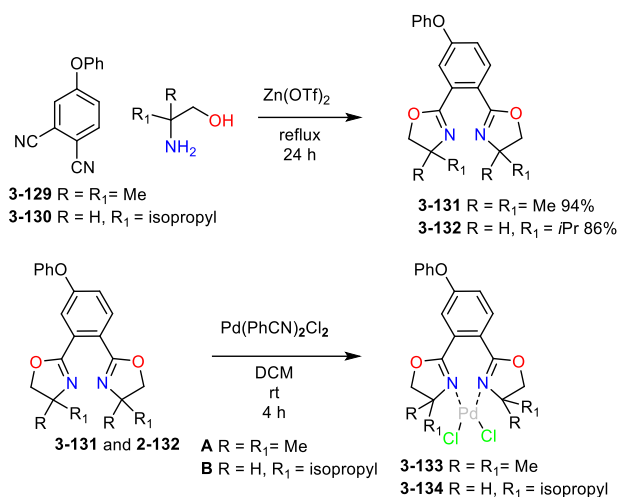
Zhang and Muthiah^[110-112] reported an interesting allylic substitution where the nucleophilic attack arises intramolecularly after the “activation” of an alkyne moiety through the Pd counter ion (OAc) compound **3-127** in combination with [(*R*)-**3-71**/Pd(OAc)₂] in acetic acid gives the lactone **3-128** with good ee (Table 20).

Table 20: Enantioselective intramolecular cyclization using BOX-Pd Catalysed.



Entry	R	Yield	ee (%)
1	Me	78	92 (<i>R</i>)
2	<i>n</i> -Pr	80	80 (<i>R</i>)
3	Ph	58	79 (<i>R</i>)
4	<i>i</i> -C ₇ H ₁₅	77	85 (<i>R</i>)
5	MeOCH ₂	67	87 (<i>R</i>)

Shakil reported the synthesis of two Pd-BOX complexes which he used for catalysing Suzuki-Miyaura and Mizoroki-Heck couplings (Scheme 14).^[113]



Scheme 17: Shakil's synthesis of complexes 3-133 and 3-134.

The BOX ligand was obtained by direct reaction between phthalonitrile and an amino alcohol catalysed by Zn(OTf)₂, subsequent of the same BOX ligand was reacted with PdCl₂(PhCN)₂ in DCM to yield the Pd complexes. Despite the ligands being achiral the author claimed an inherent chirality arising from the coordination with the Pd which induces a rigid backbone curvature with dihedral angle of 87.42(2)° and 85.7(2)°. The complex was crystallised as pseudo-racemate.

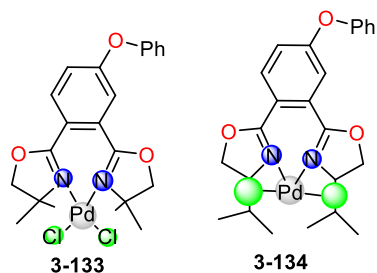


Figure 11: Complexes 3-133 and 3-134.

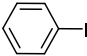
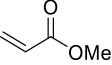
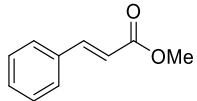
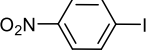
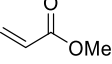
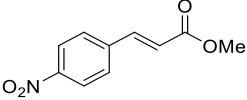
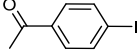
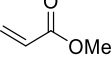
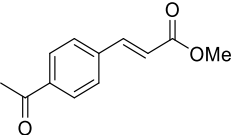
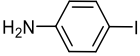
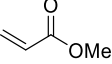
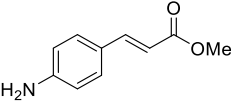
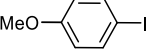
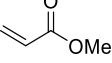
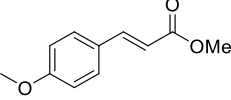
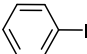
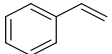
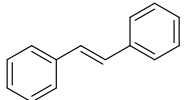
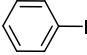
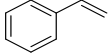
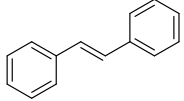
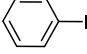
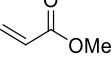
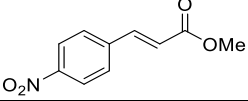
The two obtained complexes were used for catalysing the Suzuki and the Heck reaction; BOX ligands **3-133** and **3-134** allows coupling between aryl iodide and phenyl boronic acid in quantitative yield. The enrichment of both the aryl halide and phenyl boronic acid ring with

1	Pd-BOX (3-133)	100
2	Pd(OAc) ₂	93
3	PdCl ₂ (PhCN) ₂	88
4	PdSO ₄	85

Reaction conditions: Pd catalyst (0.01 mmol), iodobenzene (0.5 mmol), phenylboronic acid (0.6 mmol), K₂CO₃ (2.0 mmol), DMF (5.0 mL), 70 °C

These catalysts have also been successfully used in the Heck coupling between various aryl iodides and methyl acrylate or styrene. The aryl iodides possessing electron donating and electron withdrawing group react quantitatively with methyl acrylate whereas the reaction of the parent iodobenzene required higher temperature in order to reach competition ([Table 23](#)).

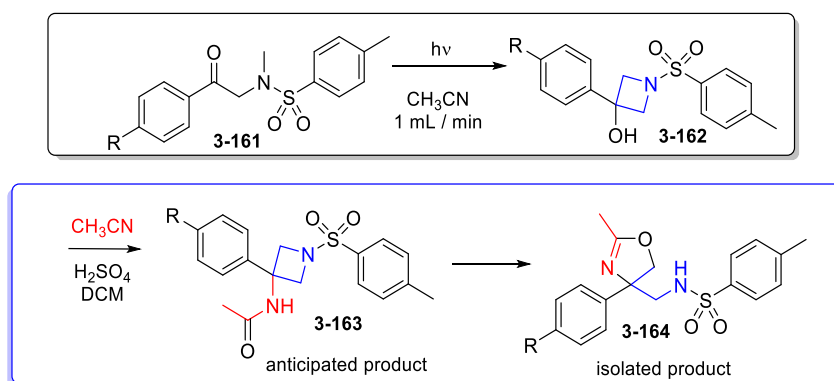
Table 23: Mizunoki-Heck coupling reaction between various aryl iodides and olefins catalysed by Pd-Box complex **3-133**^a.

Ar-I		+ $\text{CH}_2=\text{CH-R}$		$\xrightarrow[\text{K}_2\text{CO}_3, \text{DMF}, 70^\circ\text{C}, 12\text{ h}]{\text{Complex 3-133}}$		Ar-CH=CH-R	
n°	Aryl Halides	n°	Olefins	n°	Product		Yield % ^b
3-135		3-151		3-153			96
3-138		3-151		3-154			97
3-139		3-151		3-155			96
3-140		3-151		3-156			94
3-150		3-151		3-157			94
3-135		3-152		3-158			65
3-135		3-152		3-158			92 ^c
3-135		3-151		3-159			95 ^d

^a Reaction conditions: Pd-Box **3-113** or **3-114** (0.01 mmol), aryl halide (0.5 mmol), olefin (0.75 mmol), K₂CO₃ (2 mmol), DMF (5.0 mL), 70 °C, 120. ^bIsolated yield. ^cTemperature = 110 °C. ^dPd-Box (**3-114**) used

3.2 Results and discussions

In the second chapter, we described the preparation of a range of 3-hydroxyazetidines accessed via an efficient photochemical Yang reaction processed under flow conditions (Scheme 15, **3-161**→**3-162**).^[115] Having successfully demonstrated the scope, versatility and scalability of the reaction, we were particularly interested in expanding the medicinal chemistry value of the compound collection by applying simple secondary transformations to conduct functional group interconversions. As the starting materials **3-162** all possess a prominent tertiary benzylic alcohol, we first contrived to replace this group with an amide through a Ritter reaction.



Scheme 18: Formation of the 3-hydroxyazetidine via the Yang reaction and proposed Ritter reaction (blue box).

In a simple procedure, the substrate was refluxed in DCM (30 min) in the presence of 1 equivalent of sulfuric acid and an excess of acetonitrile. Although the reaction proceeded smoothly with full consumption of the starting material, to our initial surprise, the compound formed was not the expected amide **3-163** but a new cyclic, rearranged, structure **3-164** (90% isolated yield) which we determined to be a 2-oxazoline derivative (Figure 12).

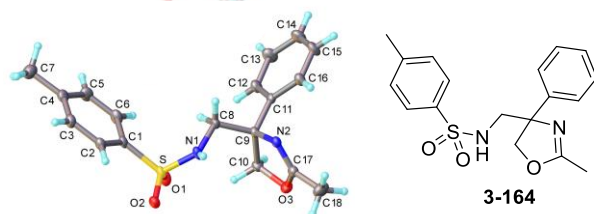
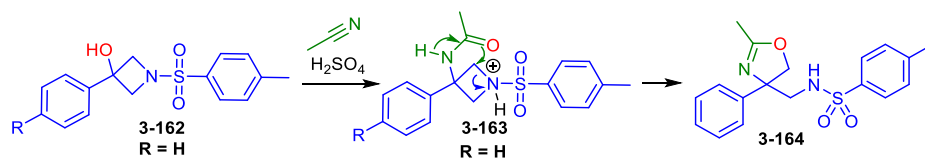


Figure 12: X-ray structure of compound **3-164** isolated from the attempted Ritter reaction.

To account for its formation, we propose a direct cascade sequence which initiates through a standard Ritter reaction. The intermediate Ritter product we propose rapidly undergoes further rearrangement in which the amide carbonyl group attacks and ring opens the azetidine **3-163**, driven by the relaxation of the 4-membered ring strain (Scheme 16).



Scheme 19: Proposed mechanism for the rearrangement of 3-hydroxyazetidines under Ritter type conditions.

Although this was not our intended transformation, this reaction represents a previously unreported and interesting rearrangement sequence leading in high yield to a set of novel oxazoline scaffolds. As such we decided to further investigate the process.

3.2.1 Optimization: Acid Screening

In an attempt to optimize the reaction, we evaluated a range of acid sources to determine their impact on the new transformation. The evaluation reactions were run with 1 equivalent of each acid source, namely, H_2SO_4 , HBF_4 , $\text{CH}_3\text{SO}_3\text{H}$ and *p*-TSA (*p*-toluenesulfonic acid) giving respectively 90%, 85%, 40% and 35% isolated yield of product **3-162** (standard 30 min reaction time). It should be noted that the use of sub-stoichiometric quantities of acid gave comparable results but required the use of much extended reaction times; this was ultimately found to be detrimental to the quality of the product isolated which showed more decomposition over prolonged reaction times. Other acids were also tested, such as acetic

acid, $\text{CF}_3\text{CO}_2\text{H}$, polyphosphoric acid (PPA), Eaton's reagent (phosphorus pentoxide - methanesulfonic acid 10:1 by wt.) and camphorsulfonic acid (CAMPHOR) but were all completely ineffective, with no product being detected (>4 h reaction time), and the starting material being recovered quantitatively. Interestingly, attempting to employ a solution of $\text{HCl}\cdot\text{Et}_2\text{O}$ resulted in the slow formation of the corresponding chloro-substituted product **3-162b** (Figure 13). It was noted that increasing the proportion of HCl over water in the mixture resulted in higher quantities of the resultant chloro product **3-162b** being detected.

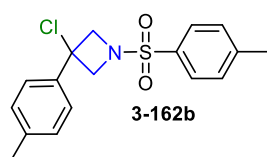


Figure 13: Reaction product obtained through treatment with hydrochloric acid.

The attempted catalysis of the transformation was also studied employing several different Lewis acids (1 equivalent). Among these FeCl_3 , ZnCl_2 , AlCl_3 and $\text{Cu}(\text{OTf})_2$ all failed to promote any reaction, whereas $\text{BF}_3\cdot\text{OEt}_2$ initially looked promising giving fast early reaction turnover but quickly becoming inactive and resulting in a maximum 50% conversion (38% isolated). We suspect that the boron trifluoride becomes rapidly deactivated by the generated water thus preventing the turnover of the desired reaction. This is evidenced by the addition of further amounts of $\text{BF}_3\cdot\text{OEt}_2$ (> 2 equivalent) which continues to progress the reaction, although the reaction mixture become increasingly complex with multiple decomposition products being observed by TLC and $^1\text{H-NMR}$.

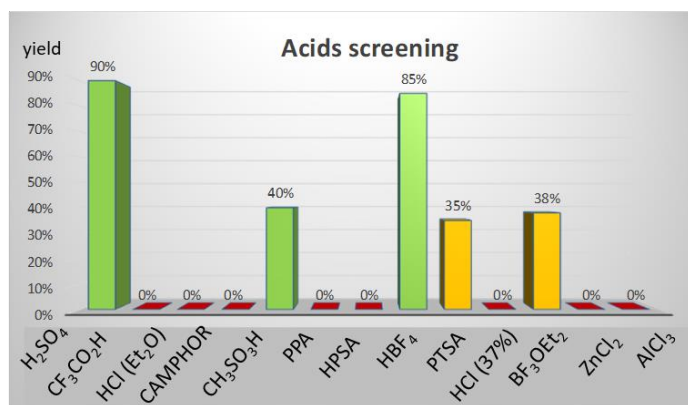


Figure 14: The results from the acid screening.

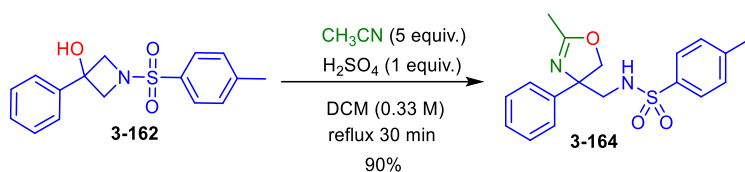
While the results obtained with H₂SO₄, CH₃SO₃H and *p*-TSA can be accounted for by their relative *p*K_a and dehydrating effect, the surprising outcome was with HBF₄ (48 wt% aqueous solution) which gave 85% based upon full consumption of the starting material. By contrast, any dilution of the other acids i.e. H₂SO₄ with water led to a significant drop in reactivity and incomplete (stalled) reaction. This seems to confirm the interesting property of the HBF₄ aqueous solution as previously noted by Stutz *et al.*^[116] who found mixtures of HBF₄ (aq.) in acetonitrile was able to rapidly cleave acetals, BOC groups and *tert*-butyldimethylsilyl ethers within minutes at room temperature, and was more effective than many other acids/solutions of acids.

In summary, H₂SO₄ gave the best conversion and yield, thus, considering factors like safety, price and availability, it remains the best choice of catalyst for further testing and optimization of the transformation.

3.2.2 Optimization: Solvent choice

Our solvent selection for the process was rather restricted due to reactivity and the solubility of the substrate and product. Chloroform was found to work equally well as DCM; ethyl acetate and THF could also be used, but the yields were reduced (~5-15%) and accompanied by unidentified minor impurities. Other potential solvents, such as toluene, xylenes, chlorobenzene and trifluorobenzene, were insufficiently solubilizing. Interestingly, the effect of reflux temperature between DCM and chloroform seemed to offer little advantage with

both reactions being complete in ~10-12 minutes and yielding identical product outcomes. Eventually the optimum conditions for performing the reaction entailed the use of 1 equivalent of nitrile (5 equivalents in case of the acetonitrile for which the excess can be easily removed by evaporation) 1 equivalent of sulfuric acid in DCM (0.33 M) refluxing the solution for 30 minutes (Scheme 17).



Scheme 20: general conditions for the synthesis of substrate **3-164**.

3.2.3 Substrate scope

Having determined some general reaction conditions, we next embarked upon an evaluation of the reaction scope in terms of both the azetidine and nitrile components. We were pleased to find the reaction proved general allowing a range of products to be assembled in good to high yield (Table 31). The rapid rate of reaction (~10 minutes) and relatively mild conditions enabled several different functional groups to be tolerated. In each case, the progression of the reaction was easily followed by LC-MS.

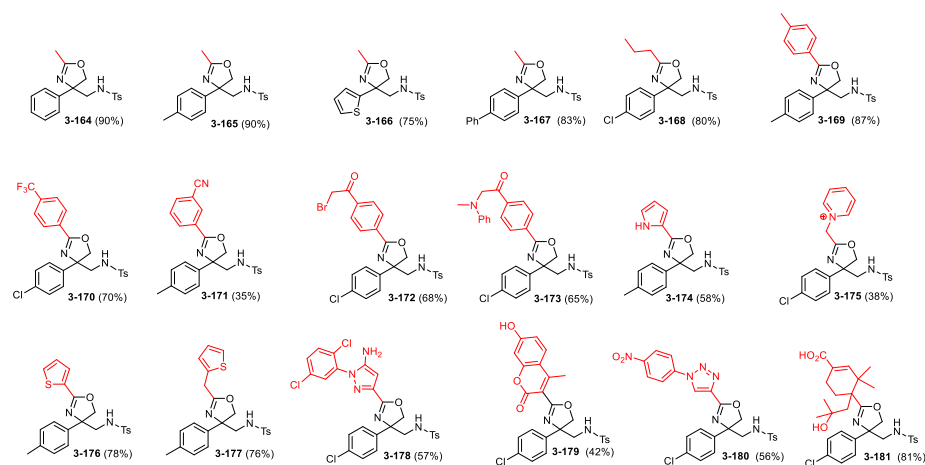


Table 8: Investigation of substrate scope.

Percentages in parentheses are isolated yields.

After testing some different structural changes with regard to the azetidinic aromatic moiety (**3-164** – **3-167**) we also made several alterations to the nitrile component. Initially we looked at extending the alkyl group (**3-168**) and then exchanging it with an aromatic ring which we functionalised in order to evaluate the compatibility of different appended groups (**3-169** – **3-173**). We then progressively increase the complexity of the nitrile derivatives with the aim of assessing the synthetic scope of the transformation. This included testing several heterocyclic species (**3-174** – **3-177**) then more varied architectures (**3-178** – **3-181**).

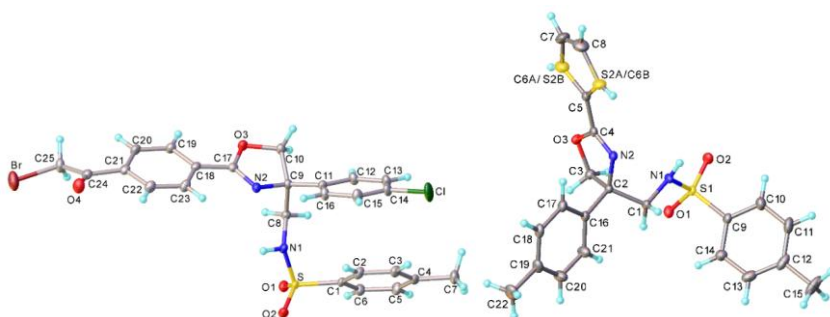


Figure 15: X-ray structures for compounds **3-172** (left) and **3-176** (right).

Several starting materials were not commercially available but had been prepared in the group previously allowing their use, these included compounds **3-178**, **3-180** and **3-181**.^[117-119] Specifically compound **3-178** was obtained starting from the 5-amino-4-cyanopyrazoles which was prepared using a flow microwave reaction between 2,5-dichlorophenyl-hydrazines and ethoxymethylene malononitrile synthesised in methanol (Figure 16).^[117]

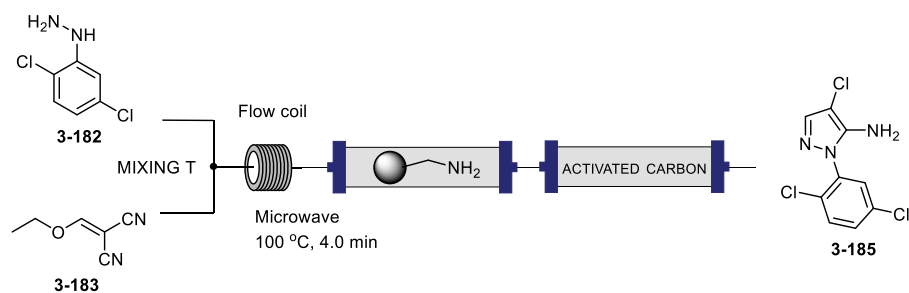
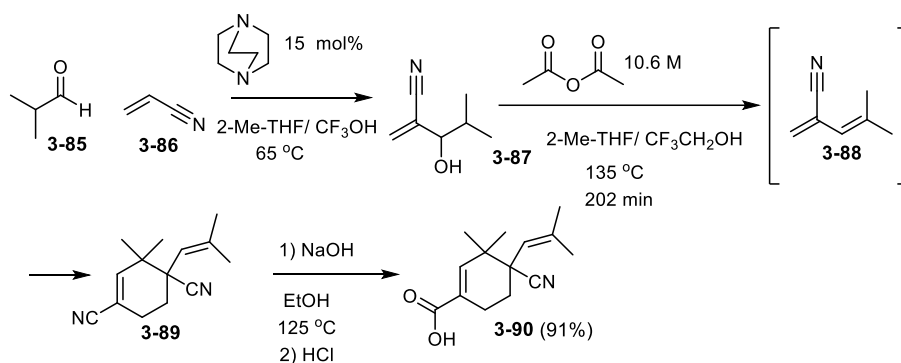


Figure 14: Flow microwave synthesis of *N*-((2-(5-amino-1-(2,5-dichlorophenyl)-1H-pyrazol-3-yl)-4-nitrile (**3-185**).

The 4-cyano-4-(2-methylprop-1-enyl)cyclohexen-1-ene carboxylic acid starting material (**3-190**) used for compound **3-181** was obtained from a Baylis-Hillman reaction between acrylonitrile and isobutyraldehyde catalysed by DABCO (15 mol-%) (Scheme 10). The intermediate was then dehydrated and cyclized in a Diels-Alder reaction which was followed by base hydrolysis to yield the desired cyclic nitrile.^[119]



Scheme 21: Synthesis of compound **3-90**.

The scope expansion of the reaction aptly demonstrates the synthetic value of the transformation exemplifying how it is possible to access complex structures. In general, it was found that simple alkyl and aryl nitriles worked well (Table 31 compounds **3-164** – **3-169**). Even basic and acidic containing functionalities proved amenable, although isolation involving neutralisation of the product mixture was more difficult and thus, resulted in lower recoveries (**3-173** – **3-175**, **3-178** – **3-181**). We also experienced issues with the isolation of compound **3-175**, which was produced as a mixed salt; additional optimisation beyond the proof of concept on this substrate was not performed. Finally, compound **3-181** could be isolated but required the use of excess acid as the hydration of the alkene moiety competes with the protonation of the azetidine alcohol required for the carbocation formation (Figure 17). Therefore, when only 1 equivalent of the acid was used, a complex mixture of the alkene **3-191**, alcohol starting material **3-162** and their corresponding mixed hydrated products (**3-181**, **3-191**) was

obtained. Whereas with an excess of acid (2.3 equivalents), selective conversion of the starting material to compound **3-181** in a respectable 81% isolated yield was achieved (Figure 11)

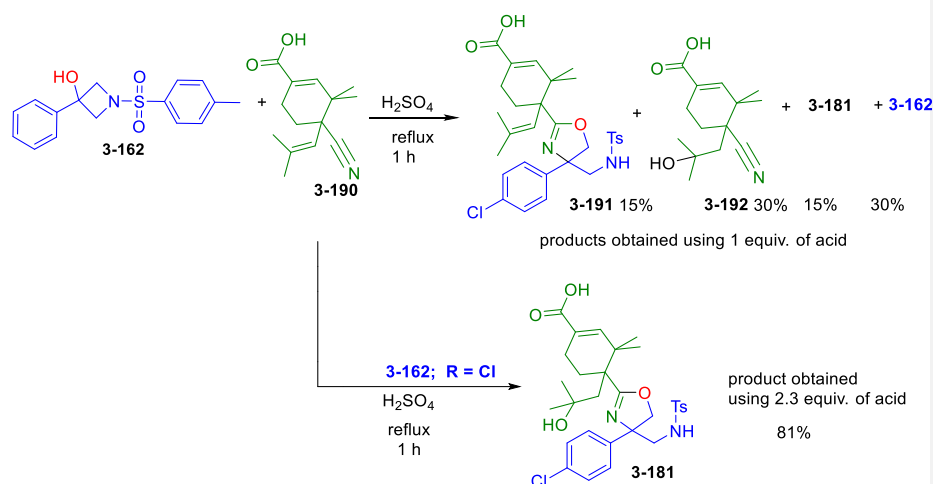
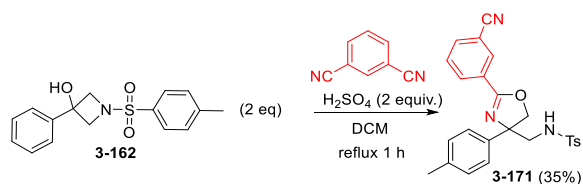


Figure 17: Cascade sequence forming hydrated compound **3-181**.

Product compositions were determined using 4-(dimethylamino)benzonitrile as internal standard on the crude reaction mixtures.

Considering the positive results obtained, we considered the possibility of preparing dyad molecules through double addition to the *bis*-nitrile precursors. Starting with 1,3-dicyanobenzene and using 2 equivalents of the azetidine (**3-162**, R = Me), we were surprised that no product from the double addition was detected. Instead, only a low yield of the mono oxazolidine **3-81** (35%) was produced. However, when observing a repeat reaction more closely, we attributed this to the poor solubility of the starting nitrile and its resulting single addition adduct **3-81**, which seemed to immediately precipitate upon formation. Overall, the limited dissolution resulted in poor mixing and ineffective reaction. Unfortunately, the use of added solvents such as DMF to help solubilize the starting materials completely shut down the reaction, presumably by attenuating the pH (protonation of the DMF). Other solvents or

additives, like the addition of EtOAc or MeOH or EtOH in order to increase the solubility of the reagent, also failed to improve the situation.



Scheme 22: Azetidine rearrangement with the bis-nitrile.

We therefore selected a more soluble *bis*-nitrile starting material, glutaronitrile, which was subjected to the same reaction conditions (2 equivalents of azetidine and 2 equivalents of H₂SO₄ in refluxing DCM). In this case, we successfully isolated from the reaction, 3 compounds; the meso **3-193** and racemic **3-194** diastereoisomers along with the corresponding mono substituted oxazolidine **3-195** (Figure 18). These were formed in a ratio of 1:1:1.1, respectively, as determined by ¹H NMR analysis of the crude reaction mixture.

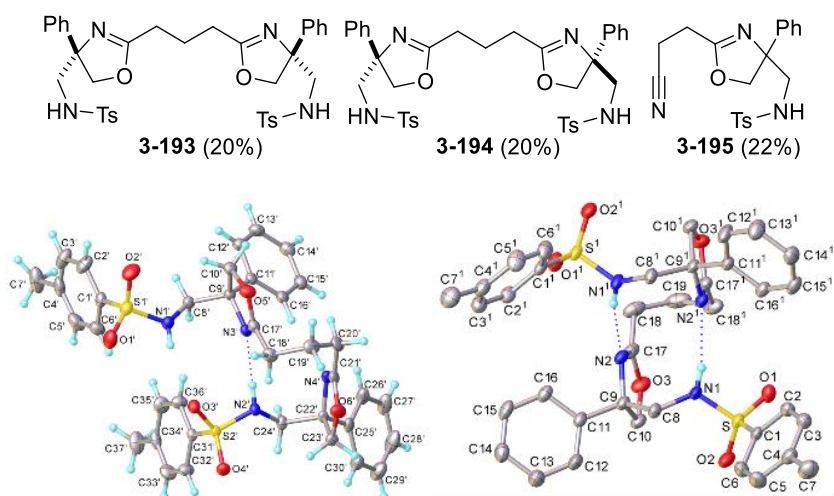


Figure 15: Reaction products of 1,3-dicyanopropane (glutaronitrile) with 3-hydroxazetidine **3-195** (*R* = Me) forming dyad molecules. X-ray images of **3-193** (left) and **3-194** (right).

The two dyads possess very different and interesting solid state and solution interactions. As can be seen from the single crystal X-ray representations (Figure 18), the racemic structure **3-**

194, forms a set of complementary hydrogen bonds creating a tight dimeric pairing (oxazole to sulfonamide NH linkage). This interaction seems to also be observed in solution as evidenced by the ^1H NMR, where the NH signals appear at a high chemical shift of 9.17 ppm (2H, CDCl_3). This same synergistic interaction is absent in the meso compound **3-193**, instead only a single intramolecular hydrogen bond occurs, a bridging H-bonding methanol molecule helps form a secondary interaction in the solid-state structure (Figure 19).

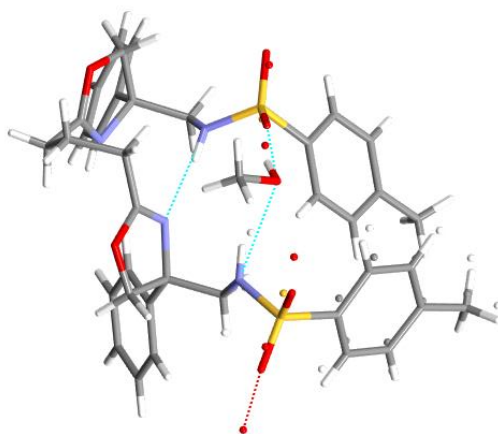


Figure 19: X-ray image of meso compound **3-193** showing the additional solvent (MeOH) H-bonding interaction.

The corresponding ^1H NMR solution state NH signals of **3-193** gives rise to a much lower resonance at 7.06 ppm (2H, CDCl_3). This data is consistent with compound **3-193** adopting a weaker set of hydrogen bond interactions. Indeed, this trend is completed when it is compared to the monomer **3-195** which shows a NH signal at 5.21 ppm (indicative of no H-bonding), this is also fully consistent with the other mono-oxazole structures (Figure 5, NH signal range 5-6.5 ppm). We therefore hypothesize that structure **3-193** is unable to hydrogen bond as tightly as **3-194** due to its mismatching stereochemistry (easily seen by comparing the X-ray forms, Figure 18) and as such adopts in solution a more dynamic structure allowing rapid exchange between the two sets of H-bonding sulfonamide and oxazole (equating to an average NH signal). This exchange process is potentially assisted by the presence of small H-bonding solvent molecules. This is exemplified when using extensively dried NMR solvent (CDCl_3). The recorded spectra of **3-193** gives broad and poorly resolved signals, yet with the addition of a H-donor/acceptor molecule i.e. H_2O or MeOH the signals immediately sharpen

giving well defined patterns and coupling. We take this as an indication of a faster exchange process in the presence of the H-bonding capable molecule. In comparison, no effect is seen in the ^1H NMR for structures **3-194** or **3-195** (Figures 20 and 21).

13135749.10.fid

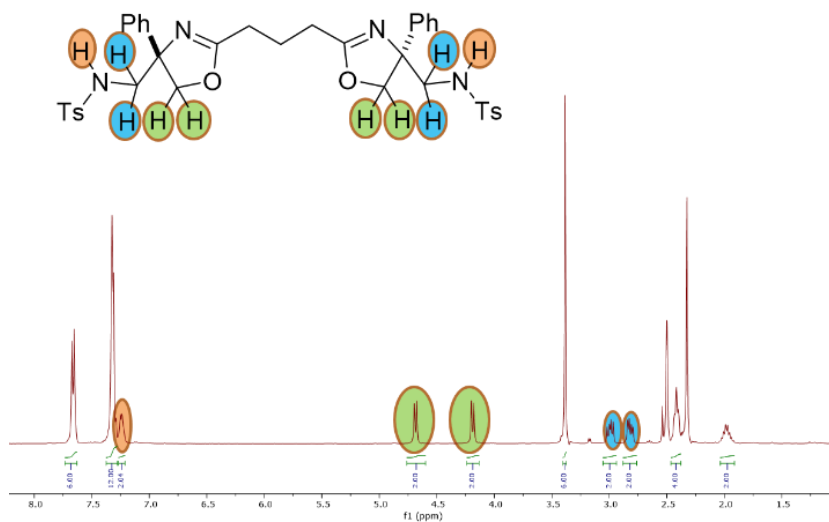


Figure 20: ^1H NMR spectra of compounds **3-193**.

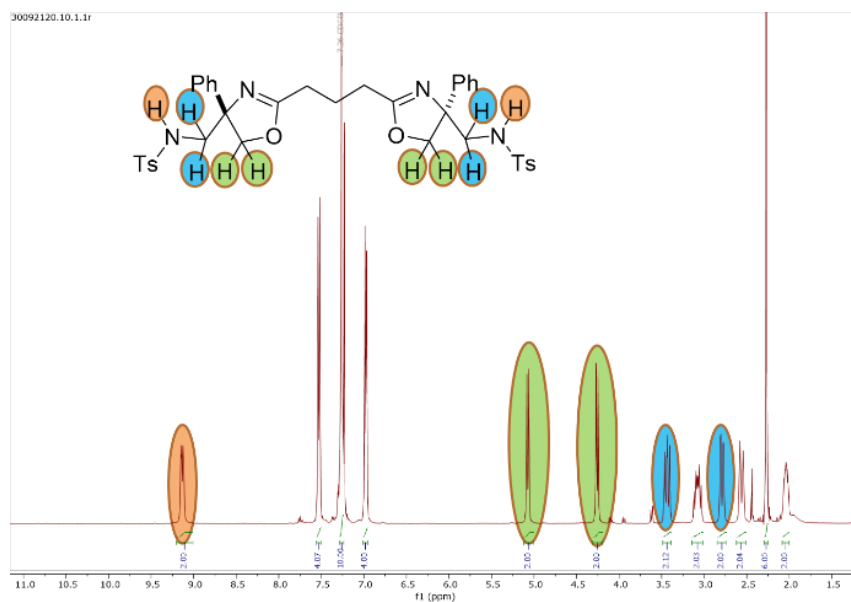
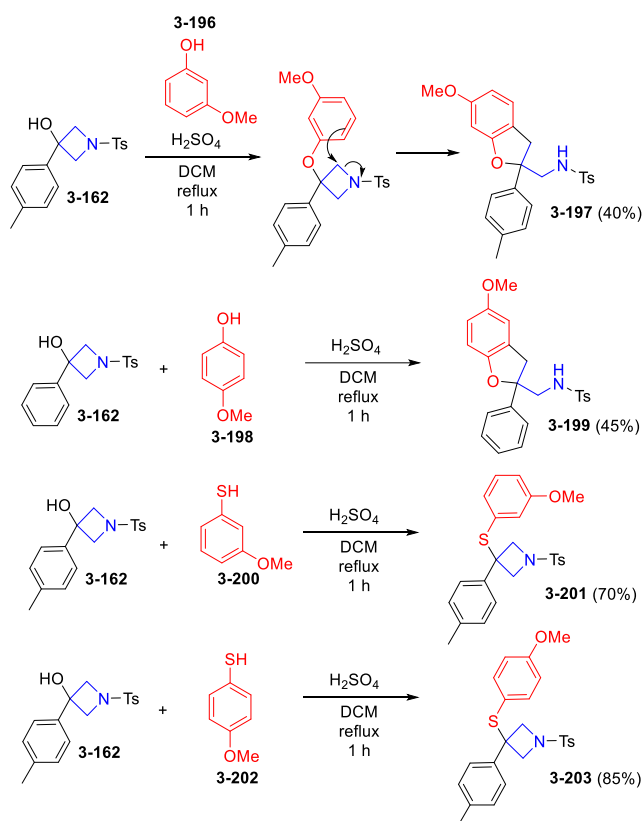


Figure 16: ^1H NMR spectra of compound **3-194**.

3.2.4 Investigating Alternative Nucleophiles

Having established that the azetidine ring could be readily opened in an intramolecular process, we considered the possibility of creating other related cascades involving for example, an aromatic ring acting as the nucleophile (Scheme 20, compounds **3-197** – **3-203**).



Scheme 23: Investigating Alternative Nucleophiles.

Initial success was immediately achieved using the 3- and 4-methoxyphenols, which each gave the rearrangement product as determined by NMR and later confirmed by single crystal X-ray analysis for compound **2-197**. However, when the alternative 3- and 4-methoxythiophenols were instead used, the azetidine was converted to the intermediate substitution product, but the secondary cyclisation was not observed, even after prolonged reaction times. We eventually managed to obtain an X-ray crystal structure of compound **2-201** (Figure 22) which clearly shows the elongated C-S bonds (C2/S2 1.825 & S2/C18 1.779 Å), this would make it impossible to adopt the correct alignment with sufficient orbital overlap between C23 – C1/C3 for the ring opening to occur. Hence, no cyclisation was observed.

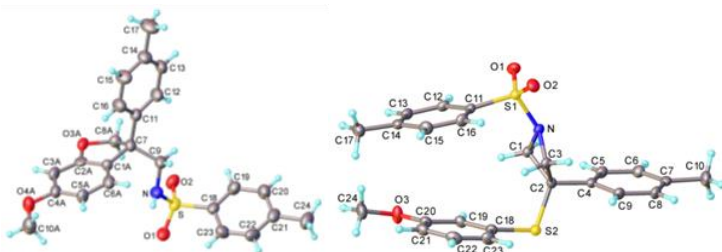


Figure 22: X-ray structure of compounds **3-199** (left) and **3-201** (right).

3.2.5 Further Intramolecular Reactions

In our initial substrate scope experiments, we had shown it was feasible to carry a bromide appendage on the nitrile component, compound **3-172** (Table 31). In addition, we explored the tosylamide nucleophilicity, which we expected to be good due to the high degree of sp^3 character suggested both by looking at the X-ray structure (Figure 6) and at the ^1H NMR NH shift and J values (NH coupling with the vicinal CH_2). To experimentally confirm the nucleophilic reactivity, we performed a displacement reaction on 2-bromo-1-(4-bromophenyl)ethanone (**3-204**, Figure 22).

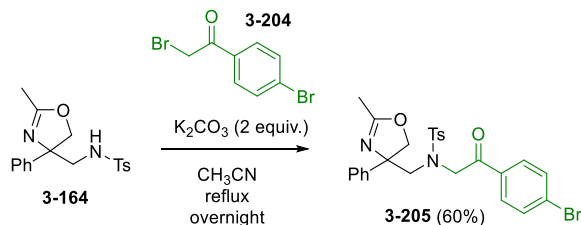


Figure 22: Synthesis of compound **3-105**.

These observations led us to explore the use of nitrile precursors which would result in products containing residual alkyl halide chains generated from the Ritter cascade (Figure 23, 19). Our proposal was that these could then enable a further intramolecular substitution reaction furnishing very interesting bicyclic products.

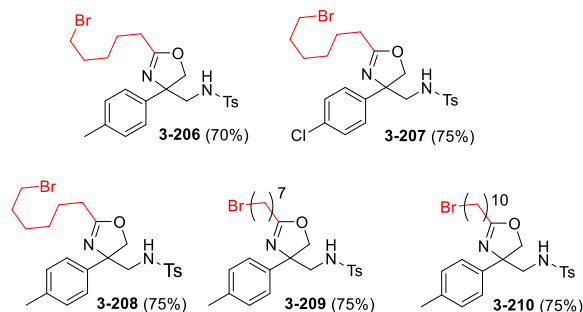


Figure 23: Products of the azetidine rearrangement prepared with pendant alkyl bromide side chains.

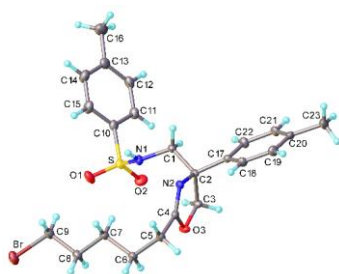


Figure 17: X-ray structure of compound **3-206**.

Following this strategy, we successfully prepared a series of suitable starting materials (**3-206** – **3-210**, Figure 23) using the previously described methodology in good isolated yields. These were then treated with K_2CO_3 under reflux in acetonitrile (36 h) to generate new cyclised compounds **3-211** – **3-215** (Figure 25). To the best of our knowledge, this type of oxazoline bridge head has never been reported before.

The difference in isolated yields of these macrocyclic compounds can be rationalised by considering both the change in ring size (ring strain) and the increasing length of the linking tether in terms of the statistical likelihood of the cyclisation event. Hence, due to the smaller ring size, **3-111**, a 10 membered ring, is a more strained structure (leads to a lower yield); whereas formation of the 15 membered ring, **3-215**, is kinetically less favoured, again resulting in a lower yield. Overall, this series of products represents a further intriguing structural diversification of the parent oxazolines via very simple chemical manipulations.

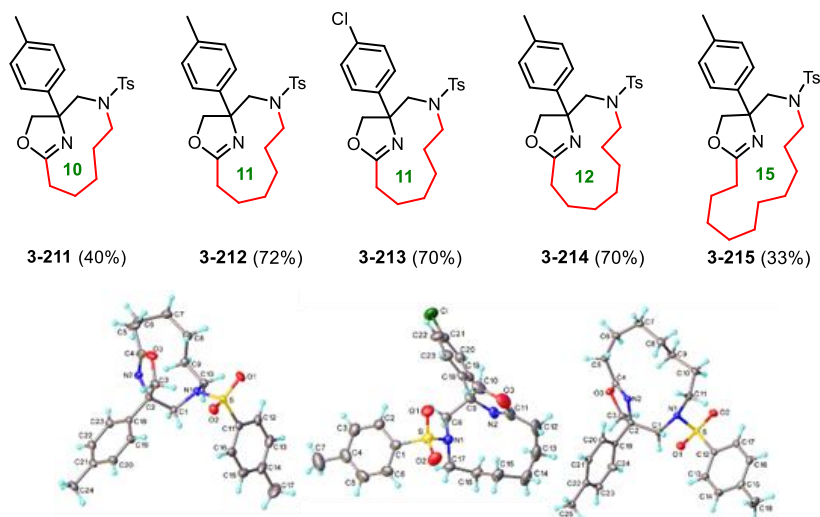


Figure 18: Intramolecular cyclization products and representative X-ray structure of compound 3-212, 3-213 and 3-214.

3.2.6 Development of a Flow Process

As these macrocyclic compounds were of particular interest as novel molecular entities, we wished to scale up their synthesis in order to access greater quantities of material for biological investigation. Therefore, the same intramolecular cyclizations were also attempted in flow where the enclosed reactor would allow higher reaction temperatures to be achieved to promote potentially faster reactions.^[120-122]

The reactions were performed using a Vapourtec-E series flow reactor system^[123] fitted with a packed column reactor containing K_2CO_3 (Figure 26). The use of a back-pressure regulator (100 psi) allowed the reaction temperature to be increased to 130 °C without changing the solvent (acetonitrile). The reaction was carried out by directing a flow stream of the starting alkyl halide (**3-206** – **3-210**) stock solution at a concentration of 0.1 M through the packed column at rate of 400 $\mu\text{L min}^{-1}$. Notably under these conditions, equitable yields were obtained whilst reducing the reaction time from 36 h to 1.5 h. This enables easy access to gram quantities of the products with a productivity of 772 mg h^{-1} (**3-113**, 72% yield), and the ability to produce 5 g in a standard 8 h working day even taking into account reactor set-up, priming, washing and shutdown.

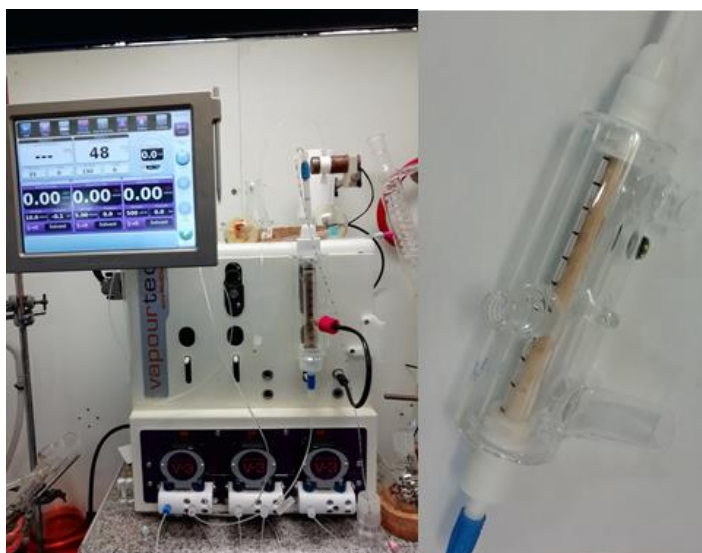


Figure 19. Flow reactor set up used for scale up of products **3-112**– **3-115**.

3.3 CONCLUSION

We have shown a novel and general Ritter based cascade involving the condensation of a nitrile and a 3-hydroxyazetidone leading to the formation of new 2-oxazoline scaffolds. The cascade can also be exploited using other nucleophilic components such as phenols, which indicates additional bifunctional nucleophiles may also be viable. In addition, we have shown that specific alkyl bromide substituted 2-oxazolines prepared using this methodology can be further cyclised in an intramolecular process to create unique bicyclic heterocycles. This last transformation has been developed in flow employing a packed column reactor reducing dramatically the reaction time and allowing the scale up of the reaction.

3.4 Future work

Following the route that lead to compounds **3-211** – **3-115** the halo nitrile chain can be functionalised in order to prepare other cyclic structures (Figure 27) this would allow the installation of an extra ring on the original structure resulting in a tricyclic product and opening the way to more interesting functionalizations.

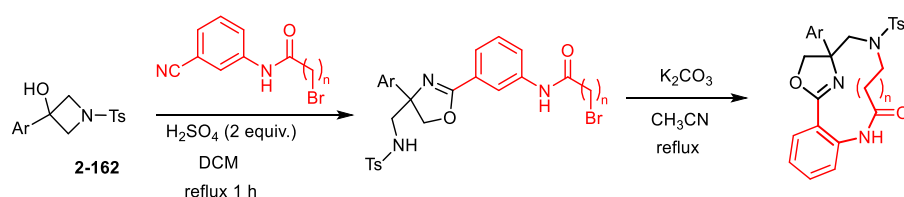
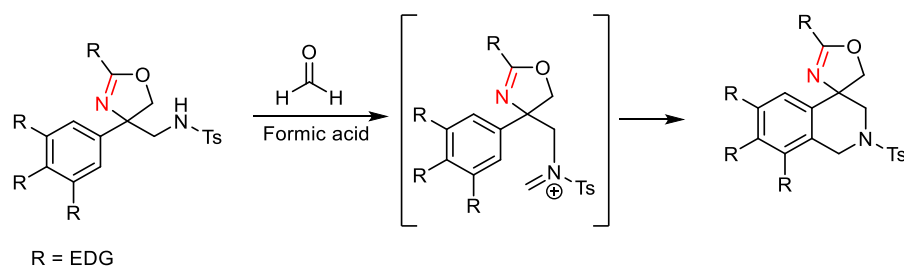


Figure 27. Proposed *Intramolecular cyclization with enriched macrocycle*

The synthesis of compound **3-205** demonstrated the nucleophilic character of compound **3-164**. The general structure of the 2-oxazolines obtained has the right features for attempting a Pictet-Spengler reaction^[114] on the original substrate. The reaction between the free nitrogen and formaldehyde would allow the generation of an electrophile that is liable to be attacked by the aromatic ring, especially if this was fictionalised with electron donating groups. The reaction would result in the cyclization of the substrate leading to a tricyclic spiro compound.

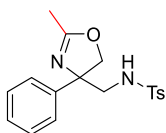


3.5 Experimental Section

General procedure for the rearrangement of 3-164 – 3-210: To a solution of 3-hydroxyazetidine **2-162** (3.15 mmol) in DCM (10 mL), was added 1 equiv. of H₂SO₄ dropwise, followed by 1 equiv. of the nitrile (6 equiv. when the nitrile was acetonitrile) dissolved in DCM (3 mL). The reaction was heated at reflux and monitored by GC/LC-mass spectra. Upon complete disappearance of the starting material, the mixture was neutralised with an excess

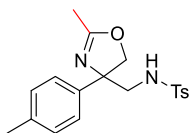
of sat. aq. Na₂CO₃, and the mixture was extracted with EtOAc, washed with brine, dried over Na₂SO₄, filtered and the solvent evaporated under reduced pressure. The resulting material was purified by chromatography column (typically with a mixture of hexane: EtOAc).

General flow procedure for the synthesis of 3-211 – 3-215: A stock solution was prepared from the appropriate alkyl halide (2 mmol, **3-206 – 3-210**) dissolved in acetonitrile (0.1 M). The solution was pumped at a flow rate of 400 μL min⁻¹ through a 100 x 6.6 mm packed column reactor (4.10 mL) filled with K₂CO₃ and equipped with adjustable end pieces. A 100 psi back pressure regulator was added to the outlet line and the column reactor heated in the Vapourtec E2 column heater at 130 °C. The acetonitrile was removed by evaporation, the residue was dissolved in EtOAc, washed with water, brine and dried over Na₂SO₄. After evaporation the resulting material was purified by chromatography column (hexane / EtOAc).



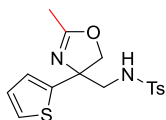
4-Methyl-N-((2-methyl-4-phenyl-4,5-dihydrooxazol-4-yl)methyl)benzenesulfonamide (3-164).

Appearance Yellow oil, 90 %; ¹H NMR (400 MHz, CDCl₃) δ 7.65 (d, *J* = 8.3 Hz, 2H), 7.32 – 7.18 (m, 9H), 5.53 (dd, *J* = 9.1, 4.6 Hz, 1H), 4.78 (d, *J* = 8.5 Hz, 1H), 4.31 (d, *J* = 8.5 Hz, 1H), 3.27 (dd, *J* = 12.8, 9.1 Hz, 1H), 3.02 (dd, *J* = 12.8, 4.6 Hz, 1H), 2.38 (s, 3H), 2.10 (s, 3H); ¹³C NMR (101 MHz, CDCl₃) δ 167.30 (C), 143.80 (C), 143.54 (C), 137.04 (C), 129.87 (CH), 128.84 (CH), 127.75 (CH), 127.02 (CH), 125.56 (CH), 75.99 (C), 75.89 (CH₂), 51.71 (CH₂), 21.59 (CH₃), 14.14 (CH₃); IR (neat) ν = 3282.4 (w), 1737.6 (m), 1696.3 (m), 1648.3 (m), 1359.0 (m), 1219.3 (m), 1211.6 (s), 1024.4 (m), 914.6 (m), 721.2 (m), 701.9 (m), 651.3 (m), 590.3 (s), 542.8 (s) cm⁻¹; HR-MS calculated for C₁₈H₂₁N₂O₃S 345.1273, found 345.1281 (Δ = -2.3 ppm, 0.8 mDa); X-ray CCDC (1985621) Unit Cell Parameters: a 15.4987(8) b 11.7051(6) c 21.9098(11) C2/c.



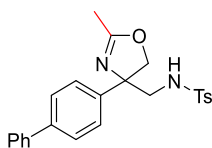
4-Methyl-N-((2-methyl-4-(p-tolyl)-4,5-dihydrooxazol-4-yl)methyl)benzenesulfonamide (3-165).

Appearance :White solid, 90% ^1H NMR (400 MHz, CDCl_3) δ 7.66 (d, J = 8.0 Hz, 2H), 7.19 (d, J = 8.0 Hz, 2H), 7.10 – 7.01 (m, 4H), 6.57 (dd, J = 9.0, 4.8 Hz, 1H), 4.84 (d, J = 8.5 Hz, 1H), 4.28 (d, J = 8.5 Hz, 1H), 3.28 (dd, J = 13.2, 9.0 Hz, 1H), 2.98 (dd, J = 13.2, 4.8 Hz, 1H), 2.38 (s, 3H), 2.30 (s, 3H), 2.11 (s, 3H); ^{13}C NMR (101 MHz, CDCl_3) δ 167.32 (C), 143.15 (C), 140.81 (C), 137.37 (C), 137.20 (C), 129.70 (CH), 129.33 (CH), 126.86 (CH), 125.30 (CH), 75.77 (CH_2), 75.77 (C), 51.41 (CH_2), 21.45 (CH_3), 20.97 (CH_3), 13.88 (CH_3); IR (neat) ν = 3468.8 (w), 2961.8 (w), 1330.4 (s), 1180.9 (m), 1147.5 (s), 1088.2 (m), 814.5 (s), 677.0 (s), 516.0 (s) cm^{-1} ; HR-MS calculated for $\text{C}_{19}\text{H}_{23}\text{N}_2\text{O}_3\text{S}$ 359.1429, found 359.1424 (Δ = -1.4 ppm, -0.5 mDa); Melting point: 120-122 $^\circ\text{C}$ (crystallised from CHCl_3).



4-Methyl-N-((2-methyl-4-(thiophen-2-yl)-4,5-dihydrooxazol-4-yl)methyl)benzenesulfonamide (3-166).

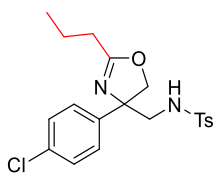
Appearance: Yellow oil, 75%, ^1H NMR (400 MHz, CDCl_3) δ 7.67 (d, J = 8.4 Hz, 2H), 7.23 (d, J = 8.4 Hz, 2H), 7.17 (dd, J = 5.1, 1.2 Hz, 1H), 6.93 (dd, J = 5.1, 3.6 Hz, 1H), 6.83 (dd, J = 3.6, 1.2 Hz, 1H), 5.86 (dd, J = 9.0, 4.9 Hz, 1H), 4.79 (d, J = 8.6 Hz, 1H), 4.37 (d, J = 8.6 Hz, 1H), 3.30 (dd, J = 13.0, 9.0 Hz, 1H), 3.15 (dd, J = 13.0, 4.9 Hz, 1H), 2.39 (s, 3H), 2.09 (s, 3H); ^{13}C NMR (101 MHz, CDCl_3) δ 168.23 (C), 147.61 (C), 143.53 (C), 137.03 (C), 129.84 (CH), 127.25 (CH), 127.01 (CH), 124.78 (CH), 122.83 (CH), 76.25 (CH_2), 74.03 (C), 51.16 (CH_2), 21.57 (CH_3), 13.95 (CH_3); IR (neat) ν = 2923.7 (w), 1656.3 (m), 1327.0 (s), 1156.8 (s), 1089.6 (s), 813.9 (m), 752.4 (m), 659.6 (s), 549.8 (s) cm^{-1} ; HR-MS calculated for $\text{C}_{16}\text{H}_{19}\text{N}_2\text{O}_3\text{S}_2$ 351.0837, found 351.0825 (Δ = -3.4 ppm, -1.2 mDa).



N-((4-([1,1'-Biphenyl]-4-yl)-2-methyl-4,5-dihydrooxazol-4-yl)methyl)benzenesulfonamide (3-167).

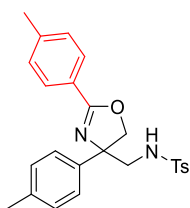
Appearance: Pale Yellow oil, 83%, ^1H NMR (400 MHz, CDCl_3) δ 7.68 (d, J = 8.3 Hz, 2H), 7.57 – 7.52 (m, 4H), 7.44 (t, J = 7.5 Hz, 2H), 7.38 – 7.34 (m, 3H), 7.24 (d, J = 8.2 Hz, 2H), 5.41 (s, 1H),

4.96 (d, $J = 8.7$ Hz, 2H), 4.49 (d, $J = 8.7$ Hz, 2H), 3.31 (dd, $J = 13.1, 9.0$ Hz, 1H), 3.17 (dd, $J = 13.1, 4.9$ Hz, 1H) 2.37 (s, 3H), 2.23 (s, 3H); ^{13}C NMR (101 MHz, CDCl_3) δ 143.71 (C), 141.13 (C), 140.30 (C), 136.85 (C), 129.94 (CH), 129.86 (C), 128.98 (CH), 128.47 (C), 127.74 (CH), 127.15 (CH), 127.06 (CH), 127.03 (CH), 125.96 (CH), 77.00 (CH_2), 75.10 (C), 51.56 (CH_2), 21.60 (CH_3), 14.25 (CH_3); IR (neat) $\nu = 2981.7$ (w), 1744.1 (m), 1233.9 (m), 1158.1 (s), 1050.9 (m), 908.8 (m), 730.3 (s), 697.6 (m), 549.8 (m) cm^{-1} ; HR-MS calculated for $\text{C}_{24}\text{H}_{25}\text{N}_2\text{O}_3\text{S}$ 421.1586, found 421.1581 ($\Delta = -1.2$ ppm, -0.5 mDa).



N-((4-(4-chlorophenyl)-2-propyl-4,5-dihydrooxazol-4-yl)methyl)-4-methylbenzenesulfonamide (3-168).

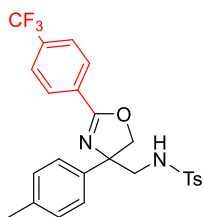
Appearance : Colourless oil, 80%, ^1H NMR (400 MHz, CDCl_3) δ 7.62 (d, $J = 8.4$ Hz, 2H), 7.23 – 7.12 (m, 6H), 5.58 (dd, $J = 8.5, 5.1$ Hz, 1H), 4.69 (d, $J = 8.6$ Hz, 1H), 4.19 (d, $J = 8.6$ Hz, 1H), 3.22 (dd, $J = 12.8, 8.5$ Hz, 1H), 3.02 (dd, $J = 12.8, 5.1$ Hz, 1H), 2.37 (s, 3H), 2.40 – 2.22 (m, 2H), 1.66 (h, $J = 7.0$ Hz, 2H), 0.95 (t, $J = 7.0$ Hz, 3H); ^{13}C NMR (101 MHz, CDCl_3) δ 170.37 (C), 143.49 (C), 142.38 (C), 136.91 (C), 133.39 (C), 129.77 (CH), 128.77 (CH), 126.99 (CH), 126.87 (CH), 75.55 (CH_2), 75.30 (C), 51.55 (CH_2), 29.94 (CH_2), 21.50 (CH_3), 19.62 (CH_2), 13.78 (CH_3); IR (neat) $\nu = 2930.7$ (w), 1630.4 (m), 1337.8 (m), 1170.3 (s), 1097.2 (s), 811.9 (s), 648.2 (s), 553.2 (s) cm^{-1} ; HR-MS calculated for $\text{C}_{20}\text{H}_{24}\text{ClN}_2\text{O}_3\text{S}$ 407.1184, found 407.1196 ($\Delta = 0.11$ ppm, 1.2 mDa); .



N-((2,4-di-p-tolyl-4,5-dihydrooxazol-4-yl)methyl)-4-methylbenzenesulfonamide (3-169).

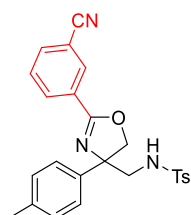
Appearance : white solid, 87% ^1H NMR (400 MHz, CDCl_3) δ 7.90 (d, $J = 8.2$ Hz, 2H), 7.66 (d, $J = 8.2$ Hz, 2H), 7.31 – 7.21 (m, 6H), 7.15 (d, $J = 7.9$ Hz, 2H), 4.96 (dd, $J = 9.1, 4.5$ Hz, 1H), 4.88 (d, $J = 8.4$ Hz, 1H), 4.46 (d, $J = 8.4$ Hz, 1H), 3.39 (dd, $J = 12.6, 9.1$ Hz, 1H), 3.22 (dd, $J = 12.6, 4.5$ Hz,

1H), 2.43 (s, 3H), 2.39 (s, 3H), 2.34 (s, 3H); ¹³C NMR (101 MHz, CDCl₃) δ 163.77 (C), 143.46 (C), 142.52 (C), 140.21 (C), 138.59 (C), 136.78 (C), 129.78 (CH), 129.46 (CH), 129.18 (CH), 128.74 (CH), 127.02 (CH), 125.56 (CH), 124.22 (C), 76.04 (CH₂), 75.73 (C), 51.75 (CH₂), 21.73 (CH₃), 21.56 (CH₃), 21.11 (CH₃); IR (neat) ν = 2981.9 (w), 1639.2 (s), 1328.2 (s), 1158.3 (s), 1088.1 (s), 1075.1 (s), 891.36 (s), 658.8 (s), 547.0 (s) cm⁻¹; HR-MS calculated for C₂₅H₂₆N₂O₃S 435.1742, found 435.1737 (Δ = -1.1 ppm, -0.5 mDa).



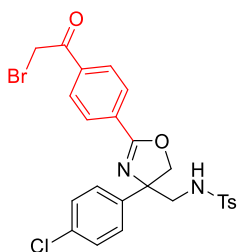
N-((4-(4-Chlorophenyl)-2-(4-(trifluoromethyl)phenyl)-4,5-dihydrooxazol-4-yl)methyl)-4-methylbenzenesulfonamide (3-170).

Appearance : colourless oil, 70%, ¹H NMR (400 MHz, CDCl₃) δ 8.07 (d, *J* = 8.1 Hz, 2H), 7.62 (m, 4H), 7.24 (d, *J* = 8.1 Hz, 2H), 7.16 (m, 4H), 5.30 (dd, *J* = 9.4, 4.6 Hz, 1H), 4.95 (d, *J* = 8.5 Hz, 1H), 4.50 (d, *J* = 8.5 Hz, 1H), 3.37 (dd, *J* = 12.8, 9.4 Hz, 1H), 3.17 (dd, *J* = 12.8, 4.6 Hz, 1H), 2.37 (s, 3H), 2.32 (s, 3H); ¹³C NMR (101 MHz, CDCl₃) δ 164.03 (C), 143.67 (C), 140.53 (C), 137.78 (C), 136.76 (C), 133.54 (q, *J* = 32.5 Hz, C), 130.51 (C), 129.89 (CH), 129.62 (CH), 129.18 (CH), 127.06 (q, *J* = 207.1 Hz, C), 127.05 (CH), 125.46 (q, *J* = 3.81 Hz, CH), 76.38 (CH), 76.28 (C), 51.91 (CH₂), 21.61 (CH₃), 21.16 (CH₃); IR (neat) ν = 3267.2 (w), 2982.2 (w), 1649.2 (m), 1321.9 (s), 1160.2 (s), 1073.1 (s), 1090.1 (s), 853.7 (m), 730.6 (s), 510.4 (s) cm⁻¹; HR-MS calculated for C₂₅H₂₄F₃N₂O₃S 489.1503, found 489.1505 (Δ = 0.4 ppm, 0.2 mDa).



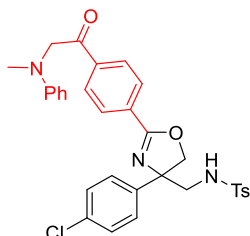
N-((2-(3-Cyanophenyl)-4-(p-tolyl)-4,5-dihydrooxazol-4-yl)methyl)-4-methylbenzenesulfonamide (3-171).

Appearance: white solid, 35%, ^1H NMR (400 MHz, $\text{DMSO-}d_6$) δ 8.15 (d, $J = 8.3$ Hz, 1H), 7.84 (t, $J = 6.9$ Hz, 1H), 7.67 (d, $J = 7.7$ Hz, 3H), 7.30 (d, $J = 7.7$ Hz, 5H), 7.15 (d, $J = 7.7$ Hz, 2H), 4.97 (d, $J = 8.4$ Hz, 1H), 4.44 (d, $J = 8.4$ Hz, 1H), 3.13 (dd, $J = 13.4, 7.9$ Hz, 1H), 2.98 (dd, $J = 13.4, 5.9$ Hz, 1H), 2.30 (s, 3H), 2.25 (s, 3H); ^{13}C NMR (101 MHz, $\text{DMSO-}d_6$) δ 162.24 (C), 142.61 (C), 141.02 (C), 137.79 (C), 136.84 (CH), 136.56 (C), 136.13 (CH), 131.36 (CH), 130.73 (CH), 129.59 (CH), 129.14 (CH), 127.63 (C), 126.53 (CH), 125.71 (CH), 117.25 (C), 112.82 (C), 76.49 (C), 75.18 (CH₂), 52.14 (CH₂), 20.97 (CH₃), 20.66 (CH₃); IR (neat) $\nu = 2979.8$ (w), 1633.9 (m), 1591.0 (s), 1328.5 (m), 1156.2 (s), 1088.7 (s), 1071.1 (m), 810.7 (s), 703.1 (m), 659.4 (s), 562.5 (m), 548.2 (s) cm^{-1} ; Melting point: 217-220 °C (hexane EtOAc); HR-MS calculated for $\text{C}_{25}\text{H}_{24}\text{N}_3\text{O}_3\text{S}$ 446.1538, found 446.1530 ($\Delta = -1.8$ ppm, -0.8 mDa).



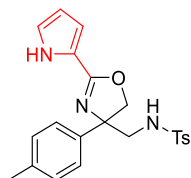
***N*-((2-(4-(2-Bromoacetyl)-phenyl)-4-(4-chlorophenyl)-4,5-dihydrooxazol-4-yl)methyl)-4-methylbenzenesulfonamide (3-172).**

Appearance :pale yellow crystals, 68%, ^1H NMR (400 MHz, CDCl_3) δ 8.04 (d, $J = 8.0$ Hz, 2H), 7.95 (d, $J = 8.0$ Hz, 2H), 7.58 (d, $J = 7.9$ Hz, 2H), 7.19 (d, $J = 7.9$ Hz, 2H), 5.18 (dd, $J = 8.7, 5.0$ Hz, 2H), 4.90 (d, $J = 8.7$ Hz, 2H), 4.43 (m, 3H), 3.31 (dd, $J = 12.8, 8.7$ Hz, 1H), 3.17 (dd, $J = 12.8, 5.0$ Hz, 1H), 2.37 (s, 3H); ^{13}C NMR (101 MHz, CDCl_3) δ 191.68 (C), 164.25 (C), 143.71 (C), 141.93 (C), 136.65 (C), 136.31 (C), 133.80 (C), 131.67 (C), 129.86 (CH), 129.19 (CH), 128.99 (CH), 128.94 (CH), 127.17 (CH), 126.93 (CH), 76.24 (CH₂), 76.12 (C), 49.84 (CH₂), 30.87 (CH₂), 22.70 (CH₃); IR (neat) $\nu = 3302.6$ (w), 1694.6 (m), 1642.0 (m), 1312.5 (m), 1151.1 (s), 1088.9 (s), 834.3 (s), 814.2 (s), 654.9 (s), 546.4 (s) cm^{-1} ; Melting point: 120-122 °C (crystallised from CHCl_3); HR-MS calculated for $\text{C}_{25}\text{H}_{23}\text{N}_2\text{O}_4^{79}\text{BrS}^{35}\text{Cl}$ 561.0250, found 561.0236 ($\Delta = -2.5$ ppm, -1.4 mDa); X-ray CCDC (1985622) Unit Cell Parameters: a 8.9040(5) b 11.4226(7) c 11.9517(7) P-1.



N-((4-(4-Chlorophenyl)-2-(4-(2-(methyl(phenyl)amino)ethyl)phenyl)-4,5-dihydrooxazol-4-yl)methyl)-4-methylbenzenesulfonamide (3-173).

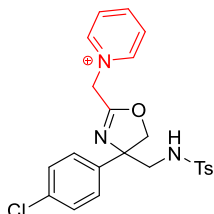
Appearance: yellow oil, 65%, ^1H NMR (700 MHz, CDCl_3) δ 8.09 (d, $J = 8.4$ Hz, 2H), 8.01 (d, $J = 8.4$ Hz, 2H), 7.62 (d, $J = 8.3$ Hz, 2H), 7.29 (s, 4H), 7.25 – 7.20 (m, 4H), 6.75 (tt, $J = 7.6, 1.0$ Hz, 1H), 6.69 (d, $J = 7.6$ Hz, 2H), 4.91 (d, $J = 8.4$ Hz, 1H), 4.81 – 4.78 (m, 3H), 4.47 (d, $J = 8.4$ Hz, 1H), 3.34 (dd, $J = 12.8, 8.6$ Hz, 1H), 3.21 (dd, $J = 12.8, 5.1$ Hz, 1H), 3.11 (s, 3H), 2.40 (s, 3H); ^{13}C NMR (176 MHz, CDCl_3) δ 196.44 (C), 164.48 (C), 149.18 (C), 143.81 (C), 141.99 (C), 138.05 (C), 136.80 (C), 133.92 (C), 131.36 (C), 129.94 (CH), 129.40 (CH), 129.25 (CH), 129.08 (CH), 127.95 (CH), 127.20 (CH), 127.01 (CH), 117.55 (CH), 112.57 (CH), 76.25 (C), 76.20 (CH_2), 59.48 (CH_2), 51.99 (CH_2), 39.73 (CH_3), 21.64 (CH_3); IR (neat) $\nu = 1697.8$ (s), 1647.8 (m), 1331.9 (m), 1159.1 (s), 1089.7 (s), 812.1 (m), 744.0 (m), 660.2 (m), 546.5 (s) cm^{-1} ; HR-MS calculated for $\text{C}_{32}\text{H}_{31}\text{N}_3\text{O}_4\text{S}^{35}\text{Cl}$ 588.1724, found 588.1714 ($\Delta = -1.7$ ppm, -1.0 mDa).



N-((2-(1H-Pyrrol-2-yl)-4-(p-tolyl)-4,5-dihydrooxazol-4-yl)methyl)-4-methylbenzenesulfonamide (3-174).

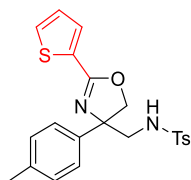
Appearance: yellow oil, 58%, ^1H NMR (400 MHz, CDCl_3) δ 10.02 (s, 1H), 7.53 (d, $J = 8.0$ Hz, 2H), 7.16 (d, $J = 8.0$ Hz, 2H), 7.08 (d, $J = 8.0$ Hz, 2H), 7.05 – 6.95 (m, 3H), 6.50 (s, 1H), 6.16 (s, 1H), 4.91 (d, $J = 8.4$ Hz, 1H), 4.28 (d, $J = 8.4$ Hz, 1H), 3.54 (dd, $J = 13.4, 9.6$ Hz, 1H), 3.03 (dd, $J = 13.4, 4.0$ Hz, 1H), 2.32 (ap. s, 6H); ^{13}C NMR (101 MHz, CDCl_3) δ 160.84 (C), 143.24 (C), 141.08 (C), 137.52 (C), 136.96 (C), 129.71 (CH), 129.52 (CH), 126.84 (CH), 125.56 (CH), 123.08 (CH), 118.64 (C), 114.77 (CH), 110.11 (CH), 75.92 (CH_2), 75.35 (C), 52.63 (CH_2), 21.58 (CH_3), 21.13 (CH_3); IR (neat) $\nu = 3333.7$ (w), 1640.9 (s), 1429.2 (m), 1307.1 (m), 1155.0 (s), 1087.3 (m), 985.1 (m),

813.7 (s), 738.3 (s), 660.4 (s), 547. 7(s) cm^{-1} ; HR-MS calculated for $\text{C}_{22}\text{H}_{24}\text{N}_3\text{O}_3\text{S}$ 410.1538, found 410.1542 ($\Delta = 1.0$ ppm, 0.4 mDa).



1-((4-(4-Chlorophenyl)-4-((4-methylphenylsulfonamido)methyl)-4,5-dihydrooxazol-2-yl)methyl)pyridin-1-ium salt (3-175).

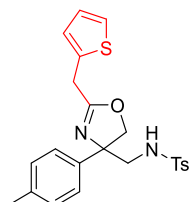
Appearance: white solid, 38%, ^1H NMR (400 MHz, CD_3OD) δ 8.92 (d, $J = 6.0$ Hz, 2H), 8.64 (t, $J = 7.9$ Hz, 1H), 8.14 (t, $J = 7.0$ Hz, 2H), 7.70 (d, $J = 7.9$ Hz, 2H), 7.35 (m, 6H), 5.62 (s, 2H), 3.98 (d, $J = 11.1$ Hz, 1H), 3.88 (d, $J = 11.1$ Hz, 1H), 3.55 (q, $J = 13.8$ Hz, 1H), 2.44 (s, 3H); ^{13}C NMR (101 MHz, CD_3OD) δ 156.27 (C), 138.12 (CH), 138.01 (CH), 135.43 (C), 130.52 (C), 129.14 (C), 124.53 (C), 121.35 (CH), 119.81 (CH), 119.58 (CH), 119.30 (CH), 118.54 (CH), 56.67 (CH_2), 54.72 (C), 53.98 (CH_2), 36.33 (CH_2), 11.97 (CH_3); IR (neat) $\nu = 2982.4$ (w), 1700.9 (m), 1493.8 (m), 1154.2 (s), 1010.0 (s), 548.8 (s) cm^{-1} ; Melting point: 227-230 $^\circ\text{C}$ (crystallised from Hexane EtOAc); HR-MS calculated for $\text{C}_{23}\text{H}_{25}\text{N}_3\text{O}_4\text{S}^{35}\text{Cl}$ ($\text{M}+\text{H}_2\text{O}$) 474.1254, found 474.1247 ($\Delta = -1.5$ ppm, -0.7 mDa).



4-Methyl-N-((2-(thiophen-2-yl)-4-(p-tolyl)-4,5-dihydrooxazol-4-yl)methyl)benzenesulfonamide (3-176).

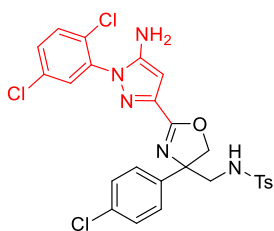
Appearance: yellow oil, 78% ^1H NMR (400 MHz, CDCl_3) δ 7.65 (m, 3H), 7.50 (d, $J = 5.0$ Hz, 1H), 7.29 – 7.19 (m, 4H), 7.19 – 7.07 (m, 3H), 4.87 (d, $J = 8.3$ Hz, 2H), 4.46 (d, $J = 8.3$ Hz, 1H), 3.37 (dd, $J = 12.6, 9.3$ Hz, 1H), 3.17 (dd, $J = 12.6, 4.4$ Hz, 1H), 2.38 (s, 3H), 2.32 (s, 3H); ^{13}C NMR (101 MHz, CDCl_3) δ 161.00 (C), 143.57 (C), 140.72 (C), 137.59 (C), 136.76 (C), 131.56 (CH), 130.77 (CH), 129.84 (CH), 129.57 (C), 129.51 (CH), 127.89 (CH), 127.05 (CH), 125.55 (CH), 76.40 (CH_2), 76.13 (C), 51.67 (CH_2), 21.60 (CH_3), 21.13 (CH_3); IR (neat) $\nu = 3056.2$ (w), 1635.0 (s), 1326.5 (s),

1159.4 (s), 1084.6 (s), 813.9 (s), 727.9 (s), 714.5 (s), 659.6 (s), 548.0 (s) cm^{-1} ; HR-MS calculated for $\text{C}_{22}\text{H}_{23}\text{N}_2\text{O}_3\text{S}_2$ 427.1107, found 427.1112 ($\Delta = 1.1$ ppm, .0.5 mDa); Melting point: 130-133 $^{\circ}\text{C}$; X-ray CCDC (1985623) Unit Cell Parameters: a 8.9040(5) b 11.4226(7) c 11.9517(7) P-1.



4-Methyl-N-((2-(thiophen-2-ylmethyl)-4-(p-tolyl)-4,5-dihydrooxazol-4-yl)methyl)benzenesulfonamide (3-177).

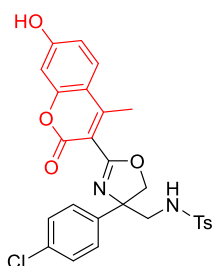
Appearance: yellow oil, 76%, ^1H NMR (400 MHz, CDCl_3) δ 7.63 (d, $J = 8.4$ Hz, 2H), 7.29 (dd, $J = 5.0, 3.0$ Hz, 1H), 7.24 – 7.19 (m, 3H), 7.13 – 7.05 (m, 5H), 5.34 (dd, $J = 9.1, 4.7$ Hz, 1H), 4.80 (d, $J = 8.5$ Hz, 1H), 4.31 (d, $J = 8.5$ Hz, 1H), 3.84 – 3.66 (m, 2H), 3.27 (dd, $J = 12.8, 9.1$ Hz, 1H), 3.04 (dd, $J = 12.8, 4.7$ Hz, 1H), 2.39 (s, 3H), 2.31 (s, 3H); ^{13}C NMR (101 MHz, CDCl_3) δ 168.17 (C), 143.47 (C), 140.60 (C), 137.47 (C), 137.00 (C), 134.46 (C), 129.83 (CH), 129.49 (CH), 128.30 (CH), 126.98 (CH), 126.12 (CH), 125.38 (CH), 122.81 (CH), 76.24 (CH_2), 75.66 (C), 51.78 (CH_2), 29.49 (CH_2), 21.56 (CH_3), 21.07 (CH_3); IR (neat) $\nu = 1649.5$ (s), 1418.9 (m), 1326.0 (s), 1161.8 (s), 1088.5 (s), 811.1 (s), 751.0 (s), 662.9 (s), 559.6 (s), 550.9 (s), 540.3 (s) cm^{-1} ; HR-MS calculated for $\text{C}_{23}\text{H}_{25}\text{N}_2\text{O}_3\text{S}_2$ 441.1307, found 441.1321 ($\Delta = 3.2$ ppm, 1.4 mDa).



N-((2-(5-Amino-1-(2,5-dichlorophenyl)-1H-pyrazol-3-yl)-4-(4-chlorophenyl)-4,5-dihydrooxazol-4-yl)methyl)-4-methylbenzenesulfonamide (3-178).

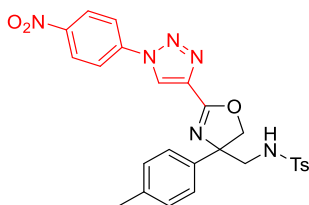
Appearance: white solid, 57%, ^1H NMR (400 MHz, CDCl_3) δ 7.67 (s, 1H), 7.61 (d, $J = 8.3$ Hz, 2H), 7.53 – 7.46 (m, 2H), 7.42 (dd, $J = 8.6, 2.5$ Hz, 2H), 7.27 – 7.18 (m, 6H), 5.36 (s, 2H), 5.28 (m, 1H), 4.63 (d, $J = 8.4$ Hz, 1H), 4.27 (d, $J = 8.4$ Hz, 1H), 3.26 (dd, $J = 12.3, 7.7$ Hz, 1H), 3.16 (dd, $J = 12.3, 5.4$ Hz, 1H), 2.40 (s, 3H); ^{13}C NMR (101 MHz, CDCl_3) δ 161.53 (C), 149.15 (C),

143.67 (C), 143.63 (C), 142.43 (C), 140.28 (CH), 136.56 (C), 135.83 (C), 133.72 (C), 133.49 (C), 131.68 (CH), 131.19 (CH), 130.49 (C), 130.14 (CH), 129.89 (CH), 128.81 (CH), 127.27 (CH), 127.01 (CH), 75.22 (C), 75.18 (CH₂), 52.10(CH₂), 21.64 (CH₃); IR (neat) ν = 3278.4 (w), 1643.4 (s), 1616.6 (s), 1157.3 (s), 1090.8 (s), 811.7 (s), 661.1 (s), 552.6 (s) cm⁻¹; HR-MS calculated for C₂₆H₂₃N₅O₃S³⁵Cl₃ 590.0587, found 590.0595 (Δ = 1.4 ppm, 0.8 mDa); Melting point: 91-93 °C (crystallised from Hexane / EtOAc).



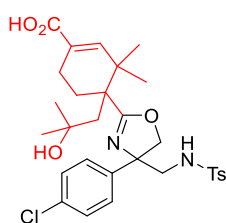
N-((4-(4-Chlorophenyl)-2-(7-hydroxy-4-methyl-2-oxo-2H-chromen-3-yl)-4,5-dihydrooxazol-4-yl)methyl)-4-methylbenzenesulfonamide (3-179).

Appearance: Yellow oil, 42%, ¹H NMR (400 MHz, CDCl₃) δ 7.76 (d, J = 7.9 Hz, 2H), 7.43 (d, J = 8.8 Hz, 1H), 7.33 – 7.27 (m, 6H), 6.88 (dd, J = 8.8, 2.2 Hz, 1H), 6.75 – 6.63 (m, 2H), 5.13 (d, J = 8.7 Hz, 1H), 4.45 (d, J = 8.7 Hz, 1H), 3.50 – 3.38 (m, 1H), 3.08 (d, J = 12.3 Hz, 1H), 2.40 (d, J = 7.2 Hz, 6H); ¹³C NMR (101 MHz, CDCl₃) δ 162.94 (C), 160.58 (C), 154.73 (C), 143.76 (C), 143.61 (C), 138.83 (C), 136.21 (C), 133.75 (C), 130.00 (CH), 129.78 (CH), 129.30 (CH), 127.35 (CH), 127.15 (CH), 126.94 (CH), 126.44 (CH), 114.98 (C), 111.82 (C), 102.17 (C), 76.39 (C), 76.29 (CH₂), 52.00 (CH₂), 21.22 (CH₃), 17.86 (CH₃); IR (neat) ν = 3453.1 (m, OH), 1595.9 (w), 1330.0 (s), 1182.1 (s), 1147.2 (s), 1088.1 (s), 909.1 (m), 815.7 (s), 675.3 (s), 603.7 (s), 562.2 (s), 515.6 (s) cm⁻¹; HR-MS calculated for C₂₇H₂₄N₂O₆S³⁵Cl 539.1044, found 539.1036 (Δ = -1.5 ppm, -0.8 mDa).



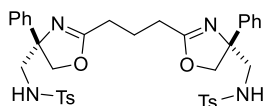
N-((4-(4-chlorophenyl)-2-(1-(4-nitrophenyl)-1H-1,2,3-triazol-4-yl)-4,5-dihydrooxazol-4-yl)methyl)-4-methylbenzenesulfonamide (3-180).

Appearance: yellow oil, 56%, ^1H NMR (400 MHz, CDCl_3) δ 9.01 (s, 1H), δ 8.48 (d, $J = 9.0$ Hz, 2H), 8.10 (d, $J = 9.0$ Hz, 2H), 7.59 (d, $J = 8.3$ Hz, 2H), 7.19 – 7.13 (m, 4H), 7.08 (d, $J = 8.0$ Hz, 2H), 6.39 (s, 1H), 5.14 (d, $J = 8.6$ Hz, 2H), 4.49 (d, $J = 8.6$ Hz, 2H), 3.49 (dd, $J = 13.4, 9.4$ Hz, 1H), 3.15 (dd, $J = 13.4, 4.6$ Hz, 1H), 2.32 (s, 3H); ^{13}C NMR (101 MHz, CDCl_3) δ 158.71 (C), 147.86 (C), 143.69 (C), 140.74 (C), 140.04 (C), 137.90 (C), 137.76 (C), 137.10 (C), 129.96 (CH), 129.71 (CH), 126.89 (CH), 125.86 (CH), 125.47 (CH), 124.65 (CH), 121.28 (CH), 42.13 (CH_2), 27.16 (CH_2), 25.13 (C), 21.63 (CH_3), 21.16 (CH_3); IR (neat) $\nu = 1487.3$ (m), 1202.1 (m), 1157.4 (m), 904.4 (s), 728.5 (s) cm^{-1} ; HR-MS calculated for $\text{C}_{26}\text{H}_{25}\text{N}_6\text{O}_5\text{S}$ 533.1607, found 533.1590 ($\Delta = -3.0$ ppm, -1.7 mDa).



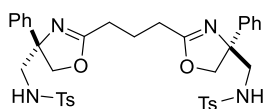
4-(4-(4-Chlorophenyl)-4-((4-methylphenylsulfonamido)methyl)-4,5-dihydrooxazol-2-yl)-4-(2-hydroxy-2-methylpropyl)-3,3-dimethylcyclohex-1-enecarboxylic acid (3-181).

Appearance: white solid, 81%, ^1H NMR (600 MHz, CDCl_3) δ 7.61 (d, $J = 8.3$ Hz, 2H), 7.32 – 7.29 (m, 2H), 7.24 – 7.19 (m, 4H), 6.62 (dt, $J = 14.4, 1.8$ Hz, 1H), 5.59 (m, 1H), 4.35 – 4.26 (m, 2H), 3.37 (dd, $J = 13.4, 7.1$ Hz, 1H), 3.17 (dd, $J = 13.4, 4.7$ Hz, 1H), 2.39 (s, 3H), 2.37 – 2.33 (m, 1H), 2.33 – 2.24 (m, 1H), 2.20 (d, $J = 13.5$ Hz, 1H), 2.06 – 1.99 (m, 1H), 1.88 (dddd, $J = 13.9, 10.1, 6.2, 3.3$ Hz, 1H), 1.75 (d, $J = 13.5$ Hz, 1H), 1.42 (s, 3H), 1.38 (s, 3H), 1.10 (s, 3H), 0.98 (d, $J = 2.5$ Hz, 3H); ^{13}C NMR (151 MHz, CDCl_3) δ 166.76 (C), 148.04 (CH), 143.51 (C), 139.77 (C), 136.68 (C), 133.68 (C), 129.77 (CH), 128.49 (CH), 127.34 (C), 127.26 (CH), 127.11 (CH), 81.52 (C), 74.65 (C), 69.21 (CH_2), 50.46 (C), 50.11 (CH_2), 45.75 (CH_2), 37.24 (C), 30.57 (CH_3), 30.06 (CH_2), 29.90 (CH_3), 29.36 (C), 26.26 (CH_3), 23.06 (CH_3), 21.73 (CH_2), 21.61 (CH_3); IR (neat) $\nu = 2986.0$ (w), 1711.9 (m), 1654.9 (m), 1248.0 (s), 1156.0 (s), 1090.6 (s), 1046.2 (m), 814.0 (m), 660.5 (s), 549.9 (s) cm^{-1} ; HR-MS calculated for $\text{C}_{30}\text{H}_{38}\text{N}_2\text{O}_6\text{S}^{35}\text{Cl}$ 589.2139, found 589.2136 ($\Delta = -0.5$ ppm, -0.3 mDa); Melting point: 88-90 $^\circ\text{C}$ (crystallised from Hexane EtOAc).



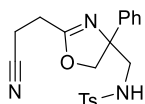
***N,N'*-(((*meso*)-2,2'-(Propane-1,3-diyl)bis(4-phenyl-4,5-dihydrooxazole-4,2-diyl))bis(methylene))bis(4-methylbenzenesulfonamide) (3-193)**

Appearance: white solid, 20%, ^1H NMR (400 MHz, $\text{DMSO-}d_6$) δ 7.66 (d, $J = 7.9$ Hz, 6H), 7.35 – 7.28 (m, 12H), 7.25 (m, 2H), 4.69 (d, $J = 8.6$ Hz, 2H), 4.19 (d, $J = 8.6$ Hz, 2H), 3.38 (s, 6H), 2.99 (dd, $J = 13.1, 7.9$ Hz, 2H), 2.82 (dd, $J = 13.1, 5.8$ Hz, 2H), 2.46 – 2.38 (m, 4H), 2.04 – 1.90 (m, 2H); ^{13}C NMR (101 MHz, DMSO) δ 167.04 (C), 144.27 (C), 142.66 (C), 137.74 (C), 129.62 (CH), 128.47 (CH), 127.25 (CH), 126.56 (CH), 125.84 (CH), 75.92 (C), 74.44 (CH_2), 52.01 (CH_2), 26.74 (CH_2), 21.92 (CH_2), 20.97 (CH_3); IR (neat) $\nu = 3338.0$ (w), 2971.0 (w), 1742.0 (w), 1663.7 (w), 1333.3 (m), 1157.0 (s), 1131.7 (m), 1092.5 (m), 818.16 (m), 700.57 (s), 664.18 (s), 543.79 (s) cm^{-1} ; HR-MS calculated for $\text{C}_{37}\text{H}_{41}\text{N}_4\text{O}_6\text{S}_2$ 701.2468, found 701.2480 ($\Delta = 1.7$ ppm, 1.2 mDa); X-ray CCDC (1985624) Unit Cell Parameters: a 11.8945(9) b 21.4091(15) c 28.158(2) P21/c.



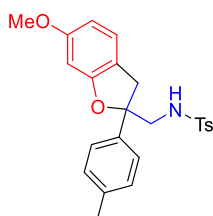
***N,N'*-(((*Rac*)-2,2'-(Propane-1,3-diyl)bis(4-phenyl-4,5-dihydrooxazole-4,2-diyl))bis(methylene))bis(4-methylbenzenesulfonamide) (3-194)**

Appearance: white solid, 20%, ^1H NMR (400 MHz, CDCl_3) δ 9.17 (dd, $J = 10.2, 3.7$ Hz, 2H), 7.56 (d, $J = 8.0$ Hz, 4H), 7.29 (s, 10H), 7.01 (d, $J = 8.0$ Hz, 4H), 5.10 (d, $J = 8.6$ Hz, 2H), 4.29 (d, $J = 8.6$ Hz, 2H), 3.47 (dd, $J = 13.7, 10.2$ Hz, 1H), 3.11 (ddd, $J = 15.0, 10.0, 8.7$ Hz, 2H), 2.82 (dd, $J = 13.7, 3.7$ Hz, 1H), 2.59 (dt, $J = 15.0, 4.5$ Hz, 2H), 2.30 (s, 6H), 2.08 (td, $J = 10.0, 8.6, 4.5$ Hz, 2H); ^{13}C NMR (101 MHz, CDCl_3) δ 170.42 (C), 143.64 (C), 142.84 (C), 138.62 (C), 129.60 (CH), 128.90 (CH), 127.86 (CH), 126.24 (CH), 124.68 (CH), 76.37 (CH_2), 76.05 (C), 50.80 (CH_2), 24.68 (CH_2), 20.98 (CH_3), 19.33 (CH_2); IR (neat) $\nu = 3062.4$ (w), 2870.2 (w), 1164.7 (s), 1147.2 (w), 1130.2 (s), 1158.7 (s), 1091.23 (s), 1010.2 (s), 912.2 (m), 723.0 (m), 764.0 (s), 554.4 (s) cm^{-1} ; HR-MS calculated for $\text{C}_{37}\text{H}_{41}\text{N}_4\text{O}_6\text{S}_2$ 701.2468, found 701.2474 ($\Delta = 0.9$ ppm, 0.6 mDa); X-ray CCDC (1985625) Unit Cell Parameters: a 15.0965(9) b 12.1682(7) c 21.8118(12) C2/c.



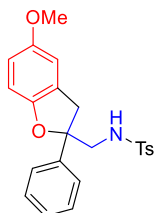
***N*-((2-(3-Cyanopropyl)-4-phenyl-4,5-dihydrooxazol-4-yl)methyl)-4-methylbenzenesulfonamide (3-195).**

Appearance: colourless oil, 22%, ^1H NMR (400 MHz, CDCl_3) δ 7.67 (d, $J = 8.1$ Hz, 2H), 7.36 – 7.30 (m, 2H), 7.30 – 7.18 (m, 5H), 5.21 (dd, $J = 8.9, 5.0$ Hz, 1H), 4.86 (d, $J = 8.6$ Hz, 1H), 4.39 (d, $J = 8.6$ Hz, 1H), 3.24 (dd, $J = 13.0, 8.9$ Hz, 1H), 3.10 (dd, $J = 13.0, 5.0$ Hz, 1H), 2.60 (t, $J = 7.1$ Hz, 2H), 2.53 (t, $J = 7.1$ Hz, 2H), 2.39 (s, 3H), 2.09 (p, $J = 7.1$ Hz, 2H); ^{13}C NMR (101 MHz, CDCl_3) δ 167.56 (C), 143.77 (C), 142.56 (C), 136.41 (C), 129.95 (CH), 129.04 (CH), 128.07 (CH), 127.02 (CH), 125.53 (CH), 119.27 (C), 76.34 (CH_2), 75.72 (C), 49.42 (CH_2), 27.22 (CH_2), 21.74 (CH_2), 21.63 (CH_3), 16.79 (CH_2); IR (neat) $\nu = 3263.6$ (w), 2177.3 (w), 1663.1 (w), 1327.7 (w), 1160.0 (s), 1091.5 (m), 906.5 (s), 727.8 (s), 702.2 (s), 551.8 (s) cm^{-1} ; HR-MS calculated for $\text{C}_{20}\text{H}_{22}\text{N}_3\text{O}_3\text{S}$ 384.1338, found 384.1335 ($\Delta = -0.8$ ppm, -0.3 mDa).



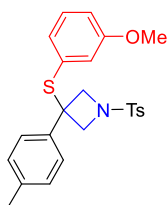
***N*-((4-Methoxy-2-(*p*-tolyl)-2,3-dihydrobenzofuran-2-yl)methyl)-4-methylbenzenesulfonamide (3-197).**

Appearance: white solid, 40%, ^1H NMR (400 MHz, CDCl_3) δ 7.65 (d, $J = 8.2$ Hz, 2H), 7.28 (d, $J = 8.2$ Hz, 2H), 7.11 (d, $J = 8.2$ Hz, 2H), 7.05 (d, $J = 8.4$ Hz, 2H), 6.89 (d, $J = 8.7$ Hz, 1H), 6.44 (d, $J = 6.5$ Hz, 1H), 4.71 (d, $J = 9.0$ Hz, 1H), 4.51 (d, $J = 9.0$ Hz, 1H), 4.26 (dd, $J = 8.5, 4.5$ Hz, 1H), 3.79 (s, 3H), 3.55 (dd, $J = 12.2, 8.5$ Hz, 1H), 3.35 (dd, $J = 12.2, 4.5$ Hz, 1H), 2.43 (s, 3H), 2.31 (s, 3H); ^{13}C NMR (101 MHz, CDCl_3) δ 162.17 (C), 161.52 (C), 143.75 (C), 139.58 (C), 137.25 (C), 136.50 (C), 129.91 (CH), 129.74 (CH), 127.18 (CH), 126.48 (CH), 125.07 (CH), 120.97 (C), 107.27 (CH), 96.75 (CH), 82.39 (CH_2), 55.65 (CH_3), 53.32 (C), 49.95 (CH_2), 21.66 (CH_3), 21.02 (CH_3); IR (neat) $\nu = 3263.0$ (w), 1621.0 (w), 1326.1 (m), 1156.2 (s), 1091.2 (m), 804.8 (m), 661.4 (m), 549.2 (s) cm^{-1} ; HR-MS calculated for $\text{C}_{24}\text{H}_{26}\text{NO}_4\text{S}$ 424.1583, found 424.1583 ($\Delta = 0.0$ ppm, 0.0 mDa); X-ray CCDC (1985642) Unit Cell Parameters: a 10.9761(8) b 11.2566(8) c 17.2670(13) P21/n



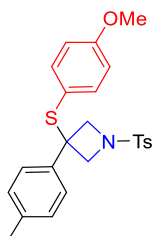
***N*-((5-methoxy-2-phenyl-2,3-dihydrobenzofuran-2-yl)methyl)-4-methylbenzenesulfonamide (3-199).**

Appearance: white solid, 45%, ^1H NMR (400 MHz, CDCl_3) δ 7.64 (d, J = 8.2 Hz, 2H), 7.33 – 7.18 (m, 7H), 6.77 – 6.70 (m, 2H), 6.59 (dd, J = 2.3, 0.8 Hz, 1H), 4.70 (d, J = 9.1 Hz, 1H), 4.64 (dd, J = 8.6, 5.4 Hz, 1H), 4.52 (d, J = 9.1 Hz, 1H), 3.69 (s, 3H), 3.61 (dd, J = 12.5, 8.6 Hz, 1H), 3.43 (dd, J = 12.5, 5.4 Hz, 1H), 2.41 (s, 3H); ^{13}C NMR (101 MHz, CDCl_3) δ 154.63 (C), 154.36 (C), 143.63 (C), 141.56 (C), 136.01 (C), 130.06 (C), 129.81 (CH), 128.98 (CH), 127.43 (CH), 127.03 (CH), 126.53 (CH), 114.57 (CH), 110.81 (CH), 110.52 (CH), 80.92 (CH_2), 55.94 (CH_3), 54.46 (C), 49.35 (CH_2), 20.57 (CH_3) cm^{-1} ; IR (neat) ν = 3270.1 (w), 2254.1 (w), 1489.1 (m), 1160.5 (m), 904.0 (s), 723.6 (s), 648.8 (s), 661.0 (s); HR-MS calculated for $\text{C}_{23}\text{H}_{24}\text{NO}_4\text{S}$ 410.1426, found 410.1445 (Δ = 4.6 ppm, 1.9 mDa).



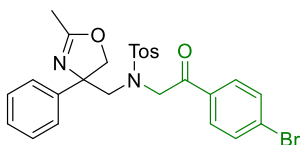
3-((4-Methoxyphenyl)thio)-3-(*p*-tolyl)-1-tosylazetidine (3-201).

Appearance: brown solid, 70%, ^1H NMR (400 MHz, CDCl_3) δ 7.63 (d, J = 8.3 Hz, 2H), 7.28 – 7.22 (m, 2H), 7.06 – 6.99 (m, 4H), 6.76 (d, J = 8.2 Hz, 2H), 6.71 (d, J = 8.8 Hz, 2H), 4.24 (d, J = 8.3 Hz, 2H), 4.13 (d, J = 8.3 Hz, 2H), 3.78 (s, 3H), 2.40 (s, 3H), 2.30 (s, 3H); ^{13}C NMR (101 MHz, CDCl_3) δ 160.83 (C), 144.16 (C), 139.16 (C), 138.04 (CH), 137.02 (C), 132.20 (C), 129.70 (CH), 128.93 (CH), 128.25 (CH), 126.17 (CH), 121.93 (C), 114.37 (CH), 61.72 (CH_2), 55.37 (CH_3), 49.32 (C), 21.64 (CH_3), 21.16 (CH_3); IR (neat) ν = 2980.5 (w), 1588.1 (m), 1465.2 (m), 1344.5 (m), 1158.2 (s), 1037.2 (m), 813.4 (m), 725.4 (s), 673.5 (s), 548.1 (s) cm^{-1} ; HR-MS calculated for $\text{C}_{24}\text{H}_{26}\text{NO}_3\text{S}_2$ 440.1354, found 440.1342 (Δ = -2.7 ppm, -1.2 mDa) Melting point: 124-126 °C crystallised from Hexane / EtOAc (1:1); X-ray CCDC (1985643) Unit Cell Parameters: a 5.9971(2) b 19.0997(8) c 20.3305(8) P-1



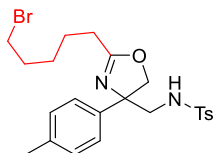
3-((3-Methoxyphenyl)thio)-3-(p-tolyl)-1-tosylazetidine (3-203).

Appearance: orange oil, 85%, $^1\text{H NMR}$ (400 MHz, CDCl_3) δ 7.66 (d, $J = 8.3$ Hz, 2H), 7.27 (d, $J = 7.7$ Hz, 2H), 7.09 (dd, $J = 8.4, 7.6$ Hz, 1H), 7.02 (d, $J = 7.7$ Hz, 2H), 6.87 – 6.79 (m, 3H), 6.72 (ddd, $J = 7.6, 1.6, 1.0$ Hz, 1H), 6.48 (dd, $J = 1.6, 1.0$ Hz, 1H), 4.26 (d, $J = 8.4$ Hz, 2H), 4.15 (d, $J = 8.4$ Hz, 2H), 3.60 (s, 3H), 2.40 (s, 3H), 2.29 (s, 3H); $^{13}\text{C NMR}$ (101 MHz, CDCl_3) δ 159.39 (C), 144.21 (C), 138.91 (C), 137.13 (C), 132.32 (C), 131.88 (C), 129.75 (CH), 129.56 (CH), 128.96 (CH), 128.25 (CH), 127.60 (CH), 126.26 (CH), 119.86 (CH), 115.64 (CH), 62.15 (CH_2), 55.13 (CH_3), 49.18 (C), 21.65 (CH_3), 21.08 (CH_3); IR (neat) $\nu = 2980.7$ (w), 1587.4 (m), 1346.8 (m), 1157.9 (s), 908.3 (m), 813.5 (m), 725.7 (s), 672.7 (s), 548.5 (s) cm^{-1} ; HR-MS calculated for $\text{C}_{24}\text{H}_{26}\text{NO}_3\text{S}_2$ 440.1357, found 440.1346 ($\Delta = -2.7$ ppm, -1.1 mDa);



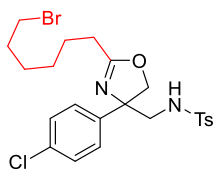
***N*-(2-(4-Bromophenyl)-2-oxoethyl)-4-methyl-*N*-((2-methyl-4-(p-tolyl)-4,5-dihydrooxazol-4-yl)methyl)benzenesulfonamide (3-205).**

Appearance: yellow oil, 60%, $^1\text{H NMR}$ (400 MHz, CDCl_3) δ 7.64 (d, $J = 8.6$ Hz, 2H), 7.61 (d, $J = 8.3$ Hz, 2H), 7.57 (d, $J = 8.4$ Hz, 2H), 7.33 – 7.31 (m, 4H), 7.24 (d, $J = 8.4$ Hz, 2H), 4.98 (d, $J = 8.7$ Hz, 1H), 4.88 – 4.70 (m, 2H), 4.33 (d, $J = 8.7$ Hz, 1H), 3.83 (d, $J = 14.8$ Hz, 1H), 3.61 (d, $J = 14.8$ Hz, 1H), 2.40 (s, 3H), 1.86 (s, 3H); $^{13}\text{C NMR}$ (101 MHz, CDCl_3) δ 192.78 (C), 166.38 (C), 144.10 (C), 143.69 (C), 136.56 (C), 134.05 (C), 132.12 (CH), 129.70 (CH), 129.34 (CH), 128.79 (CH), 128.73 (C), 127.66 (CH), 127.61 (CH), 125.82 (CH), 77.03 (C), 76.11 (CH_2), 56.58 (CH_2), 54.58 (CH_2), 21.66 (CH_3), 14.12 (CH_3); IR (neat) $\nu = 2924.2$ (w), 1672.2 (m), 1585.3 (m), 1334.8 (m), 1156.7 (s), 982.4 (s), 908.1 (s), 729.3 (s), 547.8 (s) cm^{-1} ; HR-MS calculated for $\text{C}_{26}\text{H}_{26}\text{N}_2\text{O}_4\text{S}^{79}\text{Br}$ 541.0797, found 541.0780 ($\Delta = -3.1$ ppm, -1.7 mDa).



***N*-((2-(5-Bromopentyl)-4-(*p*-tolyl)-4,5-dihydrooxazol-4-yl)methyl)-4-methylbenzenesulfonamide (3-206).**

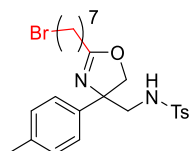
Appearance: colourless oil, 70%, ^1H NMR (400 MHz, CDCl_3) δ 7.65 (d, $J = 8.0$ Hz, 2H), 7.23 (d, $J = 8.0$ Hz, 2H), 7.16 – 7.06 (m, 4H), 5.02 (dd, $J = 9.3, 4.6$ Hz, 1H), 4.72 (d, $J = 8.5$ Hz, 1H), 4.28 (d, $J = 8.5$ Hz, 1H), 3.41 (t, $J = 6.7$ Hz, 2H), 3.24 (dd, $J = 12.6, 9.3$ Hz, 1H), 3.04 (dd, $J = 12.6, 4.6$ Hz, 1H), 2.39 (s, 3H), 2.31 (s, 3H), 1.94 – 1.83 (m, 2H), 1.78 – 1.62 (m, 2H), 1.52 (ddd, $J = 10.2, 8.4, 4.8$ Hz, 2H); ^{13}C NMR (101 MHz, CDCl_3) δ 169.88 (C), 143.55 (C), 140.82 (C), 137.48 (C), 136.82 (C), 129.92 (CH), 129.48 (CH), 127.01 (CH), 125.40 (CH), 75.88 (CH_2), 75.05 (C), 51.74 (CH_2), 33.74 (CH_2), 32.38 (CH_2), 28.56 (CH_2), 27.03 (CH_2), 25.30 (CH_2), 22.31 (CH_3), 21.09 (CH_3); IR (neat) $\nu = 3089.3$ (w), 2868.6 (w), 1651.1 (m), 1333.6 (s), 1160.0 (s), 1089.6 (s), 811.2 (s), 659.3 (m), 554.9 (s), 545.8 (s) cm^{-1} ; HR-MS calculated for $\text{C}_{23}\text{H}_{30}^{79}\text{BrN}_2\text{O}_3\text{S}$ 493.1161, found 493.1146 ($\Delta = -3.0$ ppm, -1.5 mDa); X-ray CCDC (1985626) Unit Cell Parameters: a 12.7711(8) b 11.4910(7) c 16.0665(10) P21/n.



***N*-((2-(6-Bromohexyl)-4-(4-chlorophenyl)-4,5-dihydrooxazol-4-yl)methyl)-4-methylbenzenesulfonamide (3-207).**

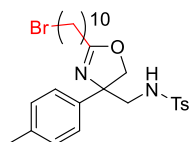
Appearance: colourless oil, 75%, ^1H NMR (400 MHz, CDCl_3) δ 7.62 (d, $J = 8.2$ Hz, 2H), 7.20 (m, 4H), 7.15 (d, $J = 8.7$ Hz, 2H), 5.44 (dd, $J = 8.7, 5.0$ Hz, 1H), 4.68 (d, $J = 8.6$ Hz, 1H), 4.20 (d, $J = 8.6$ Hz, 1H), 3.37 (t, $J = 7.0$ Hz, 2H), 3.21 (dd, $J = 12.8, 8.7$ Hz, 1H), 3.01 (dd, $J = 12.8, 5.0$ Hz, 1H), 2.37 (s, 3H), 2.35 – 2.24 (m, 2H), 1.83 (p, $J = 7.0$ Hz, 2H), 1.64 (p, $J = 7.0$ Hz, 2H), 1.52 – 1.28 (m, 4H); ^{13}C NMR (101 MHz, CDCl_3) δ 170.20 (C), 143.52 (C), 142.33 (C), 137.24 (C), 133.41 (C), 130.00 (CH), 129.78 (CH), 126.98 (CH), 126.86 (CH), 75.52 (CH_2), 75.31 (C), 51.56 (CH_2), 33.91 (CH_2), 32.48 (CH_2), 28.25 (CH_2), 27.95 (CH_2), 27.70 (CH_2), 25.83 (CH_2), 21.54 (CH_3); IR (neat) $\nu = 2932.9$ (w), 1658.0 (m), 1328.4 (m), 1157.6 (s), 1090.7 (s), 813.4 (s), 661.8 (s), 548.1

(s) cm^{-1} ; HR-MS calculated for $\text{C}_{23}\text{H}_{29}^{79}\text{Br}^{35}\text{ClN}_2\text{O}_3\text{S}$ 527.0736, found 527.0743 ($\Delta = 1.0$ ppm, 0.7 mDa).



***N*-((2-(7-Bromoheptyl)-4-(*p*-tolyl)-4,5-dihydrooxazol-4-yl)methyl)-4-methylbenzenesulfonamide (3-209).**

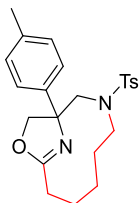
Appearance colourless oil, 75%, ^1H NMR (400 MHz, CDCl_3) δ 7.65 (d, $J = 8.1$ Hz, 2H), 7.22 (d, $J = 8.1$ Hz, 2H), 7.15 – 7.05 (m, 4H), 5.26 (dd, $J = 9.2, 4.6$ Hz, 1H), 4.72 (d, $J = 8.4$ Hz, 1H), 4.27 (d, $J = 8.4$ Hz, 1H), 3.39 (t, $J = 6.8$ Hz, 2H), 3.25 (dd, $J = 12.7, 9.2$ Hz, 1H), 3.01 (dd, $J = 12.7, 4.6$ Hz, 1H), 2.43– 2.30 (m, 2H), 2.38 (s, 3H), 2.30 (s, 3H), 1.84 (p, $J = 6.9$ Hz, 2H), 1.71 – 1.62 (m, 2H), 1.49 – 1.28 (m, 6H); ^{13}C NMR (101 MHz, CDCl_3) δ 170.14 (C), 143.42 (C), 140.94 (C), 137.34 (C), 136.88 (C), 129.77 (CH), 129.40 (CH), 126.95 (CH), 125.34 (CH), 75.74 (CH_2), 75.36 (C), 51.63 (CH_2), 34.03 (CH_2), 32.72 (CH_2), 29.00 (CH_2), 28.37 (CH_2), 28.11 (CH_2), 28.00 (CH_2), 26.04 (CH_2), 21.53 (CH_3), 21.04 (CH_3); IR (neat) $\nu = 1652.7$ (m), 906.8 (s), 726.8 (s), 661.6 (m), 551.0 (m) cm^{-1} ; HR-MS calculated for $\text{C}_{25}\text{H}_{34}^{79}\text{BrN}_2\text{O}_3\text{S}$ 521.1474, found 521.1475 ($\Delta = 0.2$ ppm, 0.1 mDa).



***N*-((2-(10-Bromodecyl)-4-(*p*-tolyl)-4,5-dihydrooxazol-4-yl)methyl)-4-methylbenzenesulfonamide (3-210).**

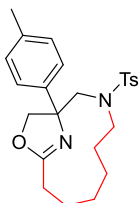
Appearance: colourless oil, 75%, ^1H NMR (400 MHz, CDCl_3) δ 7.65 (d, $J = 8.0$ Hz, 2H), 7.22 (d, $J = 8.0$ Hz, 2H), 7.13 (d, $J = 8.3$ Hz, 2H), 7.08 (d, $J = 8.3$ Hz, 2H), 5.34 (dd, $J = 9.1, 4.6$ Hz, 1H), 4.73 (d, $J = 8.4$ Hz, 1H), 4.27 (d, $J = 8.4$ Hz, 1H), 3.39 (t, $J = 6.9$ Hz, 2H), 3.25 (dd, $J = 12.7, 9.1$ Hz, 1H), 3.03 (dd, $J = 12.7, 4.6$ Hz, 1H), 2.38 (s, 3H), 2.30 (s, 3H), 1.84 (p, $J = 6.9$ Hz, 2H), 1.66 (t, $J = 7.4$ Hz, 2H), 1.47 – 1.21 (m, 14H); ^{13}C NMR (101 MHz, CDCl_3) δ 170.41 (C), 143.34 (C), 140.82 (C), 137.27 (C), 136.88 (C), 129.72 (CH), 129.35 (CH), 126.92 (CH), 125.32 (CH), 75.79 (CH_2), 75.26 (C), 51.56 (CH_2), 34.09 (CH_2), 32.79 (CH_2), 29.34 (CH_2), 29.31 (CH_2), 29.16 (CH_2),

29.13 (CH₂), 28.72 (CH₂), 28.13 (CH₂), 28.12 (CH₂), 26.10 (CH₂), 21.47 (CH₃), 21.00 (CH₃) cm⁻¹;
HR-MS calculated for C₂₈H₄₀⁷⁹BrN₂O₃S 563.1965, found 563.1970 (Δ = 0.2 ppm, 0.5 mDa).



1-(*p*-Tolyl)-3-tosyl-10-oxa-3,12-diazabicyclo[7.2.1]dodec-9(12)-ene (3-211).

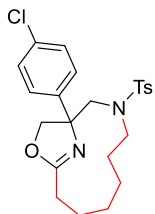
Appearance: colourless oil, 40%, ¹H NMR (400 MHz, CDCl₃) δ 7.62 (d, J = 8.3 Hz, 2H), 7.29 – 7.22 (m, 4H), 7.18 – 7.14 (m, 2H), 5.20 (d, J = 8.5 Hz, 1H), 4.20 (d, J = 8.5 Hz, 1H), 3.81 (d, J = 14.0 Hz, 1H), 3.17 – 2.96 (m, 2H), 2.77 (d, J = 13.9 Hz, 1H), 2.57 – 2.48 (m, 1H), 2.38 (s, 3H), 2.33 (s, 3H), 2.15 (ddd, J = 14.6, 11.3, 3.8 Hz, 1H), 1.99 – 1.82 (m, 4H), 1.59 (ddq, J = 10.9, 8.0, 5.2 Hz, 2H); ¹³C NMR (101 MHz, CDCl₃) δ 170.12 (C), 143.46 (C), 140.95 (C), 137.15 (C), 134.64 (C), 129.71 (CH), 129.34 (CH), 127.41 (CH), 125.77 (CH), 76.84 (C), 74.50 (CH₂), 61.57 (CH₂), 49.82 (CH₂), 29.58 (CH₂), 27.20 (CH₂), 24.55 (CH₂), 23.67 (CH₂), 21.47 (CH₃), 21.04 (CH₃); IR (neat) ν = 2923.5 (w), 1664.1 (m), 1334.6 (m), 1159.0 (s), 1014.1 (m), 908.2 (m), 815.3 (m), 728.2 (s), 712.6 (s), 646.5 (m), 547.3 (s) cm⁻¹; HR-MS calculated for C₂₃H₂₉N₂O₃S 413.1899, found 413.1895 (Δ = -1.0 ppm, -0.4 mDa).



1-(*p*-Tolyl)-3-tosyl-11-oxa-3,13-diazabicyclo[8.2.1]tridec-10(13)-ene (3-212).

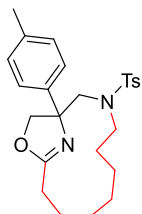
Appearance: white solid, 72%, ¹H NMR (400 MHz, CDCl₃) δ 7.65 (d, J = 8.6 Hz, 2H), 7.33 (d, J = 8.2 Hz, 2H), 7.27 (d, J = 8.6 Hz, 1H), 7.17 (d, J = 8.2 Hz, 2H), 5.52 (d, J = 8.9 Hz, 1H), 4.28 (d, J = 8.9 Hz, 1H), 3.96 (d, J = 15.0 Hz, 1H), 3.32 – 3.21 (m, 1H), 2.84 (d, J = 15.0 Hz, 1H), 2.59 (dt, J = 13.2, 4.1 Hz, 1H), 2.51 – 2.42 (m, 1H), 2.39 (s, 3H), 2.33 (s, 3H), 2.30 – 2.03 (m, 3H), 1.73 – 1.54 (m, 3H), 1.54 – 1.30 (m, 3H); ¹³C NMR (101 MHz, CDCl₃) δ 168.72 (C), 143.54 (C), 142.90 (C), 136.90 (C), 134.76 (C), 129.67 (CH), 129.25 (CH), 127.65 (CH), 125.79 (CH), 76.58 (C), 74.99 (CH₂), 61.74 (CH₂), 52.54 (CH₂), 27.78 (CH₂), 27.32 (CH₂), 26.42 (CH₂), 22.68 (CH₂), 22.27 (CH₂),

21.45 (CH₃), 20.99 (CH₃); IR (neat) ν = 2930.1 (w), 1661.9 (m), 1335.3 (m), 1160.0 (s), 984.6 (m), 816.0 (m), 697.7 (m), 548.4 (s) cm⁻¹; HR-MS calculated for C₂₄H₃₁N₂O₃S 427.2055, found 427.2042 (Δ = -3.0 ppm, -1.3 mDa); X-ray CCDC (1985644) Unit Cell Parameters: a 10.5538(7) b 21.7626(14) c 10.9319(7) P21/n



1-(4-Chlorophenyl)-3-tosyl-11-oxa-3,13-diazabicyclo[8.2.1]tridec-10(13)-ene (3-213).

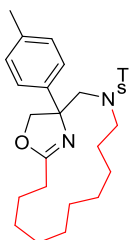
Appearance: white solid, 70%, ¹H NMR (400 MHz, CDCl₃) δ 7.55 (d, *J* = 8.0 Hz, 1H), 7.27 (d, *J* = 8.6 Hz, 1H), 7.23 – 7.16 (m, 4H), 5.42 (d, *J* = 9.0 Hz, 1H), 4.13 (d, *J* = 9.0 Hz, 1H), 3.81 (d, *J* = 15.0 Hz, 1H), 3.16 (ddd, *J* = 13.2, 11.0, 3.5 Hz, 1H), 2.71 (d, *J* = 15.0 Hz, 1H), 2.46 (dt, *J* = 13.2, 4.0 Hz, 1H), 2.42 – 2.33 (m, 1H), 2.30 (s, 3H), 2.17 – 1.94 (m, 3H), 1.68 – 1.16 (m, 6H); ¹³C NMR (101 MHz, CDCl₃) δ 169.31 (C), 144.43 (C), 143.76 (C), 134.70 (C), 133.17 (C), 129.80 (CH), 128.78 (CH), 127.74 (CH), 127.50 (CH), 76.55 (C), 74.89 (CH₂), 61.57 (CH₂), 52.65 (CH₂), 27.81 (CH₂), 27.45 (CH₂), 26.37 (CH₂), 22.66 (CH₂), 22.29 (CH₂), 21.56 (CH₃); IR (neat) ν = 2937.7 (w), 1661.0 (m), 1332.9 (m), 1155.0 (s), 1086.7 (m), 999.9 (m), 952.0 (m), 816.0 (s), 700.8 (m), 648.7 (m), 579.7 (s), 563.6 (s), 545.5 (s) cm⁻¹; HR-MS calculated for C₂₃H₂₈N₂O₃S³⁵Cl 447.1509, found 447.1508 (Δ = -0.2 ppm, -0.1 mDa); Melting point: 143-145 °C crystallised from Hexane / EtOAc. X-ray CCDC (1985645) Unit Cell Parameters: a 5.9218(6) b 21.635(2) c 17.5661(16) P21/c.



1-(*p*-Tolyl)-3-tosyl-15-oxa-3,17-diazabicyclo[12.2.1]heptadec-14(17)-ene (3-214).

Appearance: white solid, 70%, ¹H NMR (400 MHz, CDCl₃) δ 7.53 (d, *J* = 8.3 Hz, 2H), 7.27 (d, *J* = 8.3 Hz, 2H), 7.21 (d, *J* = 8.0 Hz, 2H), 7.12 (d, *J* = 8.0 Hz, 2H), 5.07 (d, *J* = 8.8 Hz, 1H), 4.38 (d, *J* =

8.8 Hz, 1H), 3.81 (d, $J = 14.8$ Hz, 1H), 3.13 (ddd, $J = 13.7, 8.3, 5.3$ Hz, 1H), 3.01 – 2.86 (m, 2H), 2.39 (m, 1H), 2.35 (s, 3H), 2.30 (s, 3H), 2.10 (dtt, $J = 15.9, 7.7, 3.3$ Hz, 1H), 1.83 (ddt, $J = 16.7, 8.7, 4.4$ Hz, 2H), 1.70 (ddt, $J = 10.6, 8.7, 3.3$ Hz, 1H), 1.66 – 1.45 (m, 4H), 1.20 (dtd, $J = 16.7, 7.7, 4.4$ Hz, 2H); ^{13}C NMR (101 MHz, CD_3OD) δ 171.41 (C), 145.28 (C), 143.36 (C), 138.35 (C), 135.27 (C), 130.86 (CH), 130.33 (CH), 128.76 (CH), 126.55 (CH), 77.78 (C), 76.92 (CH₂), 60.66 (CH₂), 51.42 (CH₂), 28.60 (CH₂), 28.37 (CH₂), 28.29 (CH₂), 25.44 (CH₂), 23.44 (CH₂), 22.47 (CH₂), 21.51 (CH₃), 21.12 (CH₃); IR (neat) $\nu = 2931.6$ (w), 1662.8 (m), 1334, 5 (m), 1159.5 (s), 1088.8 (m), 815.0 (m), 730.4 (s), 696.8 (s), 547.6 (s) cm^{-1} ; HR-MS calculated for $\text{C}_{25}\text{H}_{33}\text{N}_2\text{O}_3\text{S}$ 441.2212, found 441.2208 ($\Delta = -0.9$ ppm, -0.4 mDa); X-ray CCDC (1985647) Unit Cell Parameters: a 10.5408(7) b 11.4873(7) c 19.3042(13) P21/n.



1-(*p*-Tolyl)-3-tosyl-15-oxa-3,17-diazabicyclo[12.2.1]heptadec-14(17)-ene (3-215).

Appearance: pale yellow oil, 33%, ^1H NMR (400 MHz, CDCl_3) δ 7.59 (dd, $J = 8.3, 1.4$ Hz, 2H), 7.29 (d, $J = 8.3$ Hz, 2H), 7.24 (d, $J = 8.1$ Hz, 2H), 7.16 (d, $J = 8.1$ Hz, 2H), 4.99 (d, $J = 8.3$ Hz, 1H), 4.34 (d, $J = 8.3$ Hz, 1H), 3.78 (d, $J = 14.7$ Hz, 1H), 3.21 (dd, $J = 14.7, 10.2$ Hz, 1H), 3.10 (m, 2H), 2.39 (s, 3H), 2.33 (s, 3H), 1.77 – 1.63 (m, 3H), 1.43 – 1.11 (m, 15H); ^{13}C NMR (101 MHz, CDCl_3) δ 143.40 (C), 142.36 (C), 137.12 (C), 136.19 (C), 136.05 (C), 129.71 (CH), 129.29 (CH), 127.37 (CH), 125.80 (CH), 77.01 (C), 75.45 (CH₂), 58.15 (CH₂), 51.30 (CH₂), 29.97 (CH₂), 29.77 (CH₂), 29.70 (CH₂), 29.46 (CH₂), 29.29 (CH₂), 28.79 (CH₂), 28.41 (CH₂), 27.42 (CH₂), 25.88 (CH₂), 21.55 (CH₃), 21.09 (CH₃); IR (neat) $\nu = 2924.9$ (w), 1662.9 (w), 1334.7 (m), 1160.2 (m), 907.1 (s), 729.9 (s), 649.5 (m), 549.9 (m) cm^{-1} ; HR-MS calculated for $\text{C}_{28}\text{H}_{39}\text{N}_2\text{O}_3\text{S}$ 483.2681, found 483.2684 ($\Delta = 0.6$ ppm, 0.3 mDa).

3.6 References

- 1) Andreasch, R.; *Monatshefte für Chemie*, **1884**, *5*, 33–46.
- 2) Gabriel, S.; *Eur. J. Inorg. Chem.*, **1889**, *22*, *1*, 1139–1154.
- 3) Billman, J. H.; Parker, E. E.; U. S. Patent 2,556,791, **1951**.
- 4) Takahashi, S.; Togo, H. *Synthesis*, **2009**, 2329–2332.
- 5) Schwekendiek, K.; Glorius, F. *Synthesis*, **2006**, *18*, 2996–3002.
- 6) McManus, S. P.; Carroll, J. T.; Grohse, P. M.; Pittman, C. V. *Org. Prep. Proced.*, **1969**, *1*, 183–186.
- 7) John, A. F. *Chem. Rev.*, **1971**, *71*, *5*, 483–5057.
- 8) Hashmi, A. S. K.; Jaimes, M. C. B.; Schuster, A. M.; Rominger, F.; *J. Org. Chem.*, **2012**, *77*, 6394–6408.
- 9) Senadi, G. C.; Hu, W. P.; Hsiao, J. S.; Vandavasi, J. K.; Chen, C. Y.; Wang, J. *J. Org. Lett.*, **2012**, *14*, 4478–4481.
- 10) Oda, R.; Okano, M.; Tokiura, S.; Misumi, F. *Bull. Chem. Soc. Jap.*, **1962**, *35*, *7*, 1219–1221.
- 11) Temnikova, T. I.; Yandovski, V. *Zh. Org. Khim.*, **1968**, *4*, 178–182.
- 12) Lambert, R. F.; Kristofferson, C. E. *J. Org. Chem.*, **1965**, *30*, 3938–3939.
- 13) Trose, M.; Lazreg, F.; Lesieur, M.; Cazin, C. S. J. *J. Org. Chem.*, **2015**, *80*, 9910–9914.
- 14) Cornejo, A.; Fraile, J. M.; García, J. I.; Gil, M. J.; Martínez, V.; Mayoral, J. A.; Pires, E.; Villalba, I. *Synlett*, **2005**, *15*, 2321–2324.
- 15) Fry, E. M.; *J. Org. Chem.*, **1949**, *14*, 887–894.
- 16) Bretschneider, H.; Piekarski, G.; Biemann, K.; *Monatsh. Chem.*, **1954**, *85*, 882–883; *Chem. Abstr.*, **1955**, *49*, 15860.
- 17) Holerca, N.; Percec, V.; *Eur. J. Org. Chem.* **2000**, *12*, 2257–2263.
- 18) Evans, D.; Peterson, G. S.; Johnson, Je. S.; Barnes, D. M.; Campos, K. R.; Woerpel, K. A. *J. Org. Chem.*, **1998**, *63*, *13*, 4541–4544.
- 19) Albert, I. M.; Mark E. F. *Org. Synth.*, **1993**, *71*, 107–108.
- 20) Satoshi, M.; Yoshinobu, M.; Oderaotshi, M. K. *Org. Lett.*, **2006**, *8*, *15*, 3335–333.
- 21) Favreau, S.; Lizzani-Cuvelier, L.; Loiseau, M.; Duñach, E.; Fellous, R.; *Tetrahedron Letters*, **2000**, *41*, 9787–9790.
- 22) Kenichi, M.; Takahara, T.; Matsushita, H.; Komatsu, H.; *Org. Lett.*, **2010**, *12*, *15*, 3456–3459.
- 23) Padmavathi, V.; Mahesh K.; Subbaiah D. R. C. V.; *Arkivoc*, **2009**, 195–208.
- 24) Waschinski, C. J.; Tiller, J. C.; *Biomacromolecules*, **2005**, *6*, 235–243.

- 25) Khanum, S. A.; Khanum, N.F.; Shashikanth, M. *Bioorg. Med. Chem. Lett.*, **2008**, *18*, 4597–4601.
- 26) Hemin, T. R.; Pauvlik, J. M.; Schuber, E. V; Geiszler, A. *J. Med. Chem.*, **1975**, *18*, 1216–1223.
- 27) Gordey, E. E.; Yadav, P. N.; Merrin, M. P.; Davies, J.; Ward, S. A.; Woodman, G. M. J.; Sadowy, A. L.; Smith, T. G.; Gossage, R. A. *Bioorg. Med. Chem. Lett.*, **2011**, *21*, 4512–4515.
- 28) Waschinski, C. J.; Barnert, S.; Theobald, A.; Schubert, R.; Kleinschmidt, F.; Hofmann, A.; Saalwachter, K.; Tiller, J. C. *Biomacromolecules*, **2008**, *9*, 1764–1771.
- 29) Pirrung, M. C.; Tumey, L. N.; Raetz, C. R. H.; Jackman, J. E.; Snehalatha, K.; McClerren, A. L.; Fierke, C. A.; Gantt, S. L.; Rusche, K. M.; *J. Med. Chem.*, **2002**, *45*, 4359–4370.
- 30) Pei, Z.; Adam, W. B.; *Curr Pharm Biotechnol*, **2008**, *9*, 1, 9–15.
- 31) Gros, C.; Fahy, J.; Halby, L.; Dufau, I.; Erdmann, A.; Gregoire, J. M.; Ausseil, F.; Vispé, S.; Arimondo, P. B.; *Biochimie*, **2012**, *94*, 2280–2296.
- 32) Li, Q.; Woods, K. W.; Claiborne, A.; Gwaltney, S. L.; Barr, K. J.; Liu, G.; Gehrke, L.; Credo, R. B.; Hui, Y. H.; Lee, J.; Warner, R. B.; Kovar, P.; Nukkala, M. A.; Zielinski, N. A.; Tahir, S. K.; Fitzgerald, M.; Kim, K. H.; Marsh, K.; Frost, D.; Hing, S. R.; Sham, L. *Bioorg. Med. Chem. Lett.*, **2002**, *12*, 465–469.
- 33) Diana, G. D.; Oglesby, R.C.; Akullian, V.; Carabateas, P. M.; Cutcliffe, D.; Mallamo, J. P.; Otto, M. J.; McKinlay, M. A.; Maliski, E. G.; Michalec, S. J.; *J. Med. Chem.*, **1987**, *30*, 383–388.
- 34) Jiang, X.; Cao, Y.; Wang, Y.; Liu, L.; Shen, F.; Wang, R.; *J. Am. Chem. Soc.*, **2010**, *132*, 15328–15333.
- 35) Moraski, G. C.; Markley, L. D.; Chang, M.; Cho, S.; Franzblau, S. G.; Hwang, C. H.; Boshoff, H.; Miller, M. J.; *Bioorg. Med.*, **2012**, *20*, 2214–2220.
- 36) Miller, M. J.; Walz, A. J.; Zhu H.; Wu, C.; Moraski, G.; Mollmann, U.; Tristani, E. M.; Crumbliss, A. L.; Ferdig, M. T.; Checkley, L.; Edwards, R. L.; Boshoff, H. I.; *J. Am. Chem. Soc.*, **2011**, *133*, 2076–2079.
- 37) Thompson, A.; Donaldson, R. E.; White, C. C.; *U. S. Patent*, **1961**, *2*, 186, *Chem. Abstr.*, **1962**, *57*, 14022.
- 38) R. J. Marker, U. S. Patent 3,039,961 (**1962**); *Chem. Abstr.*, *57*, 10111 (**1962**).
- 39) Chemische Werke Huels A.-G., French Patent 1,506,154 (**1967**); *Chem. Abstr.*, *70*, 20048 (**1969**).
- 40) John, A. F.; *Chem. Rev.*, **1971**, *71*, 5, 483–505.
- 41) Wainwright, H. W.; Egleson, G. C.; Brock, C. M.; Fisher, J.; Sands, A. E. U. S. Bur. Mines, Rep. Invest., No. 4891, 19 pp (**1952**); *Chem. Abstr.*, *47*, 1357 (**1953**).

- 42) A. M. Erskine and R. M. Lydon, U. S. Patent 2,893,886 (1959); Chem. Abstr., 54, 923 (1960).
- 43) Farbwerke Hoechst A.-G., French Patent 1,371,032 (1964); Chem. Abstr., 62, 10587 (1965).
- 44) Farbwerke Hoechst A.-G., Belgian Patent 655,185 (1965); Chem. Abstr., 64, 19874(1966).
- 45) Litt, H.; Levy, A. J.; Bassiri, T. G.; Belgian Patent 666,831 (1965); Chem. Abstr., 65, 8928 (1966).
- 46) Standard Oil Co. (Ohio), British Patent 846,231 (1960); Chem. Abstr., 55, 6848 (1961).
- 47) R. J. DeGray, U. S. Patent 3,033,661 (1962); Chem. Abstr., 59, 2571 (1963).
- 48) J. Nys and J. Libeer, U. S. Patent 2,954,376 (1960); Chem. Abstr., 55, 7114 (1961).
- 49) W. J. Middleton, U. S. Patent 3,442,904 (1969); Chem. Abstr., 71, 22125 (1969).
- 50) S. Shimada, German Patent 1,299,481 (1969); Chem. Abstr., 71, 104381 (1969).
- 51) Nishiyama, H.; Sakaguchi, H.; Nakamura, T.; Horihata, M.; Kondo, M.; Itoh, K.; *Organometallics*, **1989**, *8*, 846–848.
- 52) Lowenthal, R. E.; Abiko, A.; Masamune, S.; *Tetrahedron Lett.*, **1990**, *31*, 6005–6008.
- 53) Lowenthal, R. E.; Masamune, S.; *Tetrahedron Lett.*, **1991**, *32*, 7373–7376.
- 54) Evans, D. A.; Woerpel, K. A.; Hinman, M. M.; Faul, M. M.; *J. Am. Chem. Soc.*, **1991**, *113*, 726–728.
- 55) Corey, E. J.; Imai, N.; Zhang, H. Y.; *J. Am. Chem. Soc.*, **1991**, *113*, 728–729.
- 56) Helmchen, G.; Krotz, A.; Ganz, K.T.; Hansen, D.; *Synlett*, **1991**, 257–259.
- 57) Yang, R.Y.; Chen, Y.H.; Dai, L.X.; *Acta Chim. Sin.*, **1991**, *49*, 1038–1041.
- 58) Peter, v. M.; Andreas, P.; *Angew. Chem., Int. Ed. Engl.*, **1993**, *32*, 566–568.
- 59) Sprinz, J.; Helmchen, G.; *Tetrahedron Lett.*, **1993**, *34*, 1769–1772.
- 60) Dawson, G. J.; Frost, C. G.; Williams, S. J.; *Tetrahedron Lett.*, **1993**, *34*, 3149–3150.
- 61) Zhou, J.; Tang, Y. *J. Am. Chem. Soc.*, **2002**, *124*, 9030–9031.
- 62) Laponnaz, S. B.; Gade, L. H. *Angew. Chem.*, **2002**, *41*, 3473–3475.
- 63) Bower, J. F.; Willams, J. M. *Tetrahedron Lett.*, **1994**, *35*, 7111–7114.
- 64) Kanemasa, S.; Oderaotoshi, Y.; Yamamoto, H.; Tanaka, J.; Wada, *J. Org. Chem.*, **1997**, *62*, 6454–6455.
- 65) McManus, H. A.; Guiry, P. J. *J. Org. Chem.*, **2002**, *67*, 24, 8566–8573.
- 66) Inoue, M.; Suzuki, T.; Nakada, M. *J. Am. Chem. Soc.*, **2003**, *125*, 1140–1141.
- 67) Liu, B.; Zhu, S. F.; Wang, L. X.; Zhou, Q. L.; *Tetrahedron: Asymmetry*, **2006**, *17*, 634–641.
- 68) Hahn, B. T.; Tewes, F.; Fronhlich, R.; Glorius, F.; *Angew. Chem.*, **2010**, *49*, 1143–1146.
- 69) Deng, Q. H.; Wadepohl, H.; Gade, L. H.; *Chem. Eur. J.*, **2011**, *17*, 14922–14928.

- 70) José, M. F.; José, I. G.; José A. M.; *Coord. Chem. Rev.* **2008**, *252*, 624–646.
- 71) Desimoni, G.; Faita, G.; Jørgensen, K. A. *Chem. Rev.*, **2006**, *106*, 9, 3561–3651.
- 72) Ma, S.; Wu, S. *New J. Chem.* **2001**, *25*, 1337–1341.
- 73) Evans, D. A.; Woerpel, K. A.; Scott, M. J.; *Angew. Chem.* **1992**, *31*, 430–432.
- 74) Thorhauge, J.; Roberson, M.; Hazell, R. G.; Jørgensen, K. A. *Chem. Eur. J.* **2002**, *8*, 1888–1898.
- 75) Evans, D. A.; Rovis, T.; Johnson, J. S. *Pure Appl. Chem.* **1999**, *71*, 1407–1415.
- 76) Evans, D. A.; Johnson, J. S.; Burgey, C. S.; Campos, K. R. *Tetrahedron Lett.* **1999**, *40*, 2879–2882.
- 77) Evans, D. A.; Johnson, J. S.; Olhava, E. J. *J. Am. Chem. Soc.* **2000**, *122*, 1635–1649.
- 78) Sibi, M. P.; Venkatraman, L.; Liu, M.; Jasperse, C. P. *J. Am. Chem. Soc.* **2001**, *123*, 8444–8445.
- 79) Richard E.; Atsushi, A.; Satoru, M. *Tetrahedron Letters*, **1990**, *31*, 42, 6005–6008.
- 80) Corey, E. J.; Ishihara, K. *Tetrahedron Lett.*, **1992**, *33*, 6807–6810.
- 81) Bolm, C.; Weickhardt, K.; Zehnder, M.; Ranff, T. *Chem. Ber.* **1991**, *124*, 1173–1180.
- 82) Harm, A. M.; Knight, J. G.; Stemp, G. *Synlett.*, **1996**, 677–678.
- 83) Davies, I. W.; Senanayake, C. H.; Larsen, R. D.; Verhoeven, T. R.; Reider, P. J.; *Tetrahedron Lett.*, **1996**, *37*, 813–814.
- 84) Portada, T.; Roje, M.; Raza, Z.; Caplar, V.; Zinic, M.; Sunjic, V. *Chem. Commun.*, **2000**, 1993–1994.
- 85) Fraile, J. M.; Garcia, J. I.; Mayoral, J. A.; Tarnai, T. J. *Mol. Catal. A: Chem.* **1999**, *144*, 85–89.
- 86) Østergaard, N.; Jensen, J. F.; Tanner, D. *Tetrahedron*, **2001**, *57*, 6083–6088.
- 87) Shu, F. C.; Zhou, Q. L.; *Synth. Commun.* **1999**, *29*, 567–572.
- 88) Meyer, O. G. J.; Frohlich, R.; Haufe, G.; *Synthesis*, **2000**, 1479–1490.
- 89) Haufe, G.; Rosen, T. C.; Meyer, O. G. J.; Frohlich, R.; Rissanen, K. *J. Fluorine Chem.*, **2002**, *114*, 189–198.
- 90) Evans, D. A.; Kozłowski, M. C.; Murry, J. A.; Burgey, C. S.; Campos, K. R.; Connel, B. T.; Staples, R. J. *J. Am. Chem. Soc.*, **1999**, *121*, 669–685.
- 91) Porter, N. A.; Wu, J. H.; Zhang, G.; Reed, A. D. *J. Org. Chem.*, **1997**, *62*, 6702–6703.
- 92) Yang, D.; Gu, S.; Yan, Y. L.; Zhu, N. Y.; Cheung, K. K. *J. Am. Chem. Soc.*, **2001**, *123*, 8612–8613.
- 93) Mukund, P. S.; Shankar, M.; Jake, Z. *Chem. Rev.*, **2003**, *103*, 3263–3295.

- 94) Yang, D.; Gu, S.; Yan, Y. L.; Zhao, H. W.; Zhu, N. Y. *Angew. Chem. Int. Ed.*, **2002**, *41*, 3014–3017.
- 95) Evans, D. A.; Miller, S. J.; Lectka, T.; Von Matt, P. *J. Am. Chem. Soc.*, **1999**, *121*, 7559–7573.
- 96) Evans, D. A.; Miller, S. J.; Lectka, T. *J. Am. Chem. Soc.* **1993**, *115*, 6460–6461.
- 97) Takacs, J. M.; Lawson, E. C.; Reno, M. J.; Youngman, M. A.; Quincy, D. A. *Tetrahedron: Asymmetry*, **1997**, *8*, 3073–3078.
- 98) Desimoni, G.; Faita, G.; Gamba Invernizzi, A.; Righetti, P. P. *Tetrahedron*, **1997**, *53*, 7671–7688.
- 99) Desimoni, G.; Faita, G.; Righetti, P. P. *Tetrahedron Lett.*, **1996**, *37*, 3027–3030.
- 100) Carbone, P.; Desimoni, G.; Faita, G.; Filippone, S.; Righetti, P. P. *Tetrahedron*, **1998**, *54*, 6099–6110.
- 101) Ghosh, A. K.; Cho, H.; Cappiello, J. *Tetrahedron: Asymmetry*, **1998**, *9*, 3687–3691.
- 102) Ishihara, J.; Fukuzaki, T.; Murai, A. *Tetrahedron Lett.*, **1999**, *40*, 1907–1910.
- 103) Evans, D. A.; Kozlowski, M. C.; Tedrow, J. S. *Tetrahedron Lett.*, **1996**, *37*, 7481–7484.
- 104) Davies, I. W.; Gerena, L.; Cai, D.; Larsen, R. D.; Verhoeven, T. R.; Reider, P. J. *Tetrahedron Lett.*, **1997**, *38*, 1145–1146.
- 105) Evans, D. A.; Murry, J. A.; von Matt, P.; Norcross, R. D.; Miller, S. *Angew. Chem.*, **1995**, *34*, 798–800.
- 106) Yao, S.; Johannsen, M.; Audrain, H.; Hazell, R. G.; Jørgensen, K. A.; *J. Am. Chem. Soc.* **1998**, *120*, 8599–8605.
- 107) Wolf, C.; Fadul, Z.; Hawes, P. A.; Volpe, E. C. *Tetrahedron: Asymmetry*, **2004**, *15*, 1987–1993.
- 108) Ghosh, A. K.; Shirai, M. *Tetrahedron Lett.*, **2001**, *42*, 6231–6233.
- 109) Van Lingen, H. L.; Van de Mortel, J. K. W.; Hekking, K. F. W.; Van Delft, F. L.; Sonke, T.; Rutjes, F. P. J. T. *Eur. J. Org. Chem.*, **2003**, 317–324.
- 110) Zhang, Q.; Lu, X.; *J. Am. Chem. Soc.*, **2000**, *122*, 7604–7605.
- 111) Zhang, Q.; Lu, X.; Han, X. *J. Org. Chem.* **2001**, *66*, 7676–7684.
- 112) Muthiah, C.; Arai, M. A.; Shinohara, T.; Arai, T.; Takizawa, S.; Sasai, H. *Tetrahedron Lett.*, **2003**, *44*, 5201–5204.
- 113) Shakil-H. S. M.; Ibrahim, M. B.; Fazal, A.; Suleiman, R. Fettouhi, M.; Ali, B.; *Polyhedron*, **2014**, *70*, 39–46.
- 114) Bakherad, M.; Keivanloo, A.; Bahramian, B.; Jajarmi, S. *J. Organomet. Chem.*, **2013**, *724*, 206–212.

- 115) Ruggeri, M.; Dombrowski, A. W.; Djuric, S. W.; Baxendale, I. R.; *ChemPhotoChem*, **2019**, 3, 12, 1212–1218.
- 116) Rainer, A.; Karl D.; Ruth P. S.; Arnold E. S. *Carbohydrate Res.*, **1985**, 137, 282–290.
- 117) Smith, C. J.; Iglesias-Sigüenza, J.; Baxendale, I. R.; Ley, S. V. *Org. Biomol. Chem.* **2007**, 5, 2758–2761.
- 118) Smith, C. D.; Baxendale, I. R.; Lanners, S.; Hayward, J. J.; Smith S. C.; Ley, S. V. *Org. Biomol. Chem.*, **2007**, 5, 1559–1561.
- 119) Baxendale, I. R. *Chem. Eng. Technol.*, **2015**, 38, 1713–1716
- 120) Hessel, V. *Chem. Eng. Tech.*, **2009**, 32, 11, 1655–1681.
- 121) Baxendale, I. R. *J. Chem. Technol. Biotechnol.*, **2013**, 88, 519–552.
- 122) Baumann, M.; Moody, T. S.; Smyth, M.; Wharry, S. *Org. Process Res. Dev.*, **2020**, <https://doi.org/10.1021/acs.oprd.9b00524>
- 123) <https://www.vapourtec.com/products/e-series-flow-chemistry-system-overview/>
(assessed 15/02/2020).
- 124) Pictet, A.; Spengler, T. *Berichte der Deutschen Chemischen Gesellschaft*, **1911**, 44, 3, 2030–2036.

4. Chapter 4: Exploring Photoflow Promoted Oximation of Alkanes

4.1 Introduction: Oximes

First synthesized in 1882 by the chemists Victor Meyer and Alois Janny^[1] oximes^[2] represent an important class of molecule possessing numerous applications in many different fields. An oxime is a function group entailing a hydroxyl bonded to the nitrogen of an imine. Depending on the substituent of the imino group we can distinguish between aldoxime **4-2**, ketoxime **4-3** or amidoxime **4-1** (Figure 1).

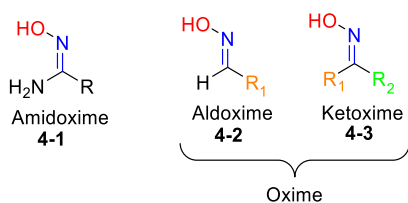


Figure 20: General oxime structures.

An oxime can potentially exist in three tautomeric forms, oxime **4-3**, nitron **4-4** and nitroso compound **4-5**^[3,4] (Figure 2).

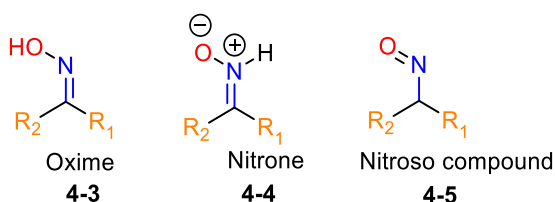
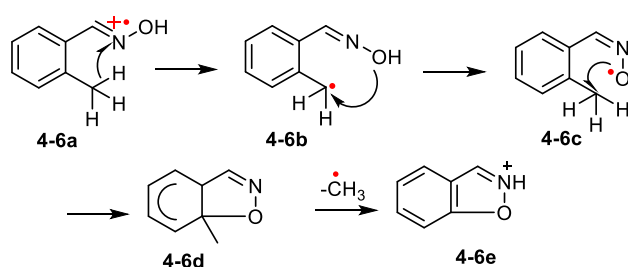


Figure 21: Tautomeric forms of oximes.

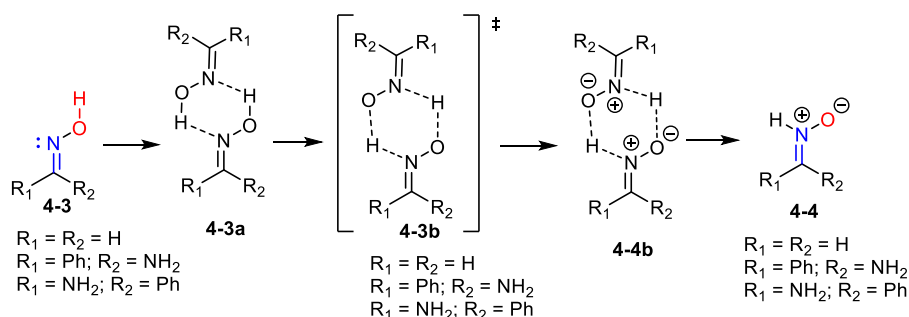
The isomerization between oxime **4-3** and nitron **4-4** was the first identified, studied and documented in 1977 by Vijfhuizen and Terlouw during their investigation using mass

spectrometry to study the loss of the methyl group from *o*-methylbenzaldoximes (**4-6a**) after electron impact (Scheme 1).^[5]



Scheme 24: Vijfhuizen and Terlouw study of the loss of the methyl group from *o*-methylbenzaldoximes

Several studies have proposed a thermal 1,2-hydrogen shift as being responsible for the tautomerism.^[6-9] In particular Yamamoto^[7] studied this proposed shift and the effect of protic solvent on the tautomerism of oximes and nitrones. However, recently it has been additionally suggested by the Lopez group that it can take place by a bimolecular mechanism involving two oximes or two nitrones^[10-15] (Scheme 2).

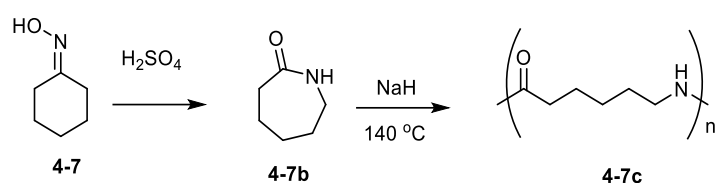


Scheme 2: Lopez bimolecular mechanism involving two molecules of oximes/nitrones.

In general the nitroso and nitronium tautomers are less stable than the corresponding oxime form.^[16] The nitronium species has proven particularly valuable in synthesis especially for cycloaddition reactions in combination with unsaturated electrophiles.^[10,11,17] The oxime shows much higher reactivity than the nitronium (**4-4**) at high pH as showed by Dignam and Hegarty in their study on the kinetics and mechanism of *E/Z* isomerisation of amidoximes in

aqueous solution. In this piece of work the authors blocked the oxime-nitrone tautomerization (**4-3**↔**4-4**) by alkylating the oxime oxygen and observing that the alkylated amidoximes at high pH isomerize at similar rates to the non-alkylated; thus deducing that it is the neutral oxime (**4-3**) and not the nitrone (**4-4**) that was the reactive species.^[11,18]

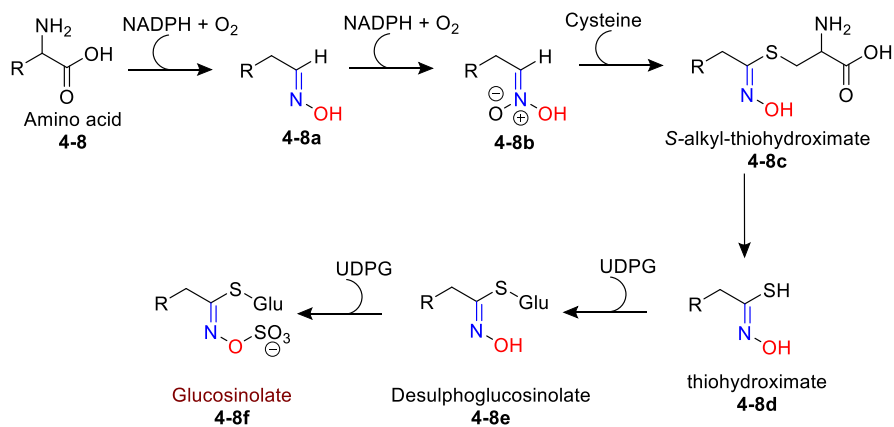
One of the most important applications of an oxime is in the synthesis of Caprolactam (**4-7b**); obtained via a Beckman rearrangement from cyclohexanone oxime (**4-7**), itself a precursor of Nylon-6 (**4-7c**; Scheme 3).



Scheme 3: Cyclohexanone oxime (4-7) a precursor of Nylon-6 (4-7b).

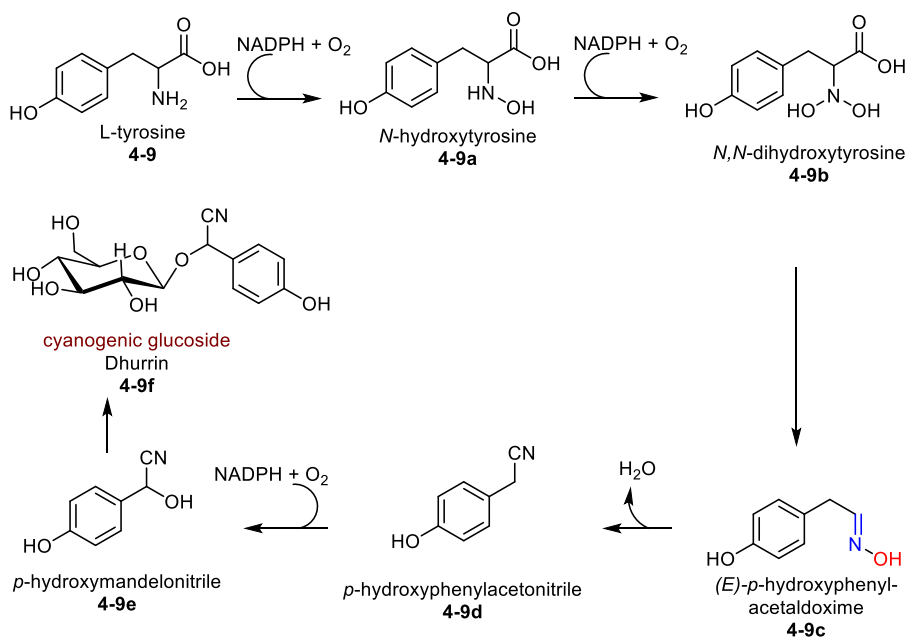
In material chemistry oximes have recently found value in the recovery of rare metals such as uranium and vanadium from seawater. In particular amidoxime groups were very promising chelating agents and thus fibrous adsorbent material functionalised with amidoxime groups have been prepared as immobilised scavengers for this purpose.^[19]

Oximes also have broad ranging biological activity. Sorensen and Moller highlighted that they are extremely abundant among plant metabolites and play key roles in plant biological systems (growth regulation and attraction of species responsible for the pollination) moreover many plant metabolites are also biosynthesised from oxime precursors, examples include Auxin, glucosinolate and cyanogenic glucosides (Scheme 4 and 5).^[20]



NADPH = Nicotinamide adenine dinucleotide phosphate
 UDPG = Uridine diphosphate glucose
 Glu = Glucose

Scheme 4: Oxime as precursor in the general biosynthesis of Glucosinolate (4-8f).



NADPH = Nicotinamide adenine dinucleotide phosphate

Scheme 5: Oxime as precursor of the cyanogenic glucoside Dhurrin (4-9f).

Their importance is also evidenced by the large number of biologically active compounds exhibiting the oxime moiety (Figure 3). Among these is a remarkable important application that oximes have as antidotes for organophosphorus compounds (OPCs).^[31] Indeed, the current standard treatment in case of Organophosphorus Poisoning includes a muscarinic ACh (acetylcholine) receptor antagonist (like atropine^[28]) to block the over-stimulation of cholinergic receptors by ACh, and an oxime like Pralidoxime (**4-10**) or Obidoxime (**4-10b**) (Figure 3) to reactivate OPC-inhibited AChE.^[28,29,30]

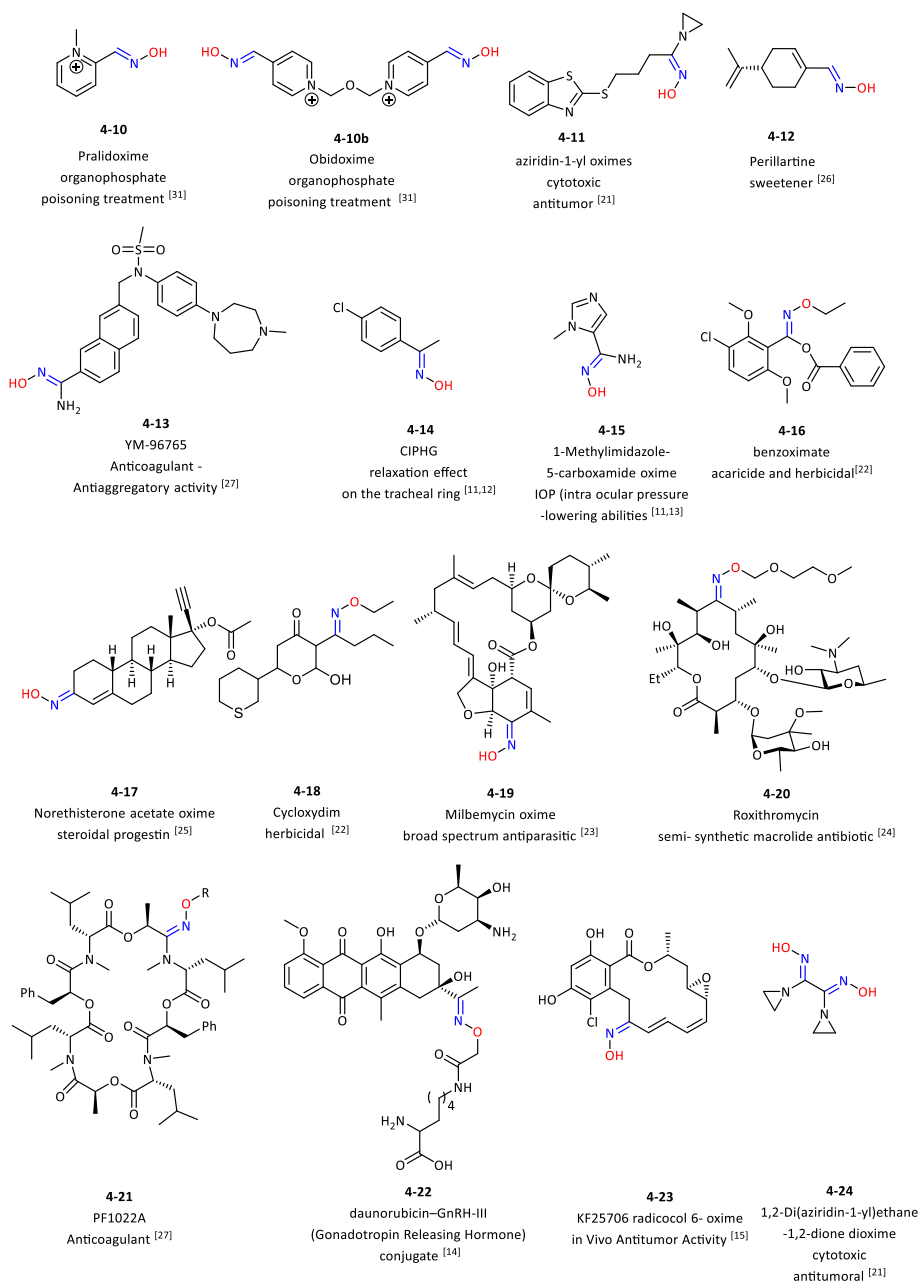
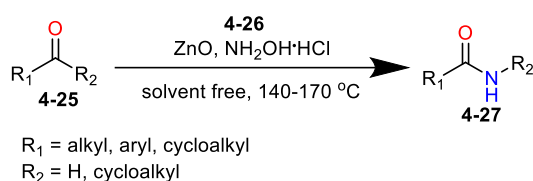


Figure 22. Examples of biologically important compounds containing the oxime moiety.

4.1.2 Synthesis of oximes

Oxime are generally obtained by the direct reaction between hydroxylamine and an aldehyde or a ketone.^[6,32,33] They can also exist as two distinct stereoisomers: the *Z* or *E* form. Although the *Z*-isomer has been shown to be the most stable, the *E* form is often also present as a minor species.^[11,4,18] Much effort has been applied towards optimising the reaction conditions to minimise by-product formation and maximise the yield of such condensations; several solvent free conditions have also been developed providing good results^[34] and the reaction has been performed using enabling technologies like microwave irradiation,^[35] ball milling^[36] and sonication.^[37]

Shanarghi and Hosseni^[38] have developed a solvent free one-pot Beckmann rearrangement of ketones and aldehydes (with hydroxylamine) promoted by heating at 140-170 °C in the presence of ZnO catalyst (Scheme 6). This procedure offers a green methodology avoiding the use of solvent and any strong Bronsted or Lewis acid which normally causes several undesired by-products to form and can be problematic to perform on industrial scale because of the associated issues of corrosion they can cause.^[39] The group applied this methodology to the synthesis of various oximes (Table 1).



Scheme 6: Shanarghi and Hosseni' one-pot Beckmann rearrangement of ketones and aldehydes.

The authors observed that when an aldehyde was stirred with hydroxylamine hydrochloride (4-26) and ZnO at 80 °C it afforded the resultant oxime in excellent yield (Table 1). The reaction was fast and allowed full conversion of the starting material in a time range of 5-15 min. Interestingly, the reaction is reported to give predominantly the *Z*-oxime isomer (OH *syn* to the aryl). Although most aldehydes reacted well, the authors observed a reduced reactivity for *meta*-substituted aromatic aldehydes which required longer reaction times (Table 1, entries 5-8). This is also in line with the findings of Schofield who also observed a reduced yield for the conversion of *meta*-substituted aldehydes to oximes when using a sulfuric acid catalyst at the same temperature of 80 °C.^[40]

Table 9: Conversion of aldehydes to oximes in the presence of ZnO.

Entry	<i>R</i>	Time (min)	Yield 4-2 (%)
1	<i>p</i> -MeC ₆ H ₄	5	100 ^a
2	<i>p</i> -OHC ₆ H ₄	5	100 ^a
3	<i>p</i> -ClC ₆ H ₄	5	100 ^a
4	<i>p</i> -MeOC ₆ H ₄	10	100 ^a
5	<i>m</i> -MeC ₆ H ₄	15	100 ^b
6	<i>m</i> -OHC ₆ H ₄	15	100 ^b
7	<i>m</i> -ClC ₆ H ₄	15	100 ^b
8	<i>m</i> -MeOC ₆ H ₄	15	100 ^b
9	<i>o</i> -OHC ₆ H ₄	5	>98 ^c
10	<i>o</i> -ClC ₆ H ₄	5	>98 ^c
11	Ph	5	100 ^d

^a 90% *Z* isomer 10% *E*, ^b 80% *Z* isomer 20% *E*; ^c 100% *Z* isomer; ^d 75% *Z* isomer 15% *E*.

Hajipour's group^[41] similarly performed the conversion of aldehydes and ketones into oximes under solvent free conditions using microwave irradiation. The process uses dry silica gel as a catalyst and allows the conversion to occur in just a few minutes with yields ranging from good to excellent (Table 2).

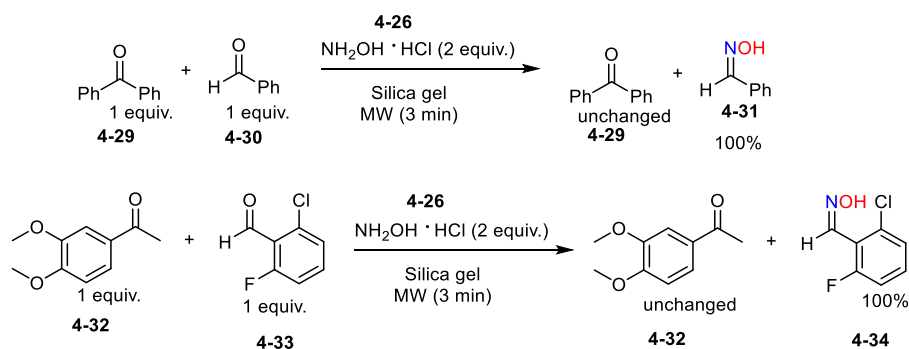
Table 10: Conversion of aldehydes and ketones in oxime under solvent free condition using microwave irradiation.

Entry	<i>R</i> ₁	<i>R</i> ₂	Power (W)	Time (s)	Yield (%)
1	Ph	H	800	50	90
2	<i>o</i> -MeOC ₆ H ₄	H	800	160	94
3	<i>p</i> -BrC ₆ H ₄	H	800	220	88
4	<i>p</i> -ClC ₆ H ₄	H	800	210	92
5	<i>p</i> -NO ₂ C ₆ H ₄	H	800	180	87
6	<i>p</i> -MeOC ₆ H ₄	H	800	140	79
7	<i>p</i> -Me ₂ NC ₆ H ₄	H	800	120	76
8	<i>o</i> -Cl, 6-FC ₆ H ₃	H	800	180	98
9	PhCH=CH	H	800	240	84
10	3,4-(MeO) ₂ C ₆ H ₃	H	800	120	86
11	Ph	Ph	800	360	50

12	3,4-(MeO) ₂ C ₆ H ₃	Me	800	270	37
13	PhCO	Ph	900	480	21
14	Ph	Me	900	240	73
15	PhCH(OH)	Ph	900	480	0
16	-[CH ₂] ₅ -		900	360	0
17	-[CH ₂] ₆ -		900	480	0

Irradiation was carried out in a domestic microwave oven (Samsung 2450 MHz, 900 W), for an optimised time and power. The temperature of the reaction reached 80-90 °C.

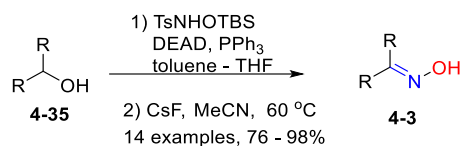
Notably, the authors reported the total inactivity of ketones under these condition and showed that their presence also didn't alter the aldehyde conversion thus providing a methodology that permits aldoximes (i.e. **4-31** & **4-34**) to be prepared even in the presence of compounds containing a ketone moiety (Scheme 7, **4-29** & **4-32**).

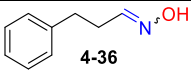
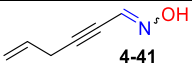
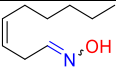
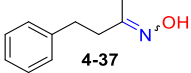
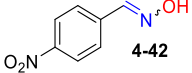
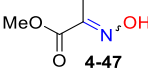
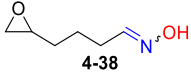


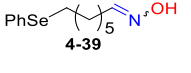
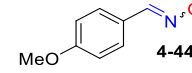
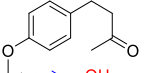
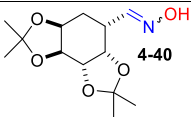
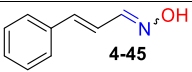


Scheme 7: The reaction condition permits the discrimination between aldehydes and ketones, with ketones being unreactive.

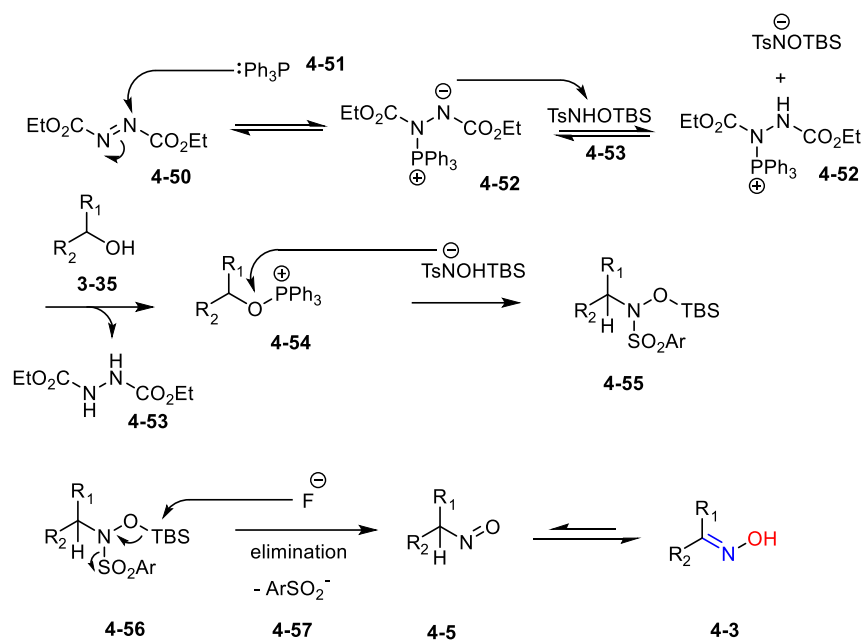
Fukuyama^[42] used *O*-TBS protected *N*-tosylhydroxylamine to obtain a variety of oximes from the corresponding alcohols, alkyl halides, or alkyl sulfonate; in particular the reagent was used under Mitsunobu conditions allowing for the facile conversion of alcohols (Table 3). The reaction generally gave excellent yields but led to a mixture of the *E,Z*-isomers.

Table 11: Synthesis of oximes starting from alcohols under Mitsunobu conditions.



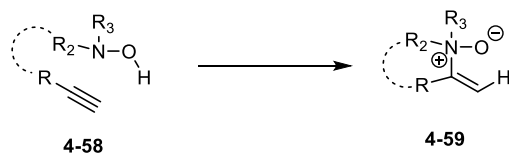
Oxime Product	Yield (%)	Oxime Product	Yield (%)	Oxime Product	Yield (%)
	99		92		89
	92		91		95
	82		94		98
	98		99		99
	90		94		

The procedure involves the conversion of the alcohol or alkyl halides first into the related alkylated hydroxylamine derivative via a Mitsunobu reaction (Scheme 8). The intermediate *O*-silyl-*N*-arylsulfonylhydroxylamine (**4-55**) is then converted to the corresponding nitrosoalkane **4-5** by elimination of sulfonate promoted by a fluoride ion attack on the silicon centre thus leading to the oxime **4-3** by tautomerization.^[42]



Scheme 8: Proposed mechanism for the Fukuyama's synthesis of oximes.

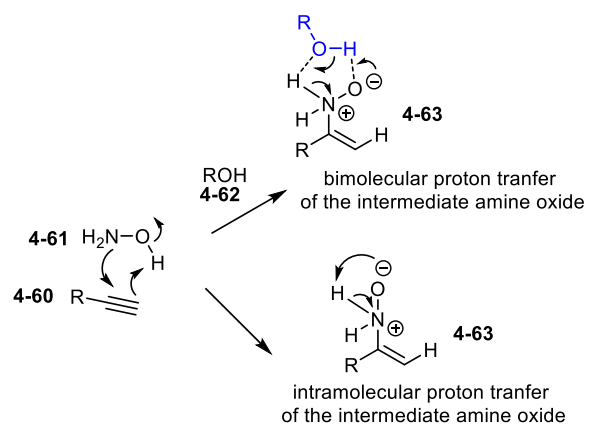
Beauchemin's group^[39a] has managed to perform the intramolecular hydroamination of alkynes and alkenes by heating them with aqueous hydroxylamine in the absence of any metal catalyst (Scheme 9 and Table 4).^[43-50]



Scheme 9: The reaction between alkyne and hydroxylamine derivative.^[39a]

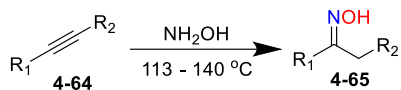
The authors proposed that some substrate have reduced reactivity due to a problematic intramolecular proton transfer and showed that the use of an additive of alcohol or water in

the reaction enhances the reactivity by promoting a more efficient bimolecular proton transfer (Scheme 10, Table 4; 4-73 - 4-75 4-77).

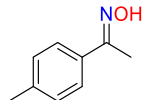
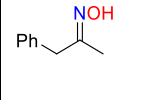


Scheme 10: Intramolecular and intermolecular proton transfer steps.

Table 12: Reaction of alkynes with aqueous NH_2OH .

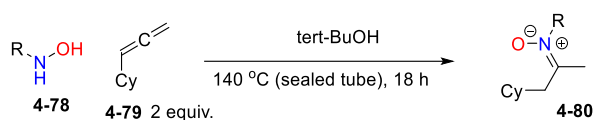


Entry	Major Product	%Yield	Entry	Major product	%Yield
4-66		87 ^a	4-72		73
4-67		83 ^a	4-73		62 ^b 86 ^c
4-68		71 ^a	4-74		55 ^b 72 ^c
4-69		45 ^a	4-75		63 ^c
4-70		75 ^a	476		71 ^b

3-71		65 ^a	3-77		31 ^b 53 ^c
^a 1 equiv. alkyne, 2 equiv. NH ₂ OH, dioxane (1 M), sealed tube, 113 °C, 16-18 h; ^b 140 °C, dioxane (2 M), 38-40 h; ^c <i>i</i> PrOH (1 M), 140 °C (microwave), 5-10 h.					

The same group^[51] also prepared a series of oximes and nitrones in good yield by direct reaction of an allene **4-79** with either aqueous hydroxylamine or *N*-alkylhydroxylamines **4-78** (Tables 5 and 6).

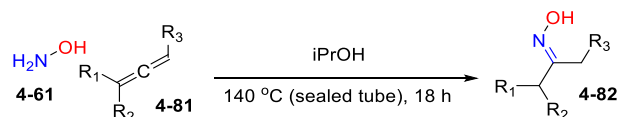
Table 13: Reaction of *N*-alkylhydroxylamines with cyclohexylallene.



Entry	R	Temp (°C)	Yield (%)
1	Cy	140	91
2	Bn	140	81
3	<i>i</i> -Pr	140	63
4	<i>sec</i> -Bu	140	49
5	CH ₂ C(CH ₃) ₃	140	47
6	<i>n</i> -C ₆ H ₁₃	140	51
7	cyclopentane	140	58
8	cycloheptane	140	71
9	norbornane	140	38

^aConditions: 2 equiv. of allene **4-79**, 1 equiv. of RNHOH **4-78**, *tert*-BuOH (0.5 M), sealed tube, 18 h.

Table 14: Reaction of aqueous hydroxylamine with allenes.

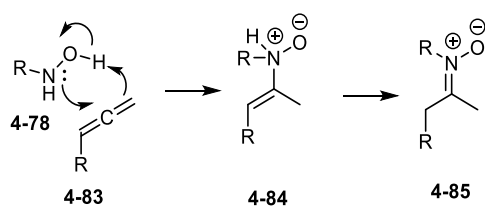


Entry	R	R ₂	R ₃	Yield (%)
1	Cy	H	H	75

2	<i>n</i> -C ₆ H ₁₃	H	H	93
3	BnO(CH ₂) ₂	H	H	99
4	TBDPSO(CH ₂) ₃	H	H	88
5	Ph	H	H	71
6	<i>n</i> -C ₆ H ₁₃	<i>n</i> -Pr	H	21 ^c
7	<i>n</i> -Pr	H	<i>n</i> -Pr	13

^aConditions: 1 equiv. of allene (2.5 M), 2 equiv. of NH₂OH, *i*-PrOH, sealed tube, 140 °C 18 h. ^c Heated in a microwave reactor at 160 °C.

A concerted five membered transition state has been proposed by the authors for this transformation^[52] (Scheme 11). The mechanism is also supported by the studies by Ciganek^[45,46] and Oppolzer^[48] on intramolecular group transfer hydroaminations with alkenes. The author also reported DFT calculations which confirmed a five-membered coplanar transition state for the concerted hydroamination process showing how the amination on the central carbon of the allene is favoured by 5.7 kcal/mol (Figure 4).



Scheme 11: Concerted five membered group transfer mechanism.

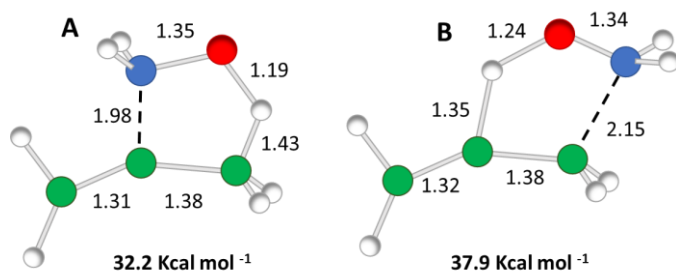
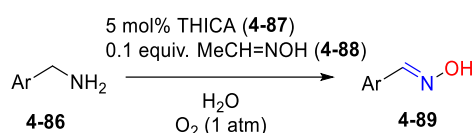


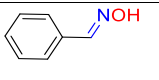
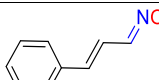
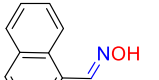
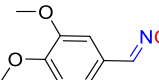
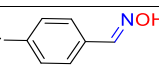
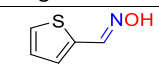
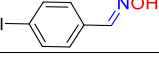
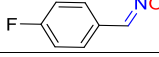
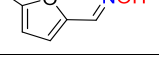
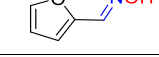
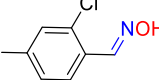
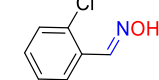
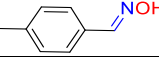
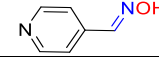
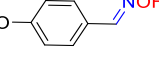
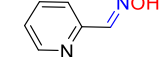
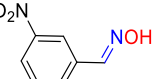
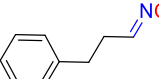
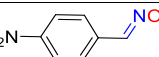
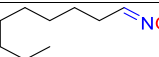
Figure 23: Energies for the two possible five-membered coplanar transition states.

In an alternative approach to oximes Jatao and Ming reported upon the aerobic oxidation of a series of primary amines generating oximes in good yields using *N,N',N''*-trihydroxyisocyanuric acid (THICA) and acetaldoxime as the catalyst (Table 7).^[53] The reaction

is metal-free and uses water as the reaction solvent. In combination with air as the oxidant the overall reaction conditions make it a green and efficient methodology for forming oximes.

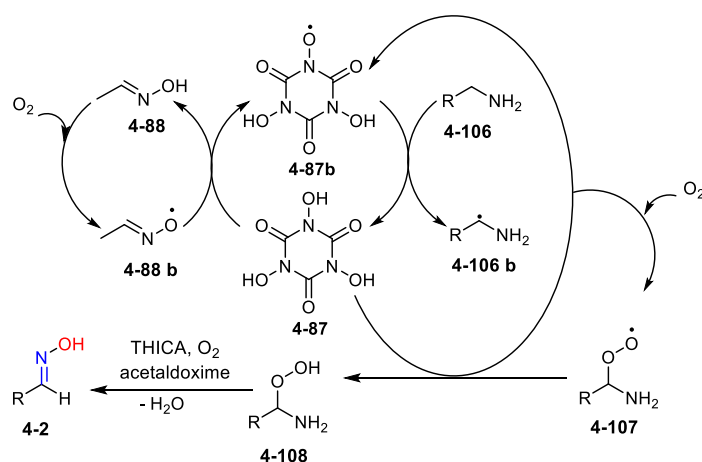
Table 15: Jatoo and Ming oximes synthesis from primary amines.



No.	Oxime Product	Time (h)	Yield (%)	No.	Oxime Product	Time (h)	Yield (%)
4-31		36	88	4-45		40	76
4-90		38	87	4-98		34	80
4-91		36	86	4-99		40	75
4-92		36	85	4-100		36	79
4-93		40	81	4-101		40	79
4-94		36	83	4-102		36	81
4-95		35	85	4-103		42	82
4-96		34	88	4-104		42	78
4-97		40	87	4-36		40	76
4-42		40	90	4-105		24	trace

Using benzylamine as a model substrate for the optimisation of the reaction conditions the authors found that THICA (*N,N,N'*-trihydroxycyanuric acid) and acetaldoxime gave the best results compared to the other catalysts screened (TEMPO and *N*-hydroxyphthalimide) and additives tested (acetoxime, dimethylglyoxime, cyclohexanone). Interestingly, amongst the various solvents screened (DMSO, DMF, EtOH, MeCN and H₂O) only water permitted the

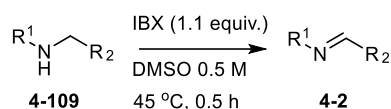
formation of the product. The authors speculated (Scheme 12) the reaction progressed with the activation of THICA (**4-87**; Scheme 12) by the NOxyl radical **4-88b** formed by a reaction between acetaldoxime **3-88** and oxygen. After radical abstraction from the primary amine **4-106** which can then react with oxygen leading to the peroxide radical **4-107**, subsequent reaction with THICA affords the hydroperoxide **4-108** and completes the catalytic cycle. The reactive peroxide species then undergoes elimination producing the oxime **4-2** (Scheme 12).



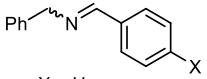
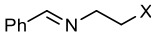
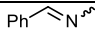
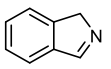
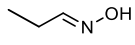
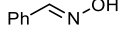
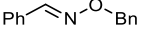
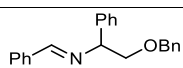
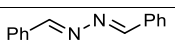
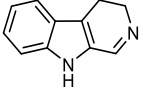
Scheme 12: A possible reaction mechanism for the aerobic oxidation of the primary amine using the THICA/acetaldoxime system.

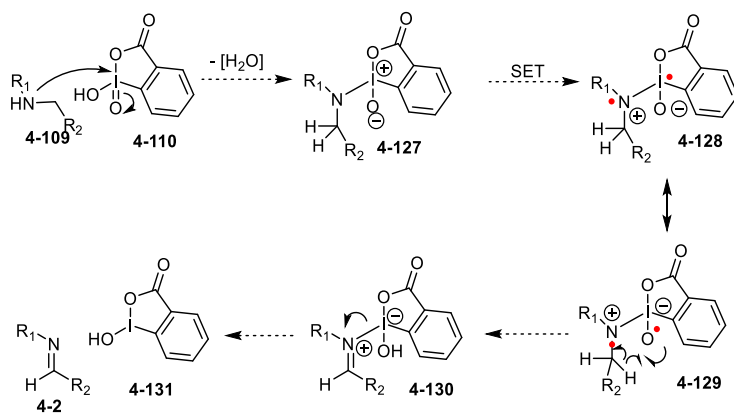
Nicolaou *et al.*^[54] studying hypervalent iodine chemistry reported that *o*-iodoxybenzoic acid (IBX) allows the oxidation of unhindered amine containing compounds to their corresponding imine and oxime counterparts. Example **4-31** and **4-124** show how starting from hydroxylamine the related oxime is obtained in great yield (Table 8). The authors proposed an anionic mechanism for the transformation (Scheme 13).

Table 16: Imine and oxime synthesis from amines with *o*-iodoxybenzoic acid.



No.	Product	Yield (%)	No.	Product	Yield (%)

4-112 4-113 4-114	 X = H X = Br X = OMe	83 91 95	4-120 4-121 4-122 4-123	 X = OH X = OBn X = NMe ₂ X = CN	79 89 77 89
4-116 4-117	 	70 3-116:3-117 = 0.8:1	4-124		90
4-31		97	4-125		98
4-118		49	4-126		94
4-119		98			



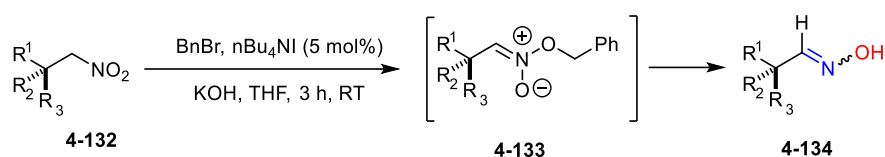
SET = (single electron transfer)

Scheme 13: Proposed SET mechanism for the oxidation of imines mediated by IBX.

Czekelius and Carreira reported^[55] the conversion of optically active nitroalkanes (**4-132**, [Table 9](#)) into chiral aldoximes **4-134** at room temperature by employing inexpensive reagents like benzyl bromide, KOH, and *n*-Bu₄NI. The reaction gave good yields ([Table 9](#)). The authors

reported that amine bases soluble in the reaction media did not produce any product, whereas the use of heterogeneous conditions KOH/THF with an added phase transfer catalyst was optimal for promoting the formation of the aldoxime. Moreover, by using chiral-HPLC assays it was demonstrated that that no racemization occurred during the process.

Table 17: Conversion of nitroalkanes into oximes.

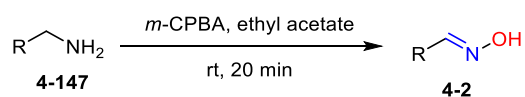


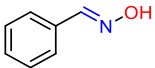
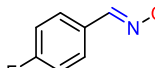
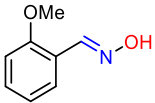
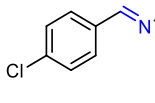
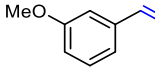
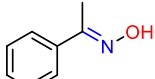
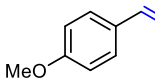
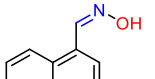
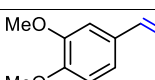
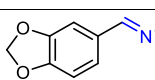
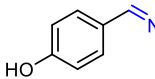
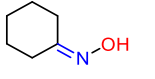
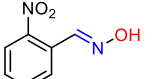
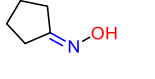
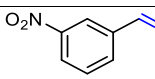
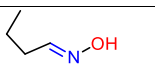
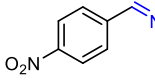
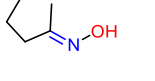
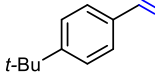
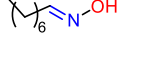
No.	product	Yield (%)	No.	product	Yield (%)
4-135		80	4-141		60
4-136		69	4-142		78
4-137		81	4-143		65
4-138		80	4-144		70
4-139		76	4-145		73
4-140		75	4-146		56

Reaction conditions: BnBr (1.1 equiv.), KOH (1.5 equiv.), *n*Bu₄NI (5 mol%) in THF at room temperature. THP = tetrahydropyran, Bn = benzyl, TBS = *tert*-butyldimethylsilyl.

It has been shown that *m*-CPBA is a good reagent for the conversion of aliphatic and benzylic amines into their related oximes (Table 10). The absence of any metal catalyst, the use of room temperature, the short reaction times required and the availability of the oxidant, along with the good overall yields makes this process a valuable tool for the synthesis of oximes.^[56]

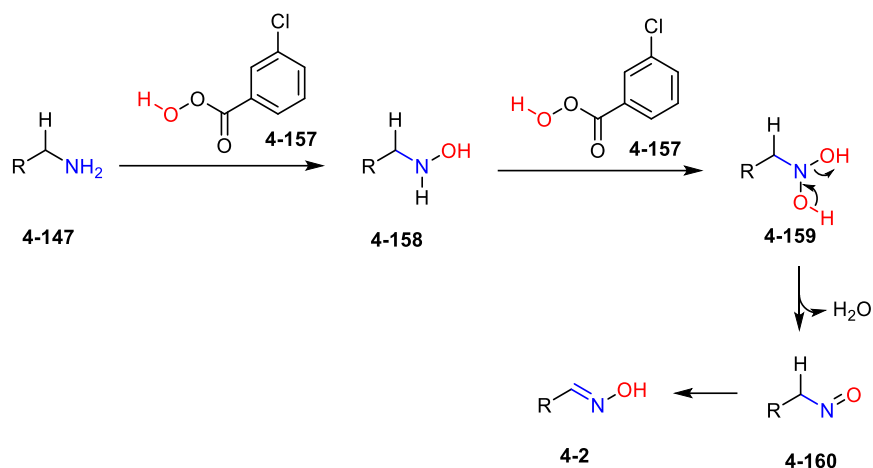
Table 18: Synthesis of oximes from amines with *m*-CPBA.



No.	Product	Yield (%)	No.	Product	Yield (%)
4-31		93	3-100		88
4-118		93	4-92		91
4-148		94	4-36		92
4-44		91	4-90		88
4-149		94	3-152		89
4-96		92	4-7		90
4-150		91	4-153		89
4-97		89	4-154		78
4-42		92	4-155		79
4-151		92	4-156		81

Reaction conditions: 2 equiv. *m*-CPBA, temperature: 30-32 °C, reaction time: 20 min.

The authors proposed a mechanism corroborated by previous studies,^[57,58] this followed a sequence implying formation of hydroxylamine by reaction of *m*-CPBA with the amine which then is oxidised again by a second molecule of the peracid which through tautomerisation leads to the final oxime (Scheme 14).

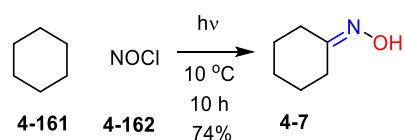


Scheme 25: A plausible reaction mechanism as proposed by Patil and Shankarling^[43].

4.1.3 Photo oximation of cyclohexane

In 1918 E.V Lynn published an article titled 'A new reaction of paraffin hydrocarbons' in this publication was outlined a new for creating an alternative process for the synthesis of ϵ -caprolactam which was normally produced by the reaction between cyclohexanone and hydroxylamine (Scheme 3). The idea was to use the photonitrosation of cyclohexane to directly produce cyclohexanone oxime **4-7** in a single step using light radiation to induce the dissociation of nitrosyl chloride (**4-162**) and functionalise the cyclohexane (**4-161**) with a nitroso group (Scheme 15). The resulting cyclohexanone oxime (**4-7**) would then be subjected to the Beckmann rearrangement to furnish ϵ -caprolactam (Scheme 2, **4-7b**).^[60,61] The main functionalization of cyclohexane (**4-161**) was carried out in a single step and the amount of ammonium sulfate produced (obtained by the reaction between cyclohexanone and hydroxylamine sulfate) was reduced by 50% compared to the traditional method and on top of that the source of nitrogen used (nitrosyl chloride, **4-162**) was considerably cheaper than hydroxylamine. The commercialization of the process started in 1963 with a production of 25

million imperial pound reaching 110 million imperial pounds after 6 years of production at the Nagoya plant^[64] (Scheme 15).



Scheme 15: The reaction of cyclohexane and nitrosyl chloride in the Toray process.

The first Nagoya commercial plant used 10 kw·h⁻¹ capacity high pressure mercury lamps which were subsequently upgraded to customised 20 kw·h⁻¹ lamps developed specifically by Toray industries^[62] in order to reduce the power consumption to 2.5 kw·h⁻¹·kg⁻¹ of oxime produced.^[64] The photoreactor used was based upon direct immersion of the light source in the reaction solution with the thermal energy being removed by a coupled water-cooling system. As the reagents and products of the process are highly corrosive (nitrosyl chloride (**4-162**), HCl, oxime hydrochloride (**4-26**)) the choice of construction material for the reactor was vital. Eventually titanium was used, although it is not directly resistant to nitrosyl chloride (**4-162**) it provided resistance to corrosion if the system is used under optimum conditions (10 °C, 10 h reaction time, 1 equivalent hydrochloric acid per equivalent of nitrosyl chloride (**4-162**)).^[64]

In 1955 the Research Department of Toyo Rayon Company published an article called “Photonitrosation of Cycloalkanes with Nitrosyl Chloride. Synthesis of Cyclohexanone Oxime”^[65] where the process for the photonitrosation of cycloalkanes and the reactor used was described (Figure 5). The cyclohexane (**4-161**) is charged to the reactor with vigorous stirring (Figure 5, item 8) where the mercury lamp provided the necessary irradiation. Nitrosyl chloride (**4-162**) and hydrochloric acid were pumped continuously into the cyclohexane solution (Figure 5, item 11). The oily product was removed from the lower part of the vessel as it was produced (Figure 5, item 2) whereas the less dense cyclohexane (**4-161**) was constantly added at the top of the reactor (Figure 5). The excess gases were conveyed in a series of 3 scrubbing vessel (Figure 5, items 3-5) containing sulfuric acid, sodium hydroxide and liquid paraffin. This allowed conversion of the nitrosyl chloride (**4-162**) into nitrosyl sulfuric acid whereas the hydrogen chloride was quenched by the sodium hydroxide and the cyclohexane captured by the paraffin.^[65]

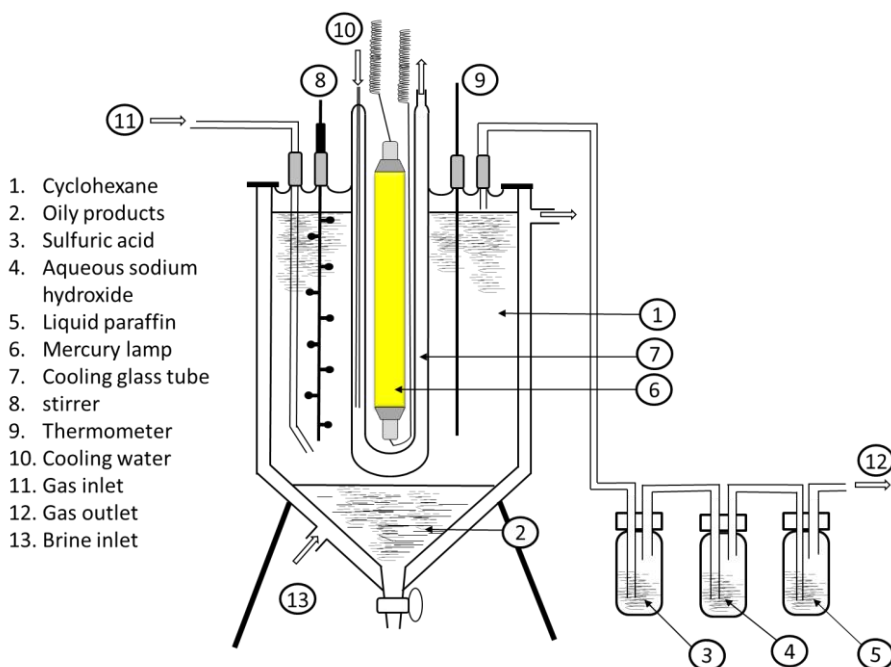
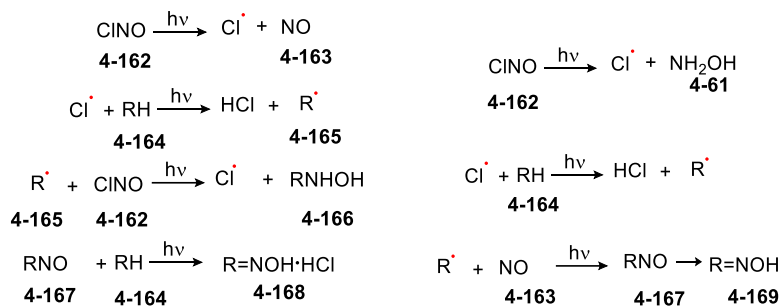


Figure 24: Schematization of the reactor set-up as used by the Toyo Rayon Company for the nitrosation of cyclohexane.



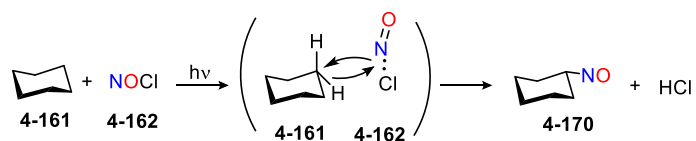
Scheme 16: Chain (left) and Non-chain (right) radical process proposed mechanisms.

Both chain (Scheme 16; left insert) and non-chain (Scheme 16; right insert) radical processes have previously been proposed to account for the reaction process.^[63] Mosher and Bunce^[63] described the study of the thermal reaction using radical initiators like benzoyl peroxide, AIBN (azobisisobutyronitrile) and PAT (phenylazotriphenylmethane) reporting the absence of

significant formation of the cyclohexanone oxime (**4-7**). They also reported an average value for the “chain length” which never exceeded unity for the formation of the product. This data, considering the values found by Muller^[70] and Mosher^[63] for the oxime formation of between 0.6 and 1.5 does not support a chain process (Scheme 16; left insert). The chain process had also been excluded by the Toray team who calculated the light quantum yield of 0.7 thus clashing with a chain reaction mechanism.^[64]

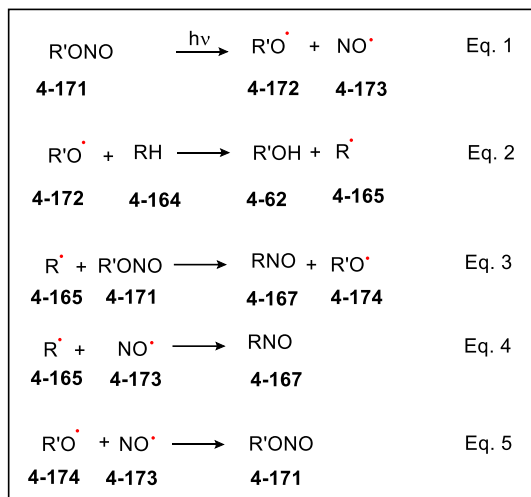
In addition the Toray’s team had extensively studied the mechanism, they claimed that the reaction took place in a cage of cyclohexane (Franck and Rabinowitch cage effect^[67]) and that this was supported by the fact that adding ¹⁵N to the nitrosyl chloride (**4-162**) gas, gave an oxime product which does not contain the ¹⁵N label. Also, in this case a chain reaction was not postulated as the mechanism for the photonitrosation because of the light quantum yield they reported which was 0.7.

Muller questioned the presence of free radicals in the reaction^[67-69] and proposed that the reaction takes place in a solvent cage and postulated a 4-centred mechanism^[70] (Scheme 17).



Scheme 26: Muller’s proposed mechanism for the nitrosation of cyclohexane.

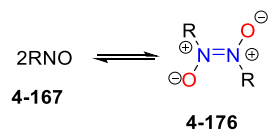
This hypothesis was rejected by Mackor and Boer who demonstrated the presence of radicals in the reaction by ESR experiments^[71,72] and proposed what is now the generally accepted mechanism^[73] (Scheme 18).



Scheme 27: Makor and Boer's mechanism.

The reaction starts with the photolysis of the alkyl nitrite **4-171** (Eq. 1) followed by proton abstraction from the alkane **4-164** (Eq. 2) leading to a second radical **4-165** which can recombine with the radical nitrosyl **4-173** affording the nitrosylated product **4-167** (Eq. 4). Equation 3 is an alternative chain reaction which could occur leading to the same product as Equation 4, **4-167**. Gray and Rathbone suggested it for methyl radicals studying the decomposition of diacetyl peroxide in *tert*-butyl nitrite.^[72] Nonetheless, separate experiments conducted by Makor^[73,74] found it mostly speculative and it is generally accepted that the main pathway for the formation of the nitrosylated product **4-167** involves Equation 4.^[75,76] The last step (Eq. 5) describes a possible recombination leading back to the formation of the starting material **4-171**.

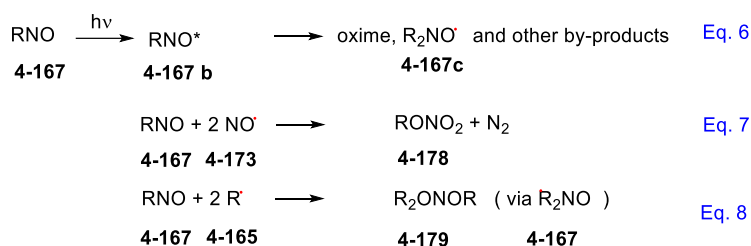
Makor reported that using cyclohexane (**4-161**) as both reagent and solvent led to the dimerization of nitrosocyclohexane^[73,74] (Scheme 19).



Scheme 28: Dimerization of the nitrosated product.

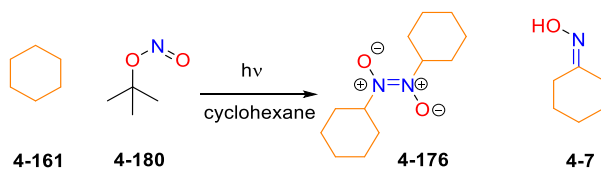
Metzger and Muller reported that the dimer can be converted into the oxime by the action of hydrochloric acid and various catalysts (*m*-CPBA^[77] or Et₃N^[78]), or upon exposure to unfiltered UV light.

Makor in his studies on the nitrosation of alkanes using several nitrites sources^[88] showed that the dimer **4-176** is less liable to decomposition compared to the monomer **4-6**. Indeed, when the dimerization is slowed down by reducing the temperature or is incomplete this results in an increase in the formation of by-products (Scheme 20). According to Makor and Boer the occurrence of detrimental reactions (leading to products not easily convertible into the desired oxime or dimer) is mainly influenced by temperature, nitrite concentration and incident light, exacting control over the conditions allows the reaction to reach a maximum final yield of 81% (based on consumed nitrite).^[73]



Scheme 29: Detrimental reactions of the involving the monomer described by Makor and Boer.

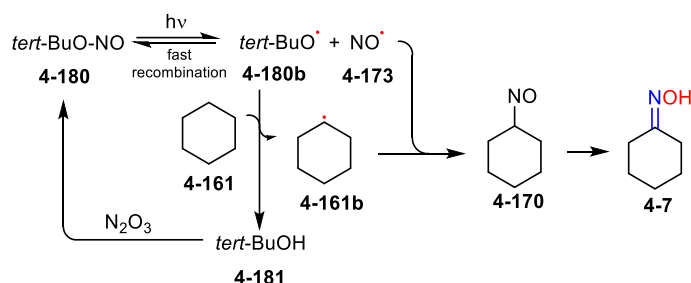
Since the nitrosyl chloride (**4-162**) is very corrosive and produces tarry by-products which deposit on the surface of the lamp and thus affects the light-efficiency. Consequently, several alternative nitrosilating agents have been investigated. In this respect *tert*-butyl nitrite (**4-180**) has received particularly attention and has been used as a model system for studying the reactivity of alkyl nitrites toward hydrocarbon functionalization^[79] (Scheme 21).



Scheme 30: The use of *tert*-butyl nitrite as nitrosating agent.

The main reaction product generated is the *trans* dimer (**4-176**; Scheme 21) with a minor amount of desired cyclohexanone oxime (**4-7**; Scheme 21) in a total yield of 81% (Ratio **4-176**:**4-6** 3:2).^[80]

The proposed mechanism entails the generation of *tert*-BuO and NO radicals (**4-180b** and **4-173**; Scheme 22) by homolytic breaking of the *tert*-BuONO (**4-180**). The *tert*-butoxide radical (**4-180b**) is believed to abstract a hydrogen atom from the cyclohexane (**4-161**) leading to the cyclohexyl radical (**4-161b**) this can then couple with NO (**4-173**) giving the nitrosocyclohexane (**4-170**) that then undergoes tautomerization to afford the cyclohexanone oxime (**4-7**)^[81] (Scheme 22).



Scheme 31: Trapp's proposed mechanism of cyclohexane photo-nitrosation.

The existence of the dimeric species **4-176** generated from the nitroso compound **4-170** has long been known and had been postulated as early as 1875 by Tilden.^[82-84] While nitroso compounds, like **4-170**, form such dimers the tautomeric oximes (**4-7**; Scheme 23) have never been observed to undergo an analogous dimerization^[85] (Scheme 23). In their article of 1996^[85] Glaser, Murmann and Barnes used an *ab initio* study of thermodynamic stabilities of diazene oxides and structural studies of the *trans*-dimer of 2-chloro-2-methyl-3-nitrosobutane (**4-5d**, Figure 6) to investigate this behaviour. They showed that the dimerization of the oxime would be energetically unfavourable therefore explaining why only one (**4-176**) out of the four (**4-182**, **4-183**, **4-184**, **4-176**) possible dimers was experimentally observed (Scheme 23).

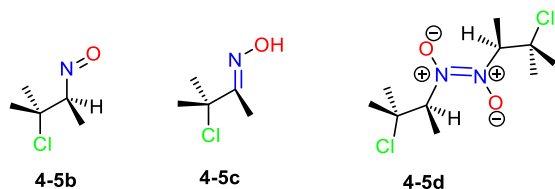
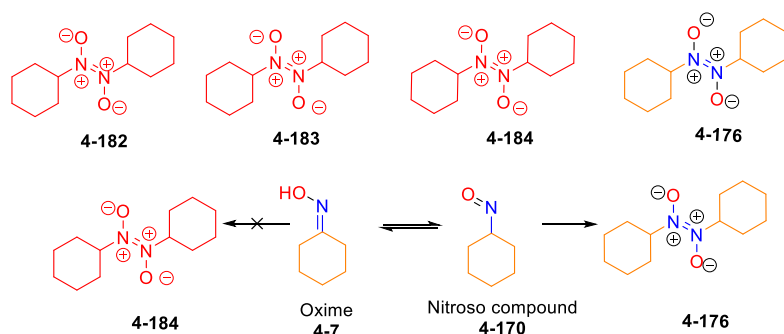


Figure 6: Tautomeric forms of 2-chloro-2-methyl-3-nitrosobutane **4-5b**.



Scheme 32: Dimerization of nitrosocyclohexane **4-170**; compounds in red are not observed

During their study on the photo-oximation of cyclohexane (**4-161**) Trapp's group reported that at 60 °C the nitrosocyclohexane dimer **4-176** was fully converted to cyclohexanone oxime (**4-7**) although a considerable amount of a black precipitate was also produced as a side product.^[81]

The UV spectra (Figure 7) of the species involved in the cyclohexane photo-oximation shows three sets of signals: a large band with maximum at 300 nm (Figure 7A) for the dimer azodioxycyclohexane **4-176** and a much smaller peak at 700 nm (Figure 7C) for the monomer nitrosocyclohexane (**4-170**). The nitrosating agents, the *tert*-butyl nitrite (**4-180**) gives two distinct peaks: one band with a large absorption between 200 and 320 nm (Figure 7B₂) and a much more complex and weaker one with multiple maxima between 320 and 430 nm (Figure 7B₁). The latter is related to the $S_0 \rightarrow S_1$ (n, π^*) absorption involving the promotion of an electron from the highest occupied non-bonding molecular orbital to an anti-bonding π^* molecular orbital.^[86]

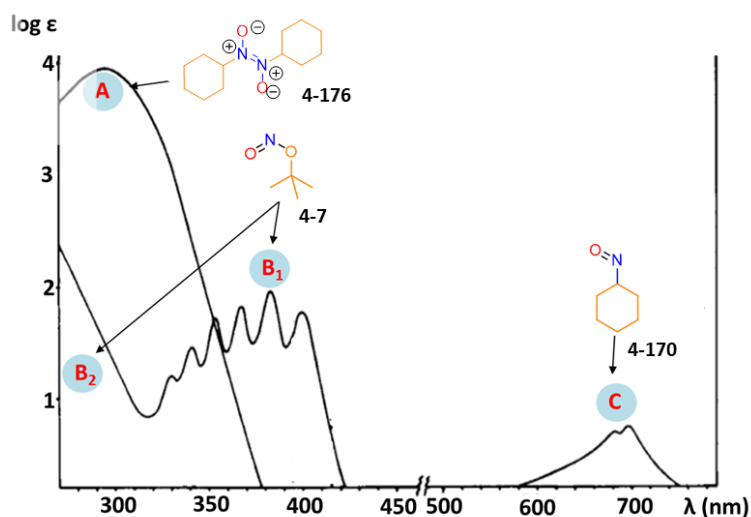
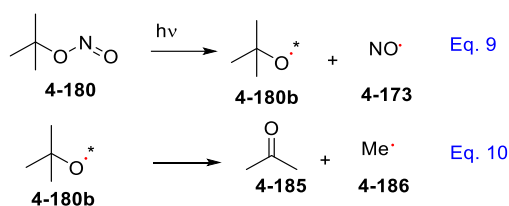


Figure 7: UV absorption spectra in cyclohexane (**4-161**) of A = dimer **4-176**; B₁ and B₂ tert-butyl nitrite (**4-180**); C = monomeric nitrosocyclohexane (**4-170**).^[88]

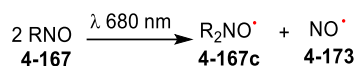
Previous studies on the photolysis of alkyl nitrites have shown that an irradiation wavelength matching with the largest of the two bands of the nitrite **4-180** (Figure 7, part B₂) induces its decomposition into nitric oxide (**4-173**), acetone (**4-185**) and a methyl radical (**4-186**). McMillan,^[87] in particular, has demonstrated that wavelengths below 366 nm lead to the dissociation of *tert*-BuONO (**4-180**) into a NO radical (**4-173**) and *tert*-BuO radical (**4-180b**) which then fragment again into acetone (**4-185**) and methyl radical **4-186** (Scheme 24).



Scheme 33: Photochemical induced *tert*-butyl nitrite (**4-180**) decomposition.

According to Makor^[73,74] lowering the wavelength applied increases the mole fraction of *tert*-BuO radical (**4-180b**) which form through dissociation, in addition he finds that low

wavelengths can also dissociate the dimer (**4-176**) and then destroy the monomeric nitrosocyclohexane (**4-170**). On the other hand, light with a wavelength matching the weaker of the nitrite's (**4-180**) absorption peaks (Figure 7, Part B₁) induce the dissociation of the nitrite with a minimum amount of by-products although this band is partially overlapping with the absorption of the dimer **4-176** (Figure 7, part A). According to Makor this sets the lower limit for the radiation suitable in the photochemical nitrosation whereas the upper limit is given by the absorption peak of the nitrosocyclohexane (**4-170**; Figure 7, part C) around 690 nm related to its $n \rightarrow \pi^*$ transition. He reported that the product of an irradiation matching with this upper limit was the unstable dicyclohexyl nitroxide^[73] which he proved by ESR spectroscopy.^[74]



*Scheme 34: Detrimental reaction leading to the photolysis of the nitrosocyclohexane monomer **4-167**.*

The choice of the light source is therefore important and made considering not just the starting nitrite **4-180** but also the two products of the reaction: the nitroso monomer (**4-170**) and the dimer (**4-176**). The region between 360-400 (Figure 7) allows the reaction to be irradiated selectively targeting the nitrite (**4-180**) without any activation of the *trans* dimer (**4-176**) of the nitrosocyclohexane (**4-170**, Figure 7, part A) or the $n \rightarrow \pi^*$ band of the monomeric nitrosocyclohexane (**4-170**; Figure 7, part C). An irradiation in this region would thus also result in a dissociation of the monomer.^[88]

One of the limitations of this type of photo-oximation is represented by the by-products obtained: the use of a mercury lamp has a relatively low efficiency in the desired absorption region and provides radiation at a lower wavelength thus generating large amounts of tarry light-absorbing by products on the glass wall of the reactor thus lowering the transmittance and reducing the selectivity.

Good results have been obtained using LED light sources using both alkyl nitrites and NOCl (**4-162**).^[89-93] Wysocky has demonstrated that using a LED set-up emitting at 365 nm the reaction proceeds in good yield leading to oxime **4-7** (for rearrangement of the nitroso) in 80% yield.^[81]

In 2019, Lebl reported the continuous version of the PNC process^[94] claiming a 66% yield for the photochemical step and showing how this transformation can benefit from a continuous process in terms of scaling-up, sustainability, reaction time and safety (Figure 8).

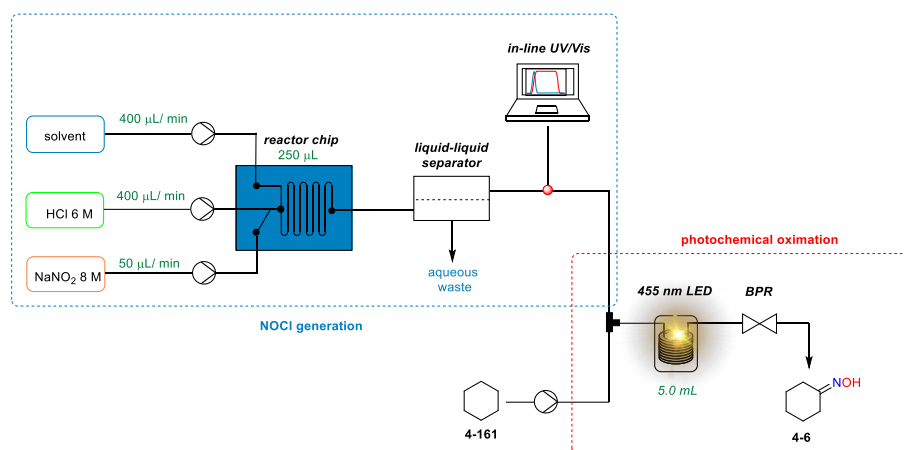


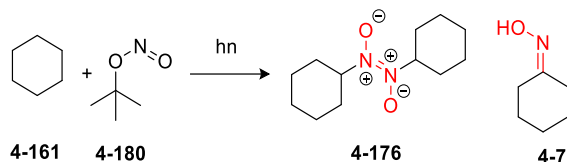
Figure 8: Lebl's continuous set-up for the generation of NOCl, purification and subsequent use in the photo-oxidation of cyclohexane.

The process can be broken down in 2 steps (Figure 8): the first being the NOCl (**4-162**) generation and second the photochemical oxidation of cyclohexane (**4-161**).

The generation of NOCl (**4-162**) is performed by direct reaction of NaNO₂ (8 M) and 6 equiv of HCl (6 M).^[95] The two reagents are mixed with a third stream of DCM as a biphasic solvent in a 250 μL chip reactor where the NOCl (**4-162**) is formed. The reagent is more soluble in the DCM and is thus extracted and separated using a continuous liquid-liquid separator from Zaiput Flow Technologies equipped with a 0.5 μm pore size PTFE membrane. The NOCl generator outlet is mixed with a stream of cyclohexane (**4-161**) using a PEEK Y-mixer at -10 °C. The merged solutions are further pumped into a Corning® Advanced-Flow Photo Reactor™ made of a 2.77 mL glass plate jacketed by heat transfer fluid and irradiated simultaneously by LED panels (λ_{max} = 395 nm) from both faces.

4.2 Results and discussion

We embarked upon the synthesis of a series of oximes using a flow approach in order to evaluate whether this methodology could further improve the results obtained in the reaction of *tert*-butyl nitrite (**4-180**) and enhance the synthetic potential of the transformation (Scheme 26).



Scheme 35: Photo-oximation of cyclohexane 4-161.

For this study we used a Vapourtec E-series 500 pumping system in combination with a UV-150 photochemical reactor unit. The photoreactor was equipped with a medium pressure mercury lamp (power adjustable from 75 to 150 W) and a 365 nm LED array lamp (total 9 W). The flow reactor consisted of a 10 mL FEP coiled tube, and the reaction temperature could be monitored using a temperature probe with an external cooling system allowing moderation (Figure 9).

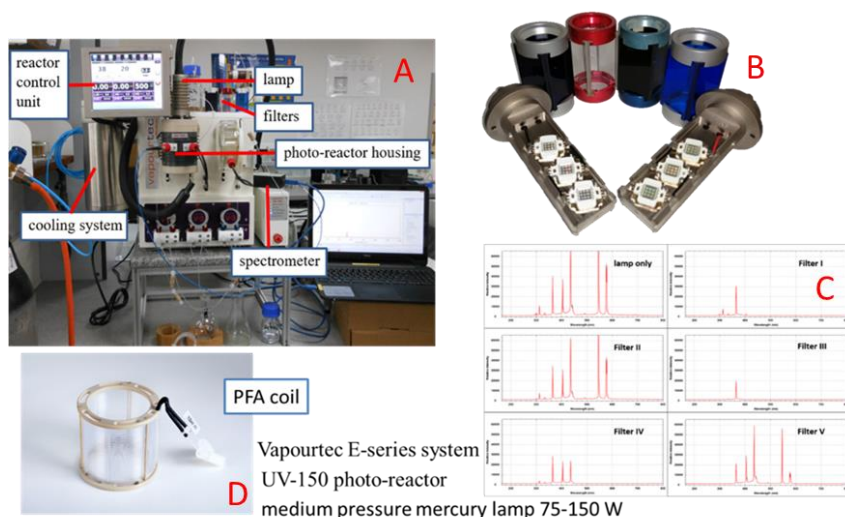


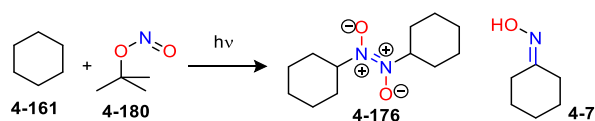
Figure 9: Flow setup used for this study: A) Vapourtec E-series system; B) UV filters and LED lamps; C) emission spectra of the medium pressure mercury lamp alone and with filters; D) 10 mL PFA coil reactor used for the transformation.

The choice of the light source for the process was influenced by the absorption spectra of the species involved in the transformation (see also above discussion). The absorption band responsible for the homolytic breaking of the *tert*-BuONO (4-180) lies between 320 and 430

nm (Figure 7, part B₁) but is partially overlapped by the absorption band of the nitroso-cyclohexane dimer **4-176** which has its maximum at 300 nm but extends to 360 nm (Figure 7, part A). Wysocki^[81] has shown that efficient activation is achieved using an emission between 365 and 405 nm therefore a 365 nm LED array lamp was also investigated. However, this low power LED array does introduce some limitation regarding luminosity and hence photon flux which can potentially lead to the necessity for extended reaction times.

To establish a flow process, we took cyclohexane (**4-161**) as a reference substrate and screened several molar ratios of reagents and flow rates in order to find optimum conditions for the oxamidation process. It was determined that a ratio of 45:1 cyclohexane (**4-161**): nitrite (**4-180**) using a flow rate of 1 mL/min provided the highest conversion (Table 11, Figure 10). The reaction gave mainly the dimer product **4-176** in accordance with previously literature reported batch results.^[81]

Table 19: Optimization of the molar ration between **4-161** and **4-180** with a flow rate of 1 mL/min; conversion based on *tert*-BuONO against an added internal standard.



Molar ratio of 4-161:4-180	%Conv. to 4-176	%Conv. to 4-7	Total %Conv. By ¹ H-NMR
10:1	32	3	35
20:1	49	8	57
30:1	51	8	59
40:1	56	9	65
45:1	55	13	68
50:1	55	9	64
60:1	57	7	64
70:1	56	8	64
80:1	55	8	63
90:1	56	8	64
100:1	54	10	64

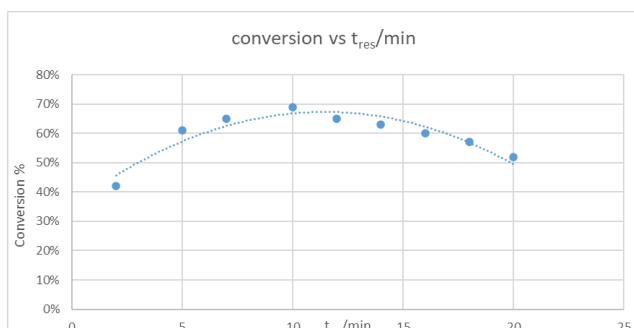
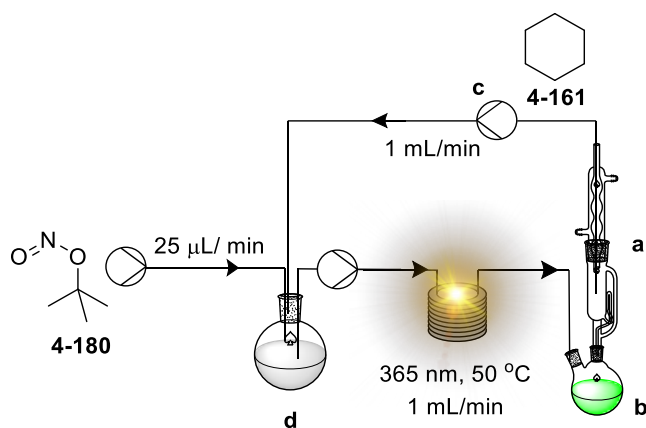


Figure 10: Residence time optimization, 10 mL FEP coil reactor using 45:1 ratio of **4-161**:**4-180**.

We also explored the need for active cooling of the photoreactor during the processing of the reaction, it was observed that higher ratios of the monomer **4-7** (4:1) were obtained directly if the temperature was allowed to stabilise around 50 °C (the non-regulated working temperature of the system). In this context it was observed that when dimer **4-176** was heated it readily interconverted to the corresponding oxime monomer **4-7**. Compound **4-176** was therefore heated neat at 100 °C for 30 min achieving quantitative conversion to the monomer form **4-7**. This is in accordance with previous observations of Burrell^[76] who calculated the dissociation constants at different temperatures.

Although it is a trivial operation to batch collect the reactor output, remove the low boiling point cyclohexane (**4-161**) leaving the products **4-176** and **4-7**, and then in a second step to heat the residue to convert it to the desired product **4-7**, we wished to establish the principles of a more continuous operation. To create a viable set-up, we also had to consider some further aspects of the reaction. During our work we had found that prolong heating of the neat oxime **3-7** led to its slow but progressive decomposition. This was though suppressed if a solvent such as cyclohexane was present. However, the low solvent reflux temperature resulted in the need for longer heating time to affect the full conversion of the compound (**4-176**→**4-7**).

Therefore, to avoid any issues with needing to regulate the rate of a continuous distillation (not drying out of the product sample) but allowing constant heating (achieving full conversion of **4-176**→**4-7**) we adopted a mixed flow and continuous distillation set-up (Scheme 27).



Scheme 36: Continuous flow recycling process for cyclohexane **4-161**.

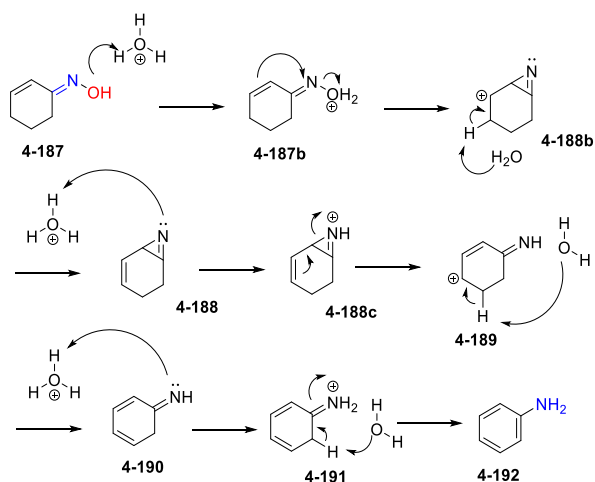
A Soxhlet extraction apparatus (Scheme 27, part a) functioned to heat the product solution (Scheme 27, part b), converting the dimer **4-176** to the oxime **4-7** *in-situ* and acting to maintain an essentially constant liquid level (Scheme 27, part a/b). In this way the unreacted cyclohexane (**4-161**) was continuously distilled and could be pumped from the top of the Soxhlet collection chamber (Scheme 27, part a, containing pure cyclohexane (**4-161**)) to a stock flask (Scheme 27, part d) where it was continuously refreshed with additional *tert*-butyl nitrite (**4-180**) at a flow rate commensurate to maintain the 45:1 reagent ratio. The stock solution (Scheme 27, part d) was itself pumped through the photoreactor with an optimised residence time of 10 min and a theoretical throughput of 1.24 g/h (*tert*-BuONO (**4-180**) processed in 1 h).

The calibrated conversion for the process was established at 54% (^1H NMR yield v's the internal standard 4-(dimethylamino)benzotrile) with the isolated yield of pure **4-7** following a batch recrystallization from 2 g of material being 36%. The system was able to be run in continuous mode for 15 h and thus generated 11.04 g (59% isolated) of the product **4-7** demonstrating the scalability and improved productivity of the process.

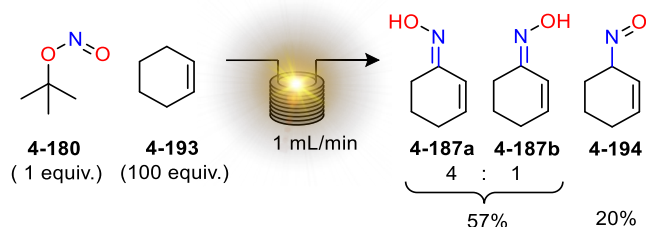
The results obtained show that the process gives good results in terms of conversion of the cyclohexane (**4-161**), the ^1H -NMR yields show that the sum of oxime **4-7** and its dimer **4-176** is comparable to that found for corresponding literature for the batch process.^[81] The slight reduction in yield for the short run, 39%, could be the result of a shorter heating time

needed for the conversion of the dimer **4-176** into the oxime **47**. Indeed, Wysocki^[81] had reported that after 180 min the conversion reached almost the max conversion considering the sum of dimer **4-176** and oxime **4-7** whereas it took additional 13 h to convert the dimeric product fully into the hydroxylamine product. Thus, this probably suggests that the conversion of the dimer **4-176** into the product **4-7** is more efficient under photolytic condition rather than thermal, hence requiring longer time. This also explains why the longer reaction run gave far greater material recovery 59% vs 39%.

Having determined the feasibility of the process for cyclohexane (**4-161**) we next explored the scope of the transformation in terms of other viable substrates. First, we tested the effect of adding unsaturation to the system, namely testing cyclohexene (**4-193**; Scheme 28), as the product would offer value as an aniline precursor via the Semmler–Wolff reaction (Scheme 28).^[96] In addition, the alkene should make cyclohexene (**4-193**) a better substrate by assisting the proton abstraction step due to the lower bond dissociation energy of the allylic hydrogen compared with the purely unsaturated hydrocarbon system (85 vs 96 kcal mol⁻¹).^[98,99]

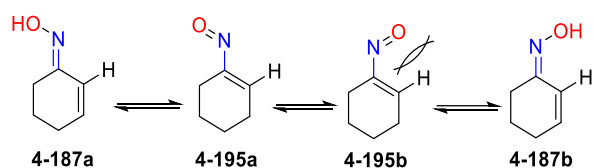


Scheme 37: Semmler-Wolff transformation of cyclohexene oxime to aniline.



Scheme 38: Photo-promoted oximation of cyclohexene (**4-193**).

The reaction produced predominantly the *anti*-diastereomer **4-187a** (Scheme 29). The two diastereomers **4-187a/4-187b** were found to exist in equilibrium, this was proven by the partial conversion of a pure sample of the major diastereomer **4-187a** to a 4:1 mixture of **4-187a:4-187b** after leaving the sample of diastereomer **4-187b** incubated for 24 h in CDCl_3 solvent (determined by ^1H NMR). The preference for the *anti*-diastereomer could be rationalised by the 1,4-interaction between the hydroxyl group and the vinylic proton in **4-187a** (Scheme 30).^[100]



Scheme 30: Equilibrium between diastereomer **4-187a** and **4-187b**.

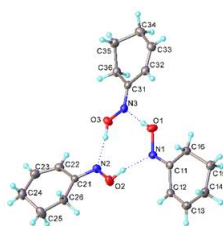
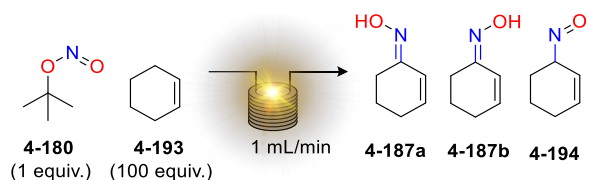


Figure 25: X-ray single crystal structure of compound **4-187a**.

Even in this case an additional rapid screening of the reagent ratio was performed finding that a large excess of cyclohexene (**4-193**) was still needed for efficient reaction.

Table 20: Optimization of cyclohexene (**4-193**) nitrosation.



Molar ratio of reagent	T/°C	Flow rate mL/min	T _{Res} min	¹ H-NMR Conv. (4-187a + 4-187b)	NMR conv. to 4-194	Total NMR conv.
100:1	50	1.0	10	57%	20%	77%
50:1	50	1.0	10	56%	18%	74%
50:1	50	1.0	10	58%	4%	62%
50:1	50	0.5	20	53%	0%	53%
50:1	50	5.0	2	17%	32%	49%
50:1	50	10.0	1	19%	23%	42%

Again, the previously established Soxhlet apparatus was used with cyclohexene as the reaction substrate allowing the product to be isolated in 70% yield (mixture of **4-187a** : **4-187b** = 3.8:1). Given the encouraging results obtained with cyclohexene (**4-193**), we next looked to expand the scope further with additional substrates (Figure 12 and Table 13).

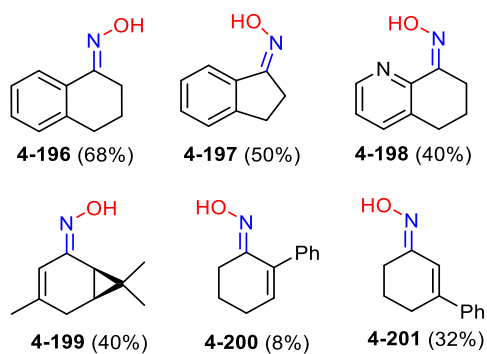


Figure 26: Expansion of substrate scope.

Table 21: Results and conditions for the photo-oxidation.

Entry	Ratio ^a	Reactor T/ °C	Flow rate (mL/min) ^b	Isolated yield
4-196	10:40:1	50	1.00	54%
4-196	20:20:1	50	1.00	68%
4-197	20:20:1	50	1.00	50%
4-198	20:20:1	50	1.00	37%
4-199	20:0:1	50	0.50	40%
4-200	20:20:1	50	1.00	8%
4-201	20:20:1	50	1.00	32%

^a Ratio indicated is precursor: *tert*-BuOH: *tert*-BuONO
^b Reactor V = 10 mL

The new substrates selected were all non-volatile therefore the removal of unreacted starting material was no longer achievable by simple evaporation and required either chromatographic separation or crystallisation. Compound **4-196** (Figure 12 and 13) was obtained starting from tetraline, the diastereoselectivity of the reaction can be explained by the preference for a conformation involving the interaction between the hydroxy group and the α -protons rather than α -*peri*-interaction with the aromatic proton (Figure 13).

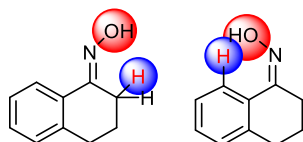


Figure 27: Possible diastereoisomers of compound 4-196.

The regioselectivity displays a strong preference for the abstraction of the benzylic proton again arising from the lower associated BDE energy (83 kcal mol⁻¹ benzylic vs 96 kcal mol⁻¹ alkyl^[101]).

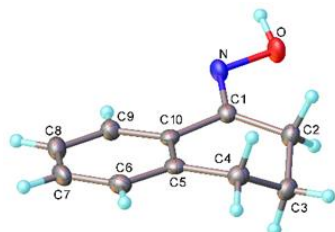


Figure 28: X-ray structure of compound **4-196**.

Compound **4-197** (Figure 15) was obtained starting from indanone, similarly to **4-196**, it was obtained as single regio- and diastereoisomer presumably due to the same kinetic and thermodynamic assumptions.

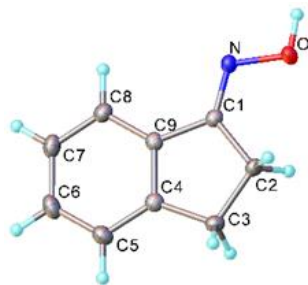


Figure 29: X-ray structure of compound **4-197**.

In order to test the reaction on a heterocyclic core, a tetrahydroquinoline system was processed under the standardised reaction conditions. Among the two possible benzylic products (Figure 16) regioisomer **4-198a** potentially can be stabilised by a hydrogen bond between the hydroxyl proton and the pyridine nitrogen and was thus considered to be the most likely product. Although there is no literature NMR available for compound **4-198a** the measured melting point for the product obtained under our conditions (190-192 °C) equates best to that reported in literature, 173-175 °C and 180-182 °C for compound **4-198a** whereas it seems to be quite different from what is reported in the literature for **4-198b** (235-236 °C and 240 °C).^[102-104]

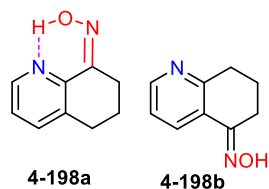


Figure 30: Possible isomers of compound 4-198.

In addition, compound **4-199** was obtained from (1*R*,6*S*)-3-carene (Figure 17). Even in this example a remarkable regio- and stereoselectivity was observed. This can be accounted for by the difference in steric hindrance between the allylic positions on the cyclohexene ring caused by the presence of the proximal methyl group (Figure 17). Interestingly, no oximation was observed on the methyl arguably because the primary radical first obtained is less stable if compare with the secondary one which arise from the abstraction on the allylic position. In addition the alignment of the C-H bond in the methyl group would require the adoption of a high energy eclipsing conformation to allow hyperconjugation and stabilisation of the developing radical, which would be restricting compared to the alternatives.

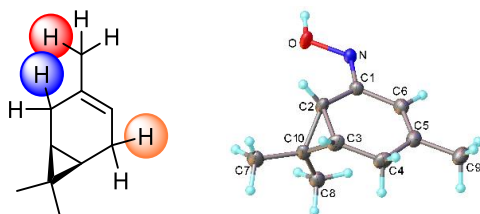


Figure 31: (1*R*, 6*S*)-3-carene and X-ray structure of compound 4-199.

Finally, regioisomeric compounds **4-200** and **4-201** were obtained starting from 1-phenylcyclohexene. The ratio 1:4 (**4-200**:**4-201**) can again be rationalised by considering the preference of the H-abstraction step, favouring the less hindered allylic proton (Figure 18).

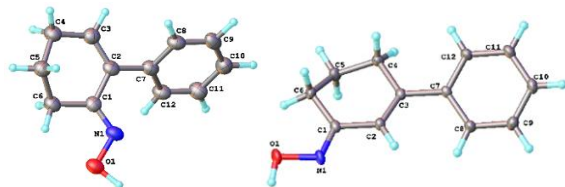
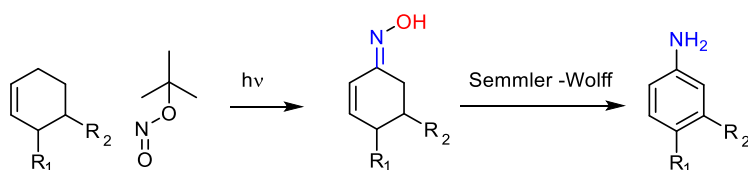


Figure 32: X-ray structures of compounds **4-200** and **4-201**.

4.3 Conclusion

In conclusion, we have reported the photoflow oximation of several alkanes and alkenes using *tert*-butyl nitrite. The flow process allows a considerably reduction in the reaction time (from hours^[81] to minutes) and the easy scale-up of the transformation. A continuous process was also investigated in order to gauge the possibility of recycling the unreacted starting material (cyclohexane). The major product remains the dimer *trans*-azodioxy cyclohexane **4-176**. Although the conversion of the dimer to the oxime can be performed thermally the high level of decomposition prevent this from being an efficient strategy and therefore more effort has still to be put into finding an alternative strategy.

In addition several substrates were subjected to the reaction condition to show the synthetic value of the transformation. The starting materials screened show that the method is applicable to a broad range of substrates thus it would be interesting to couple this method with the Semmler-Wolf reaction^[96,97] in order to access substituted anilines (Scheme 31). Indeed, if this can be successfully proven this strategy may provide an interesting and straightforward route to highly substituted anilines otherwise difficult to access due to the conflicting directing groups.



Scheme 39. Synthesis of substituted anilines by photo-oximation of cyclohexene derivatives followed by Semmler Wolff reaction.

4.4 References

- 1) Meyer, V.; Janny, A. U. *Ber. Dtsch. Chem. Ges.*, **1882**, *15*, 1164–1167.
- 2) Donohue, J. J. *Am. Chem. Soc.*, **1956**, *78*, 4172–4172
- 3) Blatt, A. H. *J. Org. Chem.*, **1938**, *3*, 91–98.
- 4) Bohle, D. S.; Chua, Z.; Perepichka, I.; Rosadiuk, K. *Chem. Eur. J.*, **2013**, *19*, 4223–4229.
- 5) Vijfhuizen, P.C.; Terlouw, J. K. *Org. Mass Spectrom.*, **1977**, *12*, 63–64.
- 6) Belmar, J.; Quezada, J.; Jiménez, C.A.; Díaz-Gallifa, P.; Pasán, J.; Ruiz-Pérez, C. *New J. Chem.* **2013**, *37*, 2002–2010.
- 7) Noguchi, M.; Okada, H.; Tanaka, M.; Matsumoto, S.; Kakehi, A.; Yamamoto, H. *Bull. Chem. Soc. Jpn.* **2001**, *74*, 917–925.
- 8) Heaney, F.; Bourke, S.; Cunningham, D.; McArdle, P. *J. Chem. Soc. Perkin Trans. 2* **1998**, 547–559.
- 9) Gotoh, M.; Mizui, T.; Sun, B.; Hirayama, K.; Noguchi, M. *J. Chem. Soc. Perkin 1* **1995**, 1857–1862.
- 10) Roca-López, D.; Darù, A.; Tejero, T.; Merino, P. *RSC Adv.*, **2016**, *6*, 22161–22173.
- 11) Sahyoun, T.; Arrault, A.; Schneider, R. *Molecules* **2019**, *24*, 2470–2489.
- 12) Vetrovsky, P.; Boucher, J. L.; Schott, C.; Beranova, P.; Chalupsky, K.; Callizot, N.; Muller, B.; Entlicher, G.; Mansuy, D.; Stoclet, J. C. *J. Pharmacol. Exp. Ther.* **2002**, *303*, 823–830.
- 13) Oresmaa, L.; Kotikoski, H.; Haukka, M.; Oksala, O.; Pohjala, E.; Vapaatalo, H.; Moilanen, E.; Vainiotalo, P.; Aulaskari, P. *Eur. J. Med. Chem.* **2006**, *41*, 1073–1079.
- 14) Sabine S.; Beáta, B. K.; Bálint, S.; Viktor, F.; László, B.; Zsuzsanna, S.; Gábor, H.; Gábor, M. *Beilstein J. Org. Chem.*, **2018**, *14*, 756–771.
- 15) Shiro, S.; Leonard, M. N.; Theodor, W. S.; Yukimasa, S.; Kazuhito, A.; Hiroaki, N.; Tsutomu A.; Yoji, I.; Chikara, M.; Tatsuya, T.; Shiro, M.; *Canc. Res.*, **1999**, *59*, 2931–2938.
- 16) Long, J. A.; Harris, N.J.; Lammertsma, K. *J. Org. Chem.*, **2001**, *66*, 6762–6767.
- 17) Novikov, A. S.; Bolotin, D. S. *J. Phys. Org. Chem.*, **2017**, *31*, 3772–3777.
- 18) Dignam, K. J.; Hegarty, A. F. *J. Chem. Soc. Perkin Trans. 2*, **1979**, 1437–1443.
- 19) a Tamada, M.; Seko, N.; Yoshii, F. *Radiat. Phys. Chem.*, **2004**, *71*, 221–225.
- 20) Mette, S.; Elizabeth, H. J. N.; Birger, L. M. *Molecular Plant*, **2018**, *11*, 95–117.
- 21) Nikitjuka, A.; Jirgensons, A. *Chem. Heterocycl. Comp.*, **2014**, *49*, 1544–1559.
- 22) Mohammed, N. H. *Herbicides Properties, Synthesis and Control of Weeds*, **2012** IntechOpen. ISBN 978-953-307-803-8.

- 23) Jung, M.; Saito, A.; Buescher, G.; Maurer, M.; Graf, J.-F. *Chemistry, pharmacology and safety: milbemycin oxime. In Macrocyclic Lactones in Antiparasitic Therapy*, Eds Vercruysse, J. & Rew, R. S., **2002**, pp 51–74. CABI Publishing, Wallingford, UK. ISBN 978-085-199-617-2.
- 24) Bahal, N.; Nahata, M. C. *Ann Pharmacother.* **1992**, *26*, 46–55.
- 25) Li, Q. G.; Hümpel, M. *Eur J Drug Metab Pharmacokinet.*, **1992**, *17*, 4, 281–291.
- 26) Nabors, O'B. *Alternative Sweeteners*, 3rd Ed., revised and expanded, **2001**, Marcel Dekker, ISBN 0-8247-0437-1.
- 27) Fylaktakidou, K. C.; Hadjipavlou, L. D. J.; Litinas, K. E.; Varella, E. A.; Nicolaidis, D. N. *Current Pharmaceutical Design*, **2008**, *14*, 1001–1047.
- 28) Marrs, T. C. *Pharmacol. Ther.*, **1993**, *58*, 51–66.
- 29) Dawson, R. M. *J. Appl. Toxicol.*, **1994**, *14*, 317–331.
- 30) Taylor, P. Anticholinesterase agents. in the pharmacological basis of therapeutics, 9th Ed.; Hardman, J. G.; Limbird, L. E. Eds. McGraw Hill: New York, **1996**; 161–176. ISBN 978-1259584732.
- 31) Buckley N. A.; Eddleston, M.; Szinicz, L. *Database Syst. Rev.*, **2005**, *1*, 1–18.
- 32) Kuruba, B. K.; Vasanthkumar, S. *Tetrahedron*, **2017**, *73*, 3860–3865.
- 33) Kool, E. T.; Crisalli, P.; Chan, K. M. *Org. Lett.*, **2014**, *16*, 1454–1457.
- 34) Sharghi, H.; Hosseini, M. *Synthesis*, **2002**, 1057–1060.
- 35) Hajjipour, A. R.; Mallakpour, S. E.; Imanzadeh, G. *J. Chem. Res.*, **1999**, 228–229.
- 36) Javad, M.; Mohammad, R. N. J.; Hamideh, H.; Mohammad, D.; Gerd, K. *ChemSusChem*, **2009**, *3*, 248–254.
- 37) Li, J. T.; Li, X. L.; Li, T. S. *Ultrason. Sonochem.*, **2006**, *13*, 200–202.
- 38) Hashem, S.; Mona, H. *Synthesis*, **2002**, 1057–1060.
- 39) Izumi, Y.; Sato, S.; Urabe, K. *Chem. Lett.* **1983**, 1649–1650.
- 40) Gregory, B. J.; Moodie, R. B.; Schofield, K. J. *Chem. Soc. B*, **1970**, 338–346.
- 41) Abdol, R. H.; Shadpour, E. M.; Holamhasan, I. *J. Chem. Res. (S)*, **1999**, 228–229.
- 42) Katsushi K.; Tatsuya, T.; Jun, S.; Tohru, F. *Org. Lett.*, **2008**, *11*, 2259–2260.
- 43) House, H. O.; Manning, D. T.; Melillo, D. G.; Lee, L. F.; Haynes, O. R.; Wilkes, B. E. *J. Org. Chem.* **1976**, *41*, 855–863.
- 44) House, H. O.; Lee, L. F. *J. Org. Chem.*, **1976**, *41*, 863–869.
- 45) Ciganek, E. *J. Org. Chem.*, **1990**, *55*, 3007–3009.
- 46) Ciganek, E. Read, J. M.; Calabrese, J. C. *J. Org. Chem.*, **1995**, *60*, 5795–5802.

- 47) Ciganek, E. *J. Org. Chem.*, **1995**, *60*, 5803–5807.
- 48) Oppolzer, W.; Spivey, A. C.; Bochet, C. G. *J. Am. Chem. Soc.*, **1994**, *116*, 3139–3140.
- 49) Oppolzer, W. *Gazz. Chim. Ital.*, **1995**, *125*, 207–213.
- 50) Cooper, N. J.; Knight, D. W. *Tetrahedron*, **2004**, *60*, 243–269.
- 51) Andre, M. B.; Joseph, M.; Marie, E. L.; Catherine, S.; Elena, D.; Lili, Z.; Serge, I. G. *Angew. Chem.* **2008**, *47*, 1410–1413.
- 52) Moran, J.; Pfeiffer, J. Y.; Gorelsky, S. I.; Beauchemin, A. M. *Org. Lett.*, **2009**, *11*, 1895–1898.
- 53) Yu, J.; Lu, M. *Synlett*, **2014**, *25*, 1873–1878.
- 54) Nicolaou, K. C.; Mathison, C. J. N.; Montagnon, T. *Angew. Chem.*, **2003**, *115*, 4211–4216.
- 55) Czekelius, C.; Carreira, E. M. *Angew. Chem.*, **2005**, *44*, 612–615.
- 56) Patil, V. V.; Gayakwad, E. M.; Shankarling, G. S. *J. Org. Chem.*, **2016**, *81*, 781–786.
- 57) Crandall, J. K.; Reix, T. *J. Org. Chem.*, **1992**, *57*, 6759–6764.
- 58) Gilbert, K. E.; Borden, W. T. *J. Org. Chem.*, **1979**, *44*, 659–661.
- 59) Lynn, E. V. *J. Am. Chem. Soc.*, 1919, *41*, 368–370.
- 60) Talukdar, E. H. S. W.; Mathur, V. K. *Solar Energy*, **1991**, *47*, 165–171.
- 62) Toyo Rayon Company. **1966**. Japan. Patent 47826.
- 61) Beckham, L. J.; Fessler, W. A.; Kise, M. A. *Chem. Rev.* **1951**, *48*, 319–396.
- 63) Melvyn, W. M.; Bunce, N. J. *Can. J. Chem.*, **1971**, *49*, 28–34.
- 64) Yoshikazu, I.; Shigeru, M. *New Chemical Processes of Monomers in the United States and Japan*, **1969**, *147*, 618–624.
- 65) Ito, Y. *Bull. Chem. Soc. of Jpn.*, **1956**, *29*, 227–230.
- 66) Franck, J.; Rabinowitsch, E. *Trans. Faraday Soc.*, **1934**, *30*, 120–130.
- 67) Rabinowitch, E.; Wood, W. C. *Trans. Faraday Soc.*, **1936**, *32*, 1381–1387.
- 68) Muller E.; Trense, U. *Tetrahedron Lett.*, **1967**, *49*, 4979–4982.
- 69) Muller, E.; Padeken, H. G.; Salamon, M.; Fiedler, G. *Chem. Ber.*, **1965**, *98*, 1893–1909.
- 70) Muller, E.; Gerhard, F.; Jurgen, H. *Chem. Ber.*, **1968**, *101*, 765–771.
- 71) Mackor, A.; Wajer, A. J. W.; de Boer, T. J.; van Voorst, J. D. W. *Tetrahedron Lett.* **1967**, *8*, 5, 385–390.
- 72) Gray, P.; Rathbone, P. *Proc. Chem. Soc.* **1960**, 316–317.
- 73) Mackor, A.; Veenland, J. U.; T. J. de Boer, T. J. *Recueil*, **1969**, *88*, 1249–1262.
- 74) Mackor, A.; Wajer, Th. A. J. W.; de Boer, Th. J.; van Voorst, J. D. W. *Tetrahedron Lett.* **1966**, 2115–2123.
- 75) Donaruma, L. C.; Carmody, D. J. *J. Org. Chem.*, **1957**, *22*, 635–639.

- 76) Burrell, E. J. *J. Phys. Chem.*, **1962**, *66*, 401–404.
- 77) Gilbert, K. E.; Borden, W. T. *J. Org. Chem.*, **1979**, *44*, 659–661.
- 78) Kakeya, N.; Abe, K.; From Jpn. Kokai Tokkyo Koho, 09003026, 07 Jan **1997**.
- 79) Dahiya, A.; Sahoo, A. K.; Alam, T.; Patel, B. K. *Chem.–Asian J.*, **2019**, *14*, 4454–4492.
- 80) Brice, S. *Photochemistry* **1971**, *2*, 675–678. <https://doi.org/10.1039/9781847554550>.
- 81) Wysocki, J. D.; Joaquim, H. T.; Richard, D.; Oliver, T.; Bernd, S.; Thomas S. *ChemPhotoChem*, **2018**, *2*, 22–26.
- 82) Mason, J.; Bronswijk, W. V. *J. Chem. Soc. A*, **1971**, 791–793.
- 83) Caldwell, S. E.; Porter, N. A. *J. Am. Chem. Soc.*, **1995**, *117*, 8676–8677.
- 84) Tilden, W. A. *J. Chem. Soc.*, **1875**, *28*, 514–518.
- 85) Rainer, G.; Kent, R. M.; Charles, L. B. *J. Org. Chem.* **1996**, *61*, 1047–1058.
- 86) Michael, H.; Josef, P. *J. Chem. Soc., Faraday Trans.*, **1992**, *88*, 2109–2110.
- 87) [McMillan, G. R.](#) *J. Phys. Chem.*, **1963**, *67*, 931–932.
- 88) Mackor, A.; Veenland, J. U.; de Boer, Th. J. *Recueil des Travaux Chimiques des Pays-Bas*, **1969**, *88*, 1251–1262.
- 89) T. Aubert, Method for preparing Lactames, comprising a photonitrosation step, followed by a Beckmann transposition step, US patent **2011**, US20110137027A1.
- 90) T. Takahashi, Y. Nishikawa, S. Morita, Method of Producing Cycloalkanone Oxime, US Patent **2015**, US20150175531A1.
- 91) R. H. Williams, J. P. Guarino, *Production of Cycloaliphatic Ketoximes*, US Patent **1970**, US3505191A.
- 92) Hirabayashi, T.; Sakaguchi, S.; Ishii, Y.; *Angew. Chem. Int. Ed.*, **2004**, *43*, 1120–1123.
- 93) Ishii, Y.; Sakaguchi, S.; Obora, Y. *J. Synth. Org. Chem. Jpn.*, **2008**, *66*, 1066–1075.
- 94) René, L.; David, C.; Oliver, C. K. *React. Chem. Eng.*, **2019**, *4*, 738–746.
- 95) J. R. Morton and H. W. Wilcox, in *Inorganic Syntheses*, John Wiley & Sons, Ltd, **1953**, pp. 48–52. ISBN 9780470132357.
- 96) Semmler, W. *Chem. Ber.*, **1892**, *25*, 3352–3354.
- 97) Wolff, L. *Justus Liebigs Ann. Chem.* **1902**, *322*, 351–391.
- 98) Alfassi, Z. B.; Feldman, L. *Int. J. Chem. Kin.*, **1981**, *13*, 771–783.
- 99) *CRC Handbook of Chemistry and Physics*, 85th ed.; Ed. D. R. Lide; CRC Press: Boca Raton, FL, **2004**. ISBN 0849304857
- 100) Aburatani, Y.; Sato, Y.; Yamamoto, T.; Ohashi, O.; Kuze, N.; Sato, E.; Sakaizumi, T. *J. Mol. Spectr.* **2006**, *237*, 1–10.

- 101) Laarhoven, L. J. J.; Mulder, P. J. *Phys. Chem.*, **1997**, *101*, 73–77.
- 102) Hayashi, E.; Suzuki, S. *J. Pharm. Soc. Japan*, **1975**, *95*, 1439–1442.
- 103) Bardakos, V.; Sucrow, W. *Chem. Ber.*, **1978**, *111*, 1780–1788.
- 104) Yanagida, A. J.; Gansser, C. *J. Het. Chem.*, **1978**, *15*, 249–251.

4.5 Experimental

4.5.1 Materials and Methods

Chemicals: The chemicals used were obtained from the companies Sigma-Aldrich / Fluka, Alfa Aesar, TCI or Fluorochem and were used without further purification.

Chromatography: For the TLC chromatography Merck TLC Aluminium oxide 60 F254 with glass backing were used. Detection was carried out either by UV absorption or by treatment of the plate with an acidic solution of potassium permanganate and drying using a handheld hot-air dryer.

NMR-Spectroscopy: The NMR spectra were recorded on a Bruker Avance-600 and Varian VNMR-700 spectrometer in the indicated solvent at a temperature of 297 K. Commercially available deuterated chloroform, methanol or DMSO was used as a solvent. The spectra were always set to the reference value of the solvent, for example chloroform (for ¹H-NMR spectra to 7.26 ppm and for ¹³C-NMR spectra to 77.00 ppm). For the exact analysis and assignment of the signals in more complex compounds, COSY, HSQC and HMBC spectra were additionally added. Chemical shifts were reported in ppm and coupling constants J in hertz (Hz). The following abbreviations were used for the multiplicities of the signals: s (singlet), d (doublet), t (triplet), q (quartet), m (multiplet).

MS-Spectroscopy: GCMS spectra were obtained using an Agilent 6890N gas chromatograph coupled with an Agilent 5973 inert mass selective detector operating in EI mode with a custom-built Anature auto sampler/injector or by Durham University Mass Spectrometry service. Electrospray (ES) mass spectra were obtained using a TQD mass spectrometer (Waters UK, Ltd; all were obtained by Durham University Mass Spectrometry service).

IR-Spectroscopy: The infrared spectra were recorded with a PerkinElmer Spectrum One IR spectrometer. The samples were measured by the ATR method (attenuated total reflection). The evaluation was limited to the bands characteristic of the compound. The position of the absorption bands in the IR spectrum was expressed in wave numbers $\tilde{\nu}$ (cm⁻¹).

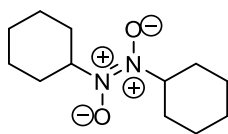
Melting point determination: The melting point was determined using an Electrothermal 9100 capillary melting point device. The melting point range was recorded for the determination of melting points for resinous solids.

General procedure for the synthesis of compounds **4-176**, **4-196/4-201**: ^tBuONO 25. mmol and 20 equivalent of the starting material are pumped through the photoreactor at 1 mL/min.

DCM 20 mL is added to the obtained mixture and the solution is stirred with activated charcoal (2 g) filtered and the solvent and unreacted cyclohexane are removed by rotavapour. The product was recrystallized from cyclohexane (compound **4-199** is purified through chromatographic column hexane: EtOAc (8:2)).

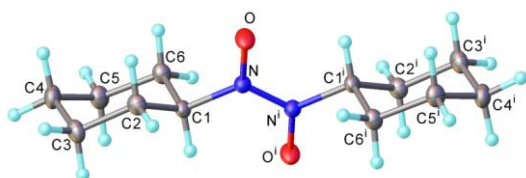
General continuous procedure for compounds **4-7**, **4-187a**, **4-187b**: t BuONO (25.1 mmol) and cyclohexane/cyclohexene (1:45 and 1:100 molar ratios) are pumped through the photoreactor at 1 mL/min and 2 mL/min and in a Soxhlet apparatus, where it is heated at reflux and the distilled solvent is re-flowed at 1 mL/min in the starting material flask where t BuONO is added, with the flow rate of the reagent adjusted to give the indicated ratio of reagents in the reactor coil, until consumption of cyclohexane. Product sublimed and recrystallised from cyclohexane (1.05 g, 37%).

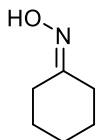
4.5.2 Compounds characterization



(E)-1,2-Dicyclohexyldiazene-1,2-dioxide (4-176).

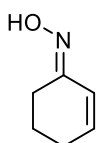
Appearance: white crystalline solid, isolated yield 55%; ^1H NMR (700 MHz, CDCl_3) δ 5.05 (tq, $J = 11.4, 3.8$ Hz, 2H), 1.93 (dd, $J = 11.4, 3.8$ Hz, 4H), 1.84 (dp, $J = 11.4, 3.5$ Hz, 4H), 1.73 – 1.57 (m, 4H), 1.35 (qt, $J = 13.0, 3.6$ Hz, 4H), 1.21 (qt, $J = 13.0, 3.6$ Hz, 4H); ^{13}C NMR (176 MHz, CDCl_3) δ 65.79 (CH), 28.36 (CH_2), 25.14 (CH_2), 24.71 (CH_2); IR (neat) $\nu = 2930.1$ (s), 2851.7 (m), 1446.5 (s), 1394.4 (s), 1191.5 (s), 1145.7 (s), 1005.2 (m), 893.4 (s), 875.3 9(m), 689.5 (s) cm^{-1} ; MS calculated for $\text{C}_{12}\text{H}_{23}\text{N}_2\text{O}_2$ 227.1256, found 227.1260 ($\Delta = 1.8$ ppm, 0.4 mDa); Melting point: 117–118 $^\circ\text{C}$; Unit Cell Parameters: a 5.5414(2) b 6.1252(3) c 9.8876(5) P-1.





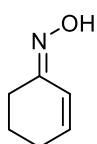
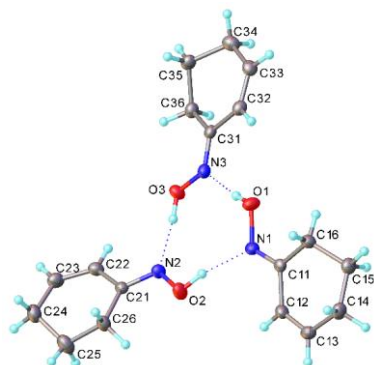
Cyclohexanone oxime (4-7).

Appearance: white crystalline solid, isolated yield 59% ^1H NMR (600 MHz, CDCl_3) δ 9.12 (s, 1H), 2.52–2.49 (m, 2H), 2.23–2.19 (m, 2H), 1.72–1.55 (m, 6H); ^{13}C NMR (151 MHz, CDCl_3) δ 160.85 (C), 32.28 (CH_2), 27.01 (CH_2), 25.94 (CH_2), 25.72 (CH_2), 24.60 (CH_2); IR (neat) ν = 3182.5 (w), 3106.7 (w), 2930.9 (m), 1163.1 (m), 1478.2 (m), 1435.2 (m), 1224.7 (w), 991.9 (s), 959.9 (s), 899.7 (m), 774.6 (m), 567.3 (w) cm^{-1} ; MS calculated for $\text{C}_6\text{H}_{12}\text{NO}$ 114.0919, found 114.0912 (Δ = -6.1 ppm, -0.7 mDa); Melting point: 89.1–89.8 °C (crystallised from cyclohexane).



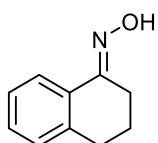
(E)-Cyclohex-2-en-1-one oxime (4-187a).

Appearance: white crystalline solid, isolated yield 55.4% ^1H NMR (600 MHz, CDCl_3) δ 6.23 (dt, J = 10.1, 4.1 Hz, 1H), 6.14 (dt, J = 10.1, 1.9 Hz, 1H), 2.65 – 2.60 (m, 2H), 2.18 (tdd, J = 6.3, 4.1, 1.9 Hz, 2H), 1.76 (p, J = 6.3 Hz, 2H); ^{13}C NMR (151 MHz, CDCl_3) δ 156.61 (C), 136.65 (CH), 124.35 (CH), 29.27 (CH_2), 25.22 (CH_2), 22.36 (CH_2), 20.88 (CH_2); IR (neat) ν = 2832.1 (m), 1636.7 (w), 1476.8 (w), 1394.1 (w), 1001.1 (s), 947.1 (s), 861.2 (s), 719.7 (s), 596.2(w) cm^{-1} ; MS calculated for $\text{C}_6\text{H}_{10}\text{NO}$ 112.0762, found 112.0734 (Δ = -25.0 ppm, -2.8 mDa); Melting point: 101.0–102.0 °C (crystallised from cyclohexane); Unit Cell Parameters: 20.516(3) 20.516(3) 7.4084(12) P-3.



(Z)-Cyclohex-2-en-1-one oxime (4-187b).

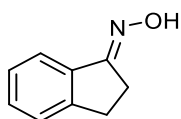
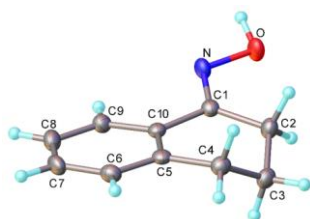
Appearance: white crystalline solid, isolated yield 14.5% ^1H NMR (600 MHz, CDCl_3) δ 6.82 (dt, $J = 10.3, 2.2$ Hz, 1H), 6.33 (dt, $J = 10.3, 4.0$ Hz, 1H), 2.41 – 2.37 (m, 2H), 2.24 (tdd, $J = 6.1, 4.0, 2.2$ Hz, 2H), 1.84 (p, $J = 6.1$ Hz, 2H); ^{13}C NMR (151 MHz, CDCl_3) δ 153.57 (C), 139.95 (CH), 117.22 (CH), 28.41 (CH_2), 26.42 (CH_2), 22.42 (CH_2); IR (neat) $\nu = 2873.0$ (m), 1636.8 (m), 1470.6 (m), 976.1 (s), 854.4 (m), 740.2 (s), 572.8 (s) cm^{-1} ; MS calculated for $\text{C}_6\text{H}_{10}\text{NO}$ 112.0762, found 112.0766 ($\Delta = 3.6$ ppm, 0.4 mDa); Melting point: 80.2–81.1 $^\circ\text{C}$ (crystallised from cyclohexane); Unit Cell Parameters: 13.643(3)20.516(3) 7.4084(12) P-3.



(E)-3,4-Dihydronaphthalen-1(2H)-one oxime (4-196).

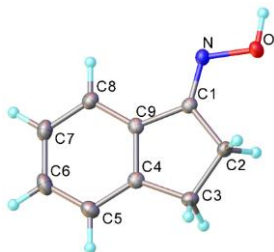
Appearance: white crystalline solid, isolated yield 68%, ^1H NMR (700 MHz, CDCl_3) δ 9.57 (s, 1H), 7.91 (d, $J = 7.6$ Hz, 1H), 7.29 (t, $J = 7.6$ Hz, 1H), 7.23 (t, $J = 7.6$ Hz, 1H), 7.18 (d, $J = 7.6$ Hz, 1H), 2.87 (t, $J = 6.7$ Hz, 2H), 2.79 (t, $J = 6.7$ Hz, 2H), 1.91 (p, $J = 6.7$ Hz, 2H); ^{13}C NMR (176 MHz,

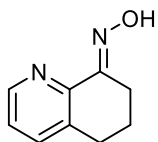
CDCl₃ δ 155.47 (C), 139.95 (C), 130.57 (C), 129.34 (CH), 128.80 (CH), 126.62 (CH), 124.16 (CH), 29.95 (CH₂), 24.03 (CH₂), 21.44 (CH₂); IR (neat) ν = 2933.8 (w), 1485.6 (w), 1305.6 (w), 962.2 (m), 948.1 (m), 886.9 (m), 737.0 (s), 657.2 (w), 466.3 (w) cm⁻¹; MS calculated for C₁₀H₁₂NO 162.0919, found 162.0916 (Δ = -1.9 ppm, -0.3 mDa); Melting point: 103.0–104.0 °C (crystallised from cyclohexane); Unit Cell Parameters: a 13.643(3) b 8.3171(16) c 15.465(3) C2/c.



(E)-2,3-Dihydro-1H-inden-1-one oxime (4-197).

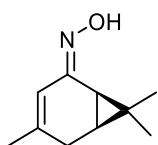
Appearance: white crystalline solid, isolated yield 50%, ¹H NMR (600 MHz, CDCl₃) δ 8.87 (s, 1H), 7.70 (d, *J* = 7.7 Hz, 1H), 7.38–7.32 (m, 2H), 7.29–7.24 (m, 1H), 3.10–3.07 (m, 2H), 3.02–2.98 (m, 2H); ¹³C NMR (151 MHz, CDCl₃) δ 164.19 (C), 148.57 (C), 136.06 (C), 130.57 (CH), 127.15 (CH), 125.75 (CH), 121.71 (CH), 28.67 (CH₂), 26.08 (CH₂); IR (neat) ν = 3044.1 (m), 2839.7 (m), 1654.4 (m), 1453.4 (m), 1431.8 (m), 1070.0 (m), 954.8 (s), 750.7 (s), 674.4 (m), 543.2 (w) cm⁻¹; MS calculated for C₉H₁₀NO 148.0762, found 148.0764 (Δ = 1.4 ppm, 0.2 mDa); Melting point: 146.0–148.2 °C (crystallised from EtOAc); Unit Cell Parameters: a 22.4110(8) b 22.4110(8) c 5.8772(2) I41/a.





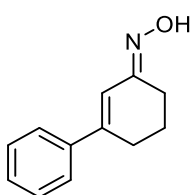
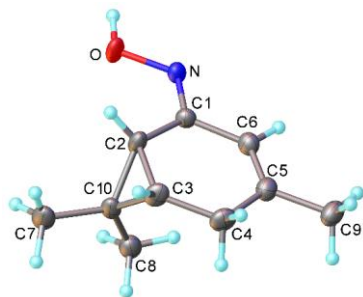
(E)-6,7-Dihydroquinolin-8(5H)-one oxime (4-198).

Appearance: yellow crystalline solid, isolated yield 40%, ^1H NMR (600 MHz, CDCl_3) δ 8.46 (dd, $J = 4.7, 1.7$ Hz, 1H), 7.41 (ddt, $J = 7.7, 1.8, 0.9$ Hz, 1H), 7.12 (dd, $J = 7.7, 4.6$ Hz, 1H), 2.86 (t, $J = 6.6$ Hz, 2H), 2.74 (t, $J = 6.1$ Hz, 2H), 1.89–1.80 (m, 2H); ^{13}C NMR (151 MHz, CDCl_3) δ 153.1 (C), 148.8 (C), 148.2 (CH), 136.9 (CH), 134.8 (C), 123.6 (CH), 29.0 (CH_2), 23.9 (CH_2), 20.8 (CH_2); IR (neat) $\nu = 2980.9$ (w), 1474.0 (m), 967.9 (s), 884.0 (s), 791.4 (s) cm^{-1} ; MS calculated for $\text{C}_9\text{H}_{11}\text{N}_2\text{O}$ 163.0871, found 163.0871 ($\Delta = -6.1$ ppm, -1.0 mDa); Melting point: 190.0–192.0 $^\circ\text{C}$ (crystallised from *i*PrOH).



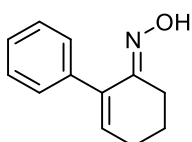
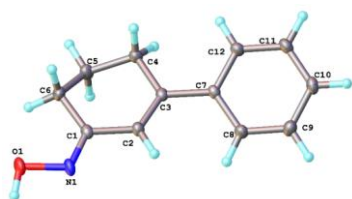
(1R,6S,Z)-4,7,7-Trimethylbicyclo[4.1.0]hept-3-en-2-one oxime (4-199).

Appearance: white crystalline solid, isolated yield 40%, ^1H NMR (400 MHz, CDCl_3) δ 5.87 (s, 1H), 2.48 (dd, $J = 20.1, 8.3$ Hz, 1H), 2.15 (d, $J = 20.1$ Hz, 1H), 1.97 (d, $J = 8.3$ Hz, 1H), 1.79 (s, 3H), 1.25 (s, 3H), 1.22 (d, $J = 8.3$ Hz, 1H), 0.91 (s, 3H); ^{13}C NMR (101 MHz, CDCl_3) δ 155.0 (C), 143.0 (C), 119.0 (CH), 28.0 (C), 27.1 (CH), 23.5 (CH_2), 22.5 (CH), 21.0 (CH_3), 19.8 (CH_3), 14.6 (CH_3); IR (neat) $\nu = 3165.3$ (m), 2863.3 (m), 1614.5 (w), 1439.6 (m), 963.0 (s), 842.2 (m), 747.8 (m) cm^{-1} ; MS calculated for $\text{C}_{10}\text{H}_{16}\text{NO}$ 166.1232, found 166.1229 ($\Delta = -1.8$ ppm, -0.3 mDa); Melting point: 122.2–123.0 $^\circ\text{C}$ (crystallised from Hexane: EtOAc); Unit Cell Parameters: a 15.248(5) b 15.248(5) c 7.249(3) P6₃.



(E)-5,6-Dihydro-[1,1'-biphenyl]-3(4H)-one oxime (4-201).

Appearance: white crystalline solid, isolated yield 32%, ^1H NMR (700 MHz, CDCl_3) δ 7.32 (m, 2H), 7.29 – 7.27 (m, 1H), 7.25 (m, 2H), 6.24 (t, $J = 4.4$ Hz, 1H), 2.69 (t, $J = 6.6$ Hz, 2H), 2.32 (td, $J = 6.6, 4.4$ Hz, 2H), 1.82 (p, $J = 6.6$ Hz, 2H); ^{13}C NMR (176 MHz, CDCl_3) δ 157.16 (C), 138.67 (C), 137.79 (CH), 136.38 (C), 129.06 (CH), 128.21 (CH), 127.50 (CH), 25.64 (CH_2), 22.98 (CH_2), 20.80 (CH_2); IR (neat) $\nu = 3163.7$ (w), 3048.1 (w), 2950.4 (w), 1439.0 (m), 981.4 (m), 943.2 (m), 877.1 (m), 753.1 (s), 687.5 (s), 615.5 (m), 452.7 (m) cm^{-1} ; MS calculated for $\text{C}_{12}\text{H}_{14}\text{NO}$ 188.1075, found 188.1070 ($\Delta = -2.7$ ppm, -0.5 mDa); Melting point: 130.8–131.4 $^\circ\text{C}$ (crystallised from hexane); Unit Cell Parameters: a 10.8828(5) b 7.5566(3) c 12.1779(5) $\text{P}2_1/c$.



(E)-4,5-Dihydro-[1,1'-biphenyl]-2(3H)-one oxime (4-200).

Appearance: white crystalline solid, isolated yield 8%, ^1H NMR (700 MHz, CDCl_3) 8.80–7.70 (br., 1H), 7.39–7.24 (m, 5H), 6.20 (t, $J = 4.4$ Hz, 1H), 2.70 (t, $J = 6.6$ Hz, 2H), 2.33 (q, $J = 5.6$ Hz, 2H), 1.84 (p, $J = 6.4$ Hz, 2H); ^{13}C NMR (101 MHz, CDCl_3) δ 157.0 (C), 138.6 (C), 137.5 (CH), 136.3 (C), 128.9 (CH), 128.1 (CH), 127.4 (CH), 25.5 (CH_2), 22.8 (CH_2), 20.7 (CH_2); IR (neat) $\nu = 2994.2$ (w), 1432.5 (w), 989.3 (m), 946.6 (s), 746.3 (s), 755.4 (s), 601.8 (m), 543.1 (m) cm^{-1} ; MS calculated for $\text{C}_{12}\text{H}_{14}\text{NO}$ 188.1075, found 188.1078 ($\Delta = 1.6$ ppm, 0.3 mDa); Melting point: 156.0–157.5 $^\circ\text{C}$ (crystallised from hexane:EtOAc); Unit Cell Parameters: a 6.2751(14) b 8.759(3) c 10.097(3).